

DISS. ETH NO. 22940

# **Development and clinical feasibility of a novel pediatric arm rehabilitation robot**

A thesis submitted to attain the degree of

DOCTOR OF SCIENCES of ETH ZURICH

(Dr. sc. ETH Zurich)

presented by

**URS WALTER KELLER**

MSc ETH ME, ETH Zurich

born on 23.02.1983

citizen of

Wildberg, ZH, Switzerland

accepted on the recommendation of

Prof. Dr. Robert Riener

Prof. Dr. Roger Gassert

PD Dr. Hubertus J.A. van Hedel

2015





# Acknowledgements

This thesis is the result of many people who helped in the last five years to transform the idea of a pediatric arm robot into the finished ChARMin system which can be applied in the clinics for rehabilitation training. Therefore, my first thanks is a general one and goes out to all the people who contributed to the successful realization of this thesis and made my last five years to a pleasant and instructive journey. I would like to thank all of them.

My biggest thanks is addressed to Robert Riener, the supervisor of my thesis. I am deeply thankful for his support during the thesis, for the possibilities he opened and the freedom he allowed in the realization of the different projects and for providing an inspiring working environment.

I would like to thank Huub van Hedel for mentoring me with great motivation and valuable inputs during the last years. His expertise and personal commitment were a great motor to realize the ChARMin project. His support in editing my documents, papers and applications was always very appreciated. I thank Roger Gassert for his commitment in co-supervising this thesis. I'm thankful for his inputs, interest and ideas as well as the scientific discussions which were a great help.

A special thanks goes out to Alessandro Rotta and Marco Bader for supporting me with their technical experience in designing and machining the robots (PASCAL, ChARMin, ARMin IV). Furthermore, great thanks to Michael Herold-Nadig for his support with the electronics of the robot, his advice and contributions to the realization of ChARMin. The discussions with him were always very fruitful and exhilarant. Thank you all guys!

I would like to thank the whole SMS team for inspiring discussions and the dynamic and friendly environment over the past years. Special thanks go to Joachim von Zitzewitz, Mark van Raai and Nicolas Gerig for always being supportive office mates and friends and Ximena Omlin for being a mental and creative enrichment of my daily life in the lab and for the great friendship we share. I thank Marco Guidali for his help with the ARMin robot. He enabled a pleasant and competent start in the ARMin group. Moreover, I thank Aniket Nagle from the SMS lab, for his tireless efforts in implementing and improving the interface software of the different robots.

Furthermore, I deeply acknowledge the valuable clinical input and support from Andreas Meyer-Heim, the occupational therapists Karin Gygax, Annina Herzog, Jan Lieber and Bärbel Rückriem, and the people from the Pediatric Rehab Research Group of the Rehabilitation Center of the University Children's Hospital Zurich, Affoltern a. A., Switzerland. I always felt welcome and integrated from the beginning, as the 'engineer' of the group.

I want to acknowledge the coauthors and contributors of the RANA (Robot-assisted neurorehabilitation of the arm) project. Namely, Sabine Schölch, Urs Albisser, Claudia Rudhe, Armin Curt and Verena Klamroth-Marganska as well as Peter Schenk, Silvia Rohner and Alexander Duschau-Wicke from Hocoma AG, Switzerland for their input on the implementation and visual representation of the assessments, as well as all the subjects and patients who kindly participated in the study.

Moreover, I want to express my appreciation to all the undergraduate students whom I supervised during the last five years and who contributed to the successful completion of the different projects and finally this thesis:

ChARMin: Alessandro Rotta (CAD design of the proximal part of ChARMin), Fabio Carrillo (Learning controller), Daniel Dörig (Design of the hand module), Sarah Nicoli (Requirements for a arm therapy robot for children), and Markus Zahner (New concepts for a pediatric ARMin).

PASCAL: Kim Pfluger (Design and realization of the PASCAL robot), Maria Rozou (Testing and extending the path control algorithm), and Evangelia Dislaki (Virtual game-like scenario).

ARMin: Fabrizio Borrello (Remote control of ARMin with an ArmeoSpring robot), Titus Bugman and Lucas Conditt (Transparency control of ARMin IV), and Tazeen Bukhari (Patient-specific arm weight compensation).

I would like to thank the financial supporters of the different projects. This work was financially supported by the Highly-Specialized Medicine Project of the canton of Zurich, the Gottfried und Julia Bangerter-Rhyner Foundation, the Mäxi Foundation, the Gaydoul Foundation, the NCCR Neural Plasticity and Repair, and the NCCR Robotics, Switzerland.

I profoundly appreciate the strong support of my family and my friends, especially Silvio Hunziker.

Finally, I particularly thank my girlfriend Helene Siegrist for accompanying my journey for over 10 years and for her unconditional support, motivation, and love.

*Zurich, 2nd September, 2015*

Urs Keller

# Contents

Acknowledgements . . . . .	iii
Contents . . . . .	v
Abstract . . . . .	ix
Zusammenfassung . . . . .	xi
Preface . . . . .	xv
Notations . . . . .	xvii
<b>1 Introduction</b>	<b>1</b>
1.1 Background . . . . .	1
1.1.1 Relevance of Arm Motor Function . . . . .	1
1.1.2 Children with Cerebral Palsy . . . . .	1
1.1.3 Triggering Neuroplasticity in Children . . . . .	4
1.2 Pediatric Rehabilitation . . . . .	5
1.3 Robot-Assisted Rehabilitation in Adults . . . . .	8
1.3.1 State of the Art . . . . .	8
1.3.2 ARMin Arm Rehabilitation Robot . . . . .	10
1.4 Robot-Assisted Rehabilitation in Children . . . . .	11
1.4.1 State of the Art . . . . .	11
1.4.2 PASCAL Robot . . . . .	14
1.4.3 What is Different in Pediatric Rehabilitation . . . . .	16
1.4.4 A Novel Pediatric Arm Rehabilitation Robot . . . . .	18
1.5 Motivation and Aim of the Thesis . . . . .	19
1.5.1 Problem Statement and Hypotheses . . . . .	19
1.5.2 Aims of the Thesis . . . . .	19
1.5.3 Challenges . . . . .	20
1.6 Thesis Outline . . . . .	20
<b>2 ChARMin Robot</b>	<b>21</b>
2.1 Introduction . . . . .	21
2.1.1 Requirements . . . . .	21
2.1.2 Improving the Transparency . . . . .	28
2.2 ChARMin Design . . . . .	29
2.2.1 Mechanics . . . . .	29
2.2.2 Actuation . . . . .	41
2.2.3 Electronics . . . . .	41
2.2.4 Virtual Reality Interface . . . . .	44
2.2.5 Safety . . . . .	48
2.3 Results . . . . .	49
2.3.1 Realization of ChARMin . . . . .	49
2.3.2 Adjustment to Patient . . . . .	49
2.3.3 Spring-Induced Compensation Torques . . . . .	51
2.3.4 Mechanical Play . . . . .	52

---

2.3.5	Static Friction . . . . .	52
2.3.6	Inertial Properties . . . . .	53
2.3.7	Torques . . . . .	53
2.3.8	First Adaptations . . . . .	53
2.4	Discussion . . . . .	53
<b>3</b>	<b>ChARMin Control</b>	<b>61</b>
3.1	Introduction . . . . .	61
3.2	Method . . . . .	63
3.2.1	Modeling . . . . .	63
3.2.2	Position Controller . . . . .	78
3.2.3	Assist-as-Needed Path Controller . . . . .	78
3.2.4	Single-Joint Controller . . . . .	86
3.2.5	Control Stability . . . . .	87
3.3	Results . . . . .	91
3.3.1	Modeling . . . . .	91
3.3.2	Position Control . . . . .	93
3.3.3	AAN Path Controller . . . . .	95
3.3.4	Control Stability . . . . .	97
3.4	Discussion . . . . .	99
3.4.1	Modeling . . . . .	99
3.4.2	Position Controller . . . . .	100
3.4.3	AAN Path Controller . . . . .	101
3.4.4	Control Stability . . . . .	103
<b>4</b>	<b>ChARMin Assessments</b>	<b>105</b>
4.1	Robot-Assisted Arm Assessments in Adult SCI Patients . . . . .	105
4.1.1	Introduction . . . . .	105
4.1.2	Method . . . . .	107
4.1.3	Results . . . . .	116
4.1.4	Discussion . . . . .	122
4.2	Robot-Assisted Assessments in ChARMin . . . . .	128
4.2.1	Introduction . . . . .	128
4.2.2	Method . . . . .	129
4.2.3	Results . . . . .	136
4.2.4	Discussion . . . . .	139
<b>5</b>	<b>ChARMin Feasibility</b>	<b>143</b>
5.1	Introduction Feasibility . . . . .	143
5.2	Method . . . . .	143
5.2.1	Participants . . . . .	143
5.2.2	Study Design . . . . .	144
5.2.3	Outcome Measures . . . . .	146
5.3	Results . . . . .	147
5.3.1	ChARMin Applicability and Settings . . . . .	147
5.3.2	Games . . . . .	153
5.3.3	Robot-Assisted Assessments . . . . .	160
5.3.4	Clinical Assessments . . . . .	173

5.4	Discussion . . . . .	174
5.4.1	ChARMin Applicability and Settings . . . . .	174
5.4.2	Games . . . . .	175
5.4.3	Robot-Assisted Assessments . . . . .	177
<b>6</b>	<b>Conclusion and Outlook</b>	<b>183</b>
6.1	General Conclusion . . . . .	183
6.1.1	ChARMin Robot . . . . .	183
6.1.2	ChARMin Control . . . . .	183
6.1.3	ChARMin Assessments . . . . .	184
6.1.4	ChARMin Feasibility . . . . .	184
6.2	Contribution of this Thesis . . . . .	185
6.3	General Outlook . . . . .	186
<b>A</b>	<b>Appendix</b>	<b>187</b>
A.1	Appendix of Introduction . . . . .	187
A.2	Appendix of ChARMin Robot . . . . .	188
A.3	Appendix of ChARMin Control . . . . .	214
A.4	Appendix of ChARMin Assessments . . . . .	220
A.5	Appendix of ChARMin Feasibility . . . . .	224
	<b>Bibliography</b>	<b>250</b>

## CONTENTS

---

# Abstract

Children with congenital or acquired neurological disorders often have impairments of their arms. This includes children suffering from cerebral palsy, stroke, spinal cord injury or other neurological disorders. The impairment often hampers the child's independence and participation in daily life. An intensive, activity-based and goal-directed upper limb rehabilitation training is essential for improvement and recovery of motor function and can prevent deterioration of arm function in children with moderate to severe impairments. In adult patients with motor or neurological disorders, such as stroke or spinal cord injury, active robotic assistance is increasingly used to achieve an intensive therapy and to actively assist and enhance neurorehabilitation. Furthermore, therapy robots have the potential for accurate assessment of motor function to diagnose the patient status, to measure the therapy progress, or to feed back the movement performance to the patient and therapist in real time. However, there is currently no actuated robot available specifically designed for the rehabilitation of children with upper extremity motor impairments.

In this thesis the development, realization and clinical implementation of ChARMin, the first actuated exoskeleton robot for pediatric arm rehabilitation, is presented. The thesis was performed at the Sensory-Motor Systems Lab, ETH Zurich, Switzerland in collaboration with the Rehabilitation Center for Children and Adolescents, Affoltern a. A., Switzerland and is divided into four main parts.

In the first part of the thesis, the ChARMin robot is presented. The robot was specifically designed to provide an intensive and motivating neurorehabilitative training for children with affected arm motor function, e.g., with cerebral palsy. It combines parallel and serial kinematics to achieve an exoskeleton with six degrees of freedom to assist and assess the shoulder, elbow, and wrist of the pediatric target group. A modular design of the robot enables the application to children aged 5 to 18 years. The parallel structure allows to keep a safe distance between parts of the robot and the patient and it reduces friction. The whole exoskeleton is highly adaptable to cover the anthropometrics for the young patients and is applicable for the left and right arm. A novel passive weight support mechanism allows for a safe operation. Furthermore, a new audiovisual therapy interface was introduced for ChARMin to motivate active participation of the child with playful game-like scenarios.

The second part introduces the control approaches implemented to support the patient's arm with the exoskeleton. Different patient-cooperative control strategies enable free arm movements, assistance as needed and complete guidance of the arm. The controllers are chosen based on the game played and the skill level of the patient. An assist-as-needed path control concept is utilized to support complex multi-axis movements on end-effector basis. For specific single-axis training an adjustable joint-based controller is used. All the controllers include a model to compensate for inertial, gravitational and frictional aspects of the robot and a dithering approach to reduce static

friction. The performance of the controllers and the compensation model were tested and the stability of the different approaches analyzed.

The third part is dedicated to the implemented set of robot-assisted assessments that encompasses kinematic, kinetic, and timing metrics for measurement of arm motor function. Before the assessments were integrated into the ChARMin robot, the applicability, safety, reliability, and comparability to clinical metrics was first investigated in adults. Twenty-four healthy subjects and five patients after spinal cord injury underwent robot-based assessments using the adult exoskeleton robot ARMin. Five different measurements were performed with the visual aid of a display. Ten kinematic, kinetic, and timing assessment parameters were extracted on joint- and end-effector level. The first results with adult subjects suggest that the measurements are widely reliable and comparable to clinical scales for arm motor function. Based on these first results, the five assessment packages were adapted and transferred to the ChARMin platform. Additionally, a new assessment was added in which the patient needs to follow a circularly moving reference on the frontal plane to measure the tracking skills.

In the fourth part the results of the first feasibility case trials are presented. The ChARMin robot, control, and assessments were tested with five pediatric patients suffering from various neurological diagnoses (stroke, cerebral palsy, and traumatic brain injury). In different sessions the patients tried the various training scenarios with different amounts of support and robot settings depending on their therapeutic goals, capabilities, and preferences. The patient characteristics showed a large variety in terms of age (from 6 to 17 years), arm function, trained side, sex, and impairment. The ChARMin robot could be adjusted to all the patients. The five patients were motivated to play various games with different levels of support ranging from free arm movements to complete guidance. Furthermore, three patients successfully performed the robot-assisted assessments two times. These first feasibility trials demonstrated a safe and good applicability of the different training modes to the pediatric target group. The robot was accepted well by the therapists and the patients. The trials revealed only minor shortcomings which need to be addressed before the start of the next extensive ChARMin feasibility study.

In conclusion, the results of this thesis demonstrate a high potential of the ChARMin robot as an advanced exercise tool for arm neurorehabilitation that optimally challenges children in the age of 5- to 18-years. Furthermore, the hardware, control, and assessment methods presented and the results with healthy and affected adults and young patients can serve as a basis for the future development of end-effector and exoskeleton-based robotic platforms.



# Zusammenfassung

Kinder mit einer erworbenen oder angeborenen neurologischen Erkrankung haben oft auch beeinträchtigte Armfunktionen. Dies betrifft unter anderem Kinder mit infantilen Zerebralpareesen, Schlaganfall, Rückenmarkverletzungen oder anderen neurologischen Störungen. Diese Beeinträchtigungen erschweren oft die Unabhängigkeit des Kindes wie auch die Teilnahme am täglichen Leben. Ein intensives, zielorientiertes Rehabilitationstraining der oberen Extremität mit aktiver Beteiligung ist wichtig für die Verbesserung und das Wiedererlangen der motorischen Fähigkeiten und kann einer Verschlechterung der Armfunktionen bei mittel- bis schwer betroffenen Kindern entgegenwirken. Für erwachsene Patienten mit motorischen oder neurologischen Störungen, wie zum Beispiel nach einem Schlaganfall oder einer Rückenmarkverletzung, werden immer öfter aktive Roboter verwendet, um eine intensive Therapie zu ermöglichen und das Neurorehabilitationstraining zu unterstützen als auch zu verbessern. Zudem bieten die Therapieroboter die Möglichkeit, die motorischen Funktionen präzise zu messen, um den Zustand des Patienten zu diagnostizieren, den Therapieverlauf festzuhalten oder dem Therapeuten und Patienten in Echtzeit eine Rückmeldung zur Qualität der Bewegung zu geben. Einen aktiven Armroboter, welcher spezifisch für Kinder mit motorischen Beeinträchtigungen entwickelt wurde, gibt es zurzeit jedoch noch nicht.

In dieser Arbeit wird die Entwicklung, Realisierung und die klinische Umsetzung von ChARMin, dem ersten aktuierten Roboter für die pädiatrische Armrehabilitation, präsentiert. Die Arbeit wurde am Labor für Sensomotorische Systeme der ETH Zürich, Schweiz, in Zusammenarbeit mit dem Rehabilitationszentrum für Kinder und Jugendliche, Affoltern am Albis, Schweiz, durchgeführt und ist in vier Hauptteile gegliedert.

Im ersten Teil der Arbeit wird der ChARMin-Roboter präsentiert. Der Roboter wurde spezifisch entwickelt, um ein intensives und motivierendes Neurorehabilitationstraining für Kinder mit beeinträchtigten Armfunktionen, wie zum Beispiel bei infantiler Zerebralparese, zu gewährleisten. Hierzu wurden parallele und serielle Kinematiken verwendet, um ein Exoskelett mit sechs Freiheitsgraden zu verwirklichen, welches die Schulter, Ellbogen und Handgelenk der pädiatrischen Zielgruppe unterstützen und ausmessen kann. Ein modularer Ansatz ermöglicht die Anwendung für 5- bis 18-jährige Kinder. Die Parallelstruktur garantiert eine sichere Distanz zwischen Roboter und Patient und reduziert die Reibung. Das Exoskelett ist in hohem Maße anpassbar an die Anthropometrie der Kinder und kann für den rechten und linken Arm eingesetzt werden. Ein neuartiger Gewichtsentlastungsmechanismus erlaubt dabei einen sicheren Einsatz. Zudem wurde für ChARMin ein neues audio-visuelles Therapieinterface eingeführt, um mit unterhaltsamen Spielszenarien eine aktive Teilnahme des Kindes anzuregen.

Der zweite Teil stellt die implementierten Regleransätze vor, welche verwendet werden, um den Patientenarm mit dem Exoskelett zu unterstützen. Verschiedene Patienten-

kooperative Regelstrategien ermöglichen dem Arm gerade soviel zu assistieren wie nötig, erlauben aber auch eine freie Armbewegung und eine komplett geführte Bewegung des Armes. Der Regler wird aufgrund des gewünschten Spieles und der Fähigkeiten des Patienten ausgewählt. Ein Pfadregler, welcher nur so stark unterstützt wie nötig, wird verwendet um komplexe Mehrgelenksbewegungen auf Endeffektorbasis zu unterstützen. Für ein spezifischeres Training mit einzelnen Roboterachsen wird ein anpassbarer gelenkbasierter Regler eingesetzt. Alle Regler verwenden ein Modell um Trägheits-, Gravitations- und Reibungsaspekte des Roboters zu kompensieren sowie einen Dithering-Ansatz (von englisch 'to dither' - zittern) um die Haftreibung zu reduzieren. Die Regelgüte und das Kompensationsmodell wurden überprüft und die Stabilität der verschiedenen Ansätze analysiert.

Der dritte Teil befasst sich mit den implementierten robotergestützten Assessments, welche kinematische, kinetische und zeitliche Metriken erfassen, um die Armmotorfunktionen zu beschreiben. Noch vor dem Integrieren der Assessments im ChARMin Roboter wurden die Anwendbarkeit, Sicherheit, Reliabilität und Vergleichbarkeit zu klinischen Metriken bei Erwachsenen untersucht. Mit 24 gesunden Probanden und fünf Patienten nach einer Rückenmarkverletzung wurden die robotergestützten Assessments mit dem ARMin Arm-Exoskelett getestet. Fünf verschiedene Messungen wurden durchgeführt und visuell mit einem Bildschirm unterstützt. Zehn verschiedene kinematische, kinetische und zeitliche Assessmentparameter wurden auf Gelenk- und Endeffektorebene extrahiert. Die ersten Resultate mit erwachsenen Testpersonen weisen darauf hin, dass die Messungen größtenteils reliabel sind und sich mit klinischen Skalen für motorische Funktionen vergleichen lassen. Basierend auf diesen ersten Resultaten wurden die fünf Assessments angepasst und auf den ChARMin Roboter übertragen. Zudem wurde ein weiteres Assessment hinzugefügt in welchem der Patient mit der Hand einem Ziel folgen muss, welches sich in der Frontalebene auf einer Kreisbahn bewegt, um die Nachfolge-Fähigkeiten zu testen.

Im vierten Teil werden die Resultate der ersten Machbarkeitsversuche mit einzelnen Patienten präsentiert. Der ChARMin Roboter, die Regler und Assessments wurden mit fünf Patienten mit unterschiedlichen neurologischen Diagnosen (Schlaganfall, infantile Zerebralparese und Schädel-Hirn-Trauma) getestet. Während dieser Tests probierten die Patienten die Trainingsszenarien mit unterschiedlicher Roboterunterstützung und -einstellung, abhängig von den jeweiligen Therapiezielen, Fähigkeiten und Präferenzen. Die Patienteneigenschaften waren sehr verschieden hinsichtlich des Alters (6- bis 17-Jahren), der Armfunktionen, der trainierten Seite, des Geschlechts und der Beeinträchtigungen. Der ChARMin Roboter konnte an alle Patienten angepasst werden. Die fünf Patienten waren motiviert verschiedene Spiele zu testen. Dabei unterstützte sie der Roboter unterschiedlich stark, von freien Armbewegungen bis hin zu komplett geführten Bewegungen. Des Weiteren haben drei der Patienten zweimal erfolgreich die robotergestützten Assessments durchgeführt. Diese ersten Machbarkeitsversuche bestätigten eine sichere und gute Anwendbarkeit der unterschiedlichen Trainingsmodi bei der pädiatrischen Zielgruppe. Der Roboter fand guten Anklang bei den Therapeuten und Patienten. Die Versuche zeigten lediglich kleinere Mängel auf, welche vor der grösseren ChARMin Machbarkeitsstudie noch behoben werden müssen.

Zusammenfassend kann gesagt werden, dass die Resultate dieser Arbeit ein grosses

Potential für ChARMin aufzeigen, als fortgeschrittenes Übungsgerät für die Armneurorehabilitation, Kinder im Alter von 5- bis 18 Jahren zu unterstützen und optimal herauszufordern. Zudem können die vorgestellte Hardware, die Regler- und Assessmentmethoden sowie die Resultate mit den gesunden und betroffenen Erwachsenen und den jungen Patienten als Grundlage für zukünftige Entwicklungen von Endeffektor- und Exoskelett-Robotern dienen.



# Preface

This thesis was performed at the Sensory-Motor Systems Lab, Department of Health Sciences and Technology, ETH Zurich, Switzerland and the Rehabilitation Center for Children and Adolescents, University Children's Hospital Zurich, Affoltern a. A., Switzerland.

Chapter 2 is based on the following manuscripts:

- U. Keller, V. Klamroth, H. J. A. van Hedel, and R. Riener, “ChARMin: A robot for pediatric arm rehabilitation,” in *Robotics and Automation (ICRA), 2013 IEEE International Conference on*. IEEE, 2013, pp. 3908–3913; Reprinted with permission, from [1], ©2013 IEEE.
- U. Keller and R. Riener, “Design of the Pediatric Arm Rehabilitation Robot ChARMin,” in *Biomedical Robotics and Biomechanics (BioRob), 2014 IEEE International Conference on*. IEEE, 2014, pp. 530–535; Reprinted with permission, from [2], ©2014 IEEE.
- U. Keller, H. J. A. van Hedel, V. Klamroth-Marganska, and R. Riener, “ChARMin: The first actuated exoskeleton robot for pediatric arm rehabilitation,” *IEEE/ASME Transactions on Mechatronics (TMECH)*, 2016, *in press*.

Section 3.2.3 from Chapter 3 is based on the following manuscript:

- U. Keller, G. Rauter, and R. Riener, “Assist-as-needed path control for the PASCAL rehabilitation robot,” in *Rehabilitation Robotics (ICORR), 2013 IEEE International Conference on*. IEEE, 2013, pp. 1–7; Reprinted with permission, from [4], ©2013 IEEE.

Section 4.1 from Chapter 4 is based on the following manuscript:

- U. Keller, S. Schölch, U. Albisser, C. Rudhe, A. Curt, R. Riener, and V. Klamroth-Marganska, “Robot- assisted arm assessments in spinal cord injured patients: A consideration of concept study,” *PloS one*, vol. 10, no. 5, 2015; Reprinted with permission, from PLOS ONE<sup>1</sup>.

Appendix A.3.1 in Chap. A is based on the following manuscript:

- U. Keller, M. Guidali, L. Conditt, and R. Riener, “Novel recording and control strategies for robotic therapy,” in *Automed Conference*, vol. 286, 2012, pp. 55–56; Reprinted with permission, from VDI Verlag 2015.

Certain passages were taken directly from the publication or, where appropriate, with slight modifications from these references. Some paragraphs that appeared in the published or submitted manuscripts were removed to reduce redundancy in this thesis.

---

<sup>1</sup>PLOS applies the Creative Commons Attribution (CC BY) license to published work, it states free immediate access to, and unrestricted reuse of, original works of all types, when the source is properly cited.



# Notations

## Abbreviations

AAN	Assist-as-Needed
AFG	Advanced Force Gauge
AHA	Assisting Hand Assessment
ARW	Arm Reachable Workspace
BBT	Box and Block Test
ChARMin	Children ARMin
ChAxis	ChARMin Axis Current Control Boards
CIMT	Constraint-Induced Movement Therapy
COV	Coefficient of Variation
CP	Cerebral Palsy
DoF	Degree of Freedom
ElEx	Elbow Extension
ElFl	Elbow Flexion
ElPr	Elbow Pronation
ElSu	Elbow Supination
ETH	Eidgenössische Technische Hochschule (Swiss Federal Institute of Technology)
FS	Full Scale
GHJ	Glenohumeral Joint
GMFM	Gross Motor Function Measurement
GRASSP	Graded and Redefined Assessment of Strength, Sensibility and Pre- hension
HSAb	Horizontal Shoulder Abduction
HSAd	Horizontal Shoulder Adduction
ICC	Intraclass Correlation Coefficient
IK	Inverse Kinematics
MACS	Manual Abilities Classification System
MAS	Modified Ashworth Scale
MMT	Manual Muscle Test
MTS	Modified Tardieu Scale
NHPT	Nine-Hole-Peg Test
PASCAL	Pediatric Arm Support Robot for Combined Arm and Leg Training
QOM	Quality of Movement
RCoR	Remote Center of Rotation
ROM	Range of Motion

## Abbreviations (continued)

RPM	Resistance to Passive Movement
SCI	Spinal Cord Injury
SCIM	Spinal Cord Independence Measure
ShAb	Shoulder Abduction
ShAd	Shoulder Adduction
ShER	Shoulder External Rotation
ShEx	Shoulder Extension
ShFl	Shoulder Flexion
ShIR	Shoulder Internal Rotation
Std	Standard Deviation
TBI	Traumatic Brain Injury
VLT	Van Lieshout Test
VR	Virtual Reality
WrEx	Wrist Extension
WrFl	Wrist Flexion
3D	Three Dimensions <i>or</i> Three Dimensional

## Scalars, Vectors, and Matrices

Scalars are denoted by lower case italic letters. Vectors are written in bold and italic lower case letters. A vector is composed of the scalar elements  $x_i$ . Matrices are denoted by bold upper case letters and are composed of elements  $m_{ij}$  ( $i$ -th row,  $j$ -th column).

$x$	scalar
$\mathbf{x}$	vector
$\mathbf{X}$	matrix
$\mathbf{X}^T$	transposed of matrix $\mathbf{X}$
$\dot{\mathbf{x}}, \ddot{\mathbf{x}}$	equivalent to $\frac{d}{dt}\mathbf{x}$ and $\frac{d^2}{dt^2}\mathbf{x}$



## Variables

The most frequently used variables are subsequently listed.

$\mathbf{p}$	Cartesian coordinates, $\mathbf{p} = (p_x, p_y, p_z)^T$
$\mathbf{p}_{ee}$	Robot end-effector position
$\mathbf{p}_{NN}$	Nearest neighbor position
$\mathbf{v}_{ee}$	End-effector speed
$\mathbf{q}$	Joint angles, ChARMin: $\mathbf{q} = (q_1, q_2, q_3, q_4, q_5, q_6)^T$ , PASCAL: $\mathbf{q} = (q_1, q_2, q_3)^T$
$\dot{\mathbf{q}}$	Joint speed
$\ddot{\mathbf{q}}$	Joint acceleration
$\mathbf{M}(\mathbf{q})\ddot{\mathbf{q}}$	Inertial terms of the equations of motion
$\mathbf{C}(\dot{\mathbf{q}}, \mathbf{q})\dot{\mathbf{q}}$	Coriolis terms of the equations of motion
$\mathbf{G}(\mathbf{q})$	Gravitational terms of the equations of motion
$\mathbf{J}$	Jacobian
$\mathbf{f}$	Forces applied at the end effector, $\mathbf{f} = (f_x, f_y, f_z)^T$
$\boldsymbol{\tau}$	Robot joint torques
$\tau_{spring}$	Spring torque applied to ChARMin joint axis 2
$\tau_f$	Coulomb and viscous friction torque of the ChARMin joints
$\tau_{comp}$	Torques computed by the compensation model of the robot
$\tau_{int}$	Interaction torques between the human and the robot



# 1 Introduction

## 1.1 Background

### 1.1.1 Relevance of Arm Motor Function

The arms and hands are essential tools to reach, grasp, gesture, feel, touch, feed, discover, play and have many other important functions. The success story of this tool started with the bipedal upright walking about 3.6 million years ago [7], which freed the arms and hands to develop the highly functional, precise, sensitive and fine-motor tools we use to interact with our environment.

An important phase in humans to develop these motor functions is typically an age between 4 and 10 years where fundamental movement patterns are refined [8]. These functions are learned during childhood in close connection with our cognitive skills [9, 10] which highlights the crucial relation between physical grasping and the intellectual grasping of the world. These versatile arm functions and their acquisition can be impaired in children with a congenital or acquired brain injury, hampering a normal development, the participation and independence in daily life, and the experience of the world. This includes children suffering from a neurological disorder such as cerebral palsy (CP), spinal cord injury (SCI), multiple sclerosis or another traumatic or non-traumatic brain injury.

### 1.1.2 Children with Cerebral Palsy

CP is one of the most prevalent neurological disorders in children affecting up to 2.5 per 1'000 children born in Northwestern Europe [11] and with an overall prevalence worldwide of 2.1 per 1'000 live births [12]. This is also represented by the impairment group of the patients in Switzerland, e.g., in the Rehabilitation Center for Children and Adolescents in Affoltern am Albis (Fig. 1.1). CP describes a group of permanent disorders of the development of movement and posture, causing activity limitations that are attributed to non-progressive disturbances that occurred in the developing fetal or infant brain [13]. These activity limitations in CP (and other congenital or acquired brain injuries) often hamper the child's independence and participation in daily life [14].

The motor functions in patients suffering from CP usually increase in early life and depend on the level of impairment. There are indications that the functional improvements are less in children with congenital brain lesions as in children with acquired lesions that show more spontaneous recovery [15]. Children with inborn brain lesions might have developed compensatory strategies over many years while children with acquired brain lesions often show more potential for restoring physiological selective voluntary movements [15].

Various assessment tools were used to measure the motor function and capabilities in children with CP and with different levels of impairment. Holmefur et al. [16] analyzed the development of motor function in children with unilateral CP in the early

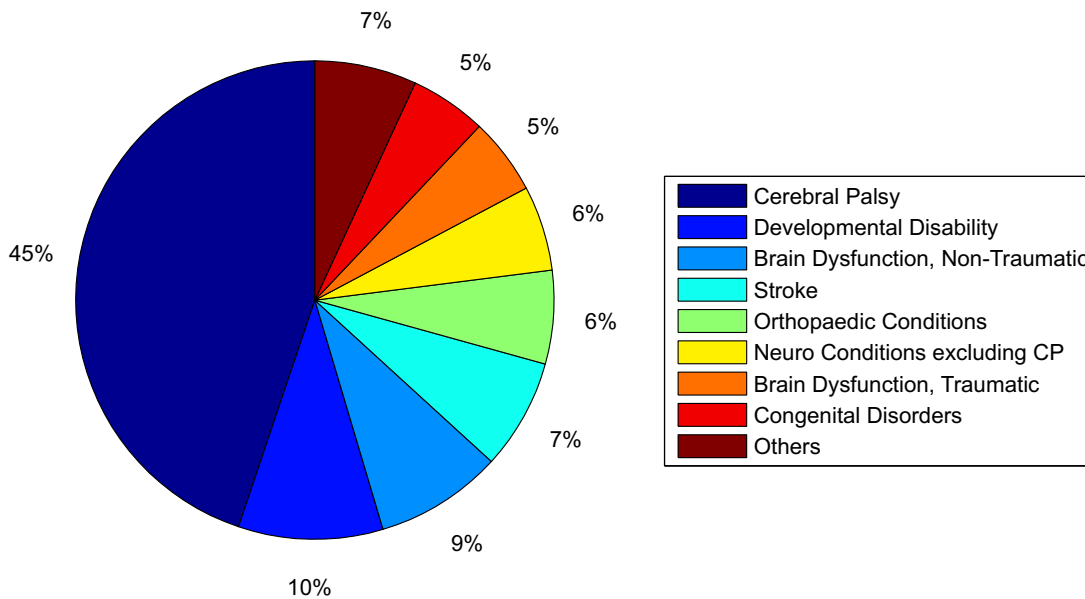


Figure 1.1: Children impairment group of the patients at the Rehabilitation Center for Children and Adolescents in Affoltern am Albis, Switzerland (2012, n=174).

years using the Assisting Hand Assessment (AHA; measures the use of the affected hand in bimanual performance; score ranges from 22 to 88) and the Manual Abilities Classification System (MACS; describes how children with CP use their hands to handle objects; score ranges from I to V). Children with a higher 18-month AHA score reached higher ability levels with a higher progression rate than children with a low 18-month AHA score (Fig. 1.2 a). The AHA limit reached was higher for children with lower MACS levels (low MACS scores correspond to better handling).

Hanna et al. [17] showed that the hand and arm motor functions can be further improved, stagnate or even deteriorate dependent on the severity of the impairment. In their study, the hand function was assessed in children with CP and upper extremity involvement (n=51) using hand and upper extremity skill assessments. Hand function was measured with the Peabody Developmental Motor Scales. This standardized measure evaluates fine motor function in the domains of grasping, hand use, eyehand coordination and manual dexterity. Possible raw scores range from 0 to 224 (Fig. 1.3 a). Furthermore, the general arm function was measured with the Quality of Upper Extremity Skill Test (QUEST). QUEST scores range from below 0 to 100 (Fig. 1.3 b). Both assessments showed a tendency for the scores to peak and decline. In a later publication Hanna et al. [18] showed similar results using the 66-item Gross Motor Function Measurement (GMFM-66)<sup>1</sup>. They found that children and youth with levels III, IV, and V are at risk of losing motor function, with the greatest declines apparent in level IV. The motor functions seem to peak at an age of about six to seven years (Fig. 1.2 b). The GMFM assessment focuses on mobility. However, the Gross Motor Function Classification System (GMFCS), which is based on the GMFM, highly correlates with assessments for upper extremity motor function, like the MACS [19].

<sup>1</sup>The GMFM-66 measures capability or what a child can do in a standardized environment. Items include tasks related to lying and rolling, sitting, crawling and kneeling, standing, walking, running and jumping [18].

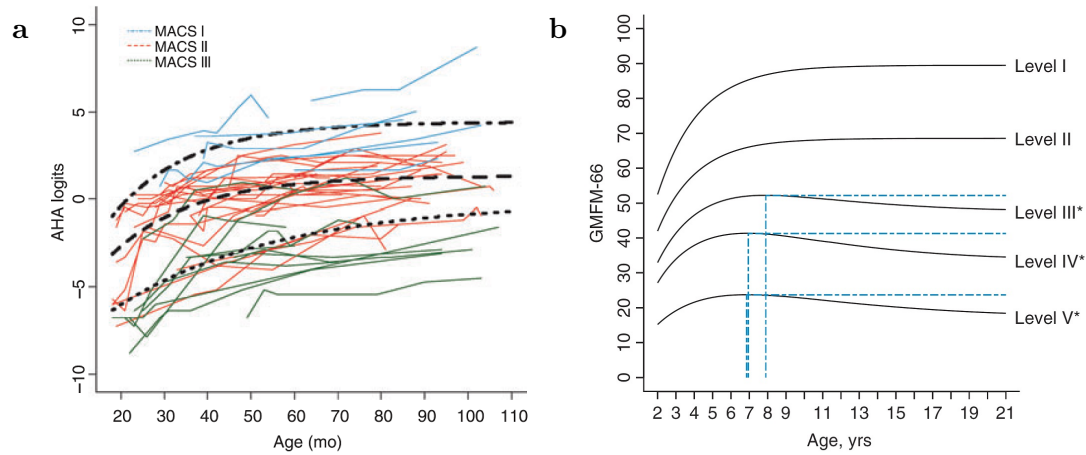


Figure 1.2: Development of motor function in children with CP. **(a)** Improvement of arm function (AHA) dependent on the MACS level (source: [16]). **(b)** Improvement of mobility (GMFM-66) dependent on the GMFCS level (source: [18]).

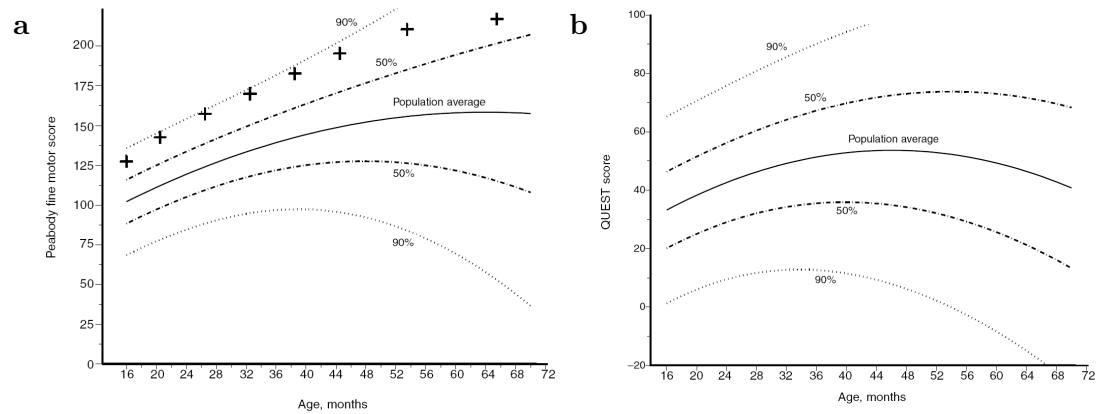


Figure 1.3: Development of arm and hand motor function in children with CP indicated by **(a)** the Peabody Developmental Motor Scales for hand function (source: [17]) and **(b)** the QUEST assessment for upper extremity motor skills (source: [17]).

In summary, children suffering from CP often have functional disorders depending on the severity of the impairment. These disorders are permanent and might get worse during the development of the child. Here, a therapeutic intervention is critical with the goal to not only improve and recover motor function but also to prevent its deterioration in children with moderate to severe CP. This intervention has to be based on clinical evidence and on the knowledge of the underlying neurological principles in order to provide an optimal patient-tailored rehabilitative training. Therefore, a short insight is given into brain plasticity after a neurological impairment (Sec. 1.1.3) and further important key aspects of an effective rehabilitation training are discussed (Sec. 1.2).

### 1.1.3 Triggering Neuroplasticity in Children

To learn a new task or to recover after a neurological impairment (such as CP, stroke, or SCI), the brain capitalizes on the ability to reorganize neural networks [20,21]. This neural reorganization can be within the function network or even include structures which were previously responsible for other functions [22]. This mechanism is usually referred to as brain plasticity. For rehabilitation purposes it is crucial to know how neuroplasticity can be triggered or enhanced after a neurological damage to learn or relearn motor functions (Fig. 1.4). Reactivation of brain structures may be induced by motor imagery, observations of movements, passive training or constraint-induced movement training (CIMT) [20]. CIMT therapy forces the patient to intensively use the affected arm or hand while the unaffected or less affected arm or hand is constrained. In adult stroke patients, CIMT was shown to re-expand cortical motor areas [23]. Nonuse of the affected extremity, however, can lead to decrease of the brain motor area size [24].

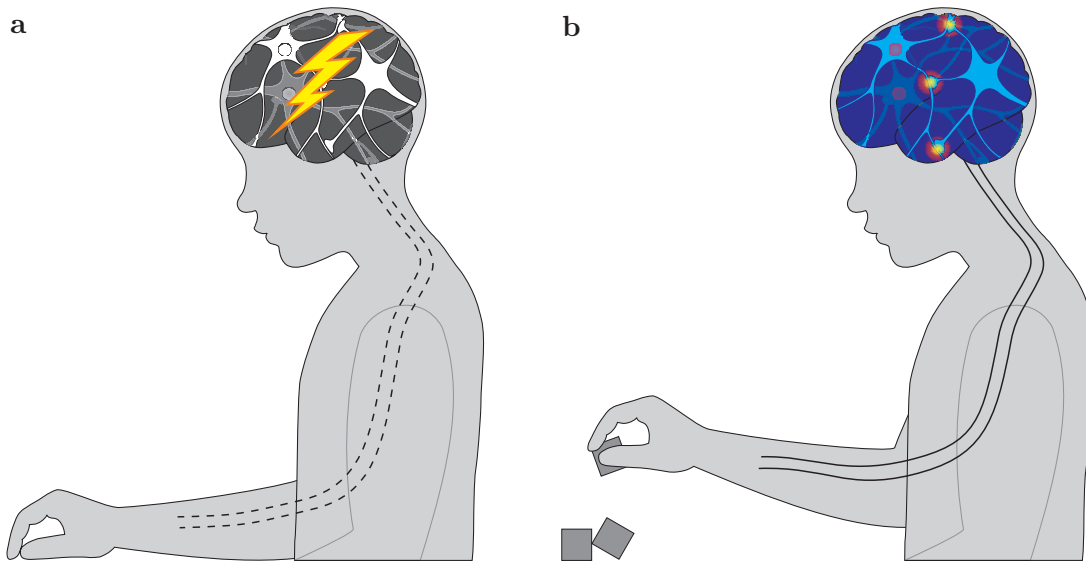


Figure 1.4: **(a)** A neurological impairment, such as CP, can hamper the motor commands to control the arm as well as the sensory signals, leading to movement disorders. **(b)** The neuroplasticity of the brain enables the reorganization of neural networks and pathways to learn or relearn motor functions during an intensive, activity-based and task-specific arm motor function training.

As in adults, an intensive rehabilitation training (e.g., with CIMT) with active participation was shown to be essential for cortical reorganization in children [25–27]. Compared to adults, children can recover more fully from brain injuries [25] and plasticity mechanisms are enhanced in the developing brain. Moreover, children with CP have a remarkable ability to recover from early brain injuries [28] which does not seem to be age-dependent among children [29].

These findings highlight that an intensive rehabilitative intervention of the affected limb is critical to trigger brain plasticity in children.

## 1.2 Pediatric Rehabilitation

As described in the previous section, brain plasticity is an important aspect of habilitation and rehabilitation of motor function in children with neurological disorders<sup>2</sup>. An intensive, activity-based, and task-specific upper limb (re)habilitation training seems to exploit the concept of plasticity of the central nervous system and thus to improve motor recovery [27]. A comprehensive rehabilitative intervention should, therefore, try to cover these aspects. Additionally, there is clinical evidence for other key attributes of neurorehabilitation therapy. The following subsections discuss these key aspects which are important and beneficial for improvement of motor function in children with congenital or acquired neurological disorders.

### Intensity

In this thesis, the term 'intensity' of a training refers to the number of movement repetitions, training sessions and use of the affected arm in a given time period. Different studies already highlighted the benefit of training intensity on motor recovery in children [27, 31] and pointed out that the intensity should be more than what is applied during standard care [32]. As mentioned above, this intensity can be achieved with CIMT and a forced use of the affected arm. This therapy was shown to be effective for upper-extremity function in children with CP [33].

Children with CP have an initial slower learning rate compared to typically developed children and a delayed improvement is expected [34]. Therefore, when working with children with unilateral CP, sufficient practice (two to three times more than for typically developed children) is important.

In adult rehabilitation an intensive training has a favorable effect on motor recovery [35, 36] and motor learning. According to the power law of practice, acquisition of skilled performance is determined solely by the number of times a task is practiced [37]. This aspect is also important for pediatric rehabilitation as first results suggest that motor rehabilitation in children has traits of motor learning in healthy subjects [38]. The number of time practiced in this context does not mean a repetition of the same identical movement, however, the movement has to be varied to achieve a 'repetition without repetition' (Bernstein principle [39]).

### Goal-Directed Therapy

Therapy should be goal-directed, working on the goals identified by children and their caregivers [32]. In a study of 44 children with CP a goal-directed functional therapy was compared with an activity focused therapy [40] using the Pediatric Evaluation of Disability Inventory (PEDI) with the result that the goal-directed training demonstrated clear gains for children with CP in everyday activities and gross motor function.

---

<sup>2</sup>The term habilitation was introduced as rehabilitation refers to the true recovery where undamaged brain and/or spinal regions are recruited, which generate commands to the same muscles as were used before the injury [30]. However, in children with congenital brain damage new function are learned (habilitation) rather than previously existing circuits are recovered (rehabilitation).

### **Activity-Based Training**

Motor activity is important to establish and reinforce the neuromuscular pathways in children [41]. Contrary the lack of activity can lead to an elimination of unused or less-used pathways [42], following the 'use it or lose it' principle. Studies have shown that active involvement in the motor pattern generation resulted in greater motor learning than passive movement [43]. During rehabilitation training, active participation is highly relevant to trigger neuroplasticity and to significantly improve the therapy outcome in adults [44] as well as in children [42]. Therefore, contemporary motor learning approaches use activity-based training approaches for children [32] and adults [45].

### **Task-Specific Movements**

Activity-based training is important but also has to be meaningful for cortical reorganization and functional recovery to occur [46]. Task-specific training, therefore, plays a major role in motor learning in young and adult patients with neurological impairment [27, 46, 47].

### **Early Onset**

The first years of a child's life are characterized by fast neural development. During this time, the child adapts its sensory-motor patterns to more and more complex functions [48]. Children with CP have abnormal sensory-motor patterns from the beginning and they will develop abnormal functional patterns which leads to contractures and structural deformities [48]. Therefore, very early treatment in most cases will give quicker and better results and is a critical factor for the treatment [48]. This potential for a more complete recovery may diminish throughout the course of early development [41]. Similar findings pointing towards an early onset can also be found for stroke and other neurological disorders [46].

However, rehabilitation before the age of 4 years is controversially discussed. While Law et al. (1997) [49] see no direct benefit of intensive therapy for children below 4 years, Eliasson et al. (2015) [50] indicated a mCIMT training (a modified and less intensive version of CIMT) at the age of 2 to 3 years may have a positive impact on long-term development.

### **Strength Training**

For children and young adults with CP literature provides evidence, although it is limited, that strength training programs may provide positive strength benefits [51]. The general consensus across studies is that strength can be predictably increased through a properly designed short-term program but very likely needs to be continued regularly to retain benefits [41].

### **Motivation**

According to the International Classification of Functioning, Disability and Health (ICF) [52], motivation is defined as a mental function that produces the incentive to act.



In adult stroke patients, exposure to stimulating and complex environments and involvement in tasks or activities that are meaningful to the adult individual serves to increase cortical reorganization and enhance functional recovery [46].

In pediatric rehabilitation motivation is a critical determinant of functioning and achievement and essential for learning new skills [53] and to provoke an active participation [44]. Motivation in children with CP can be related to greater persistence in performing tasks and a better physical functioning and psychosocial well-being [54]. The motivation of the child depends on a lot of aspects. Fewer limitations in self-care, communication and social skills, a higher IQ and better motor ability are associated with higher motivation [55]. Furthermore, a negative impact of the child's disability on the family, hyperactivity and peer problems were associated with lower motivation [55]. Positive social behaviors were positively correlated with motivation. In addition, children with acquired lesions appear sometimes more motivated compared to those with congenital lesions [15].

### **Therapy Session Structure**

Different therapy structures and strategies are still discussed. There are indications that for children with CP a therapy may be more effective when provided regularly (once or twice a week) rather than in blocks of treatment [56]. However, there is no consent on the effect of the two strategies.

Another aspect of the training structure is the decomposition of complex movements. Recent studies indicate that multi-joint movements are not superior to single joint movements in stroke patients [57] and that motor learning can be improved when decomposed in anatomical complements [58]. However, comparable investigations with young patients have not yet been performed.

### **Assessment**

To provide a patient-tailored rehabilitation therapy for the child, which addresses the individual needs of the young patient, it is important to know the status and the skills of the patient. When the motor function of the patient is known, the therapy can be modulated according to the capabilities of the patient. Therefore, the arm motor function has to be measured objectively by using reliable, valid and responsive assessment tools [32].

### **Assistance**

Often, an intensive training as mentioned above can only be achieved when the patient is assisted and supported to actively perform the movements on his own. A possibility is to increase the weight support against gravity. Gravity compensation facilitates active arm movement excursions without impairing motor control and is a valuable modality in conventional or robot-aided therapy to increase the intensity of training for mildly impaired adult patients [59]. Results with a passive gravity support system for children with arthrogryposis indicated the benefits of assisting the arm [60]. This assistance can be provided by the therapist or by an active or passive robotic system supporting the arm during the therapy. The latter is discussed later (Sec. 1.4).

Conventional therapy usually tries to address these different aspects to achieve an effective rehabilitation training. The requirements to provide a repetitive high-intensity rehabilitation training while assisting and motivating the patient makes the manually-assisted training very labor-intensive. Moreover, the conventional clinical assessments often show deficits in terms of reliability, validity and sensitivity [61]. Here, rehabilitation interventions can capitalize on new tools and devices which complement and support the conventional manually-assisted therapy. For adult patients, robots are more and more used as a promising tool to assist and assess arm rehabilitation and to cover various of these important key aspects.

## 1.3 Robot-Assisted Rehabilitation in Adults

### 1.3.1 State of the Art

Children [14] as well as adults [62] who suffer from lesions of the central nervous system, e.g., spinal cord injury or stroke often have problems to use their affected arm during daily life, which can affect their independence negatively. These patients profit from rehabilitative interventions that aim to regain certain functionalities. As shown above, an intensive training triggers neuroplasticity and is essential for the recovery of motor functions in children but equally in adults [36].

In adult human stroke subjects, actuated robotic technologies are more and more used to complement conventional rehabilitation interventions, as they can provide a task-specific [63], activity-based [45], intensive [35] training while assisting and assessing the patient. Furthermore, virtual reality (VR) scenarios are used together with the robots to motivate the patient to actively participate and provide online augmented feedback about the patient's performance [64,65]. Moreover, robots have been shown to have a positive effect on the rehabilitation process in adult patients with neurological disorders [66–70].

The acceptance and the number of robots for clinical care are continuously increasing. Predictions for the rehabilitation robot market size expect a growth from \$43.3 million in 2014 to reach \$1.8 billion by 2020 (published in a study by WinterGreen Research, 2014, MarketPublishers.com). It is often assumed that the robotic therapy costs more than conventional therapy. However, robot-assisted therapy has similar total health cost as usual care or intensity matched physical therapy [71] and can be a valuable and economically sustainable aid for rehabilitation [72].

The American heart association integrated robot-assisted therapy in its guidelines and states for stroke care: 'Robot-assisted therapy offers the amount of motor practice needed to relearn motor skills with less therapist assistance. Most robots for motor rehabilitation not only allow for robot assistance in movement initiation and guidance but also provide accurate feedback' [73]. Furthermore, the guidelines state that robot-assisted upper extremity therapy can improve motor function during the inpatient period after stroke.

Different robotic platforms for adult arm rehabilitation and arm assistance were built in the last two decades, including active and passive robots with end-effector or exoskeleton kinematics for the arm, single joints, or the hand. Tab. 1.1 gives a non-exhaustive overview of different existing robot platforms. Not all the robots in Tab. 1.1 have been used for clinical studies. A list of the robots used for clinical studies can be found in Lo et al. 2012 [74].

		Active	Passive
End-effector based	planar	1992 InMotion ARM (MIT Manus) [75], 2012 ReaPLAN [76], 2005 Ju robot [77]	2006 ARMON [78], 2009 ARMassist [79]
	3D	1998 Nagai-8DOF [80], 2001 ARM Guide [81], 2002 <i>MIME system</i> [82], 2005 MACARM [83], 2005 REHAROB [84] <sup>c</sup> , 2005 NeReBot [85], 2007 iPAM [86] <sup>c</sup> , 2011 arm skate [87], 2011 ReoGo [88], 2011 ROBIN System [89], 2013 BioMotionBot [90], 2014 Armotion [91]; HapticMaster-based: 2006 ADLER [92], 2003 Act <sup>3D</sup> [93] 2007 Gentle/G (GENTLE/s) [94]	<i>Swedish Helparm (Swedish Slings)</i> <sup>a</sup> , 2006 TheraJoy [95], 2007 Freebal (ArneoBoom <sup>b</sup> ) [96]
Exoskeleton based	planar	2007 MEDARM [97]	
	3D	1999 pMA powered exoskeleton [98], 2005 MGA Exoskeleton [99], 2006 UL-EXO7 [100], 2007 ARMin [101], 2007 L-EXOS [102], 2007 REHAROB [103], 2007 RUPERT [104], 2008 ABLE [105], 2009 Limpact [106], 2009 NEUROExos [107], 2010 BONES [108], 2011 MAHI Exo-II [109], 2012 CAREX [110], 2012 ArneoPower <sup>b</sup> [111]	2007 Dampace [112], 2010 ArneoSpring <sup>b</sup> [113], 2014 MUNDUS exoskeleton robot [114]
Single joint robots <sup>d</sup>		1995 <i>Bimanual Lifting Rehabilitator</i> [115], 1999 Cozens robot [116], 2003 <i>Bi-Manu-Track (Arm Trainer)</i> [117]	
Hand/Wrist systems		2005 HWARD [118], 2006 HIFE [119], 2007 Haptic Knob [120], 2007 Gentle/G end effector [121], 2007 Alpha-Prototype II [122], 2008 Reha-Digit [123], 2008 HandCARE [124], 2009 Kinetic Maestra Portable Hand CPM [125], 2009 HenRiE [126], 2010 HEXORR [127], 2011 ReHaptic Knob [128], 2013 AMADEO [129], Vector 1 <sup>e</sup> , DigiGlide XT Portable Hand <sup>f</sup>	2007 SaeboFlex [130], 2014 SCRIPT prototype (SP1) [131], ManovoSpring <sup>b</sup> [132]

Table 1.1: Overview of available active and passive robotic systems for adult arm rehabilitation. For commercial products without a preceding research prototype, the date of the first appearance in publications is stated. *Italic* font is used for bimanual setups. In brackets are earlier names or different names for the platform. <sup>a</sup>Kinsman Enterprises INC. <sup>b</sup>Hocoma AG, Switzerland. <sup>c</sup>Robot consisting of two end-effector robots attached to the upper and forearm. <sup>d</sup>Training single joint at once, but may be reconfigured for other joints. <sup>e</sup>Lantz Medical, Indianapolis, US. <sup>f</sup>Kaiser Medical, US.

Robotic technology is not only applied to stroke but also SCI patients [5,133–135] and multiple sclerosis patients [136,137]. Moreover, rehabilitation robots have the potential to provide objective, sensitive, and reliable measurements of kinematic, kinetic, and timing parameters of the patient’s arm (details in Sec. 4.1.1).

There are critical comments to rehabilitation robotics saying that robot-assisted arm training is questionable because the equipment is expensive and often there are alternative ‘strong evidence’ interventions [138]. However, a recently published paper indicates that robotic arm therapy using the ARMin robot is superior to other interventions regarding activities of daily living and arm function [69].

### 1.3.2 ARMin Arm Rehabilitation Robot

The ARMin arm rehabilitation robot for adults is referenced in several sections of this thesis (e.g., in Sec. 2.2.1 or Sec. 4.1) and is, therefore, presented here in more detail. Four versions of the arm therapy robot ARMin have been designed and evaluated by the groups of Riener and Dietz/Curt of ETH Zurich and University of Zurich [5,64,101] (Fig. 1.5). ARMin is used for arm neurorehabilitation of adult patients suffering from stroke or SCI. The robot is characterized by an exoskeleton structure. The latest prototype has seven degrees of freedom allowing 3D shoulder rotation, elbow flexion/extension, elbow pro-/supination and wrist flexion/extension. A hand actuation module supports opening and closing of the hand. The patient is sitting on a chair and is fixed in the ARMin robot by the use of cuffs around the upper arm, forearm, and the fingers. The robot can be adjusted to the patient by changing the exoskeleton length settings for the upper arm, forearm and hand as well as the shoulder height. The same robot can be used for the training of the left and right arm by changing the hardware configuration. Mechanical end limits are provided for safety reasons to not overstretch joints or collide with the patient.

ARMin is the research version of the ArmeoPower (Hocoma AG, Switzerland). The kinematics, joint ranges and actuation are comparable. The ARMin robot features different control modes covering the range from a tracking only setting, where the robot’s weight and friction are compensated, to complete guidance of the arm. In between, a path control approach can be used to assist the patient as needed, e.g., for the training of activities of daily living.

ARMin IV is the latest version of the robot and was realized by the author of this thesis (ARMin IV, Fig. 1.5). ARMin IV is equipped with 6 degrees of freedom (DoF) force/torque sensors to measure small interaction torques between the patient and the robot. The sensors were mounted to better account for the reduced arm strength in SCI patients. Furthermore, the sensors allow for better transparency of the robot. Moreover, different assessments were implemented to test arm motor function in SCI patients (details in Sec. 4.1).

The ARMin robot was shown to be an effective tool for arm rehabilitation [69] but it can not be used for pediatric rehabilitation. With a minimum forearm length of 0.24 m, ARMin is adjustable to male adolescents aged 14 years and older and to female adults. However, there are other robotic platforms which have already been tested with children, or were specifically developed for children. An overview is given in the next section (Sec. 1.4).



Figure 1.5: ARMin IV shown with a subject performing an activity of daily living training scenario.

## 1.4 Robot-Assisted Rehabilitation in Children

### 1.4.1 State of the Art

In contrast to robot-assisted rehabilitation in adults, only a few studies that have been performed with rehabilitation devices for children and there are only a few commercial therapy devices available (Tab. 1.2). Preliminary results suggest that robot-assisted therapy might increase functional strength and improve isolated movements of the upper extremities in patients with CP [27] or improve motor function following childhood stroke [139].

For children with mildly affected arm function the YouGrabber system (YouRehab AG, Switzerland) can be used for rehabilitation therapy [140] (Fig. 1.6 a). The YouGrabber consists of two gloves which are visually tracked and detect grasping of the patient. Furthermore, it is interfaced with a display that allows for a game-based training. The system can be used bilaterally and trains spatial multi-joint movements including the shoulder, elbow, and wrist. For mildly to moderately affected children aged 5 years and older the ArmeoSpring Pediatric (Hocoma AG, Switzerland) can be used for arm training (Fig. 1.6 b). This robot features a passive spring mechanism to support the arm of the children against gravity. Various game scenarios can be played by performing multi-joint or single-joint movements including shoulder, elbow, and wrist. A pressure-sensitive hand module allows to trigger events in the gaming software. Another arm rehabilitation device which can be applied for children is the PABLO System (Tyromotion, Austria) [145] (Fig. 1.6 c). The system consists of different devices (PABLO Sensorgriff, PABLO Multiball, and PABLO Multiboard). Position and force sensors allow to assess hand strength and range of motion as well

		Active	Passive
End-effector based	planar	1992 InMotion ARM (MIT Manus) [75], 2012 ReaPLAN [76]	2006 ARMON [78], 2009 YouGrabber <sup>b</sup> [140]
	3D	2010 NJIT-RAVR system [141], <i>DIEGO</i> <sup>a</sup> [142]	2011 PABLO <sup>a</sup> system [143]
Exoskeleton based	planar		
	3D		2010 ArmeoSpring Pediatric <sup>c</sup> [144]
Single joint robots <sup>d</sup>			
Hand systems		2013 AMADEO <sup>a</sup> [129]	

Table 1.2: Overview of available robotic systems for pediatric arm rehabilitation. For commercial products without a preceding research prototype, the date of the first appearance in publications is stated (when possible a publication with pediatric application). *Italic* font is used for bimanual setups. In brackets are earlier names or different names for the platform. <sup>a</sup>Tyromotion GmbH, Austria. <sup>b</sup>YouRehab AG, Switzerland. <sup>c</sup>Hocoma AG, Switzerland. <sup>d</sup>Training single joint at once, but may be reconfigured for other joints.

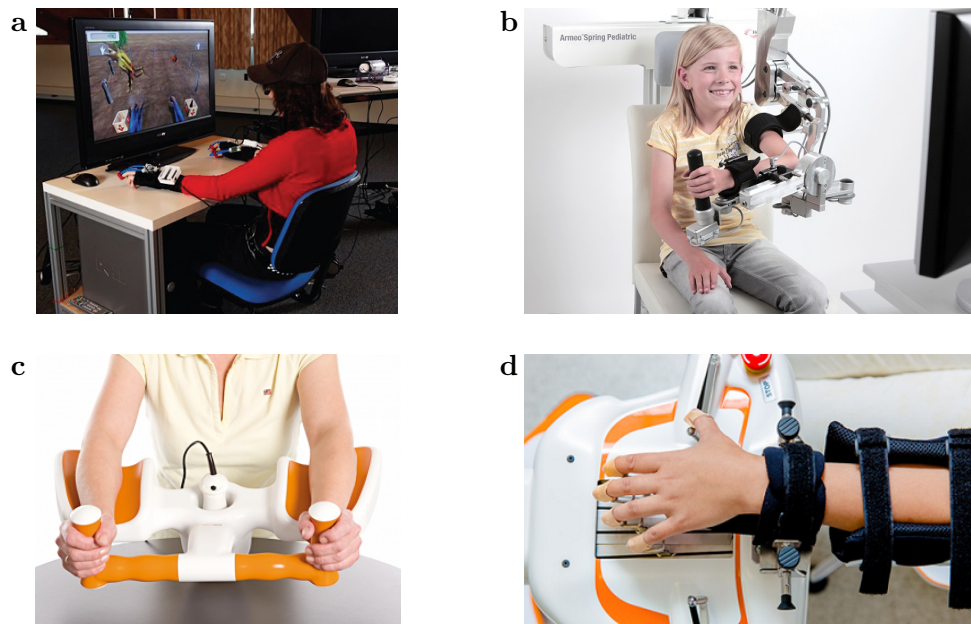


Figure 1.6: Robotic systems that have been tested with children; (a) YouGrabber (YouRehab, Switzerland) [140], (b) ArmeoSpring Pediatric (copyright Hocoma AG, Switzerland), (c) PABLO system (copyright Tyromotion, Austria), (d) AMADEO (copyright Tyromotion, Austria).

as to train movements that involve shoulder, elbow, and wrist. Two other Tyromotion products which can be applied for rehabilitation in children are the AMADEO [145] (Fig. 1.6 d) for hand and finger rehabilitation as well as the DIEGO robot which is an active rope robot to support bimanual arm training against gravity [142]. Furthermore, the PASCAL robot (described in Sec. 1.4.2) can be used for children with mild to moderate CP to support the arm weight during grasping movements in space.

For moderately to severely affected children active robot assistance of the arm might be necessary. Not only to compensate for gravity but to provide directional support towards a desired position in space. First results have been reported with different actuated end-effector platforms originally designed for adults. The InMotion2 [139,146] is an actuated planar end-effector robot and was used in several studies with children suffering from hemiplegic CP or childhood stroke (Fig. 1.7 a). The NJIT-RAVR system can be utilized for training of spatial movements and was tested with children with hemiplegic CP [141] (Fig. 1.7 b). The REAPlan [147] end-effector robot is for planar movements in the transversal plane (Fig. 1.7 c). Recently the REAPlan robot was used for the first single-blinded randomized control trial applying the robot for pediatric arm therapy [147]. Sixteen children with CP participated in the study, split in two groups receiving either robot-assisted therapy or conventional therapy. The study concludes that robot-assisted therapy is effective in children with CP. The results of all these preliminary studies indicate that children may benefit from robots used during arm therapy, which was also suggested in the review of Aisen et al. [27].

Virtual reality (VR) treatment appears to be an effective rehabilitation tool for use with adult patients [148] and children with CP [149]. It has the capacity for making otherwise impossible or uninteresting activities to be accomplished in an engaging, challenging environment and lets the child forget about the repetitive and frequent



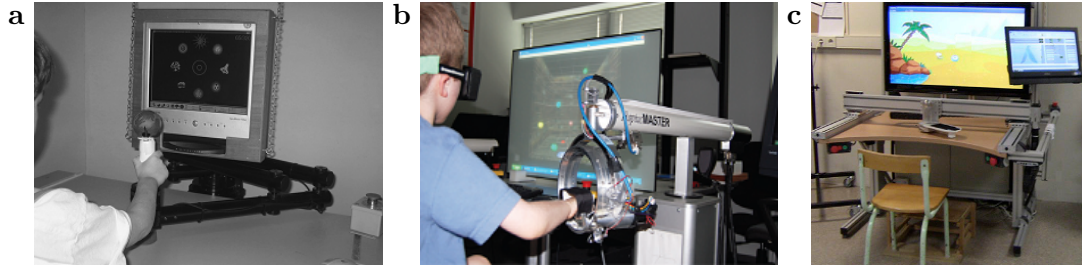


Figure 1.7: Robotic systems that have been tested with children suffering from CP or childhood stroke; (a) InMotion2 [146], (b) NJIT-RAVR system [141], (c) REAPlan [147] (adapted from original publication).

arm movements that it is performing [15, 149, 150]. Therefore, along with the robot, immersive VR scenarios are often used in pediatric rehabilitation (e.g., Fig. 1.7) to distract children from monotonous and repetitive exercises, to motivate the patient’s active participation [65], and to provide feedback about the patient’s performance [151].

#### 1.4.2 PASCAL Robot

The PASCAL robot is referenced in other sections of this thesis (e.g. Sec. 3.2.3) and is, therefore, introduced here as an example of a pediatric arm rehabilitation robot. PASCAL (Pediatric Arm Support robot for Combined Arm and Leg training, [152]) is an end-effector-based robot to support arm movements in space (Fig. 1.8). This robot can be combined with the commercial gait orthosis Lokomat<sup>®</sup> (Hocoma, Switzerland, [153]) to train combined movements of arm and legs. The target group is children and adolescents with CP or other neurological lesions and with mild spasticity aged 6 years and older. The robot can apply arm gravity support or directional support for grasping movements in space.

PASCAL was developed in the framework of the iMiC (Innovative Movement-Therapies in Childhood) project in collaboration between the Sensory-Motor Systems Lab, ETH Zurich, Switzerland and the Rehabilitation Center for Children and Adolescents in Affoltern a. A., Switzerland. The robot was realized by Kim Pfluger, supervised by Alexander König and the author of this thesis.

PASCAL is an end-effector-based robot with three active degrees of freedom (DoF) (Fig. 1.9) [152]. The robot is fixed to the combined center of mass of the human arm (as suggested by Herder et al. [78]) by means of a cuff (Fig. 1.8).

A parallel kinematic structure and a motor rotating it around the vertical axis allow for movements of the end effector in three translational degrees of freedom. The cuff itself contains two more passive DoF (Fig. 1.9) to ensure that only interaction forces are present and no torques are applied to the human arm. In other words, there is no control over the direction that the forearm is pointing. A more detailed analysis of the kinematics is given in Appendix A.1.1.

The robot is completely backdrivable<sup>3</sup> and a force sensor (JR3, USA) is mounted close to the end effector (Fig. 1.8, blue cylinder close to the elbow) to measure interaction forces and torques for assessments and control purposes.

<sup>3</sup>The term backdrivable is used to characterize an actuated axis which can be moved by the user when the robot is not powered.



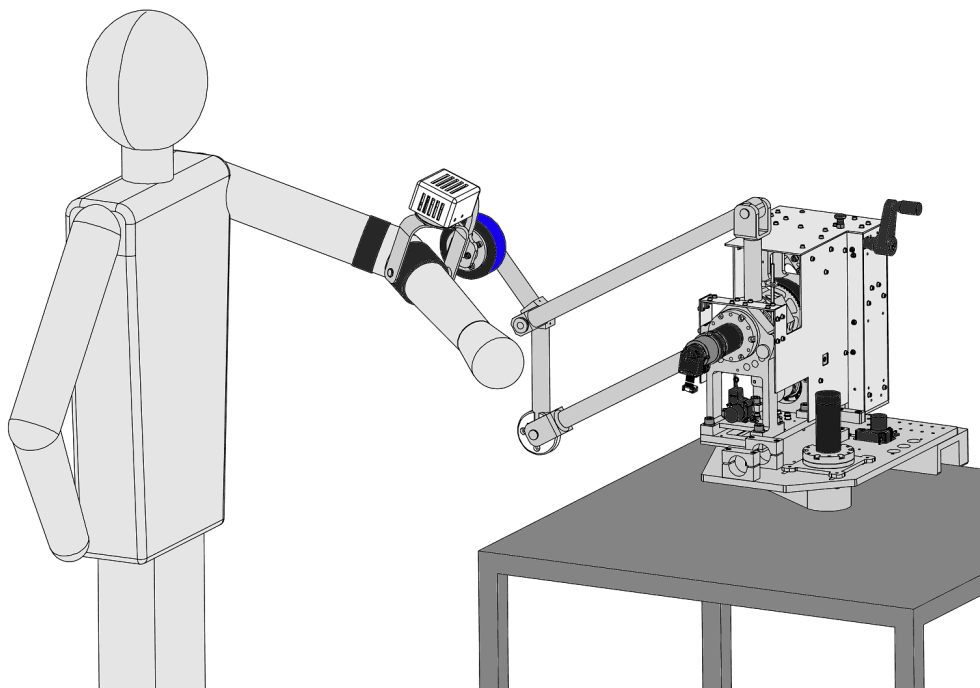


Figure 1.8: Visualization of the PASCAL robot attached to the combined center of mass of the arm. The avatar is a simplified body model of a 13-year-old child. A picture of the real PASCAL system can be found in Appendix A.1.

As the robot is used in close interaction with humans, different mechanical, software, and electrical safety measures guarantee the overall safety of the patient: Mechanical and software limits are provided on axis level. Brakes are provided for the two horizontal motors to block the according axes if necessary (e.g., when the therapist releases the handheld safety switch or there is a power loss) and an electro-magnet is used to connect the cuff to the robot which can release the patient in case of emergency. Moreover, it is a benefit in handling, as the cuff can be attached before the patient is connected with the robot. In addition, there are redundant sensors for each axis, a watchdog for software supervision, plausibility checks in the software and saturation limits for controller values as well as a restricted end effector speed to 1 m/s. PASCAL also features an adaptable passive gravity compensation for the two parallelogram actuators to support the motors which need to lift the main part of the load.

A change-of-side mechanism is not provided and the current version can only be used for the left arm. The robot can be adjusted to the patient with the cuff and the gravity support that can be changed.

PASCAL is for children and adolescents with mildly to moderately affected arm function, who can already train dual tasks with combined reaching and walking. Children with moderate to severe motor impairments need more active support of the arm posture, e.g., in the form of an adult or pediatric ARMin robot.

The example of the PASCAL robot and the overview of the pediatric robots in the previous section show that a majority of the robots, which are used for children are based on robots for adult rehabilitation or are used for both, children and adults. This rises the question what the specific differences are between adult and pediatric

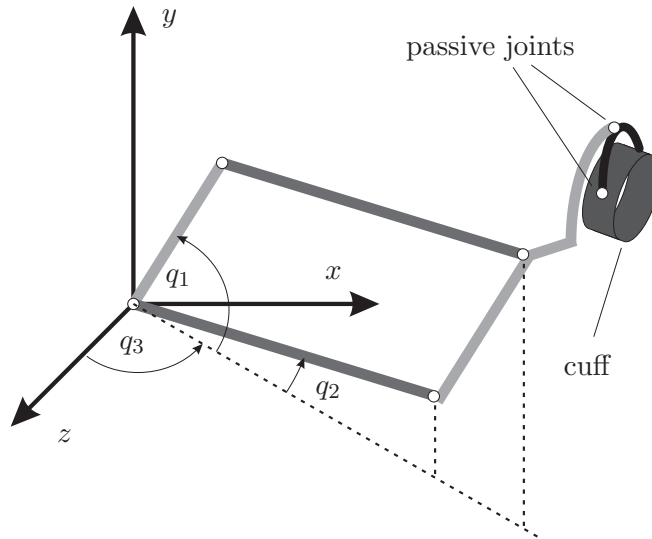


Figure 1.9: Kinematic structure of the PASCAL robot. The angles  $q_1$ ,  $q_2$  and  $q_3$  represent actuated joints.

arm rehabilitation training and, whether, it is possible to provide an optimal pediatric therapy with the same rehabilitation concepts that we use for adult patients.

### 1.4.3 What is Different in Pediatric Rehabilitation

In Sec. 1.2, the different key features for pediatric rehabilitation were listed. It also showed that most of these aspects are similar to adult rehabilitation where an intensive, goal-directed, activity-based, task-specific, early onset, assisted, and assessed rehabilitation training is crucial for the recovery of arm motor function. Nevertheless, there are several aspects in which the young patient differs from an adult patient. These differences need to be considered to provide the best possible rehabilitation training. The most important aspects are quickly discussed in the following paragraphs.

#### Anthropometry and Strength

The most obvious difference is the body size of the child. However, it should be stated here that children are not small adults. Not only is the extrapolation from adult data not adequate [154], but also do the children who suffer from a neurological diagnose often have growth impairments.

The strength characteristics show that joint torques in adults are significantly higher than in children, even when normalized to body mass [155]. This difference is even higher when comparing to young patients with impaired arm motor function which are often weaker than their peers.

#### Type of Impairment

In children with CP, the impairment is congenital or acquired in the first years. As a consequence, the impairment detracts normal skill acquisition and development of arm function. As stated above, for children with congenital lesions (especially severely affected), the goal is to maintain rather than improve motor function. While in adults

after a neurological disorder (and often children with pediatric stroke or traumatic brain injury), therapies focus more on recovery of arm function from before the impairment, in children with CP there is usually no state to regain and all the skills have to be learned first. Hence, the term habilitation is more and more used for children with CP instead of rehabilitation to emphasize this difference.

In general, the prevalence of neurological disorders in children (e.g., CP with a prevalence of 2.1 % worldwide [12]) is much lower than in adults (e.g., stroke with a prevalence of 2.6 % in the US [156]).

### **Motivation**

As mentioned above (Sec. 1.2), motivation is essential for both, adult and pediatric rehabilitation to stimulate the patient to actively participate in an active arm therapy training. The adult patient with neurological impairments such as stroke or SCI is often intrinsically motivated to perform the arm training, knowing that the therapy can help to improve or regain arm and hand function. Moreover, for adults the social factor positively affects the patient's motivation, e.g., clear and revisable goal-settings, an attempt to make the patient feel that their views on rehabilitation are valid and welcome, acceptance of the patients' idiosyncrasies, avoiding to clash with the value system of the patient or a warm, approachable and competent therapist [157]. Children with CP, however, are less aware of what can be achieved with the training and tend to be frustrated easier than adults when reaching their limits with the affected arm, i.e., the intrinsic motivation to use the affected arm is lower. Here, the young patient has to be motivated extrinsically with spoken rewards and other incentives from the therapist or by providing an enriched, attractive and non-distracting environment that lets the patient use the affected arm without permanently thinking about the training performed. Here, game-like scenarios and VR environments have the potential to provide a training environment to motivate the patient and provoke a prolonged training. It seems that especially children and youths can immerse easily in such game environments and accept the training with rehabilitation technologies in combination with VR environments very well [15].

By changing the amount of support of the robot, such that the patient can perform a movement on his own and by adapting the difficulty settings of the VR task, the patient can be optimally challenged, i.e., the child is not bored or over-challenged. This is often referred to as being 'in the flow'. The flow is an immersed mental state of focused motivation (theory of flow [158]).

### **Motor Learning**

The difference between motor learning in children and adolescents was rarely investigated and is discussed controversially. On one hand, there seem to be similar traits in pediatric habilitation and adult motor learning [38], but on the other hand, there are clear motor learning differences between children and adults [159].

### **Safety**

Compared to adults, it is more difficult to instruct a child to sit still and perform a particular task. This leads to stricter safety requirements for devices which are used in close interaction with children, i.e., when needed the patient has to be released quickly

and no sensitive or dangerous parts should be close to the patients head or trunk in case that the young patient makes unexpected movements.

#### 1.4.4 A Novel Pediatric Arm Rehabilitation Robot

Compared to adult rehabilitation there are only a few robotic devices available which have been tested with children. Most of these tests were performed with robots which were originally built for adult rehabilitation and with mildly to moderately affected children. However, the previous section indicated that there are clear differences between the rehabilitation approaches in adults and children. An active robot for children with moderately to severely affected arm functions, specifically designed to cover the key aspects of pediatric arm rehabilitation (Sec. 1.2) and accounting for the differences between adults and children (Sec. 1.4.3) is still missing.

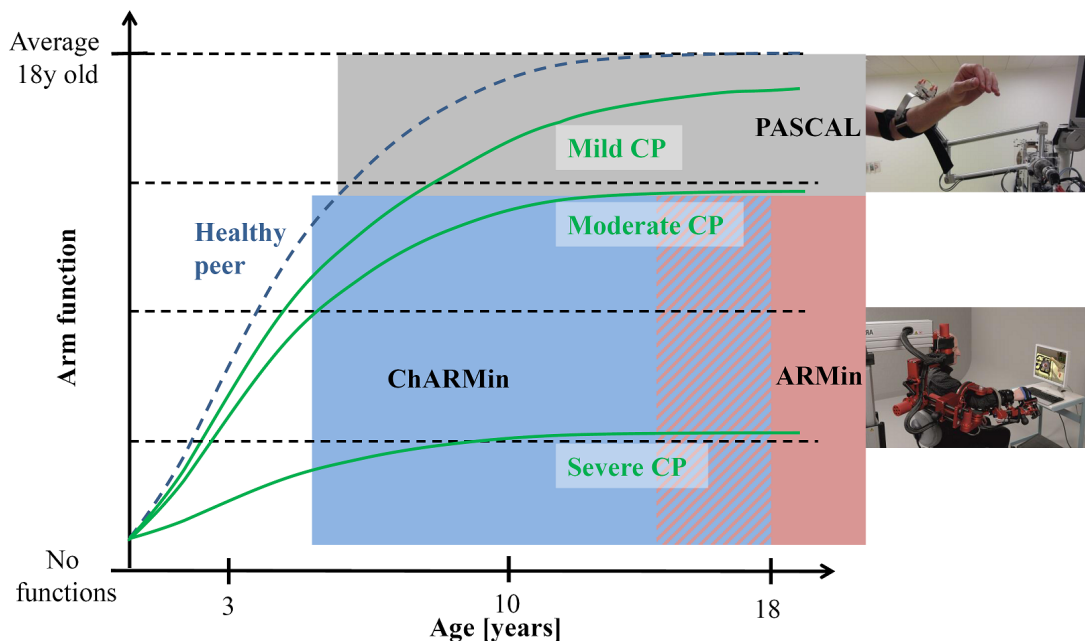


Figure 1.10: Illustration of the development of arm motor function in children with CP (based on GMFCS/GMFM data [18,160] for children with CP; the GMFM was shown to correlate well with the MACS assessment [19]) together with the target group (age and severity) that the robots PASCAL (gray), ARMin (rose) and a children version of ARMin (ChARMin, blue) cover. The range of ChARMin and ARMin overlap slightly as male adolescents aged 14 years and older can already use the ARMin robot.

Based on the knowledge of the adult ARMin robot (Sec. 1.3.2), a novel children ARMin (ChARMin) prototype could address the challenging requirements of the pediatric target group, provide an intensive, task-specific and activity-based training, actively assist different therapy modes (such as single-joint or multi-joint arm training), motivate the patient by means of a VR scenario, and enable assessments of arm motor functions in patients with moderately to severely affected arm motor functions.

In Fig. 1.10, an illustration of the potential fields of application of ChARMin and the other two introduced robotic platforms, ARMin and PASCAL, is given dependent on

the severity of the patient arm impairment and the age of the patient. While end-effector robots, such as the PASCAL robot, are typically used for arm rehabilitation training in mild to moderately affected patients, exoskeleton-based systems, such as the ARMin or ChARMin, can cover the range from moderately to severely affected patients.

## 1.5 Motivation and Aim of the Thesis

### 1.5.1 Problem Statement and Hypotheses

Children with a neurological disorder such as cerebral palsy often suffer from impaired arm motor function hampering their participation in daily life. An intensive, activity-based and task-oriented rehabilitation can help to increase the arm function and prevent deterioration. This rehabilitation training can be provided by robotic technology. While rehabilitation robots are regularly used for adult therapy, there are only a few platforms available for arm rehabilitation training of children and youths. Moreover, there is currently no actuated exoskeleton robot available for pediatric arm rehabilitation to actively assist and assess arm motor function during complex arm movements as well as single-joint movements. Based on first findings of robotic devices applied to children and the successful use of active-assistive devices in adults, the hypothesis was formulated that an active patient-tailored, robot-assisted and motivating arm therapy complementing conventional therapy can be applied to children with moderate to severe CP. Furthermore, it is hypothesized that robot-assisted arm assessments can provide an applicable, safe, reliable and comparable tool to measure arm motor function in patients with neurological disorders.

### 1.5.2 Aims of the Thesis

The aim of this thesis is to design and build the active pediatric arm support robot ChARMin to provide an intensive, task-specific, activity-based and motivating exercise tool to assist single-joint and multi-joint movements and assess children and youths with affected arm motor function such as children with CP. This aim involves the following aspects which are the four building blocks of the thesis:

1. **ChARMin robot** - Design and realization of an active child-specific arm rehabilitation robot hardware which is safely applicable to the anthropometric range of the pediatric target group and an audiovisual interface to motivate an active participation of the child during the therapy.
2. **ChARMin control** - Implementation of a patient-cooperative support strategy to assist children with different levels of arm impairment and with different therapy goals during the robotic rehabilitation session.
3. **ChARMin assessments** - Development of robot-assisted assessments to measure various kinematic, kinetic, and timing aspects of arm motor function.
4. **ChARMin feasibility** - Test of the resulting robotic hardware, control paradigms, and assessments in first feasibility case trials with children and youths with affected arm motor function.

### 1.5.3 Challenges

The specific technical challenge in designing an active pediatric arm rehabilitation setup is to find the optimal robotic hardware and interface that satisfy the needs given by the pediatric target group. This involves the clinical goals, arm anthropometry, kinetics, joint range of motion and workspace, operability, technical and safety constraints, movement support and the patient's motivation. Apart from the technical challenges, the control and assessment software of the robot present more methodological challenges. Here, the requirement is to find a comfortable, cooperative, and sensitive patient-robot interaction which assists and assesses the arm while trying to intervene as little as possible and as much as needed with the patient. The control needs to follow a patient-cooperative approach to allow an active participation of the young patient and to support the arm movement only when needed. The robot-assisted assessments have to accurately measure different parameters describing the patient's arm functions. The implementation of these assessments is a balancing act between a robot which has to be able to counteract a strong patient and a robot which transparently follows the patient's movements.

## 1.6 Thesis Outline

This thesis is structured in four main building blocks as described above in the 'Aims of the Thesis' (Sec. 1.5.2). Following the first introduction chapter ('1 Introduction') the second chapter ('2 ChARMin Robot') presents the development and realization of the pediatric ChARMin arm rehabilitation robot hardware, including the electronics, actuation, safety and the game-like visual interface. The third chapter ('3 ChARMin Control') describes the different patient-cooperative control modes for complex multi-joint support (position controller in Sec. 3.2.2, assist-as-needed path controller in Sec. 3.2.3) and single-axis support (single-joint controller in Sec. 3.2.4) implemented for the ChARMin robot. The fourth chapter ('4 ChARMin Assessments') is divided in two sections. The first section describes the robot-assisted assessment packages which were implemented in the ARMin IV robot and tested with adult SCI patients (Sec. 4.1). The second section contains the adaptations and extensions for the robot-assisted ChARMin assessments (Sec. 4.2). In the fifth chapter ('5 ChARMin Feasibility'), first feasibility case trials with pediatric patients are presented. In the last chapter, a general conclusion is drawn for the thesis and an outlook is given for future work ('6 Conclusion and Outlook').

## 2 ChARMin Robot

This chapter presents the design of the ChARMin robot. The requirements in the introduction below form the basis for the subsequent sections which show the detailed concept and design of the robot. The design section introduces the details of the kinematics of the different axes, the passive gravity compensation, the change-of-side mechanism and other adjustment and hardware aspects. Moreover, the actuation of the robot, the newly developed electronics, the virtual reality interface, and the features that guarantee a safe application are presented in the according sections.

### 2.1 Introduction

The conceptualization of the new robotic system is strongly influenced by various aspects and requirements as formulated by therapists in terms of arm anthropometry, joint range of motion, kinetics, patient's motivation, assistance by the robot, operability by the therapist, available therapy modes, safety and further technical requirements. These specific requirements will be stated in more detail below. An overview is given in Fig. 2.1. Most of the requirements directly depend on the pediatric target group which is, therefore, encircled by all the subsequent requirements in the graphical representation.

#### 2.1.1 Requirements

##### Target Group



The main requisite is that the robot has to cover the size range of 5- to 18-year-old children with arm motor impairments, such as CP. Children younger than 5 years are not included as robot-assisted therapy is considered to be unsuitable for them. On the one hand, the child is usually fixed in the robot for more than 30 min during the therapy and the child has to sit calmly and focus on the task, which is difficult to achieve in very young children. On the other hand, there are indications that there is no immediate benefit of an intensive training for children up to 4 years [49].

According to the therapists, the goals of the robotic therapy are to increase (i) range of motion and workspace, (ii) strength and (iii) quality of movement. The joints that should be included in active training are:

1. Horizontal shoulder ab-/abduction (HSAb/HSAd)
2. Shoulder extension/flexion (ShEx/ShFl)
3. Shoulder internal/external rotation (ShIR/ShER)
4. Elbow extension/flexion (ElEx/ElFl)
5. Elbow pronation/supination (ElPr/ElSu)
6. Wrist extension/flexion (WrEx/WrFl)

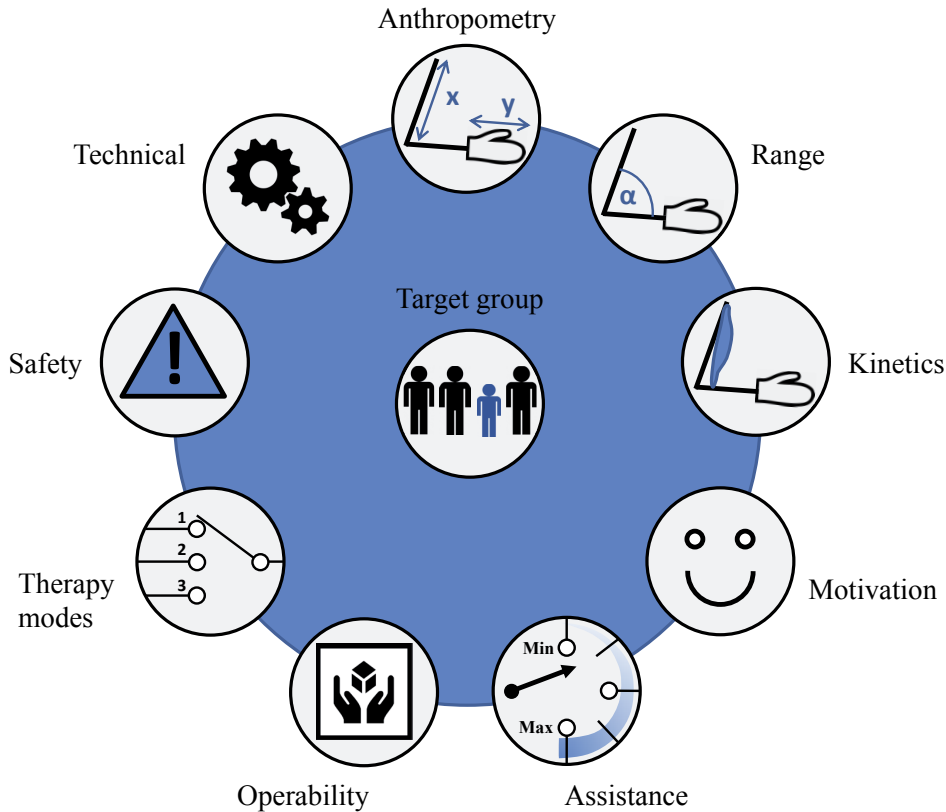
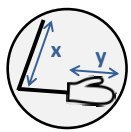


Figure 2.1: Overview of the different requirements for the development of the new pediatric arm rehabilitation robot ChARMin.

Moreover, an active or passive hand module should be provided which detects the pressure the child applies with the hand. The robot structure should allow for vertical displacement of the glenohumeral joint (GHJ) of the shoulder as it is explained in Fig. 2.2.

### Anthropometry



Children with early-manifesting disorders like CP often show growth retardation [161], which requires that the robot is designed according to the anthropometry data of this specific group. Due to insufficient data regarding anthropometry of arm segments in children with CP, the data was deduced from healthy children whose body height corresponds to that of a child with CP at a certain age. For example, the 50th percentile of the body height of a 5-year-old child with CP (gross motor function classification system level V) corresponds to approximately the 50th percentile value of a 3-year-old healthy child [162]. Consequently, anthropometrical data from healthy children aged from 3 to 18 years has to serve as a basis to design the mechanical structure of the robot. The upper limit for anthropometric data was set to the 95th percentile of healthy 18-year-old subjects, such that also adolescents whose growth was not affected can be trained with the robot. To cover these different arm sizes of the target group, the robot must be highly adaptable. The anthropometric ranges which the robot needs to cover for the upper arm, forearm, wrist-to-handle distance, and arm circumference are given in Tab. 2.1.



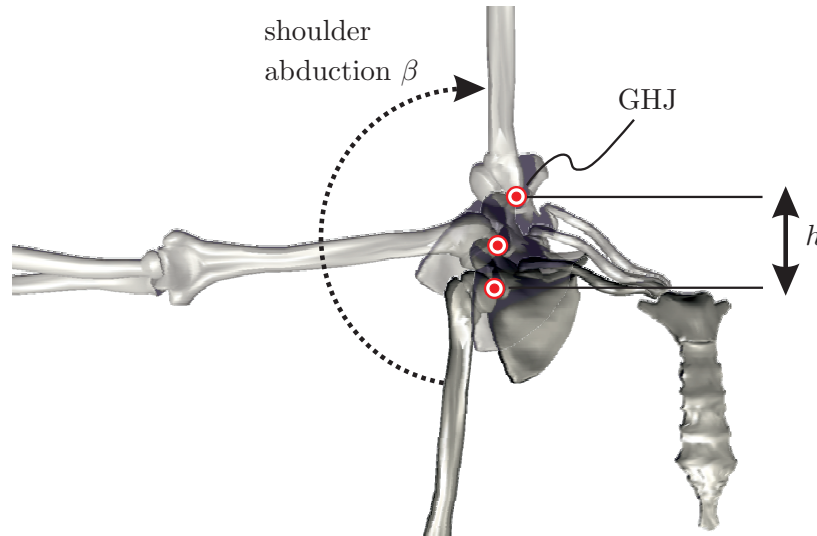


Figure 2.2: Vertical shoulder movement ( $h$ ) of the glenohumeral joint (GHJ) during shoulder ab-/adduction ( $\beta$ ).

Additionally to the adaptations of the length values and arm circumference, the device also needs to be adaptable to the shoulder height of the patient. All the anthropometric data were extracted from [163].

<b>Anthropometric arm measurement</b>	3 years	13 years	18 years (50th)	18 years (95th)
Upper arm length [cm] <sup>a</sup>	16.7	29.2	31.8	34.4
Upper arm circumference [cm]	15.8	23.0	27.5	31.5
Forearm length [cm] <sup>b</sup>	13.5	23.0	25.1	28.0
Forearm circumference [cm]	15.7	21.9	24.8	28.0
Wrist-to-handle distance <sup>c</sup> [cm]	4.2	6.7	7.3	7.8
Sitting shoulder height [cm]	~ 60	~ 80	~ 100	-

Table 2.1: Anthropometric data of healthy children aged 3, 13, 18 years - 50th percentile - and 18 years - 95th percentile [163]; The values are for combined sexes; <sup>a</sup>acromion-radiale length, <sup>b</sup>radiale-stylon length, <sup>c</sup>estimated to be 40% of the hand length.

## Range



For the six relevant arm joints mentioned above it is important to know the clinically meaningful range of motion (ROM) they should cover. In the literature, maximum range values for functional activities of daily living for 9 to 12-year-old children can be found [164]. The desired ROM that the robot should cover was based on the values underlying these movements and on additional feedback from the therapists in the Rehabilitation Center, Affoltern a. A., Switzerland (Tab. 2.2). The angle definitions are according to the convention found in the Appendix A.2.4. A large flexion angle for the wrist is desired in order to better position a child with a spastic and, therefore, with a strongly bent wrist.

Range of motion	Min. angle [°]	Max. angle [°]
Shoulder horizontal add-/abduction	-20 <sup>a</sup>	90 <sup>a</sup>
Shoulder extension/flexion	-58 <sup>b</sup>	152 <sup>b</sup>
Shoulder internal/external rotation	-47 <sup>b</sup>	54 <sup>b</sup>
Elbow extension/flexion	12 <sup>b</sup>	117 <sup>b</sup>
Elbow pronation/supination	-90 <sup>a</sup>	90 <sup>a</sup>
Wrist extension/flexion	45 <sup>a</sup>	-90 <sup>a</sup>

Table 2.2: Desired range of motion that the robot should cover, derived from literature (<sup>b</sup>)[164] and/or by therapists (<sup>a</sup>). The range shows mean values plus standard deviation (Std). The angles are defined according to the convention found in Appendix A.2.4.

### Kinetics



The robot should be strong enough to guide a paralyzed arm and counteract a spastic arm and, therefore, prevent a possible collision with the patient's body. Furthermore, the robot should resist even a relatively strong patient when using the robot as an assessment tool to determine isometric force.

Therefore, data from healthy subjects was used to estimate the torques that the robot should be able to apply at each joint (Tab. 2.3). Values for horizontal shoulder ab-/adduction and elbow pronation/supination could not be found. However, based on the knowledge from the ARMin robot a torque of 20 Nm for horizontal shoulder ab-/adduction and 8 Nm for elbow pronation/supination was selected that the pediatric robot should be able to apply temporarily for the 18-year-old patient.

Kinetics	5 years	13 years	18 years
Shoulder abduction [Nm]	6.9 <sup>a</sup>	35.2 <sup>b</sup>	41.0 <sup>c</sup>
Shoulder adduction [Nm]	7.3 <sup>a</sup>	~40.0 <sup>d</sup>	52.9 <sup>c</sup>
Shoulder internal rotation [Nm]	7.8 <sup>a</sup>	~27.5 <sup>d</sup>	34.8 <sup>c</sup>
Shoulder external rotation [Nm]	5.9 <sup>a</sup>	~19.8 <sup>d</sup>	25.7 <sup>c</sup>
Shoulder horizontal ab-/adduction [Nm]	-	-	20.0 <sup>f</sup>
Elbow extension [Nm]	8.8 <sup>a</sup>	27.6 <sup>b</sup>	32.2 <sup>c</sup>
Elbow flexion [Nm]	8.5 <sup>a</sup>	34.3 <sup>b</sup>	42.8 <sup>c</sup>
Elbow pronation [Nm]	0.9 <sup>a</sup>	2.1 <sup>e</sup>	8.0 <sup>f</sup>
Elbow supination [Nm]	0.9 <sup>a</sup>	2.6 <sup>e</sup>	8.0 <sup>f</sup>
Wrist flexion [Nm]	1.5 <sup>a</sup>	4.4 <sup>e</sup>	19.1 <sup>c</sup>
Wrist extension [Nm]	0.7 <sup>a</sup>	1.7 <sup>e</sup>	10.0 <sup>c</sup>

Table 2.3: Joint torques of healthy subjects (50th percentile both genders); <sup>a</sup>isometric values [165], <sup>b</sup>isometric values [166], <sup>c</sup>isokinetic values (30 °/s) for subjects aged 20 to 29 [167], <sup>d</sup>interpolated values due to a lack of data, <sup>e</sup>isometric values for 10 year old children [165], <sup>f</sup>taken from ARMin robot values for adults [168].

## Motivation



In the introduction, it was highlighted that motivation is crucial for children to promote an active participation during the arm training. The child's motivation can be triggered by different means including feedback from the therapist, an appealing and comfortable design of the robot, its use in non-distracting surroundings or with a virtual reality interface that accounts for the specific interests of children. For adults who are more intrinsically motivated, the interface is often used to visualize the real task which has to be learned, e.g., performing activities of daily living with ARMin. Children, however, need a VR interface which has to cover other aspects:

- Gaming - Game-based therapy to motivate the child and, therefore, to increase the duration of the training.
- Variety - Various scenarios to provoke curiosity, to account for children with different interests, to keep the training exciting over a longer period by changing the scenario, and to train different arm movements.
- Immersion - An immersive environment lets the child forget the repetitive tasks performed, e.g., by using an exciting gameplay, beautiful scenery, colors, acoustic feedback, an appealing character, etc.
- Reward - The game provides highscore lists to compare with previous scores or with other patients. Other rewards can, e.g., appear in the game in the form of bonus elements for good performance.

## Assistance



The robot has to display different modes of assistance to account for different motor disorder, severities of impairment and different game scenarios. Furthermore, the kind and amount of assistance needs to be adjustable by the therapist. Therefore, different control modes need to be provided by the robot:

- Free movement - The robot follows the patient arm and intervenes as little as possible, e.g., for assessments or motor learning experiments.
- Gravity support - The robot compensates the arm weight to a desired amount. The amount of support can be adjusted by the therapist, e.g., for mildly to moderately affected patients who do not need directional support, but a reduction of the arm weight to train longer before the arm fatigues.
- Assist-as-needed - The robot assists the arm when the patient is not able to perform a certain arm movement. The amount of support can be adjusted by the therapist, e.g., for moderately to severely affected patients who need assistance to reach a desired position.
- Complete guidance - The robot controls the position of the arm and guides the movement, e.g., for movement instruction, mobilization of the arm or for measuring arm properties.
- Single-joint support - Single-joint training is applied when the focus is on selective training of single joint movements or when multi-joint movements are still too

difficult to train. Here, the robot locks a desired arm posture and only supports the movement and game-play in a single axis chosen by the therapist.

- Holding posture - The robot fixes a posture, e.g., to help positioning the patient or to measure isometric strength.

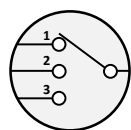
### Operability



Regarding operability and handling the robot has to be easily adjustable to the patient's arm which also includes a change-of-side mechanism that allows the therapist to change between left and right arm training. Furthermore, the robot has to be mobile for transportation and positioning relatively to the patient.

The use of the robot has to be intuitive and supported with instructions and a comprehensive manual. Parts that are in contact with the patient should be exchangeable for cleaning, e.g., the cuffs to fix the robot to the patient. The therapist interactions with the keyboard, mouse, or other input devices should be kept at a minimum such that the therapist has its hands free for patient fixation, robot teaching, etc.

### Therapy modes



Based on the knowledge acquired with the ARMin robot and other pediatric arm and hand rehabilitation devices, different therapy modes were defined which have to be implemented for interventions with the new robot covering the robot setup, calibration, games, mobilization, and assessments:

- Setup - A dedicated interface is needed to enter patient-specific information and to support the therapist in positioning and adjusting the robot.
- Calibration - A calibration routine is used to define the range of motion, Cartesian workspace, and other thresholds to scale the games to the skills of the patient.
- Games - Various games have to be provided covering single-joint movements and multi-joint movements.
- Mobilization - A therapy mode to teach and repeat a movement should be implemented to repeatedly mobilize the patient's arm.
- Assessments - Robot-assisted assessments that measure arm motor functions should be included.

### Safety



A set of crucial requirements is related to the safety of the robot. This includes the safety of the patient, therapist, third party, and the robot itself. The mechanical precautions guarantee safety independent from any electrical or software components:

- Increased distance between the patient's head and trunk and the robot. (In contrast to ARMin where the horizontal shoulder rotation is actuated from top of the shoulder joint, leading to mechanical parts that are close to the patient's head as seen in Fig. 1.5).

- Passive gravity compensation of the robot to support the motors and to ensure a safe position in case of power loss.
- Mechanical measures to make sure that the robot stays in the anatomical joint range of the human arm.
- Quick release of the patient has to be guaranteed in case of unexpected events, e.g., strong spasticity or epileptic seizure. This includes a backdrivable robot to move in a safe position also when unpowered.
- The therapist must be able to switch off the robot and stop the therapy session at any point in time.
- No sharp edges and no pinch point.
- The robot needs to be conform with the norms EN 60601-1, ISO 14971, EN 980 and IEC 62304.

In addition to all the technical requirements, there need to be more electrical and software features to assure the safety of the patient, e. g., constraining the joint torques and ROM, supervise the controller (speed and force limits, plausibility checks), redundant sensors for all joints or a safety switch. The control software and other supervision elements have to check continuously for the plausibility and operability of the system.

### Technical



The last aspect covers technical requirements that have to be fulfilled to assure a proper functionality, durability, and performance of the hardware as well as state-of-the-art engineering principles for human-machine interaction:

- No backlash ( $<1^\circ$ ) and backdrivable joints (static friction  $<1$  Nm) that are movable in the case of power loss.
- Dimensioning the robot with a safety factor on the loading to achieve longer durability and stability.
- Designing the robot such that the maintenance can be performed efficiently.
- Trying to reduce the weight of the robot where possible.
- Using redundant and sensitive sensors to increase safety, control performance, and assessment accuracy.
- Improving the power-to-weight ratio to achieve a powerful and compact design.
- Enabling a quick change of location of the robot, i.e., having a mobile robot and using standard power supply.
- Reaching a position control bandwidth of at least 2 Hz.
- Achieving a high mechanical transparency<sup>1</sup> of the robot to account for smaller and weaker patients.

---

<sup>1</sup>The transparency of the robot is a measure for undesired interaction forces between the robot and the human arm. In this context, a difference is made between the desired forces applied to support the human arm and the disturbing forces that counteract the movement of the robot and the patient and, therefore, reduce the transparency. Factors that influence the transparency of the robot are mainly the mass and inertia of the robot, but also disturbing torques coming from joint friction or connecting cables.

- Keeping the weight of the robot at a minimum while maintaining stability and durability of the device.

### 2.1.2 Improving the Transparency

For a good transparency of the robot, i.e., reduced undesired interaction forces between the robot and the user, the mechanics, control, and electronics have to be considered.

#### Mechanics

The robot joints have to be backdrivable, which can be fulfilled with an appropriate choice of actuator and transmission components (Sec. 2.2.2). Furthermore, the joints need to have little static- and dynamic friction. Here, a remote center of rotation (RCoR) kinematics structure is a promising candidate to reduce friction compared to previous designs (Sec. 2.2.1). The mass and inertia of the robotic structure have a great influence on the mechanical transparency. Therefore, the goal during the construction phase was to keep the mass and inertia at a minimum. However, the load cases are difficult to predict and to guarantee the safety of the robot, the stability of the structure was weighted more than a highly lightweight structure for the first prototype. Lastly, the joints should have little backlash. Harmonic drives are known for having minor backlash. However, the size and costs of the units are both considerable, such that harmonic drives should only be used where critically needed.

#### Control

An important software measure to improve the transparency of the robot is by actively compensating mass, friction, and inertia with a dedicated compensation model of the robot (details in Sec. 3.2.1). Static friction, however, is more difficult to compensate. In the adult ARMin, for example, friction torques were quite high and ranged from 0.2 Nm (elbow) to 2.4 Nm (shoulder).

Additionally to the friction compensation, using force sensors is another option to improve the transparency of the robot by measuring the interaction forces/torques between the robot and patient (e.g., ARMin IV [6] or the iPAM system [169]). ARMin IV is equipped with 6 DoF force/torque sensors right below the arm cuffs and, therefore, as close as possible to the patient's arm. Appendix A.3.1 provides more information about the placement of the sensors as well as the modeling and control using the force/torque sensors. By using this force/torque information for the control of the robot, the transparency can be increased, as shown in first tests with ARMin IV [6].

A third option is the use of series elastic actuators (SEA) which can decouple the inertia of the robot from the user and, therefore, improve the transparency. This approach needs elastic elements between the actuator and the user as well as a dedicated controller.

#### Electronics

Cables can have a negative influence on the robot dynamics [170]. Therefore, the number of cables and the weight of electronic components should be reduced where possible.

## 2.2 ChARMin Design

### 2.2.1 Mechanics

The new ChARMin (Children ARMin) prototype evolved from the ARMin rehabilitation robot (Sec. 1.3.2). The ARMin robot was designed for adult rehabilitation and only partially fulfills the requirements for a pediatric therapy robot. The very young and heterogeneous target group has specific needs regarding adaptability, kinetics, safety features, friction, and the visual interface which require new technical methods and solutions for the pediatric version of the robot. Downscaling the adult ARMin is therefore not suitable, as children are not just small adults (Sec. 1.4.3). Therefore, the decision was taken to move from the adult ARMin design to a new and specific pediatric design.

#### Exoskeleton vs. End Effector

In general, two different robotic concepts for human-machine interaction are distinguished: Exoskeletons and end-effector robots. End-effector-based robots are connected with the patient's hand or forearm at one point (e.g., InMotion2 [146] or the NJIT-RAVR system [141] in Fig. 1.7 or the PASCAL robot, Sec. 1.4.2). Exoskeleton-based devices, in contrast, have a structure resembling human arm anatomy, and the robot's rotation axes often correspond to that of the human arm (e.g., ARMin [171] in Fig. 1.5). A list of exoskeletons and end-effector robots for adult patients is given in Tab. 1.1. There are several reasons for choosing an exoskeleton-based approach for the new ChARMin robot:

- Each arm joint can be controlled independently, which enables to define arm postures completely and to train physiological movements without compensatory or synergistic patterns. This is specifically important for severely affected patients.
- The device can provide a wider joint range of motion and workspace for the hand, thus allowing the training of three-dimensional functional tasks.
- Joint torques can be measured independently, which is necessary for the isometric strength or resistance assessment.
- Single joints can be supported or resisted for specific joint training. For end-effector robots, in contrast, it is difficult to generate an isolated movement for a single joint [172].
- Mechanical limits for each joint prevent hyperflexion or hyperextension, and thus a potential injury of the joint.

The disadvantages of the exoskeleton over an end-effector robot are the more complex design, the higher inertia of the robot, and the more difficult patient positioning and fixation. However, for our robot which is applied to moderately to severely affected children and which will be used as an assessment tool, the advantages of an exoskeleton outbalance the disadvantages.

## Modular Design

One of the main challenges in designing the robot was the range of 5 to 18-year-old children (requirement 2.1.1). First ideas for a robot structure for this target group were sketched (Appendix A.2.5) and used as a starting point for further iterations with engineers from the SMS Lab and the occupational therapists from the Rehabilitation Center in Affoltern a. A. This led to a first conceptual CAD drawing of the robot (Appendix A.2.5). With these first conceptual drafts of the robot, it became apparent that the anthropometric range of the target group is too large to cover the whole age range with a single exoskeleton. Furthermore, a robot with dimensions for an 18-year-old patient that can deliver torques to move a completely paralyzed arm could be a safety risk when applied to a 5-year-old child.

As a consequence, a modular approach of the hardware was chosen (Fig. 2.3). The ChARMin robot consists of a proximal part (Fig. 2.3 a) that can be used for the whole target group aged 5 years and older. For the distal module (Fig. 2.3 b), two different sizes are available and can be exchanged according to the patient's age and arm size. The smaller distal module covers a range from approximately 5- to 13-year-old children while a second module can be used for children aged 13 years and older. This modular design allows to have an exoskeleton that fits the patients needs better in terms of size and torques that can be applied.

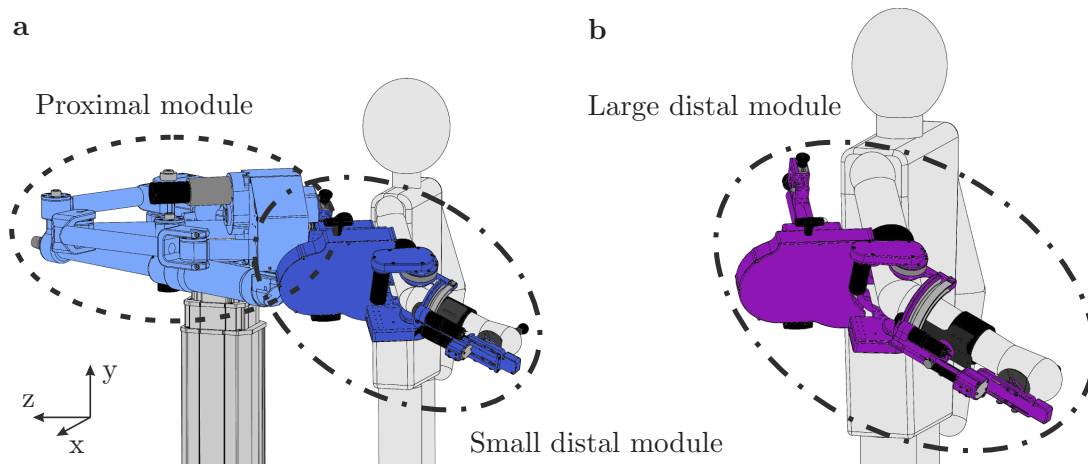


Figure 2.3: Modular design of the ChARMin robot. (a) ChARMin robot shown with the small distal module for 5- to 13-year-old children. (b) Large distal module for children aged 13 years and older. The two avatars are simplified body models of a 5-year-old and an 18-year-old patient.

### The Six Actuated Axes of ChARMin

In the following subsections, the structure of the robot will be presented by focusing on the single joints. A definition of the ChARMin axes is given in Fig. 2.4.

**Axis 1: Horizontal shoulder ab- and adduction (HSAb/HSAd)** The first axis of the robot actuates the horizontal shoulder ab- and adduction. The requirement to move the actuator away from the head of the patient led to a new parallel kinematics



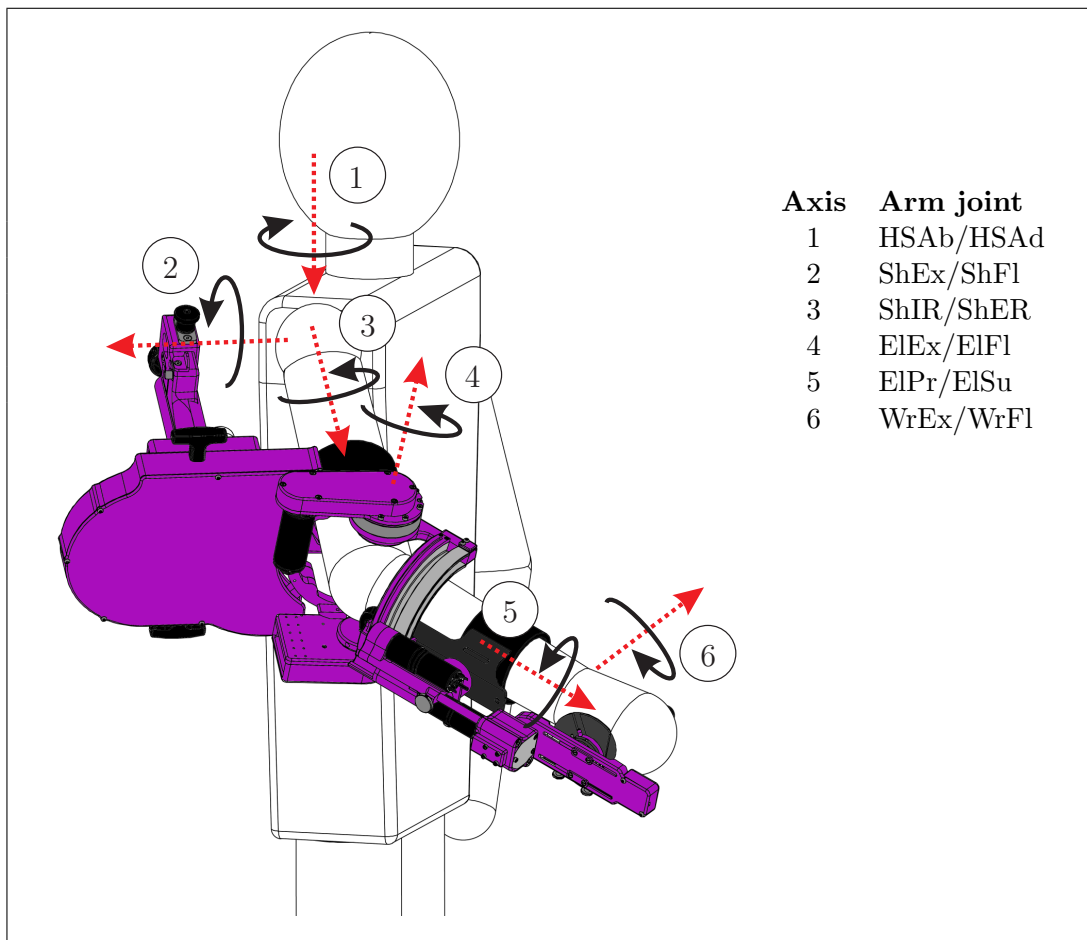


Figure 2.4: Definition of the six ChARMin joint axes.

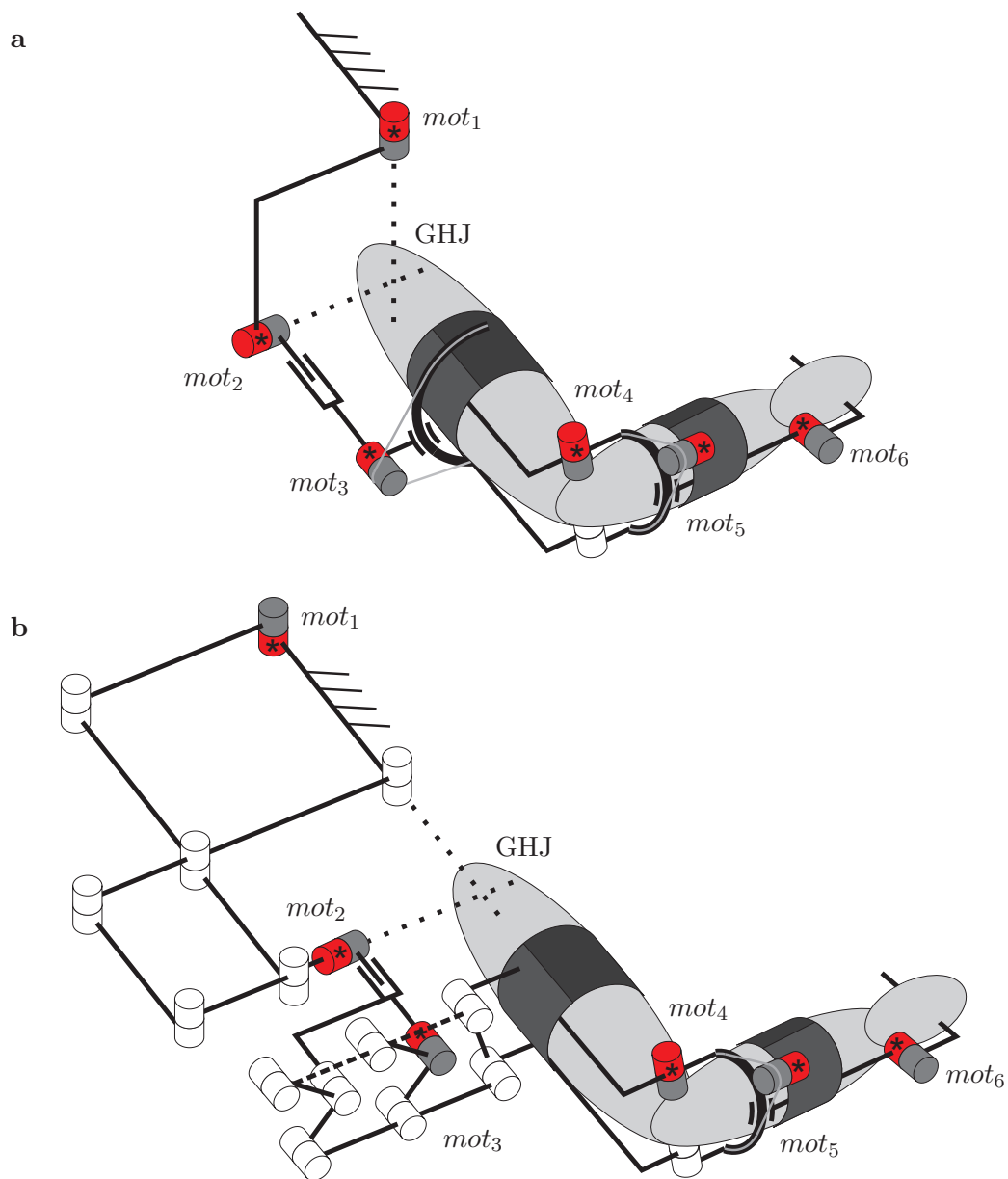


Figure 2.5: Kinematic chain of (a) the ARMin kinematics [171] compared to (b) the ChARMin kinematics structure, shown with a simplified model of an arm (light gray). The red cylinders marked with a star (\*) represent the motors. The dark gray cylinders are the gears and the white ones are the passive joints.  $mot_x$  is the motor moving axis number  $x$ . The dotted auxiliary lines are pointing to the GHJ = Glenohumeral joint. The dashed line is a standard link but dashed to improve the illustration.

structure, in contrast to the serial structure of ARMin (Fig. 2.5). The parallel kinematic structure used is referred to as a remote center of rotation (RCoR) kinematics. A simplified model of the RCoR can be seen in Fig. 2.6, where the light blue structure is moving the shoulder in horizontal ab-/adduction. This RCoR allows to actuate ( $mot_1$ ) the robot in a remote center and to transfer this rotation to the glenohumeral joint (GHJ) of the shoulder. An offset angle  $\theta$  allows to optimally set the kinematic range of the robot to the functional RoM of the patient. The link connections which are represented as white circles are passive joints in the parallel structure.

This design has similarities with a structure suggested in the US Patent 2008/0304935 [173] (A more detailed comparison can be seen in Appendix A.2.3). However, the proposed design here has a reduced number of joints and the way the arm is attached to the structure is different.

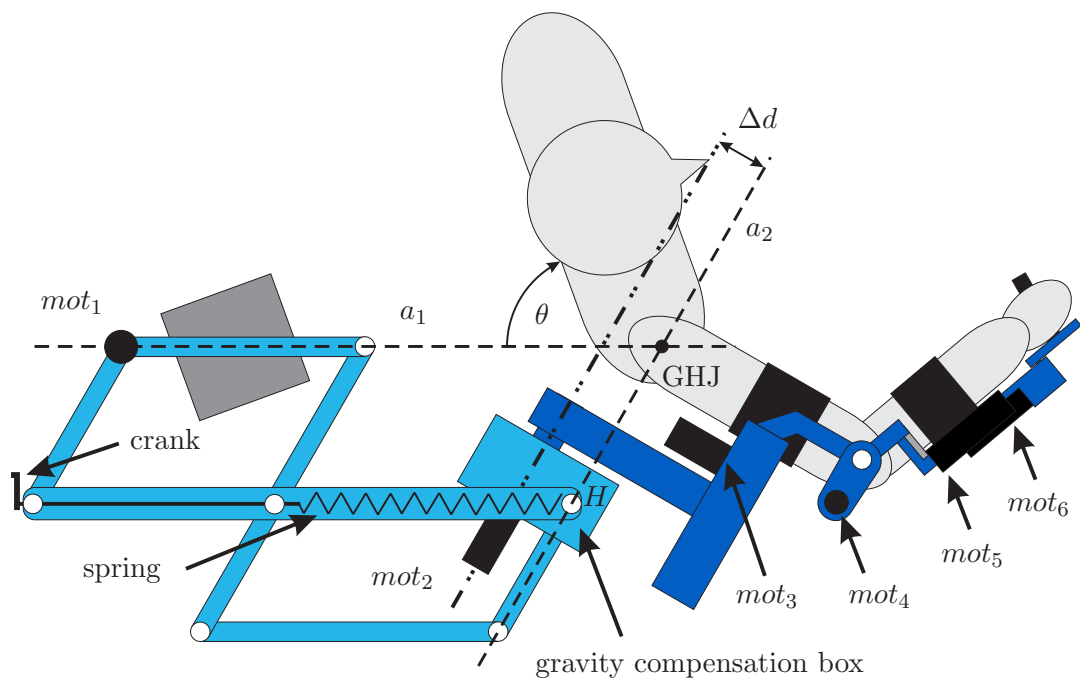


Figure 2.6: Simplified representation of ChARMin with the remote center of rotation mechanism for the horizontal shoulder ab-/adduction (top view) [1]. The six actuators are labeled with  $mot_1$  to  $mot_6$ . GHJ = Glenohumeral joint.

**Axis 2: Shoulder extension and flexion (ShEx/ShF1)** The second axis  $mot_2$  actuates the shoulder extension and flexion. This axis is mounted at the end of the parallel structure. During extension and flexion of the shoulder, the vertical translation of the GHJ of the upper arm cannot be neglected [171] (Fig. 2.2). To account for that displacement of the human physiological axis, an offset  $\Delta d$  was introduced between the GHJ of the shoulder and axis  $mot_2$  (Fig. 2.6 and visualization in Fig. 2.7). The offset  $\Delta d$  was chosen to be 30 mm which is in the lower range of the typically used offset in the ARMin robot (25-40 mm). This configuration results in a vertical movement of the GHJ joint depending on the ab-/adduction angle  $\beta$  of the shoulder and following a circular segment [171].

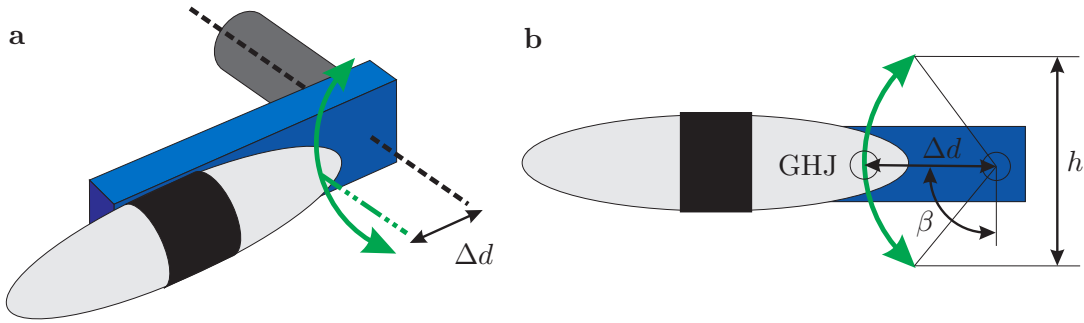


Figure 2.7: Visualization of the effect of an axis misalignment on the vertical shoulder rotation. **(a)** The dashed line is the axis of rotation of the actuator. The dash-dotted line is the temporary axis of rotation of the GHJ. The curved arrow indicates the movement of the GHJ. **(b)** The ab-/adduction of the shoulder ( $\beta$ ) leads to a vertical displacement  $h$  of the GHJ.

**Axis 3: Shoulder internal and external rotation (ShIR/ShER)** The ARMin robot has several issues with respect to the internal/external rotation axis, such as high friction forces caused by the curved guidance and the transmission belt (Fig. 2.8 a) and a quite large safety distance between this axis and the patient to avoid collisions with the patient's trunk.

As it is difficult to place an actuator on the rotation axis around the center line of the upper arm, another RCoR mechanism was applied that promises less friction as the ARMin design and allows to bring the arm closer to the patient's body without collision while still covering the required range. This parallel structure was originally introduced by Stienen et al. 2009 [106] and allows to rotate the upper arm around its longitudinal axis (Fig. 2.8 b, c, d).

**Axis 4: Elbow extension and flexion (ElEx/ElFl)** The fourth actuated joint in ChARMin is the elbow axis. The actuator axis is arranged parallel to the human elbow joint axis (Fig. 2.6) and the transmission between the axes is done via a belt.

**Axis 5: Elbow pronation and supination (ElPr/ElSu)** The fifth axis consists of a curved guidance to rotate the forearm (Fig. 2.5 and Fig. 2.9). No commercial curved guidance was found which is small enough and stands the high cross torques. Therefore, the curved guidance was built in-house.

**Axis 6: Wrist extension and flexion (WrEx/WrFl)** The motor of the sixth axis is positioned in parallel to the forearm and the torque is applied to the wrist joint via a bevel gear (Fig. 2.9).

**Axis 7: Hand module with pressure bulb** The hand of the user grabs a rubber bulb that can measure grip pressure (Fig. 2.9). The bulb has a  $10^\circ$  inclination to the front which makes it more comfortable to hold (according to the therapists operating the robot). An active hand module, as it was used for ARMin (Fig. 1.5), was designed (by Daniel Dörig in a semester thesis [174]) but not realized for the first prototype (Appendix A.2.1).

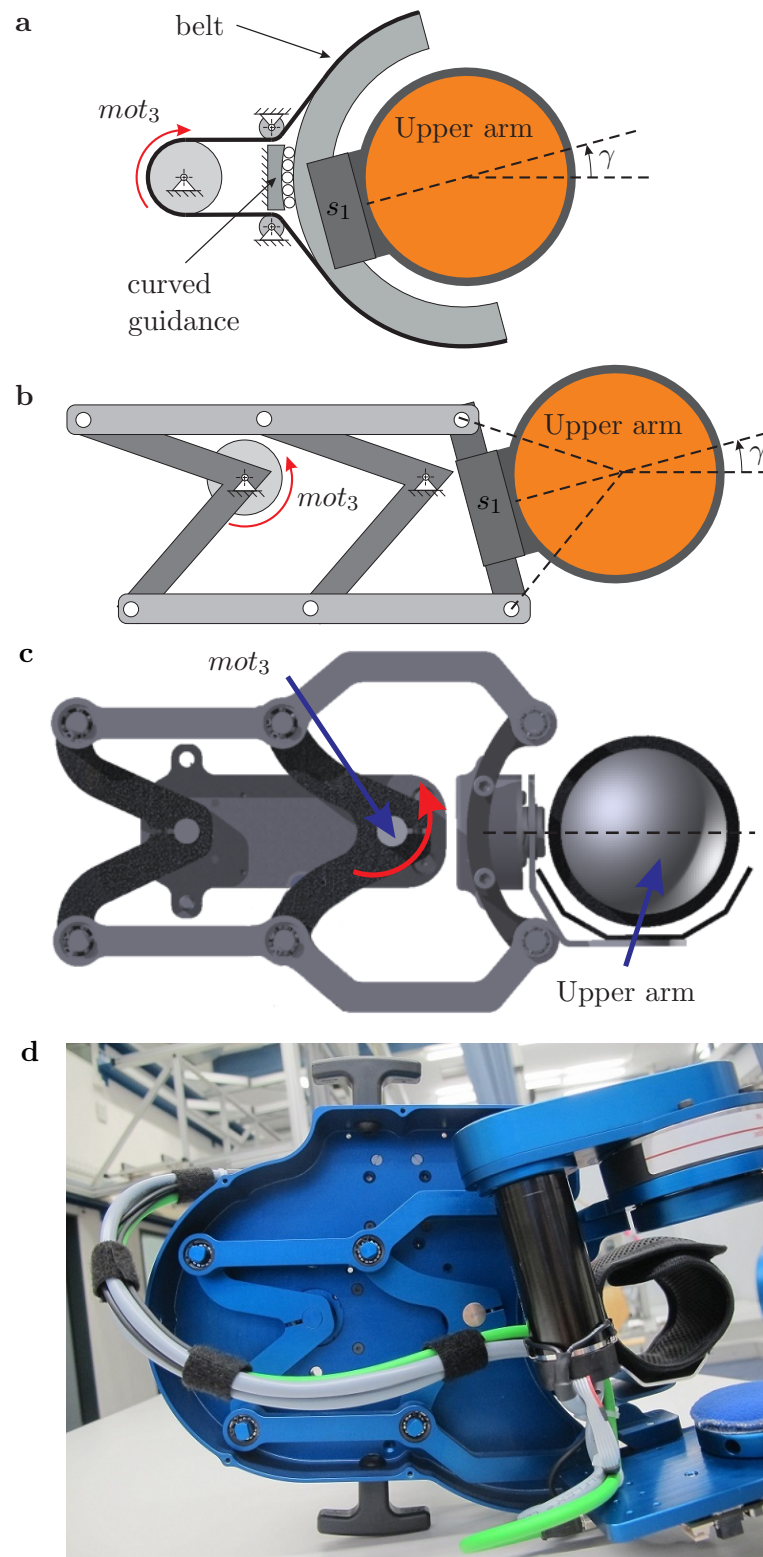


Figure 2.8: Simplified representation of (a) the ARMin and (b) the ChARMin design for the internal/external rotation of the shoulder (axis 3). A force/torque sensor  $s_1$  can be mounted directly between the cuff and the kinematic structure. The kinematics are based on Stienen et al. [106]. (c) shows the technical drawing of the RCoR concept and (d) the parallel kinematics embedded in the robot.

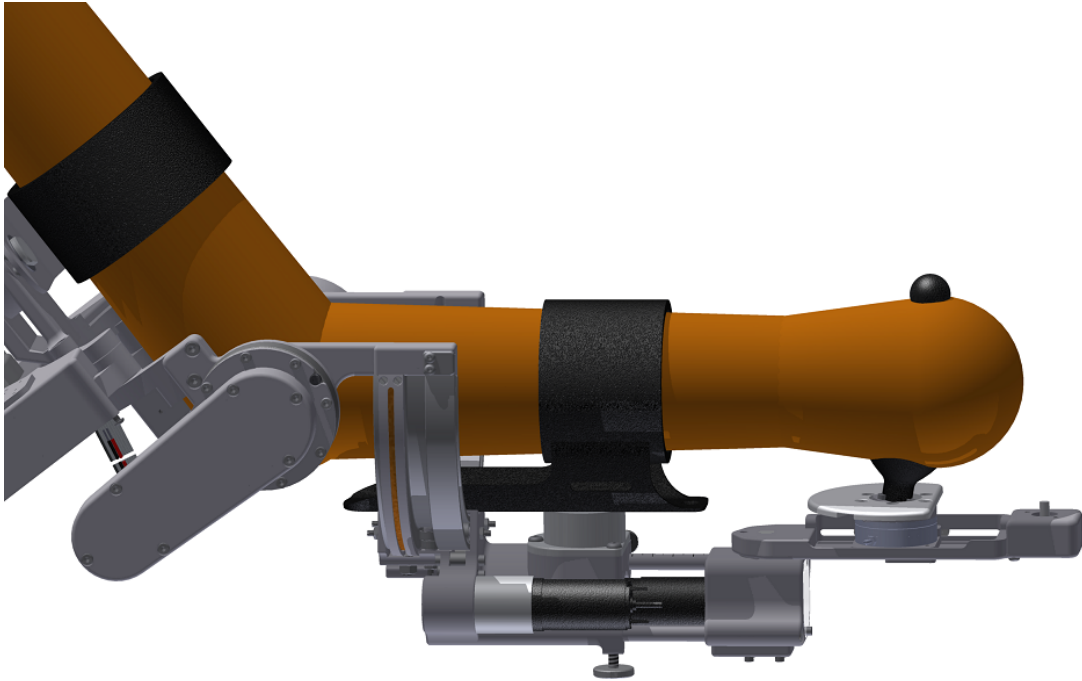


Figure 2.9: Forearm of the ChARMin robot with the curved guidance for elbow pronation/supination and the actuation for wrist flexion and extension. The black pressure bulb is grasped by the patient and measures the grasping pressure applied.

### Passive Gravity Compensation of the Robot

To prevent the robot from falling down in the case of power loss and to support the motor for axis  $mot_2$ , a passive gravity compensation is included in this axis (compensation box in Fig. 2.6, Fig. 2.11). In order to achieve this compensation, a spring  $E$  is attached in an offset distance  $d_s$  to the rotation shaft  $mot_2$  (Fig. 2.10) using a rope that is deflected by different small pulleys  $J$ .

The spring attached to point  $A$  produces a torque acting on the axis  $mot_2$  (Fig. 2.11). The tension spring required is integrated into the parallel structure described above (indicated by the zigzag line in Fig. 2.6). However, the rope coming from the spring has to cross axis  $H$  to arrive at the compensation box (Fig. 2.6). This introduces an unwanted torque in the parallel structure unless the rope and the rotation axis are collinear in the location where they pass each other (Fig. 2.10,  $G$ ).

The torque which is needed to compensate the weight of the robot arm is dependent on the angle  $\beta$ , i.e., when the angle  $\beta$  is  $0^\circ$  or  $180^\circ$  there is no need for compensation. The maximum support is required, when the arm is horizontal and  $\beta$  is  $90^\circ$ . This results in a desired passive compensation of the robot  $\tau_{spring,des}$  with a sinusoidal shape as shown in Fig. 2.12 with the dotted line.

The torque which is produced by the new spring compensation mechanism was calculated from the simplified model in Fig. 2.13 which is based on the hardware design Fig. 2.10. The following relation can be found (according to the xy-coordinate system

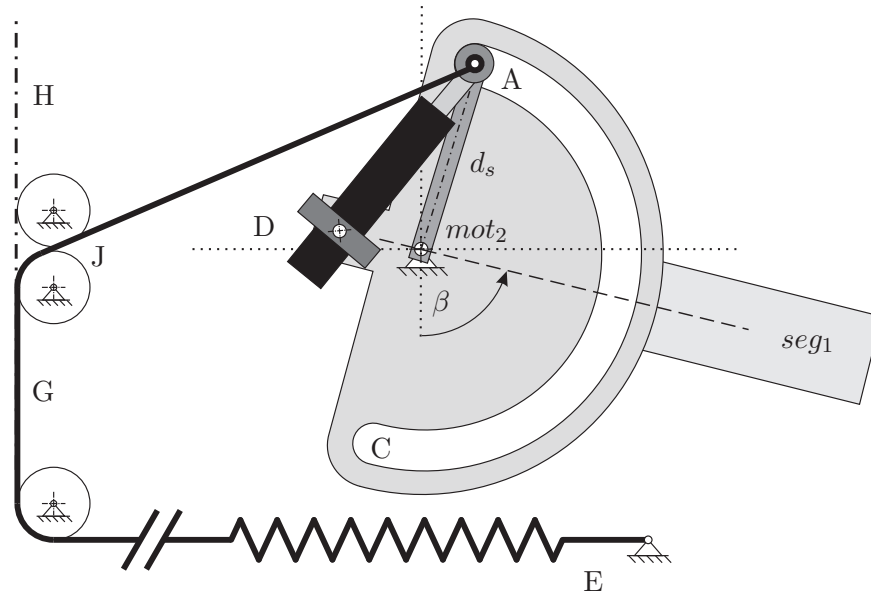


Figure 2.10: Simplified representation of the gravity compensation mechanism with the deflection pulleys (J), dampers to decelerate the toggling mechanism (D), axis 2 ( $mot_2$ ), axis of rotation of the parallel RCoR structure (H), location where rope passes along the axis of rotation (G), offset attachment point for the rope (A), and the spring (E) [1].

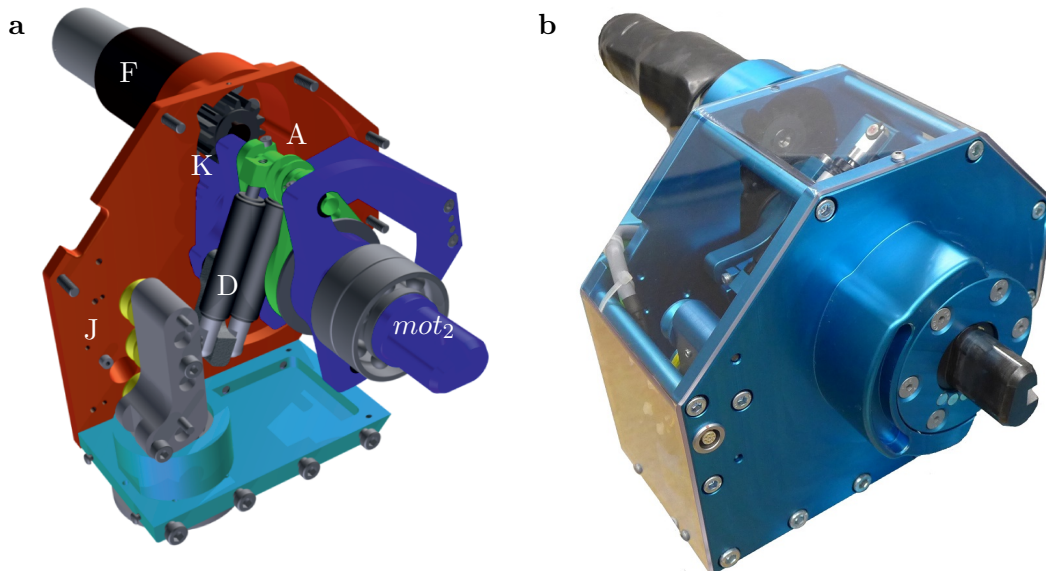


Figure 2.11: Passive gravity compensation with a toggling mechanism for changing the direction of the compensation torque. (a) Technical design of the mechanism with the spring attachment point (A), dampers (D), motor with gear (F), deflection pulleys (J) and the custom gear (K); (b) Finished hardware.



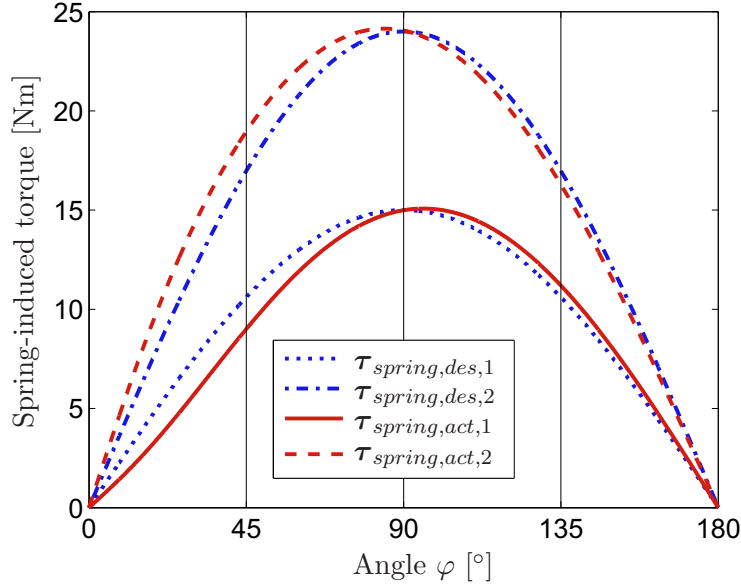


Figure 2.12: Compensation torque produced by the spring mechanism. The desired compensation torque is shown in blue ( $\tau_{spring,des,1}$ ,  $\tau_{spring,des,2}$ ) where the first load condition is with the robot only and the second condition is together with a heavy arm and high spring pretension. The actual compensation torque is shown in red ( $\tau_{spring,act,1}$ ,  $\tau_{spring,act,2}$ ). The shoulder flexion/extension angle  $\beta$  is given by  $\pi - \varphi$ .

indicated in the figure):

$$\mathbf{l}_3(\varphi) = \begin{pmatrix} -l_1 - l_2 \cos(\pi - \varphi) \\ -l_2 \sin(\pi - \varphi) \\ 0 \end{pmatrix} \quad (2.1)$$

Given the spring stiffness  $c_{spring}$  and the pretension force  $f_{\varphi_0}$  which is present at  $\varphi = 0$ , the force in the rope  $\mathbf{f}_{rope}$  can be calculated:

$$\mathbf{f}_{rope}(\varphi) = (c_{spring} \cdot (\|\mathbf{l}_3(\varphi)\| - l_1 + l_2) + f_{\varphi_0}) \cdot \mathbf{l}_3(\varphi) / \|\mathbf{l}_3(\varphi)\| \quad (2.2)$$

The spring torque  $\tau_{spring}$  is computed as the cross product between the rope force  $\mathbf{f}_{rope}$  and the lever arm  $\mathbf{l}_{arm}$ :

$$\tau_{spring} = \mathbf{l}_{arm} \times \mathbf{f}_{rope}, \quad \text{with } \mathbf{l}_{arm} = \begin{pmatrix} l_2 \cos(\pi - \varphi) \\ l_2 \sin(\pi - \varphi) \\ 0 \end{pmatrix} \quad (2.3)$$

The compensation curve for the new mechanism  $\tau_{spring,act}$  (solid line in Fig. 2.12) has a slight deviation from the optimal sinusoidal shape.

To account for different arm weights and different torques induced by the length settings in the robot, the spring pretension can be changed using a crank (Fig. 2.6). The spring mechanism produces up to 24 Nm, while the compensation curve is still close to a sinusoidal shape (dashed and dash-dotted line in Fig. 2.12).



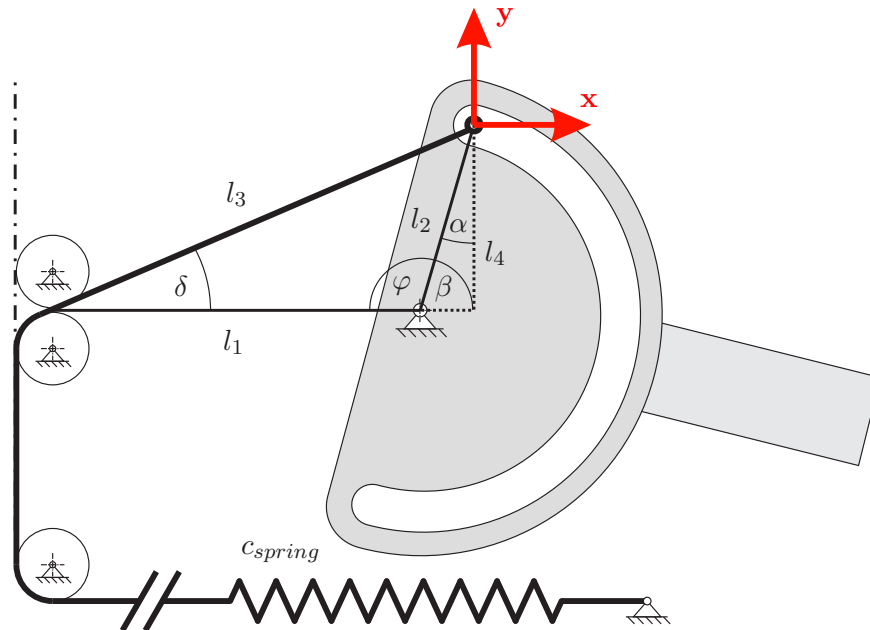


Figure 2.13: Simplified representation of the passive compensation mechanism used to derive the spring compensation torques.

### Change-of-Side Mechanism

The robot has to be adaptable to be used with both arms. Therefore, a change-of-side mechanism is provided. To change the side configuration, the whole exoskeleton is rotated around the horizontal axis  $a_1$  (Fig. 2.6) and angle  $\theta$  is adjusted. The robot is shown in both configurations in Fig. 2.15. As a consequence, the passive gravity compensation applies the offset torque in the wrong direction. That is why, secondly, the gravity compensation has to be changed to invert the passive compensation. This is done by a novel mechanism located in the compensation box. By temporarily removing the mechanical end stop for axis  $mot_2$ , the robot arm can be moved to  $\beta = 0^\circ$  (Fig. 2.14 a). In this position, the spring attachment point starts moving from position  $A$  to the opposite side  $C$  (Fig. 2.14 b). This produces high speeds for the spring attachment point, which can be decelerated with a damper  $D$ . Finally, the spring attachment point is in the new location and the shoulder flexion/extension axis is brought back in the operational range (Fig. 2.14 c). Now, the offset torque is acting in the desired direction.

### Adjusting the Robot to the Patient

To avoid unwanted interaction torques coming from misaligned axes, the robot has to be optimally adapted to the patient. This can be achieved by length adaptation mechanisms for the upper arm and forearm and by cuffs that are adaptable to the circumference of the patient's arm. In order to simplify the positioning of the shoulder, two lasers are provided pointing to the GHJ of the patient along the axes  $a_1$  and  $a_2$  in Fig. 2.6. This positioning is done by adapting the height of the lifting column in the back of the robot and wheels allow to move the robot relatively to the patient. The experience with the ARMin robot showed that it is difficult for the therapist to

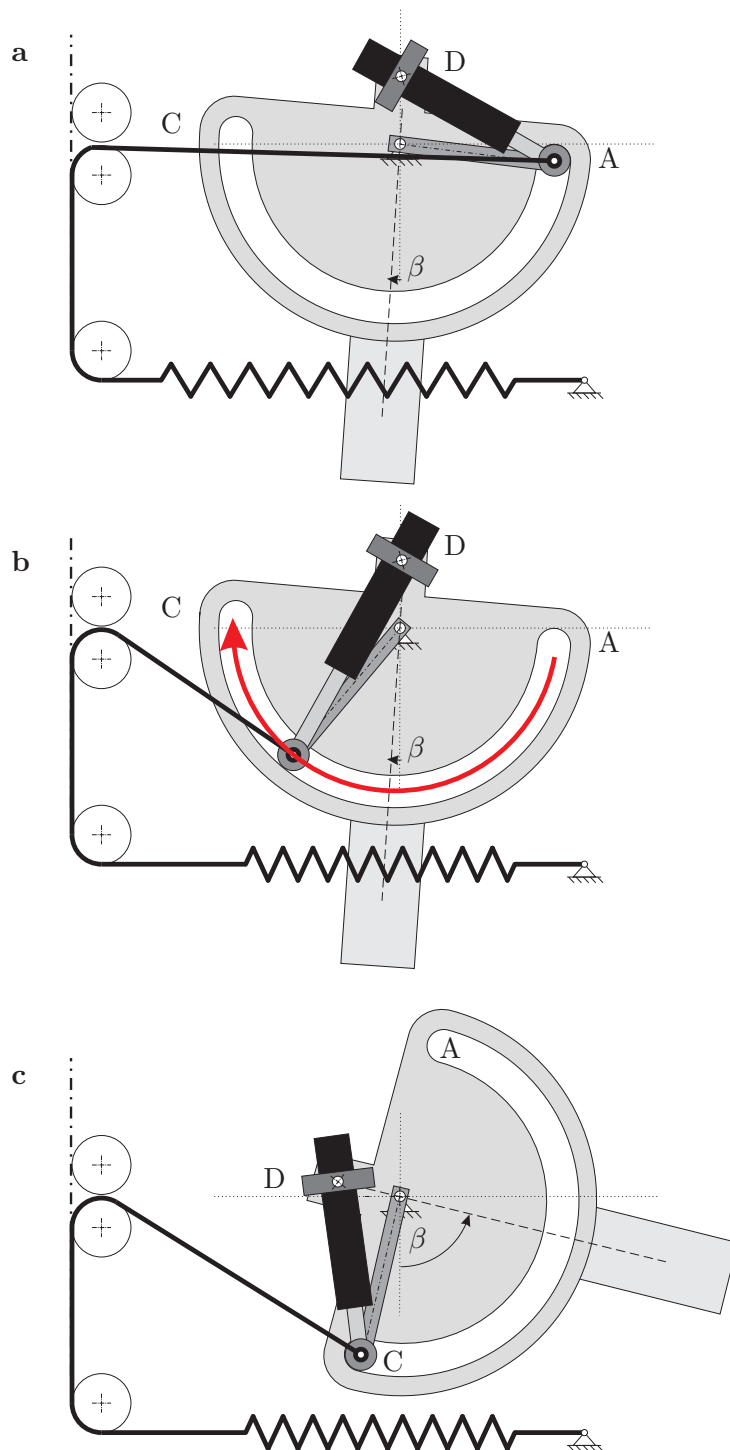


Figure 2.14: Reversing the compensation mechanism when changing from right to left arm configuration. **(a)** Removing the mechanical end stop and move the exoskeleton in the downward direction. **(b)** Arriving at  $\beta = 0^\circ$  the spring attachment point moves from position *A* to position *C*, damped with damper *D*. **(c)** The robot can now be rotated to the other arm side configuration and the spring attachment point is brought back inside the operational joint range.

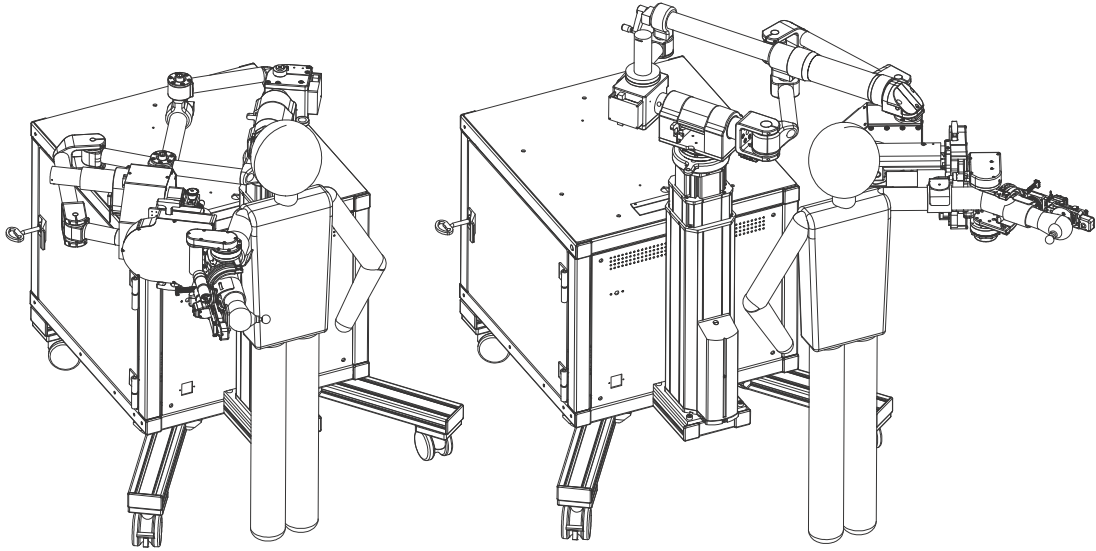


Figure 2.15: Visualization of the ChARMin robot for the right and left arm use, shown with the simplified model of a 5-year-old child.

instruct the patient to keep the position of the shoulder and to hinder the patient from doing compensatory movements with the shoulder. In the ChARMin robot, a distance sensor was mounted on the robot which can detect when the patient shoulder moves too far away from the required position. The sensor is mounted on the proximal part of the robot and points along axis  $a_1$  (Fig. 2.6).

### 2.2.2 Actuation

Electric actuation is the most common actuation principle for rehabilitation robots [172, 175]. Because of its good power-to-weight ratio, compact design, low noise level, backdrivability and its unproblematic use in clinical environments electric motors were as well used for the ChARMin robot. The actuation of the robot was chosen using the torque estimations from the requirement section (Sec. 2.1.1).

The exoskeleton is actuated with electric Maxon DC motors in combination with either harmonic drives or planetary gears. The first two actuators are on the proximal robot module and are, therefore, identical for the whole age range. However, the motors on the distal part are being exchanged together with the distal module. The different actuator-transmission combinations and the corresponding nominal torques can be found in Tab. 2.4. The values listed are for the robot equipped with the smaller (s) as well as the larger (l) distal module.

### 2.2.3 Electronics

**ChAxis - Current control boards** In previous robot control setups, all the motor drives were located in the back of the robot (similar to Fig. A.8, bottom left). This led to a lot of cables reaching from the back of the robot to the motors, encoders, and potentiometers of each joint. Since the new ChARMin setup is modular and has an exchangeable distal part, it is important to reduce this cabling, as the cables need to be unplugged each time the module is exchanged. Furthermore, it is known that

Axis	Maxon Motor	Gear	Ratio (1:x)	Nominal torque
1 (s, l)	RE40	HD, CSG-17-120	120	18.0 Nm
2 (s, l)	RE40	Custom gear & MG, GP 52C	162	22.7 Nm
3 (s)	RE35	MG, GP 42C	113	8.6 Nm
4 (s)	RE30	HD, HFUS-14-100	101	6.3 Nm
5 (s)	RE25	MG, GP 26A & belt gear	250	5.0 Nm
6 (s)	DCX22	MG, GPX22	414	4.7 Nm
3 (l)	RE35	MG, GP 32 HP	159	11.8 Nm
4 (l)	DCX32L	HD, HFUS-14-100	101	9.1 Nm
5 (l)	RE25	MG, GP 26A & belt gear	363	8.3 Nm
6 (l)	RE25	MG, GP26A	278	6.5 Nm

Table 2.4: Actuation, transmission, and nominal torques for the six axes of the ChARMin robot for the small (s) and large (l) distal module. HD=Harmonic drive. MG=Maxon gear.

cables have an influence on the robot joint dynamics [176]. This influence is usually nonlinear and can vary over time and is, therefore, rather difficult to model. In the ChARMin robot, a different approach was taken, where the motor drives for the distal part are located directly on the exoskeleton close to the actuator.

Each of these 'axis controllers' (Fig. 2.16) encompasses the current controllers for two actuators as well as two encoder inputs, two digital outputs, a digital input and three analog inputs. The communication between the boards and the real-time system is implemented using a CAN 2.0 B interface. With these axis controllers, the cabling is reduced to a power cable and a cable for the CAN bus communication. The axis controller boards were developed and built in-house and are very small in size (52x63x18 mm). More technical details about the axis current control boards can be found in Tab. 2.5.

Board interface	
Board supply voltage	48 V
Communication	CAN 2.0 B
Transfer rate	1 Mbit/s
Motor interface	
Max output current	5.5 A
Output voltage	-48 ... +48 V
Sample rate current controller	22.05 kS/s
Encoder input	20 bit
Optional I/O's	
3 Analog inputs	10 bit
1 Digital input	5 V TTL
2 Digital outputs	5 V TTL

Table 2.5: Technical specification of the ChARMin axis current control boards.

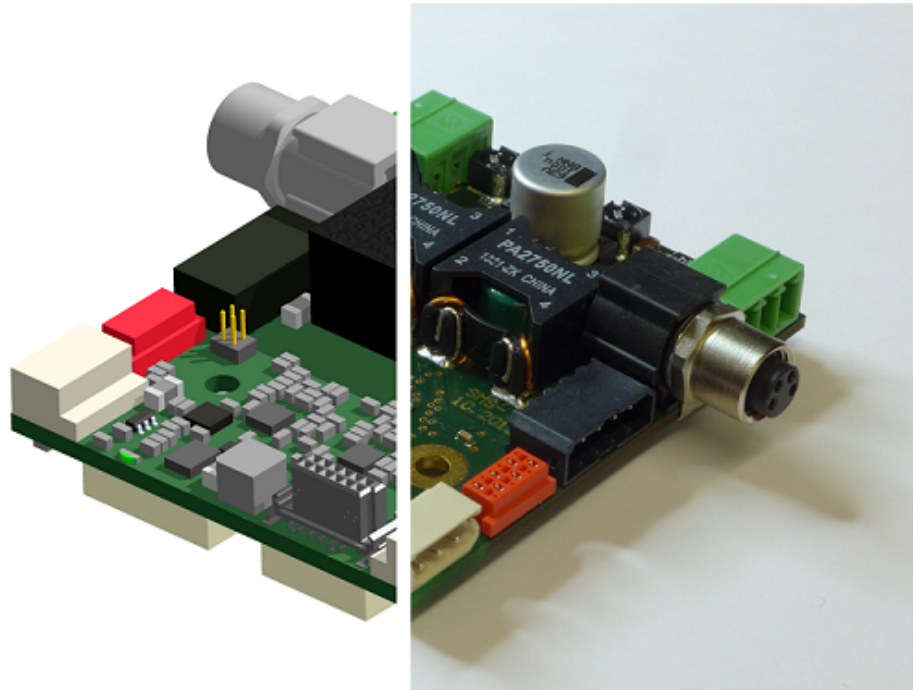


Figure 2.16: Technical drawing (left) and the finished hardware (right) of the newly developed axis controller boards used on the distal part of the ChARMin robot for current control of the actuators and to read sensor information.

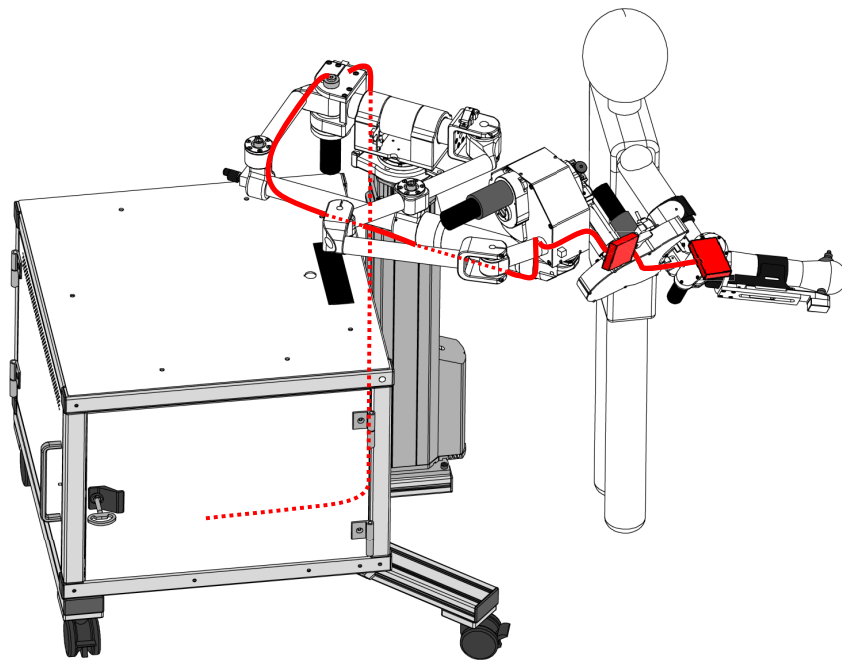


Figure 2.17: Conceptual drawing of the location of the axis control boards on the distal part of the robot and the interconnecting CAN bus and power line.



Figure 2.18: This print screen shows the main menu of the interface software with the different therapy modes. The six available standard games are located at the top and right part of the screen. The button list on the left allows to change the patient settings ('Patient'), to run the assessments ('Assessments'), to calibrate the angular- and end-effector workspace as well as the hand pressure threshold ('Kalibration'), to mobilize the arm in a teach and repeat mode ('Mobilisation'), to change the patient profile ('Profil wechseln'), to connect to another gaming interface using the RehabConnex server ('RehabConnex'), and finally to exit the interface ('Beenden'). Furthermore, the interface shows the currently active patient profile on the bottom center and a warning for incorrect shoulder positioning in the bottom right corner.

### 2.2.4 Virtual Reality Interface

The interface for ChARMin was implemented in the Unity game system (Unity Technologies) by Aniket Nagle. The sample rate for the interface is approximately 15 ms. The communication between the xPC real-time control computer and the visual interface is done using the UDP protocol. Currently, 94 game- and control parameters are sent to the xPC real-time computer and 51 robot parameters are sent back to the unity software. The interface is mostly programmed in German, as the therapists and the majority of the children are German-speaking. To increase the immersion and motivation, a large screen with 32" diagonal is used.

When starting the interface software, the user is asked to check the brakes of the robot wheels, to test the foot pedal, and to select the currently used distal module. After choosing and adapting (when needed) the patient profile the user gets to see the main screen (Fig. 2.18). Here, the different games and other training modi can be chosen, which are subsequently presented.

#### Patient Settings

The patient settings are used to enter the robot length settings and parameters and further information which might be useful for the therapist for a reproducible posi-

tioning (e.g., chair height and a field for free commenting). The patient settings mode also provides assistance for the patient positioning with laser and detection of wrong shoulder position with a proximity sensor pointing to the GHJ. For the second a warning is prompting on the interface screen when the shoulder of the patient moves too far away from the correct position (red message on the bottom right on the interface screen Fig. 2.18). Additionally, the robot can be actively held in any posture to allow the therapist to use both hands for the patient fixation.

### Gaming Interface

Six different games can directly be started from the main menu (Fig. 2.18). The various games are designed to motivate the child for active participation and to train different arm movements. The six games are:

**Ball** The ball game is a single-joint game where a ball is rolling down an inclined plane and has to be hit with a horizontally moving bar at the bottom of the screen (Tab. 2.6 a). The position of the bar is controlled with one of the six ChARMin joint axes defined by the therapist.

**Whack-a-mole** The whack-a-mole game can be played in a single-joint or multi-joint mode. The end-effector is represented with a hammer on the screen (Tab. 2.6 b). The hammer stays at a predefined height above a table, independent of the real end-effector height, and can be moved in the transverse plane. By applying pressure to the handle, the hammer moves down to the table to hit moles which appear from holes in the table. For the single-joint mode, the game is reduced to a single row of three wholes and the hammer is moved horizontally by changing the joint angle of the axis chosen by the therapist.

**Tennis** In the tennis game, the racket is moved in the frontal plane by changing the hand position. The ball which is shot by the computer opponent has to be caught (Tab. 2.6 c). A visual aid can be enabled to show where the ball needs to be hit, for patients who have problems to estimate where the ball will arrive.

**Spaceship** In the spaceship game, a spaceship is selected and during the constant speed flight in space blue target spheres have to be collected and approaching obstacles need to be avoided (Tab. 2.6 d).

**Diver** The diver in this game is walking with constant speed on the sea floor and is hunting treasures (Tab. 2.6 e). The robot end-effector position is used to move around the cross hairs of the diver's bubble gun. The aim is to collect as many treasures as possible (to increase the score) while shooting approaching pirate fishes, obstacles, and air bubbles (to refill the air tank).

**Airplane** The player chooses an airplane or a bird and flies through the sky. The airplane is moved in the frontal plane by changing the robot's end-effector position. The aim is to collect balloons (to increase the score) and hearts (energy refill) while avoiding other flying objects (Tab. 2.6 f).

All the games are scaled to the workspace, joint angles, and hand pressure previously defined in the calibration menu. Each game has its settings that can be used to adapt the difficulty of the game, the visual appearance, the duration of the game and the



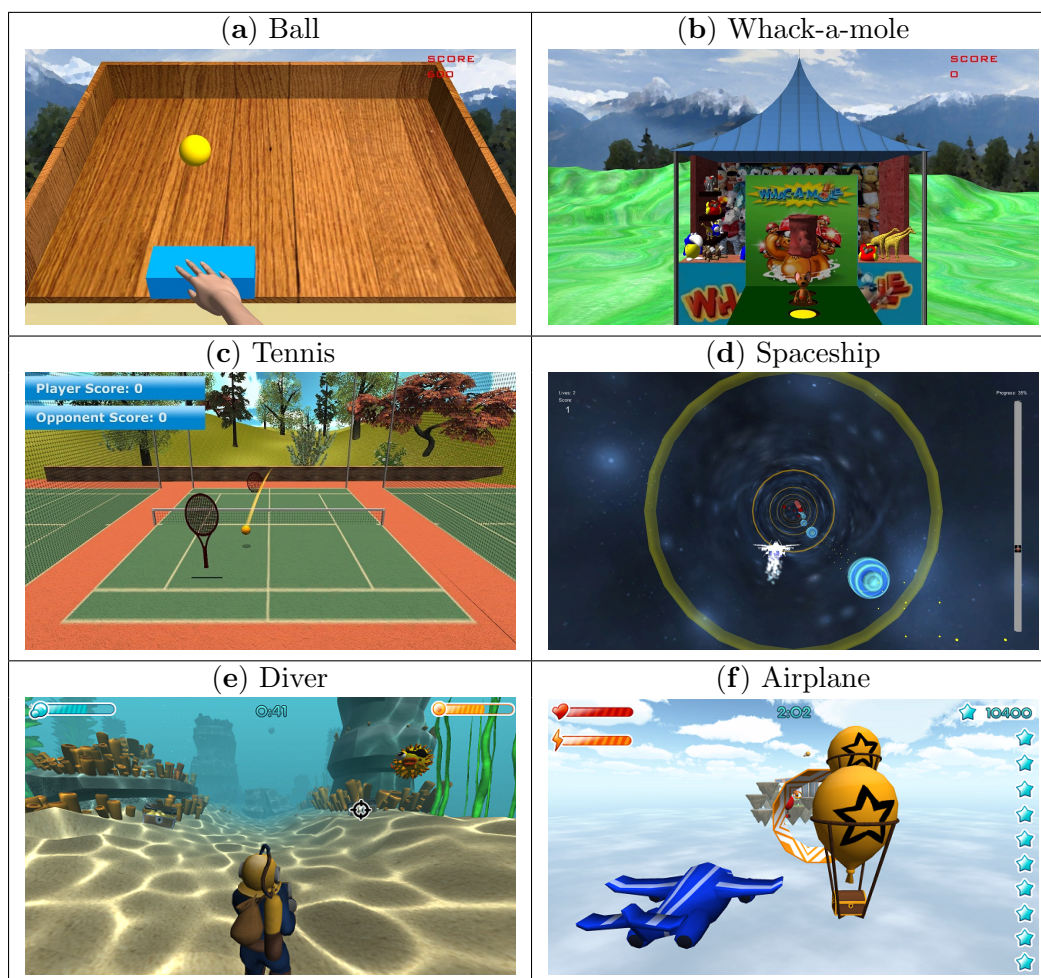


Table 2.6: Screenshots of the six games which can be played with the arm therapy robot ChARMin.

support the robot should provide. In each game, the arm support can continuously be changed from free non-supported movements to completely guided movements (detailed information about the controllers in Sec. 3). These adjustment possibilities allow optimal support of the patient to provide a challenging training environment. In advance of the ChARMin feasibility study, the acceptability of this interface was tested with five patients using the ArmeoSpring (Hocoma AG, Volketswil, Switzerland).

### Assessments

The six different robot-assisted arm assessment packages which are available can be started from the interface main menu. The assessments were evaluated in adult SCI patients (Sec. 4.1) and tested in first case trials with children (Sec. 5.3.3). The assessments are presented in more detail below in Sec. 4.1.2 and Sec. 4.2.2.

### Calibration

The calibration menu is intended to define the Cartesian workspace (x-, y- and z-direction) which the hand can cover and the joint range for all axes. This information



is used to define the range in which the games are played, i.e., where a target has to be positioned such that it can be reached. The calibration of the workspace only affects the multi-joint games, whereas, the joint range settings are used for the single-joint games such as the ball and the whack-a-mole game (in single axis mode). Finally, the maximum bulb pressure is recorded which can be applied by the user. To trigger events in the gaming software, an 80 %-threshold of the maximum pressure has to be reached.

### Mobilization

The mobilization mode allows teaching an arbitrary movement to the ChARMin robot. This movement trajectory is recorded, filtered, and replayed by the ChARMin robot as long as the therapist desires. This mode was earlier introduced for the adult ARMin robot [101] and was required for the pediatric version as well (requirement 2.1.1).

### RehabConnex

The ChARMin robot can be connected to other software interfaces using the RehabConnex server which was developed in the framework of the iMiC (Innovative Movement-Therapies in Childhood) project [177]. Currently, the Tornalino game (Fig. 2.19), developed by the ZHdK Zurich (Zürcher Hochschule der Künste - Zurich University of the Arts, Switzerland), can be played additionally to the six standard games presented above.

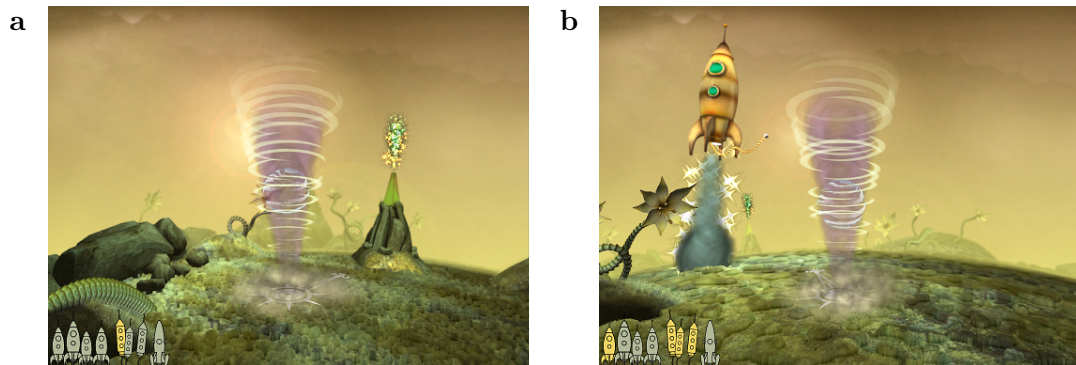


Figure 2.19: The Tornalino game (ZHdK Zurich, Switzerland) can be played with the ChARMin robot using the RehabConnex Server developed in the iMiC project. The hand movement of the patient is transformed to the movement of a Tornado which moves on the surface of a small planet. The task is to (a) collect the sparks from a volcano and (b) to launch a rocket by igniting its fuze.

### 2.2.5 Safety

Different mechanical, electrical, software-related, and operator-related safety features are used to assure that the robot can be used in the clinical environment with children:

**Mechanics** The robot hardware features mechanical end stops for all joints and all length adjustments and a passive spring mechanism ensuring that the robot is statically balanced in case of power loss (Sec. 2.2.1). In this context, a quick release of the patient has to be enabled. Furthermore, the joints are backdrivable and the device has no sharp edges.

**Electronics** Different sensors are mounted to supervise the functionality of the robot, i.e., redundant position sensors for each joint, a dead-man switch pedal and two emergency stop buttons for the therapist to unpower the motors and stop the therapy session at any point in time. Furthermore, four sensors are provided to measure the temperatures of the motors 3 to 6, a sensor to check for correct left/right configuration and a proximity sensor to monitor the proper fixation of the distal module. A watchdog electronic supervises the functionality of the real-time control computer.

**Software** The three different software units (interface software, control software, and ChAxis software) in the ChARMin architecture (Fig. 2.20, light blue boxes) fulfill supervision and safety-related tasks. The control software has to continuously check for plausibility and operability of the system. This includes observation of the end-effector speed (max. 1.0 m/s), checking the electronic supply voltage (48 V and 5 V levels), supervision of position-control errors, comparison between desired and actual motor current, checking the connectivity and operability of the current control boards and testing the plausibility of the sensor range and the received commands from the interface and current control boards. A list of errors that the control software can detect is appended in A.2.2. Moreover, the Unity software and the peripheral axis control boards check for plausibility of the values and for functionality of the real-time computer. The small distal module has a dangerous pinch point which is protected with a touch sensor which stops the robot immediately when contacted.

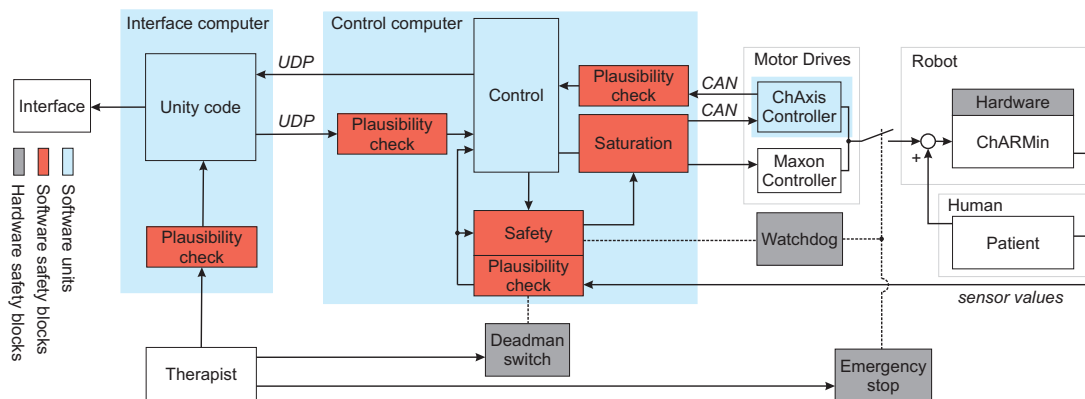


Figure 2.20: Overview of the software architecture and the existing software, electronic and hardware safety features.

**Operability** An extensive handbook, biannual robot maintenance, a monthly safety check and a password protected computer are provided and only educated staff may use the robot.

**Norms** The robot was built according to the norm for medical electrical equipment (EN 60601-1), the international standard for the application of risk management to medical devices (ISO 14971), the clinical investigation of medical devices for human subjects - good clinical praxis (ISO 14155) and the international standard for medical device software (IEC 62304).

## 2.3 Results

### 2.3.1 Realization of ChARMin

The very first prototype for preliminary tests of the software and control only had 4 DoF (Appendix A.2.5). The distal DoF for pro-/supination of the forearm and wrist extension/flexion were added afterwards and, therefore, the robot extended to 6 DoF. The presented design of ChARMin has 6 DoF and was developed according to the clinical and technical requirements described in the requirements section (Sec. 2.1.1) of this chapter. The different features described in the previous design section were realized in the robot. All the non-standard robotic parts were fabricated in-house in our workshop by our expert multi-skilled mechanics. The resulting ChARMin hardware is presented in Fig. 2.21.

A first challenge was to cover the large range of the pediatric target group, which was solved by using a modular design of the robot. The first two axes cover the whole range while the more distal DoF can be exchanged for 5 to 13 and 13 to 18 years old children respectively. In Fig. 2.21 it can be seen that the proximal and two distal parts were anodized in different colors for an easy differentiation between the modules and to achieve a children-friendly appearance of the robot.

The finalized ChARMin prototype with its six DoF has a passive gravity compensation to reduce the torques and, therefore, the size of motor 2 that lifts most of the robot arm weight. When unpowered, the robot is statically balanced and backdrivable. The spring pretension can easily be adapted, according to the distal module which is mounted on the robot. The small distal module weighs 5.7 kg and the larger one 7.5 kg. The change of side and exchange manipulations are working as intended, however, it is important to follow a clear step by step procedure which has to be practiced and which is not straightforward.

### 2.3.2 Adjustment to Patient

#### Length Settings

The resulting ChARMin length characteristics are for the upper arm (0.21 m ... 0.36 m), forearm (0.14 m ... 0.29 m) and the wrist-to-handle distance (0.05 m ... 0.10 m), the circumference of the upper arm ( $40 \cdot 2\pi$  m ...  $100 \cdot 2\pi$  m) and forearm ( $40 \cdot 2\pi$  m ...  $75 \cdot 2\pi$  m), as well as the sitting shoulder height (0.90 m ... 1.30 m). The detailed ranges for the different modules are listed in Tab. 2.7. The corresponding range for the length scales on the robot is given in Tab. 5.8.

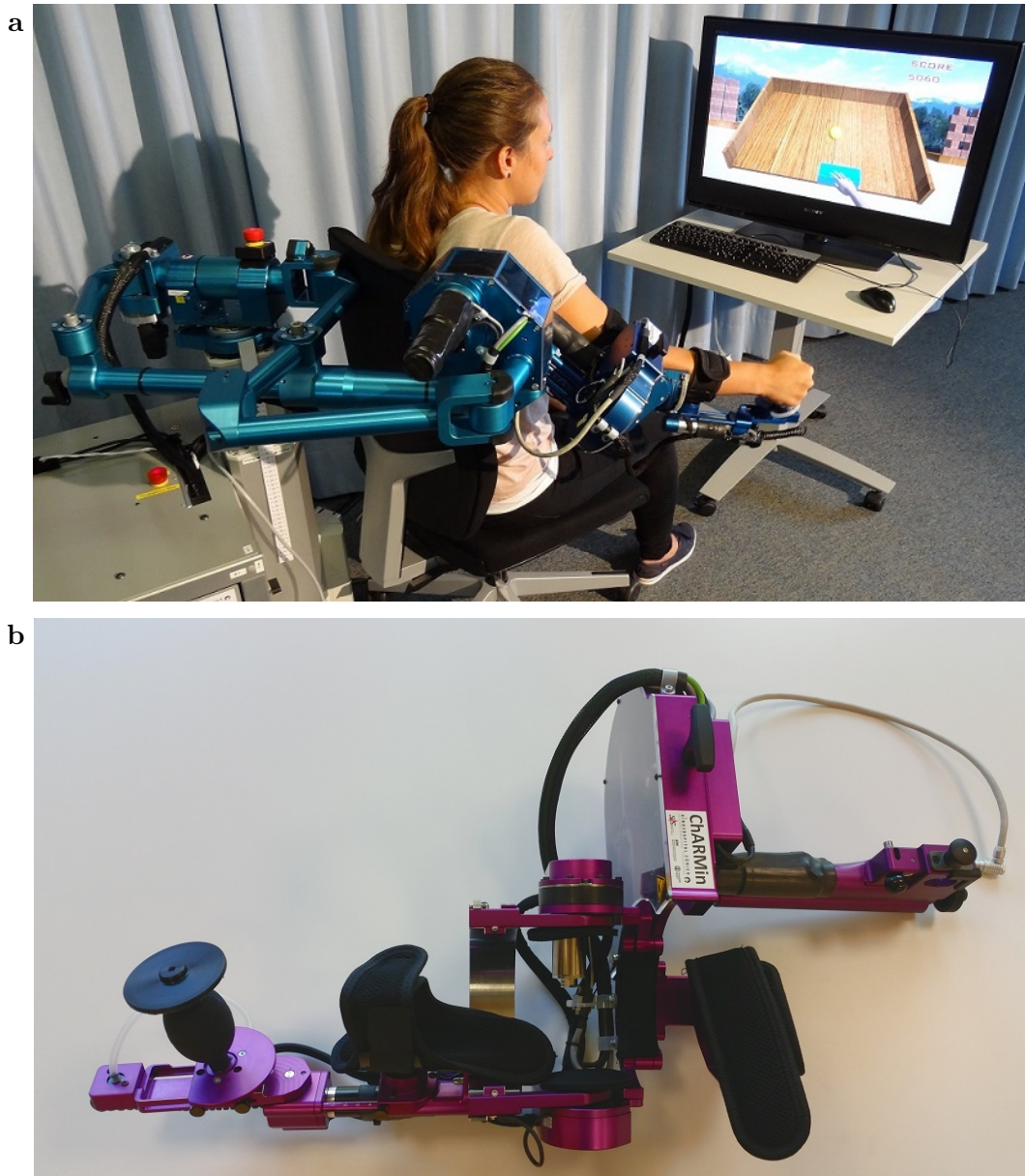


Figure 2.21: (a) First ChARMin prototype with six DoF and a healthy subject. The picture shows a possible setup with the audiovisual display for the therapy. (b) Larger distal module for ChARMin that covers 13- to 18-year-old children.

	Small distal part		Large distal part	
	Min	Max	Min	Max
Shoulder height [mm]	900	1295	900	1295
Upper arm length [mm]	211	336	233	363
Upper arm circumference [mm]	$40 \cdot 2\pi$	$70 \cdot 2\pi$	$60 \cdot 2\pi$	$100 \cdot 2\pi$
Forearm length [mm]	129	204	187	288
Forearm circumference [mm]	$40 \cdot 2\pi$	$75 \cdot 2\pi$	$40 \cdot 2\pi$	$75 \cdot 2\pi$
Wrist-grip distance [mm]	46	71	52	102

Table 2.7: Range for the length adjustment of the small and large distal module. Shoulder height is measured from the floor. Forearm length is measured from the epicondyles to the wrist joint.

Axis	Min. angle [°]	Max. angle [°]	Static friction [Nm]	Joint inertia [kg·m <sup>2</sup> ]	Mech. play [°]
1	-10	95	1.6	2.45	0.05
2	50	130	3.0	0.82	0.63
3	-30	70	0.6	0.11	0.45
4	0	120	0.5	0.06	0.03
5	-90	90	0.2	0.09	0.10
6	-70	70	0.2	0.09	1.39

Table 2.8: Achievable joint range of ChARMin (for both, the small and the large distal module) for axis 1 to 6 and the static friction, joint inertia and mechanical play of the small distal module.

### Joint Range

The ROM of the robot joints covers most of the activities of daily living (Tab. 2.8). The joint range of the two distal ChARMin modules does not differ. In the direction of the internal rotation the range was reduced using mechanical end stops to avoid collisions with the legs of the sitting patient. The shoulder extension is likewise reduced, to stay above 50°. As a consequence, the shoulder extension axis can currently not exceed 130°, due to the symmetry of this axis for the left and right arm configuration. But this range covers most functional activities as defined by [164].

### 2.3.3 Spring-Induced Compensation Torques

To validate the spring compensation model, the torque was recorded which the motor needs to apply to move axis 2 when no distal module is attached and only the compensation torque is acting on the motor axis. For this test, axis 2 was moved with a position controller in the whole range of axis 2. The results are shown in Fig. 2.22. When moving against the spring compensation mechanism, the motor additionally needs to overcome the joint friction to move the axis, while moving in the same direction in which the compensation acts, the friction is overcome by the spring compensation mechanism. As a consequence, the first measurement is the spring compensation torque with the joint friction (blue line). The second measurement is the spring compensation torque with the friction subtracted (green line). The mean between the two measurements is, therefore, the torque from the spring compensation

mechanism (black line). The spring model used for the control is plotted in Fig. 2.22 in red. The model matches very well the torques generated by the spring compensation mechanism.

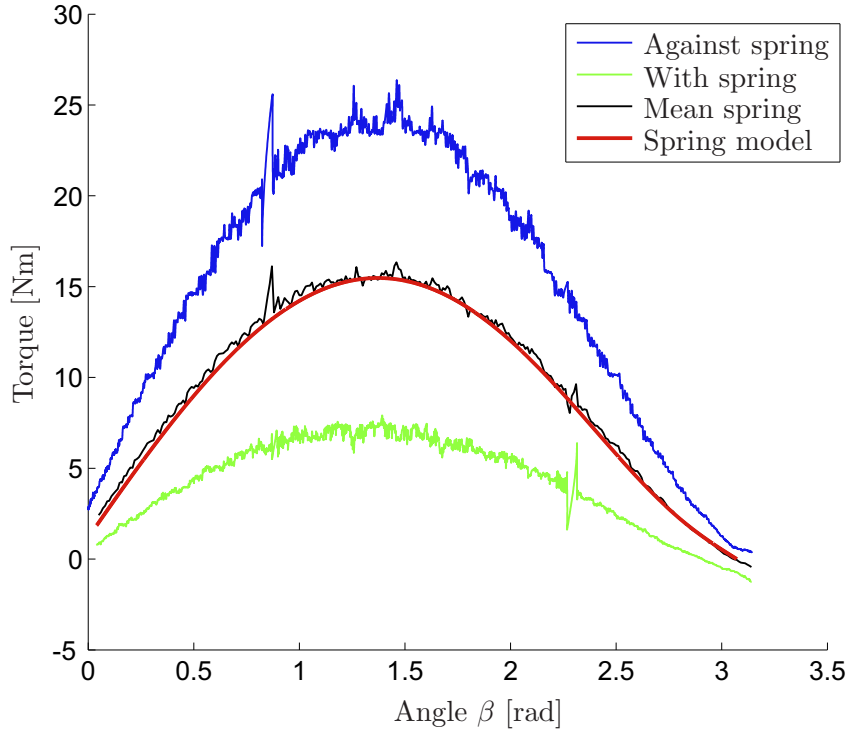


Figure 2.22: The model for the spring compensation mechanism was validated by measuring the motor torque needed to move the passive gravity compensation mechanism, when no distal module is mounted. The top graph is the torque needed when moving against the direction in which the compensation torque is acting. The lowest graph shows the torque required to move in the direction of the compensation. The graphs in the middle show the mean values and the spring model used for the compensation.

### 2.3.4 Mechanical Play

The mechanical play was measured by comparing the analog sensor value with the digital sensor value, as these sensors are located on the two opposite sides of the mechanical play, i.e., the planetary gear, the belt transmission or the curved guidance. The mechanical play coming from a bending structure cannot be evaluated, when only the absolute and digital sensor are compared. However, the mechanical play due to a bending structure is expected to be rather low. The results are shown in Tab. 2.8. Axes 1 and 4 have little mechanical play, because of the harmonic drives used.

### 2.3.5 Static Friction

The static friction torque was measured with an externally applied force sensor, type 9205, KISTLER, Switzerland. The force needed to initiate a joint movement was recorded and the joint torque calculated. The static friction values are listed in Tab. 2.8.

### 2.3.6 Inertial Properties

The inertia of the first axis was calculated by using a least squares fit of a spring-mass-damper model to the motor torques needed to follow a reference sine chirp signal. The inertia for the more distal axes (2 to 6) was estimated using the CAD model of the ChARMin exoskeleton. The results are listed in Tab. 2.8. The estimated robot inertias around the motor axis ( $I_a$ ) were calculated by adding the reflected inertia of the motor ( $n^2 \cdot I_m$ , with  $n$  being the gear ratio) to the estimated link inertia ( $I_l$ ) around the axis with the robot length settings in the middle of the adjustable range:  $I_a = I_l + n^2 \cdot I_m$ .

### 2.3.7 Torques

The torques that the robot can apply (Tab. 2.4) will be enough to provide support during the therapy and can temporarily be overloaded if needed, e.g., for the strength assessment. The torques for the first two axes are high compared to the other axes as they are mounted on the proximal part and, therefore, move more mass than the others. Moreover, these two axes actuate the shoulder joint which is very strong.

### 2.3.8 First Adaptations

After preliminary tests with the finished prototype, a couple of improvements had to be included in the robot. The ball bearing for the custom-made curved linear guidance in the small distal module did not withstand the rather high torques that are produced when applying forces to the hand module or performing the bandwidth test. Therefore, the ball bearings were removed and slide bearings were introduced. This change increases the static friction but sustains the torques. Furthermore, plastic slide bearings inside the toggling mechanism had to be replaced with brass bearings. At the elbow and close to the upper arm cuff additional cushions had to be mounted to avoid that the patient's arm touches metal parts of the robot.

## 2.4 Discussion

In this chapter, the hardware and interface of the new ChARMin arm robot for children with CP was presented. ChARMin was built at the SMS Lab, ETH Zurich, Switzerland, in collaboration with the Rehabilitation Center for Children and Adolescents, Affoltern am Albis, Switzerland and is the successor or the ARMin robot for adults (a comparison between the two robotic platforms is given in Appendix A.2.6). It was shown how the challenges given by the pediatric target group influenced the geometric design, the kinematics, the actuation, the electronics and the implemented safety features in the ChARMin robot. The technical data sheet for ChARMin can be found in Appendix A.2.6. The design is based on clinical and technical requirements stated in the beginning of the chapter (Sec. 2.1.1). An overview of the different requirements is given in Fig. 2.23 and the according solutions are summarized in Tab. 2.9 and 2.10. In the following, the different requirements will quickly be discussed.

**Target group** The challenging requirements to cover the anthropometric range of the target group could be met with a modular design which includes serial and parallel kinematic structures to achieve a highly adjustable and safe design of a robot that can cover children aged 5 years and older. The robot actuates six joints including shoulder,

Table 2.9: Summary of the most relevant clinical and technical requirements for the CHARMin robot (Part I).

Requirement	Details	Implementation/solution
Target group	Cover children aged 5 to 18 years Actively support six arm joints Active or passive hand module	Modular design Exoskeleton with six actuated joint axes Passive pressure-sensitive hand module <sup>a</sup>
Anthropometry	Adaptable to all arm size	Robot adaptable to the upper arm, forearm, hand length, shoulder height, and arm circumferences <sup>b</sup>
Range	Cover joint range for functional activities	Maximized robot joint ranges while ensuring safety <sup>c</sup>
Kinetics	Counteract a spastic arm and hold posture during isometric strength assessment	Actuators and gears dimensioned to get close to the joint torques that a healthy subject can apply <sup>d</sup>
Motivation	Keep the patient motivated during the arm training	Audiovisual interface with various game-based virtual reality scenarios to motivate the child for active participation
Assistance	Support of the patient arm as needed to keep the training challenging but not boring or over-straining	Arm support can continuously be changed from free arm movements to completely guided movements

<sup>a</sup>Active support desired. <sup>b</sup>With minor limitations for growth-retarded severely affected 5-year-old children. <sup>c</sup>The joint range is restricted in shoulder extension and shoulder internal rotation for safety reasons. <sup>d</sup>Only axes 1 and 5 cover the joint torque of a healthy subject. The others range between approx. 30% (elbow flexion) and 75% (shoulder flexion) of a healthy subject (when shortly operated at double nominal current).



Table 2.10: Summary of the most relevant clinical and technical requirements for the ChARMin robot (Part II).

Operability	Easily adjustable	Robot is mobile and can be easily adjusted with a lifting column and several cranks
Therapy modes	Applicable for right and left side Mobilization Assessments Games	Mechanism to turn the exoskeleton to the opposite side A movement can be taught to the robot and replayed Robotic-assisted assessments measure arm motor functions Single- and multi-axis games to motivate the patient
Safety	No mechanical parts close to the trunk or the head Always stay in the anatomical joint range Safe robot position in case of power loss Quick release of the subject at any time The therapist can always switch off the robot Checking plausibility and operability of the system	Remote center of rotation kinematics for the shoulder Mechanical joint end stops Passive gravity compensation and backdrivable joints Only two Velcro® fasteners for quick release of the arm A foot pedal or hand switch powers the robot Watchdog, redundant sensors, supervision of signals, etc.
Technical	Little static and dynamic friction Little backlash Position control bandwidth of at least 2 Hz	Parallel kinematics, choice of drive trains and dithering Harmonic drives where possible <sup>e</sup> Position control bandwidth of 2.1 Hz or higher in all joints

<sup>e</sup>Axes 2, 3, 5, and 6 have no harmonic drive and, therefore, increased mechanical play (Tab. 2.8).

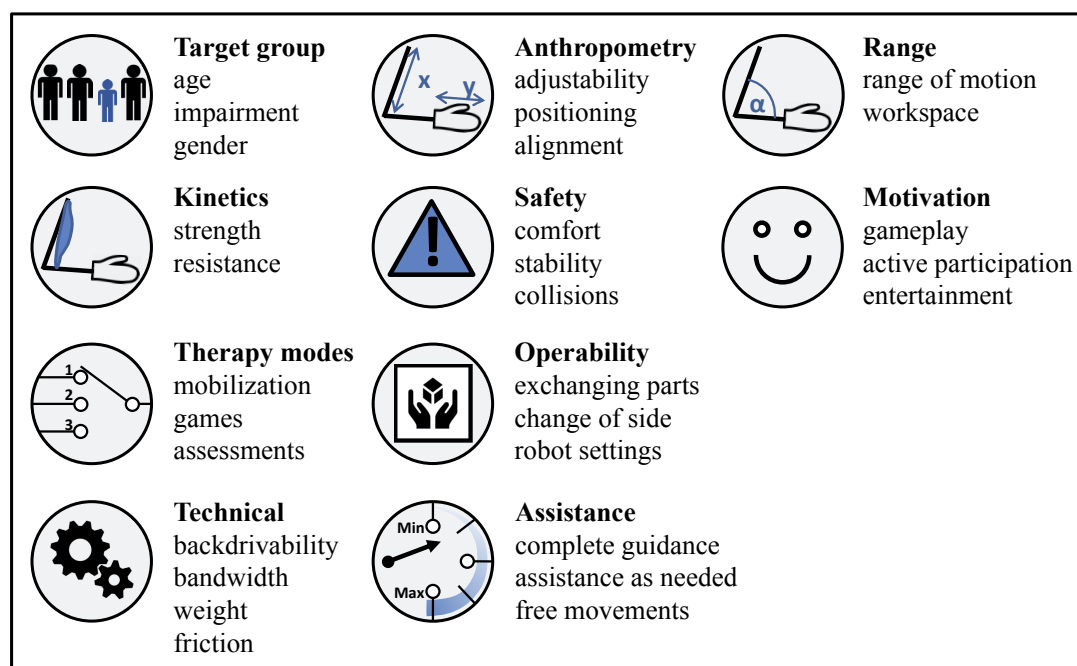


Figure 2.23: Summary of the different requirement categories and aspects covered by the new robotic design.

elbow and wrist for either the left or right arm. The hand grasps a pressure-sensitive bulb which is used to trigger events while playing the games. To allow the vertical displacement of the GHJ, an offset was introduced in axis 2. Contrary to the adult device, this distance had to be fixed and could not be realized to be adaptable as in ARMin.

**Anthropometry** Different robot length settings allow to adjust the robot to the length of the upper arm, forearm, and hand, to the height of the shoulder and the circumference of the different arms. The upper arm length of the robot is not sufficiently short for 3-years-old children. Furthermore, the length characteristics given in the requirements (Tab. 2.1) for the upper arm are for the acromion-radiale length which is slightly longer than the distance needed. As a consequence, the positioning of a severely affected 5-year-old child leads to an increase shoulder offset and larger vertical shoulder movements. It needs to be considered individually for severely affected and young patients, whether this produces problems in the applicability of the robot.

**Range** The range of motion for axes 2 (shoulder extension) and 3 (shoulder internal rotation) was reduced for safety reasons. However, as movements to these regions of the workspace are not instructed this reduction should not restrict the user's arm movement.

**Kinetics** The nominal torque that can be applied by the robot is slightly less than what a strong person can apply. In case that these torques are too small, the motors could be overloaded to produce up to five times the nominal torque. However, this will require a more detailed model of the motor winding temperatures.

**Motivation** An audiovisual interface (Fig. 2.21, screen in **a**) is used to provoke active participation of the child by using six different game-like training scenarios. Moreover, the interface software can serve as a middleware and connect to other games, such as Tornalino [177]. First preliminary trials with the gaming interface and the passive ArmeoSpring robot showed good acceptance by the patients and the potential to motivate the child to play the games (own observation).

**Assistance** All the six joints of the robot are actuated to actively assist or guide the patient's arm on single-joint and multi-joint level. The control strategies to support the patient are introduced in the ChARMin control chapter (Chap. 3).

**Operability** The robot can be used for the left and right arm and the distal module can be exchanged. A drawback of the system is that the weight of the distal module might lead to difficult handling of the 'change-of-side' mechanism and may hamper the exchange of the distal module. It requires practice and needs evaluation by therapists in the clinical environment.

The robot is mobile with lockable wheels for transportation and for positioning with respect to the patient. The cuffs and cushions provided ensure a soft and comfortable fixation of the patient. All the parts which are in contact with the patient (including the cuffs, cushions and the rubber bulb) can be exchanged and cleaned when needed.

**Therapy modes** Different therapy modes can be chosen with the software interface including game scenarios, mobilization, calibration, and assessments. Furthermore, the interface is used to setup the robot and to instruct and assist the therapy.

**Safety** Safety requirements could be fulfilled regarding the hardware, electronics, control software, and operability.

Compared to the adult ARMin robot, the actuator of axis 1 was moved away from the child's head (Fig. 2.24). A parallel kinematic structure is used to actuate this joint. This structure provides the requested range but makes it impossible to include the existing passive gravity compensation mechanism. Therefore, a novel mechanism was developed which can be used for the left and right arm configuration of the robot. The produced offset torque deviates slightly from a desired sinusoidal shape but the motor can account for this using the accurate model for the spring compensation mechanism derived above (Sec. 2.3.3). For safety reasons this mismatch is not critical, as the robot arm is still enough compensated to not fall down quickly in case of power loss. For all the joints mechanical end stops are provided. The patient is attached to the robot with cuffs using Velcro<sup>®</sup> fasteners for quick release at any point in time. The backdrivable joints also allow to move the robot when unpowered and, therefore, to better release the patient.

To guarantee the safety of the robot and to receive approval for the application of the robot with children, different technical norms had to be fulfilled and applied to the robot. The robot is conform with the norms EN 60601-1, ISO 14971, EN 980, EN ISO 14155 and IEC 62304 and its use was approved by the Swissmedic (Swiss Agency for Therapeutic Products, reference number: 2015-MD-0009).

**Technical** The robot joints have small backlash, are backdrivable and have sensitive and redundant position sensors.

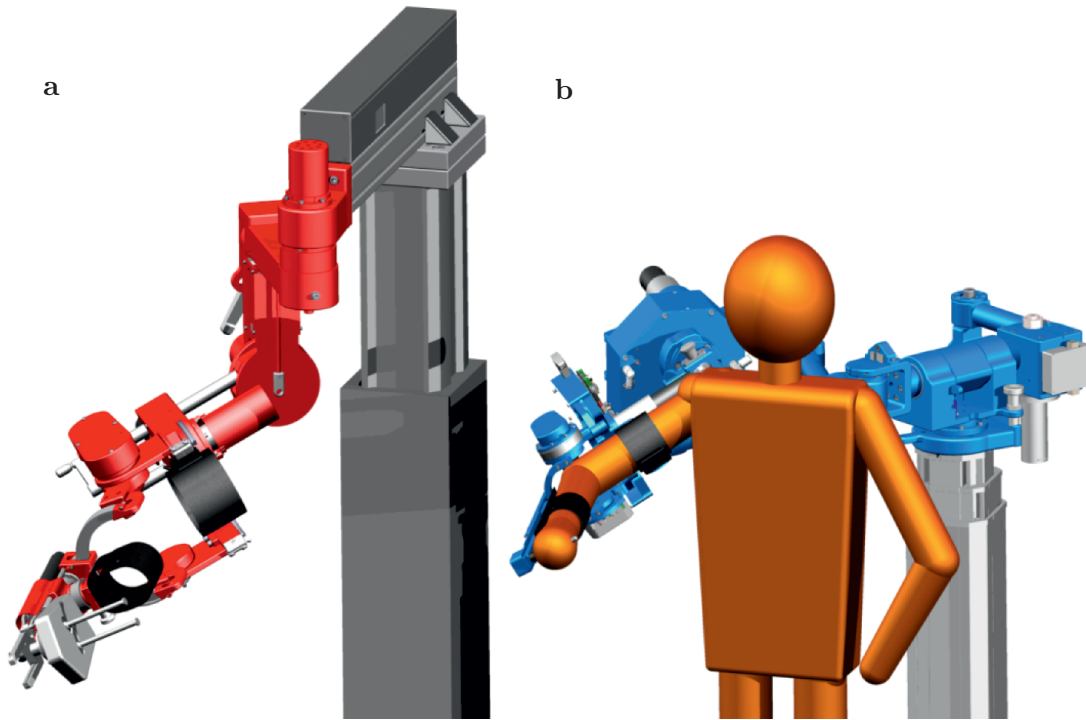


Figure 2.24: The two arm exoskeletons (a) ARMin and (b) ChARMin (shown with a simplified body model of a 13-year-old child).

For a transparent robot, the static friction has to be as low as possible. All the joint axes (mainly the first two axes) still have quite some static friction (Tab. 2.8). A comparison with the friction torques measured for ARMin IV (Tab. 2.11) reveals that the static friction for axis 1 is much higher in ChARMin (1.6 Nm) than in ARMin (0.2 Nm). The increased static friction probably comes from the parallel kinematic structure, as the other components such as the actuators and gears are comparable in the two robots. The static friction in axis 2 is in both robots quite high because of the passive gravity compensation mechanism affecting the joint friction. The static friction in axis 3 is much smaller in ChARMin, which can be assigned to the parallel kinematic structure, which has less friction than the curved guidance with the belt transmission. The drive train in axis 4 is very similar in both robots and, therefore, it is not surprising that the static friction is identical.

ARMin joint	Friction torque [Nm]
Axis 1 (Shoulder horizontal add-/abduction)	0.2
Axis 2 (Shoulder extension/flexion)	2.4
Axis 3 (Shoulder internal-/external rotation)	2.1
Axis 4 (Elbow extension/flexion)	0.5

Table 2.11: Static friction in the ARMin IV joints was measured for the first four joint axes.

The transparency could be reduced with the decentralized current controller setup which decreased the cabling and, therefore, the disturbing forces coming from the cables. The transparency could potentially be further improved by using force/torque

sensors, by reducing mass and inertia of the robot or by using a SEA approach. The SEA design, however, was excluded because of the quite slow movements during the therapy. A series elastic actuation is rather interesting for more dynamic movements. Moreover, the elasticities of the SEA have to be as close as possible to the interaction point, as the inertia of robotic parts between the elasticity and the human arm can not be compensated. This requires a SEA design with several degrees of freedom, which leads to a complex design (as in [178] or [179]). Exoskeleton designs with a SEA on joint level were introduced before [180], however, with rather heavy actuators (1.3 kg) which cannot be used for the exchangeable distal part of the ChARMin robot. The negative influence of the cables on the transparency of the robot was reduced in our new electronics design. The motor drives are directly located on an axis control board on the corresponding robot axis, which reduces the cabling to only one data cable and a power cable along the robot structure.

Compared to existing actuated arm robots that have been used with children [141, 146, 147], the exoskeleton structure of ChARMin has several advantages including the large range of motion, the completely defined arm posture, and the possibility to train and measure single-joint movements as well as three-dimensional reaching movements in space.



# 3 ChARMin Control

## 3.1 Introduction

In the previous chapter, the hardware and the interface of the ChARMin robot was described. To perform the assessments and games implemented in the interface a dedicated control is needed which moves the robot exoskeleton and supports the patient. It is required for the robot that the active assistance covers the range from free non-supported arm movements to completely guided movements (Sec. 2.1.1) to support young patients with different levels of impairment. An active contribution to the movement is crucial for the effectiveness of the rehabilitation training. To motivate the patient's active contribution to these movements, it is important that the robot is not completely guiding the arm but cooperatively assisting the arm as much as needed. An assist-as-needed (AAN) controller can help the patient to complete a movement and allows for position and timing errors, since making errors is known to drive motor learning [181], while fixed guidance rather hampers the learning process [182]. As a further enhancement, the game-like scenarios with audiovisual feedback can instruct and challenge the patient and motivate to remain active during the training.

In the literature, various support strategies have been described to assist the patient. A detailed review of haptic control strategies, especially for the training of complex movements, can be found in Sigrist et al. 2012 [183]. First, impedance control approaches aim to increase the compliance of the robot in order to allow the patient to deviate from a predefined trajectory [184]. But to promote an active contribution of the patient to the arm movement, controllers were introduced that try to minimize the robot support and allow for spatial freedom while providing sufficient support that the patient can fulfill the desired task, e.g., controllers following an AAN approach [185, 186]. However, these control strategies do usually not allow for temporal freedom. A solution to this problem is the use of a virtual tunnel which is rendered around a given path in space, rather than using a predefined trajectory [186, 187]. This allows freedom in terms of timing and possible deviation from the path and enables the patient to vary the movement and to perform the 'repetitions without repetition' (according to Bernstein [39]). This kind of controller is often referred to as path controller and has been used for supporting periodic movements in task space [188, 189] and in joint space [190, 191] as well as for point-to-point movements of the arm [64, 187].

The less support the patient needs and the more the patient performs the movement on his own, the more important it becomes, that the robot is not hindering the movement of the patient and behaves transparent (as stated in the requirements, Sec. 2.1.2). Therefore, the friction and mass of the robot should be compensated. For this reason, an accurate model of the robot was developed and is further explained below. For patients who only need gravity compensation without a directional support and for the assessments, a simple arm gravity compensation model is foreseen. For severely affected patients and instructional purposes, a position control can be applied for complete guidance of the arm.

Finally, to train complex three-dimensional arm movements as well as individual joint movements, multi-joint and single-joint movements have to be assisted.

To cover all these requirements for the different levels of impairment, the single- and multi-joint support, and the various game-scenarios, different control paradigms were implemented depending on the training mode and support chosen. An overview of the training modes and the controllers used is given in Tab. 3.1. The mentioned controllers are discussed in the following sections.

Mode	Component	Controller used
Setup	Hold posture	Position control <i>with current posture as RP</i>
	Testing GC	Free movement <i>with GC</i>
Calibration	Workspace	Free movement <i>with GC</i>
	Joint angles	
	Hand pressure	
Mobilization <sup>a</sup>	Record	Free movement <i>with GC</i>
	Reply	Position control <i>with previously recorded RP</i>
Assessments	ROM	Position control <i>with predefined posture as RP</i> Free movement <i>with GC for single joint</i>
	WORKSPACE	Free movement <i>with GC</i>
	QOM	Free movement <i>with GC</i>
	STRENGTH	Position control <i>with predefined posture as RP</i>
	RPM	Position control <i>with RP inside passive ROM</i>
	CIRCLE	Free movement <i>with GC</i>
Games	Ball	Free movement <i>with GC</i> Single-joint support
	Whack-a-mole	Free movement <i>with GC</i>
	Tennis	Free movement <i>with GC</i> AAN path control Position control <i>with online calculated RP</i>
	Spaceship	Free movement <i>with GC</i> AAN path control Position control <i>with online calculated RP</i>
	Diver	Free movement <i>with GC</i> AAN path control Position control <i>with online calculated RP</i>
	Airplane	Free movement <i>with GC</i>

Table 3.1: Control strategies used for the different therapy modes. GC = Gravity compensation, RP = Reference positions. <sup>a</sup>The recorded joint angle data during the mobilization modus is simplified using splines before it is saved for a later reply (according to [168]).

### Control Architecture

An overview of the control architecture is given in Fig. 3.1. The controllers for ChARMin are implemented in MATLAB/Simulink (MathWorks) and are executed on a PC system using the xPC target real-time environment (Fig. 3.1, *xPC real-time PC*). The sampling frequency of the control system is 500 Hz. A second computer is



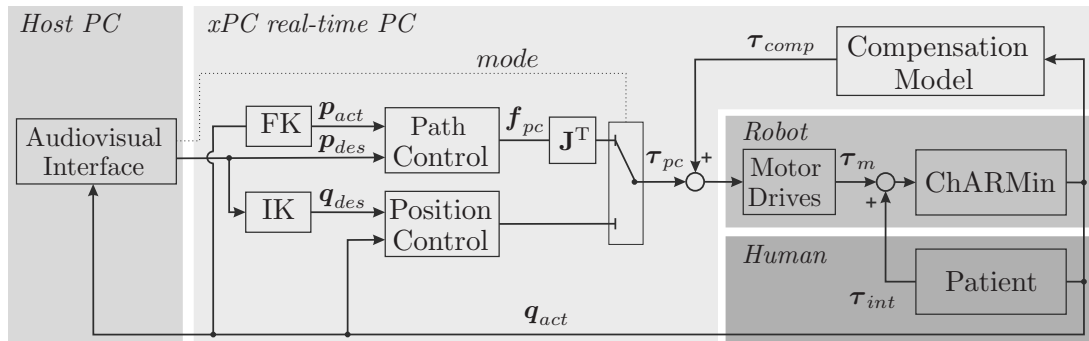


Figure 3.1: Simplified scheme of the ChARMin control system shown with the path- and position controller. Additional controllers for arm mobilization (teach and repeat), single joint support or the simple compensation control are not shown in the chart. Inverse kinematics uses the swivel angle kinematics described in [192]. FK = Forward kinematics; IK = Inverse kinematics;  $\mathbf{p}$  = Cartesian coordinates;  $\mathbf{q}$  = joint coordinates.

used for the audiovisual interface (Fig. 3.1, left). According to the chosen training mode, the controller is selected on the target computer (e.g., path control or position control). The controllers receive information from the visual interface about the positions to support or guide to  $(\mathbf{p}_{des}, \mathbf{q}_{des})$  as well as the current joint angles of the robot ( $\mathbf{q}_{act}$ ). Additionally to this feedback loop, the compensation model block includes the inverse dynamic model (Sec. 3.2.1) of the robot as well as a compensation of the passive spring mechanism (Sec. 2.3.3) and a dithering signal to reduce static friction (Sec. 3.2.1, details below). While the outer control loop is closed by the position- or path controller, the inner loop is a current controller which is executed on the motor drives. For axes 1 and 2 Maxon ADS E 50/5 drives are used in the electric cabinet (Fig. 2.21 a, box bottom left). For axes 3 to 6 in-house built current control boards are used which are directly located on the distal module [2] (details in Sec. 2.2.3).

## 3.2 Method

### 3.2.1 Modeling

A precise model of the robot is necessary to actively compensate for dynamics and static aspects of the robot. This model reduces disturbing interaction torques and improves the control performance by using the inverse dynamics model as a feedforward compensation term, as indicated with the compensation model block in Fig. 3.1.

#### Simplified Robotic Model

For the model-based compensation, a simplified model of the robot was used. The robot was divided into segments which are moved by the actuators, i.e., the mass between the actuated axes. The resulting 6 segments are shown in Fig. 3.2 with gray circles. Each segment has an assigned coordinate system (Fig. 3.2). For each segment, the mass was defined using the CAD model of the robot. The center of mass was calculated according to its assigned coordinate system. Furthermore, the inertia of each segment according to the actuated axis was computed. While the inertia for

axis 2 to 6 was extracted from the CAD model, this procedure was not be applied to the parallelogram structure of axis 1. Instead of calculating the inertia of all the parallelogram components, it was more intuitive and precise to measure the inertia by moving the structure with a position controller and a sine chirp signal reference without the distal part and to fit a spring-mass-damper model to the data received. Segment 2 can change in length when the upper arm length is adjusted. To account for this, the parameters for segment 2 were derived from the two different subsegments 2a and 2b, where 2b is dependent on the upper arm length. The resulting physical parameters for segment 2 (the mass, center of mass and inertia) are also length dependent. This simplified model can be used for further analysis of the robot's dynamics.

### Simplified Human Arm Model

Supporting the patient's arm against gravity is important to provoke active arm movements of the patient (Sec. 1.2). Therefore, a model-based arm gravity compensation is used. Depending on the arm gravity support which is required by the patient, the therapist can change the amount of arm weight which the robot should support against gravity. The patient arm is modeled with three different point masses in the upper arm, forearm and hand. The location and mass of the different mass points was determined using the anthropometric information from Winter 1990 [193]. The masses of the arm segments are given with respect to the body weight (BW):

$$\begin{aligned} \text{Upper arm mass} &= 0.028 \cdot \text{BW} \\ \text{Hand mass} &= 0.006 \cdot \text{BW} \\ \text{Forearm mass} &= 0.016 \cdot \text{BW} \end{aligned}$$

The distance of the centers of mass (CoM) from the shoulder-, elbow- and wrist joint is given with respect to the according segment lengths:

$$\begin{aligned} \text{Upper arm CoM} &= 0.436 \cdot \text{Upper arm length} \\ \text{Forearm CoM} &= 0.43 \cdot \text{Forearm length} \\ \text{Hand CoM} &= 0.506 \cdot \text{Hand length} \end{aligned}$$

### Equations of Motion

The equations of motion were calculated to obtain a dynamic model of the robot which can be used to compensate the robot in the control. With the simplified model from the previous section, the positions and speeds of the centers of mass can be described in the initial coordinate system, dependent on the segment lengths, the posture of the robot, and the chosen distal module. Given the position and the speed of the centers of mass (using the same rotational matrices as for the direct kinematics in Sec. 3.2.1) the kinetic energy  $T$  and the potential energy  $V$  can be calculated (which was done using Wolfram Mathematica 8). With the resulting terms, the equations of motion were calculated using the Lagrange equation:

$$\frac{d}{dt} \frac{\partial T}{\partial \dot{q}_i} - \frac{\partial T}{\partial q_i} + \frac{\partial V}{\partial q_i} = \tau_{ext} \quad (3.1)$$

where  $\tau_{ext}$  is the torque that is applied externally by the gravity compensation spring (more details below in Sec. 2.2.1).

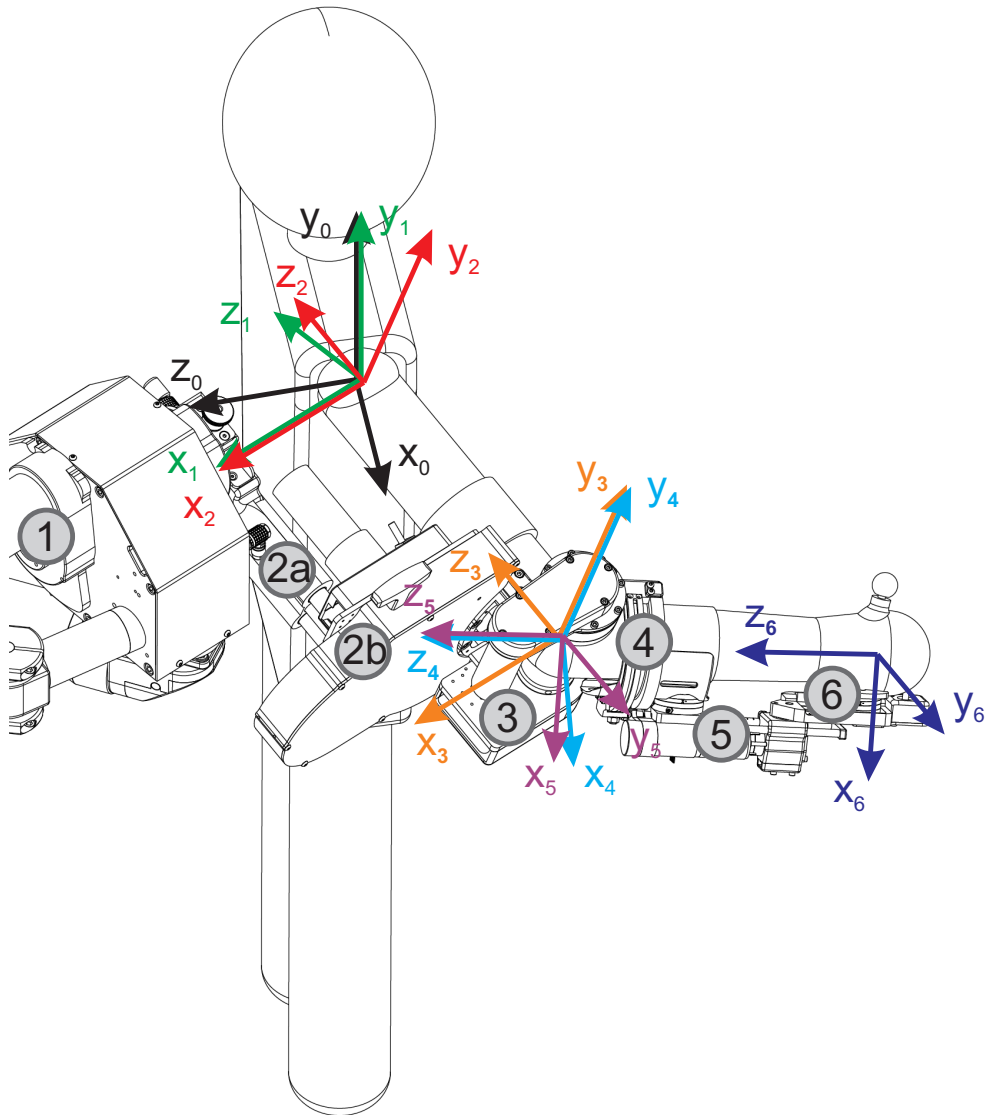


Figure 3.2: Coordinate systems (COS) for the six ChARMin segments. The different segment numbers are encircled.  $COS_0$  is the initial reference coordinate system of the trunk and the visual interface, where the x and y axis build an intuitive 2D system on the interface screen.  $COS_1$  is rotated vs  $COS_0$  when the shoulder is horizontally ab-/adducted.  $COS_2$  is rotated vs  $COS_1$  when the shoulder is flexed/extended.  $COS_3$  is rotated vs  $COS_2$  when the shoulder is internally/externally rotated.  $COS_4$  is rotated vs  $COS_3$  when the elbow is flexed/extended.  $COS_5$  is rotated vs  $COS_4$  when the forearm is pro-/supinated.  $COS_6$  is rotated vs  $COS_5$  when the wrist is flexed/extended.

Applying the Lagrangian formalism leads to equations of motion of this form:

$$\mathbf{M}(\mathbf{q})\ddot{\mathbf{q}} + \mathbf{C}(\dot{\mathbf{q}}, \mathbf{q})\dot{\mathbf{q}} + \mathbf{G}(\mathbf{q}) - \boldsymbol{\tau}_{spring} = 0 \quad (3.2)$$

where  $\mathbf{M}(\mathbf{q})\ddot{\mathbf{q}}$  are the inertial-,  $\mathbf{C}(\dot{\mathbf{q}}, \mathbf{q})\dot{\mathbf{q}}$  the Coriolis and  $\mathbf{G}(\mathbf{q})$  the gravitational terms.  $\boldsymbol{\tau}_{spring}$  is the torque that is applied externally by the gravity compensation spring (details in Sec. 2.2.1). Additionally, a Coulomb- and viscous friction model ( $\tau_{f,i}$ , more details below 3.2.1) was integrated.

An analysis of the inertia-, Coriolis-, gravity- and friction contributions to the overall compensation torque was performed to detect negligible contributions. For this simulation, all the robot axes were moved simultaneously with sinusoidal movements over the whole joint range and the contributions of the different terms in the equations of motion calculated. The results are presented in Sec. 3.3.1.

For the human arm model, the equations of motion can be calculated analogously to the robot's dynamics using the Lagrange equations 3.1 (given the masses and distances). However, only the gravity terms were used for the compensation of the human arm in the robot.

**Kalman filter** To compute the equations of motion (Eq. 3.1), the joint accelerations are required. The acceleration estimate from a double time derivative of the encoder measurement does not result in a sufficiently smooth signal. Therefore, a Kalman filter [194] was used to improve the estimation. The following linear discrete-time model was utilized for each axis:

$$\begin{aligned} x_k &= Ax_{k-1} + w_{k-1}, \quad w \sim N(0, Q) \\ y_k &= Cx_k + v_k, \quad v \sim N(0, R) \end{aligned}$$

$$\text{with } A = \begin{bmatrix} 1 & T_s & T_s^2/2 \\ 0 & 1 & T_s \\ 0 & 0 & 1 \end{bmatrix} \text{ and } C = [1 \quad 0 \quad 0],$$

where  $x$  is the state vector  $[q, \dot{q}, \ddot{q}]^T$ ,  $T_s$  is the sample time and  $y$  is the encoder measurement. For the Kalman filter used, only the signals from the encoders are needed which are located on the six joint axes. For the covariance matrix  $Q$  the variances were derived from the maximally expected joint accelerations. From the robot bandwidth cutoff frequency (Sec. 3.3.2) the maximal acceleration was estimated that can occur ( $a_{max}$ ). This acceleration was then used as the standard deviation of the acceleration variance. The variances for position and speed were achieved by simple integration from the acceleration variance:

$$Q = \text{diag}\left(\frac{1}{2}a_{max}^2 \cdot T_s^2, \quad a_{max}^2 \cdot T_s, \quad a_{max}^2\right) \quad (3.3)$$

This stated Kalman filter was compared to other Kalman filters with different covariance matrices. For this reason the position controller was used with a chirp position reference signal. The signal started at 0.001 Hz and increased to approximately 1 Hz. The chirp reference signal allows to easily differentiate twice to receive the actual acceleration which can be compared with the estimated acceleration (assuming that the robot can follow a given trajectory close enough).

**Example of axis 1** The position control bandwidth for axis 1 is 2.1 Hz (Sec. 3.3.2) measured with an angle amplitude of  $5^\circ$ . By means of this maximal position signal ( $\varphi = 5^\circ \cdot \sin(\omega) = 5^\circ \cdot \sin(2\pi f)$ ), the maximal acceleration can be derived by taking the second derivative. It follows that the resulting maximal acceleration for the first axis is  $a_{max} = 5^\circ / 180^\circ \cdot \pi \cdot (2 \cdot \pi \cdot 2.1)^2 = 15.2 \text{ rad/s}^2$  which is a maximum change of 0.03 rad/s each sample time of 2 ms. This value is used to calculate the  $Q$  matrix in Tab. 3.2. The presented approach to find the  $Q$  matrix was tested against other covariance matrices (Fig. 3.3). While lower standard deviations for the acceleration lead to more delay, higher standard deviations tended to follow the noise of the encoder signal more. The filtered signal which is based on the above calculated standard deviation shows a good and smooth filtering performance. The delay of the filter is approx. 60-80 ms between the differentiated reference signal and the Kalman acceleration (peak-to-peak). The delay comes mostly from the filter. 5-10 ms come from a suboptimal position tracking. For the other axes the standard deviations used for the covariance matrix  $Q$  (Eq. 3.3) are 0.03, 0.06, 0.19, 0.10, 0.25 and 0.17 rad/s for the axes 1 to 6, respectively (Tab. 3.2). For axis 4 a standard deviation of 0.21 rad/s was calculated, however, better results were achieved for a standard deviation of 0.10 rad/s. The covariance  $R$  was set to  $1.0e-7$ .

	Std [rad/s]	Covariance matrix ( $Q$ )
Axis 1	0.03	diag(1.80e-9, 1.80e-6, 900.00e-6)
Axis 2	0.06	diag(7.20e-9, 7.20e-6, 3.60e-3)
Axis 3	0.19	diag(72.20e-9, 72.20e-6, 36.10e-3)
Axis 4	0.10	diag(20.00e-9, 20.00e-6, 10.00e-3)
Axis 5	0.25	diag(125.00e-9, 125.00e-6, 62.50e-3)
Axis 6	0.17	diag(57.80e-9, 57.80e-6, 28.90e-3)

Table 3.2: Standard deviations used and according covariance matrices used for the Kalman filter for the six axes. For axis 4, a standard deviation of 0.21 rad/s was theoretically calculated, however, better results were achieved for Std = 0.1 rad/s.

### Coulomb and Viscous Friction Compensation

A Coulomb- and viscous friction model was integrated which has no discontinuities when the joint speed is close to zero:

$$\tau_{f,i} = k_{1,i} \cdot (1 - e^{-k_{2,i} \cdot |\dot{q}_i|}) \cdot \text{sign}(\dot{q}_i) + k_{3,i} \cdot \dot{q}_i \quad (3.4)$$

where  $k_{1,i}$ ,  $k_{2,i}$  and  $k_{3,i}$  are tunable parameters. To test the validity of this model, the joint friction was measured in axis 1. For this measurement, the axis was moved in the position control mode with a constant speed reference trajectory, while the torque was recorded, which was needed to maintain this speed. The resulting torques, depending on the angle and speed of the joint, can be found in Fig. 3.4. To test whether there is an angle-dependency of the friction, the first model consisted of two planes for the positive and negative joint speeds. However, the angle-dependency is not given (which can be seen in Fig. 3.4) and the friction model from above (Eq. 3.4) is sufficient (bold blue line in the middle of the two planes).

For the other axes, the model (Eq. 3.4) was fitted by moving the robot joint with three

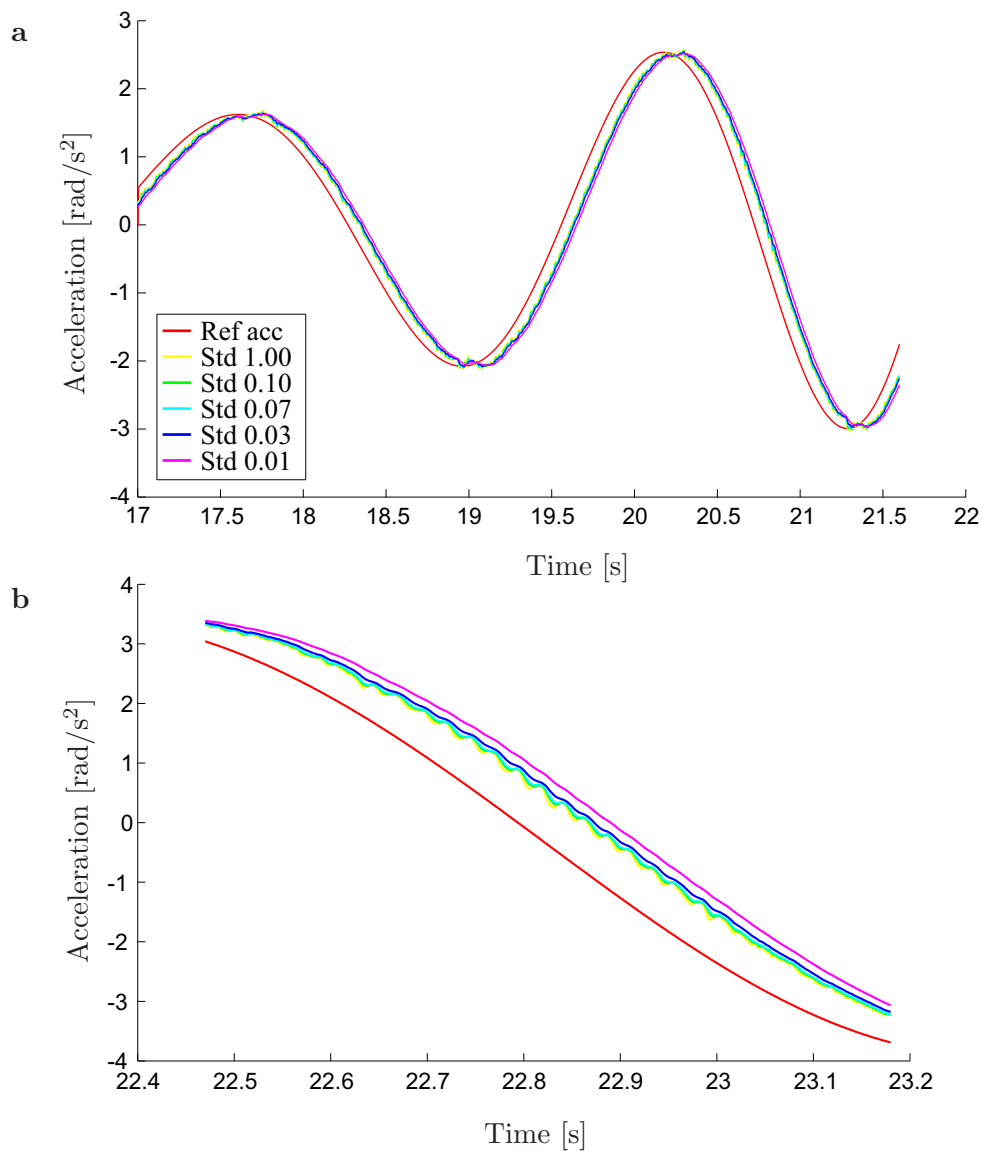


Figure 3.3: (a) Example of the Kalman filter action for the first axis during a sinusoidal movement with an amplitude of  $20^\circ$  for different covariances used. The covariance calculated based on the maximal acceleration leads to the best result (0.03 rad/s). Covariances used were 1, 0.1, 0.07, 0.03, 0.01. (b) Zoomed-in view of the Kalman filter signals at a later time point.

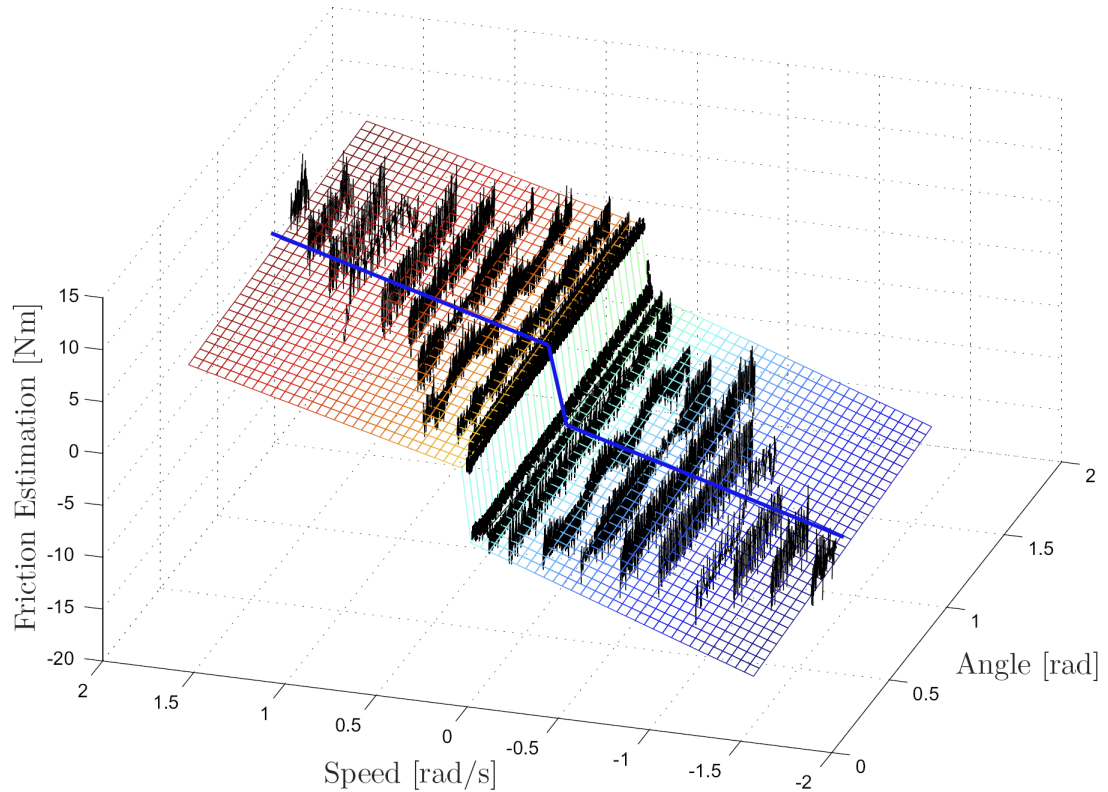


Figure 3.4: Torque needed to move the robot axis 1 at different constant speeds. The higher the speed, the shorter was the distance where the speed could be reached and, therefore, the data samples are reduced (black). An extended planar friction model is shown (grid) as well as the Coulomb- and viscous friction model (blue line) (from Eq. 3.4).

different constant speeds ( $2^\circ/\text{s}$ ,  $10^\circ/\text{s}$ ,  $50^\circ/\text{s}$ ). An example of the resulting friction torques and the fitted models can be found in Fig. 3.5 for the small distal module in positive joint direction.

The friction model had to be adapted manually. Usually, the parameters had to be slightly reduced, as joint oscillations occurred in certain robot postures (different from the postures measured for the model fit). For axis 5 the parameters had to be increased after changing the ball bearings to plastic slide bearings. The currently used friction parameters can be found in Tab. 3.3.

The dynamic friction model (Eq. 3.4) was exemplarily tested for axis 1. This axis is only moving horizontally and, therefore, not gravity affected and allows for an independent measurement of the dynamic friction. The robot joint was moved with constant speeds between  $2^\circ/\text{s}$  and  $30^\circ/\text{s}$  in positive and negative direction with and without the friction compensation. The resulting motor torques can be seen in Fig. 3.6. The mean reduction of motor torque due to the friction compensation was between 57 % and 86 % for slow and fast movements, respectively. To ensure that the joint is not overcompensated and to avoid stability issues, the friction is not completely compensated [195]. The remaining torque for axis 1 is 1.3 Nm.

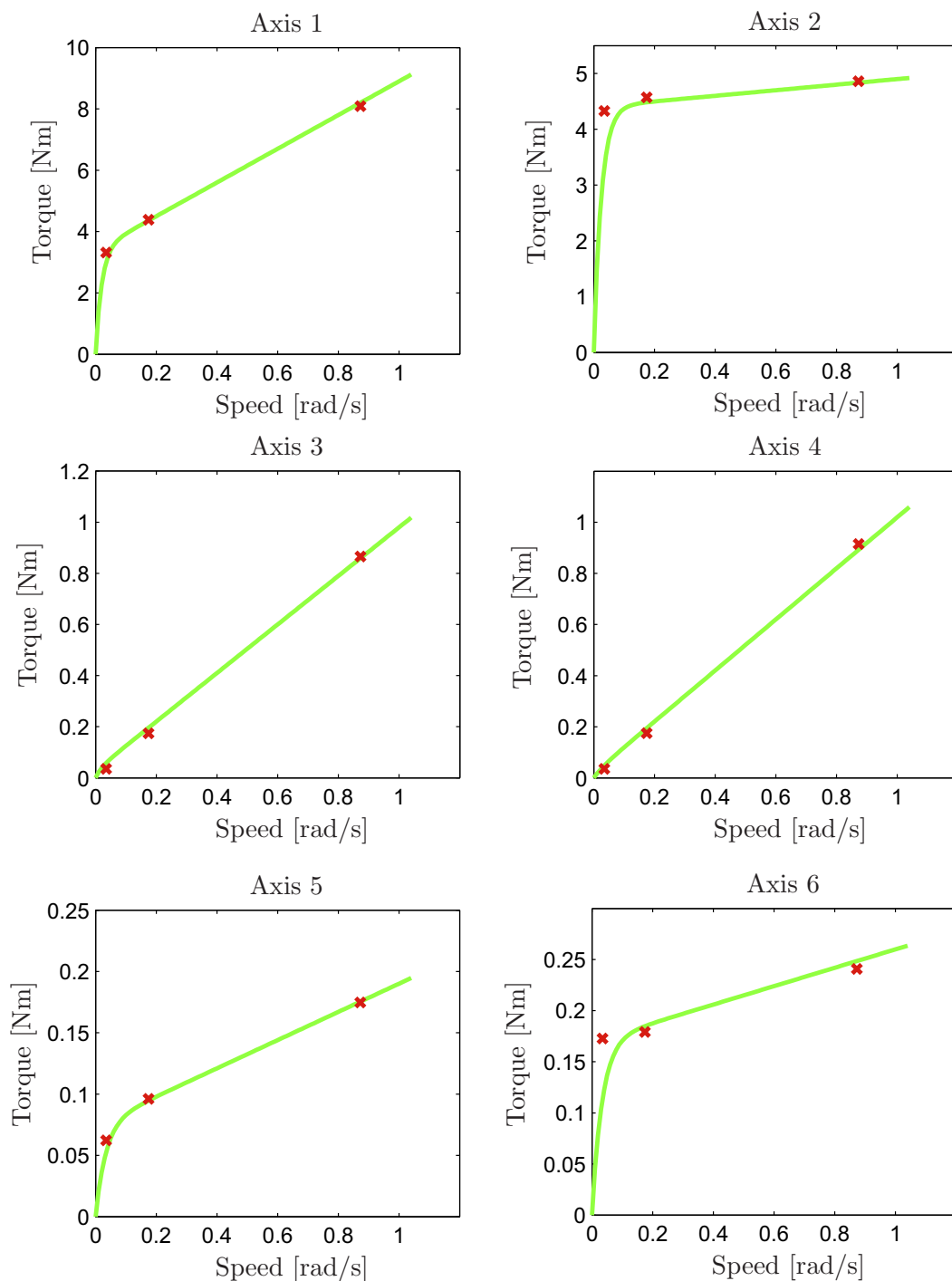


Figure 3.5: Example of the Coulomb and viscous friction model (green line) fitted to resistance torques measured while the robot moved the joints at three different constant speeds (red crosses). Values are only shown for a single direction and equipped with the small distal module.



Axis	Coulomb friction coeff. $k_1$ [Nm]	Viscous friction coeff. $k_2$ [Nms/rad]	Exponential rise coeff. $k_3$ [ ]
1	3.3	5.5	50
2	3.0	0.4	5
3 (s)	0.25	0.1	30
4 (s)	0.9	0.7	60
5 (s)	0.65	0.13	10
6 (s)	0.12	0.05	30
3 (l)	0.3	0.03	20
4 (l)	0.8	0.4	60
5 (l)	0.3	0.05	10
6 (l)	0.15	0	15

Table 3.3: Friction parameters for the small and large distal module.

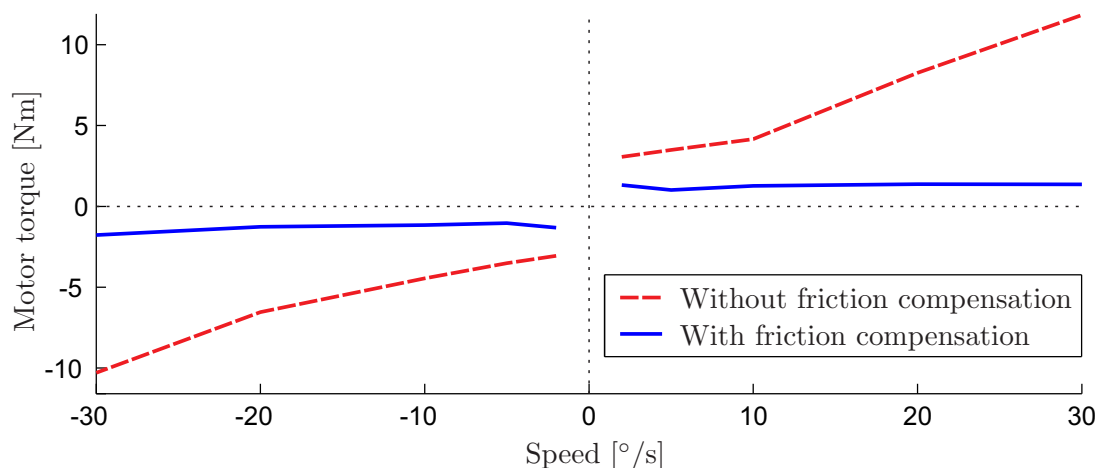


Figure 3.6: Effect of the friction compensation model on the torque needed to move the robot axis. The plot shows the required torque to move axis 1 with (blue line) and without (dashed red line) friction compensation.

### Static Friction and Dithering

**Static friction** Coulomb- and viscous friction can be compensated with the previously mentioned approach in Sec. 3.2.1 (Eq. 3.4). However, static friction from the mechanical transmission cannot be compensated with this model (a list with the static torques in the different ChARMin axis can be found in Tab. 2.8). The main problem is that at zero joint speed, there is no information about the direction, in which the patient wants to start moving and, therefore, no torque can be applied to help initiating the movement. Possible solutions are:

1. When the direction of the target is known, in which the patient wants to move, this information can be used to forward the torque needed to initiate the movement [196].
2. Using a force/torque sensor close to the patient's arm to detect small forces and using this information to start moving the robot. However, this approach also needs a precise model of the patient's arm to discriminate between interaction

forces due to arm weight, spasticity, spasms, joint stiffness, etc. and voluntarily applied forces to move the robot.

ChARMin is currently not equipped with force or torque sensors to extract directional information nor should the joint movement direction be predefined. Therefore, a dithering approach was tested to reduce static friction.

**Dithering** Dithering is a straightforward and well-known way to reduce or overcome static friction. It was first discussed in the 60s and has been used for a long time [197, 198]. Dither can be introduced electronically or mechanically by a vibrator, as was done in early auto pilots. An interesting form of this was utilized in gyroscopes for autopilots in the 1940s [198]. There, the dither signal was obtained simply by a mechanical vibrator. The effect of the dither is that it introduces extra forces that makes the system move before the stiction level is reached. The effect is thus similar to removing the stiction [198].

Applied to our robot, a dithering signal is applied electronically by the motor as soon as the motor speed drops below a predefined speed limit (0.001 rad/s).

The pattern applied in our application was a sinus signal. The advantage of the sinusoidal signal is the predefined amplitude and the fact, that the force changes smoothly between both directions compared to, e.g., a uniform distributed noise. The sinus signals ranged from 0 to 20 Hz to stay outside the hearing range (according to [199] only under very favorable conditions individuals can obtain tonal characteristics as low as 12 Hz). Different phase shifts ( $0^\circ$ ,  $90^\circ$  and  $180^\circ$ ) were tested for the sinus signal and the resulting torques averaged to reduce the effect that for low frequencies the timing of the maximal sinus amplitude may affect the torque needed to start moving.

First, each dithering signal was applied alone to test whether the robot gets instable. When the robot stayed stable, a small linearly increasing torque was overlaid to detect how much additional torque was needed to initiate the movement. In Fig. 3.7, an example of the tested sinus frequency-amplitude combinations and the measured static torques is shown for the first axis. This measurement can be used to find the frequency-amplitude combination with the minimal static torque to initiate a movement for both joint directions (red crosses in Fig. 3.7). In the end, only one single dithering signal can be applied per joint. Therefore, the frequency-amplitude combination was chosen with the smallest mean static torque between both directions (orange circle in Fig. 3.7).

The finally achieved reduction in static joint torque was measured with an externally applied Kistler 1-DoF force transducer. The results are presented in Sec. 3.3.1.

## Kinematics

The forward kinematics and inverse kinematics model of the robot are needed to determine the end-effector position of the robot from its joint angles and vice versa (Fig. 3.1).

**Forward kinematics** The forward kinematics model is used to calculate the end-effector position from the single joint angles. The end-effector position can be determined by multiplication of the different rotational and translational transformation

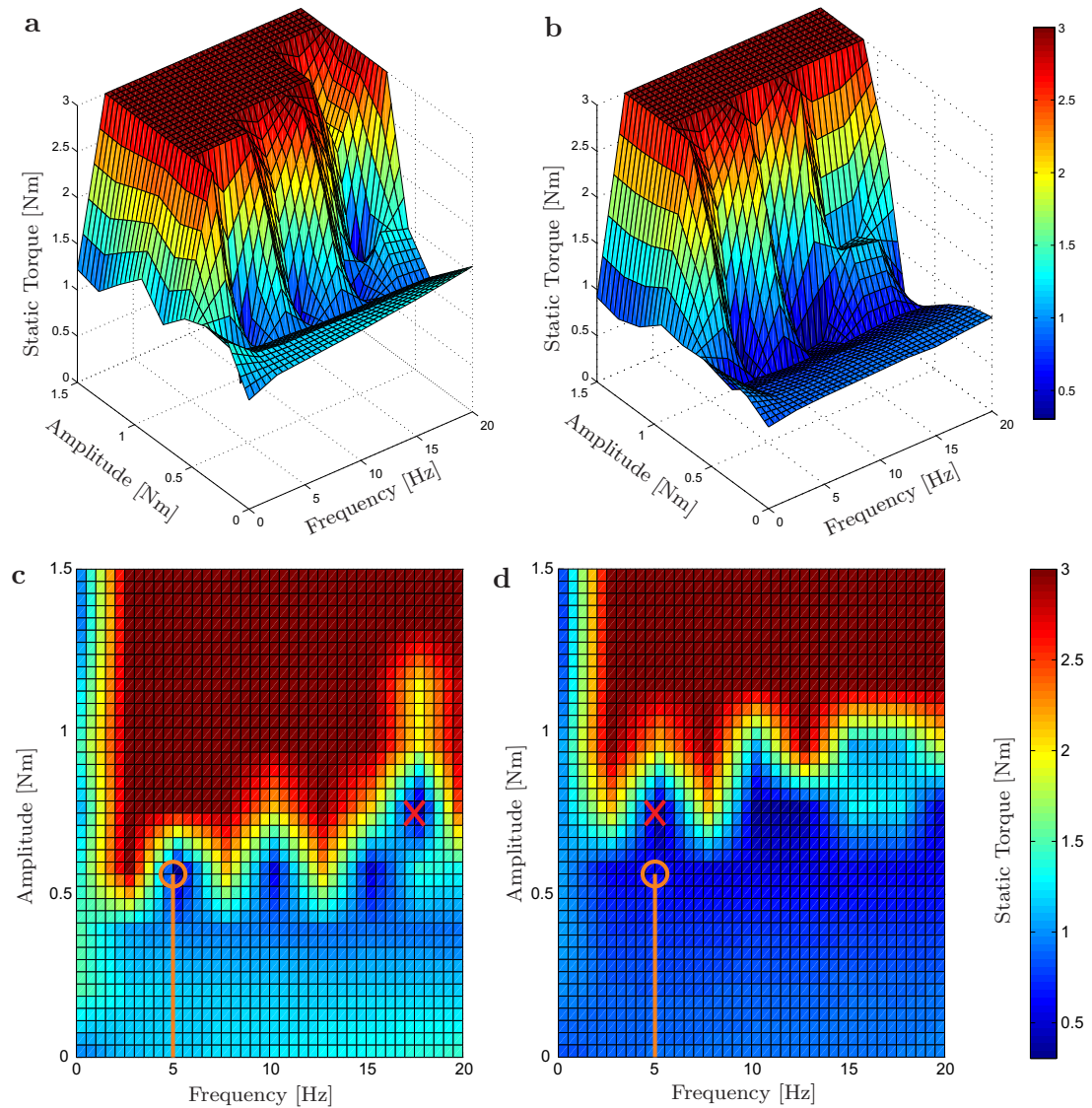


Figure 3.7: Static friction measured when different sinusoidal dithering signals are applied for axis 1, tested in both joint directions. When the dithering signal alone resulted in a joint movement, the frequency-amplitude combination was assigned a value of 3 Nm. This helps for visual purposes and to detect the location with minimal static friction torque (red cross). (a) and (b) show the static friction measurements for the positive and negative direction in 3D. (c) and (d) show the measurements in top view. The orange circle indicates the combination with the same frequency and amplitude in both directions which is finally used in the robot.

matrices (as introduced by Denavit-Hartenberg):

$$\mathbf{p}_{ee} = \mathbf{T}_{01}\mathbf{T}_{12}\mathbf{T}_{23}\mathbf{T}_{lu}\mathbf{T}_{34}\mathbf{T}_{ll}\mathbf{T}_{45}\mathbf{T}_{56}\mathbf{T}_{lh} \quad (3.5)$$

where the different transformation are defined with respect to the coordinate system defined in Fig. 3.2:

$$\begin{aligned} \mathbf{T}_{01} &= \begin{bmatrix} \cos(q_1) & 0 & -\sin(q_1) & 0 \\ 0 & 1 & 0 & 0 \\ \sin(q_1) & 0 & \cos(q_1) & 0 \\ 0 & 0 & 0 & 1 \end{bmatrix}, \quad \mathbf{T}_{12} = \begin{bmatrix} 1 & 0 & 0 & 0 \\ 0 & \cos(-q_2 + \frac{\pi}{2}) & \sin(-q_2 + \frac{\pi}{2}) & 0 \\ 0 & -\sin(-q_2 + \frac{\pi}{2}) & \cos(-q_2 + \frac{\pi}{2}) & 0 \\ 0 & 0 & 0 & 1 \end{bmatrix}, \\ \mathbf{T}_{23} &= \begin{bmatrix} \cos(q_3) & \sin(q_3) & 0 & 0 \\ -\sin(q_3) & \cos(q_3) & 0 & 0 \\ 0 & 0 & 1 & 0 \\ 0 & 0 & 0 & 1 \end{bmatrix}, \quad \mathbf{T}_{34} = \begin{bmatrix} \cos(-q_4) & 0 & -\sin(-q_4) & 0 \\ 0 & 1 & 0 & 0 \\ \sin(-q_4) & 0 & \cos(-q_4) & 0 \\ 0 & 0 & 0 & 1 \end{bmatrix}, \\ \mathbf{T}_{45} &= \begin{bmatrix} \cos(q_5) & \sin(q_5) & 0 & 0 \\ -\sin(q_5) & \cos(q_5) & 0 & 0 \\ 0 & 0 & 1 & 0 \\ 0 & 0 & 0 & 1 \end{bmatrix}, \quad \mathbf{T}_{56} = \begin{bmatrix} 1 & 0 & 0 & 0 \\ 0 & \cos(q_6) & -\sin(q_6) & 0 \\ 0 & \sin(q_6) & \cos(q_6) & 0 \\ 0 & 0 & 0 & 1 \end{bmatrix}, \\ \mathbf{T}_{lu} &= \begin{bmatrix} 1 & 0 & 0 & 0 \\ 0 & 1 & 0 & 0 \\ 0 & 0 & 1 & -L_u \\ 0 & 0 & 0 & 1 \end{bmatrix}, \quad \mathbf{T}_{ll} = \begin{bmatrix} 1 & 0 & 0 & 0 \\ 0 & 1 & 0 & 0 \\ 0 & 0 & 1 & -L_l \\ 0 & 0 & 0 & 1 \end{bmatrix}, \quad \mathbf{T}_{lh} = \begin{bmatrix} 1 & 0 & 0 & 0 \\ 0 & 1 & 0 & 0 \\ 0 & 0 & 1 & -L_h \\ 0 & 0 & 0 & 1 \end{bmatrix}. \end{aligned}$$

The origin of the Cartesian coordinate system is placed in the shoulder of the patient.  $L_u$ ,  $L_l$ , and  $L_h$  are the lengths of the upper arm, forearm, and the distance from the wrist to the handle.

**Jacobian** The Jacobian is needed to calculate the joint torques from the desired end-effector forces (e.g., Fig. 3.1).

$$\boldsymbol{\tau}_{joint} = \mathbf{J}^T \cdot \mathbf{f}_p \quad (3.6)$$

The Jacobian also describes the transformation from the joint speed to the end-effector speed:

$$\mathbf{v}_{ee} = \mathbf{J} \cdot \mathbf{v}_q \quad (3.7)$$

This relation (Eq. 3.7) can be used to derive the Jacobian. First, the end-effector speed is calculated using the time derivative of the end-effector position described with respect to the origin of the Cartesian coordinate system. In a second step, the terms of the end-effector speed  $\mathbf{v}_{ee}$  are brought into the form from Eq. 3.7. These operations were performed in Wolfram Mathematica 8. The resulting Jacobian is dependent on the angular positions and the chosen robot arm lengths.

**Inverse kinematics** Due to the redundancy in the human arm, there exists an infinite number of solutions to reach a given point in space. This set of solutions is reduced by defining the swivel angle<sup>1</sup> (introduced by Badler 1996 [200]). However, the challenge remains to find an appropriate swivel angle. Several publications close

<sup>1</sup>The swivel angle is the rotation angle of the plane defined by the upper and lower arm around a virtual axis that connects the shoulder and wrist joints [192].

with a conclusion that a function to define the swivel angle is difficult to find, as it depends on the subject, the kinematics, dynamics, comfort, and the hand orientation [201, 202]. Different models exist for the inverse kinematics (IK) of the arm using the swivel angle [192, 203]. For ARMin, a swivel angle based inverse kinematic was used where the swivel angle is dependent on a relation between the external shoulder rotation [170], the hand pronation and the hand orientation based on Marotta et al. 2003 [204]. However, the hand orientation was usually fixed and, therefore, the shoulder external rotation and pronation/supination were both constant  $0^\circ$ .

For the inverse kinematics in the ChARMin exoskeleton, two different inverse kinematics were tested. For simplification of the inverse kinematics it was assumed that the wrist (axis 6) and pro-supination (axis 5) do not contribute to the end-effector position. Consequently, the inverse kinematics can be solved analytically and the IK only calculates angles for the first 4 joints of the exoskeleton. The first IK chosen was similar to the one used in ARMin with a fixed external rotation of  $10^\circ$ . A slightly externally rotated posture was chosen, as usually the children are in an internally rotated arm posture and an externally rotated grasping position is useful for therapy (according to the therapists). However, too much external rotation restricts movements to the lower end of the workspace. The second IK tested was the one suggested by Kim et al. [192]. To test whether the different inverse kinematics have valid solutions, the IK was applied to different randomly chosen end-effector positions. In order to illustrate and compare the solutions, end-effector positions were chosen in the frontal plane (z-axis: -0.3m for the small module and -0.35m for the large module). The solutions for the two different IK can be seen in Fig. 3.8 (large module, right side, upper arm length 6, lower arm length 5 and hand length 3). The first subfigure (Fig. 3.8 a) shows the IK according to Kim (in the following referred to as Kim IK). In the second subfigure (Fig. 3.8 b) the constant rotation solution is plotted. To better compare these two inverse kinematics the third subfigure (Fig. 3.8 c) shows an overlay of both kinematics. The blue markers show end-effector positions which have a solution with both IK approaches. The black markers are regions that have only a solution with the constant rotation solution and the green markers indicate areas which can only be reached using the Kim IK. The Kim IK has a larger workspace in high positions and covers the right side slightly better. For lower areas, not all the end-effector positions have a valid solution using the Kim IK. However, this region is not very important to reach as it is too close to the legs of the patient (legs indicated in Fig. 3.8 c with the black rectangle). Furthermore, the Kim IK leads to elbow positions which are closer to the trunk than the constant rotation solution for lower positions (Fig. 3.9 left side). The constant rotation solution has less workspace in the top and bottom region, however, it has a larger workspace to the left and has always valid solutions inside the reachable workspace. Moreover, the elbow is further away from the child's trunk. For higher end-effector positions, the posture the constant rotation solution has a quite high and sometimes uncomfortable elbow position (Fig. 3.9 right side). As a consequence, the IK chosen for the ChARMin robot is a combination of both, i.e., for positive y-values the Kim IK is used and for negative y-values, the constant rotation solutions is applied to get rid of the region with non-reliably solutions and to increase the reachable workspace to the lower left (Fig. 3.8 d). Given the whole range indicated in the figure (x: -0.3 ... 0.5 and y: -0.35 ... 0.4), the Kim IK had no valid solution in 57.79% of the positions and the constant rotation in 65.03% of the positions. The combination of both IKs has no solution in 59.43% of the positions. This whole range is larger than

what is used for the games, however, it shows that the combined IK solution does not affect the number of valid solutions of the IK.

This mixed solution can only be applied, as the IK is never being calculated continuously to determine desired positions, which would lead to discontinuities when the y-value changes its sign. In the control used for the ChARMin robot, the IK is calculated for the desired position and subsequently a minimal jerk profile trajectory for each single joint is determined to reach the target in a predefined time, i.e., the IK is only calculated once before the movement is performed.

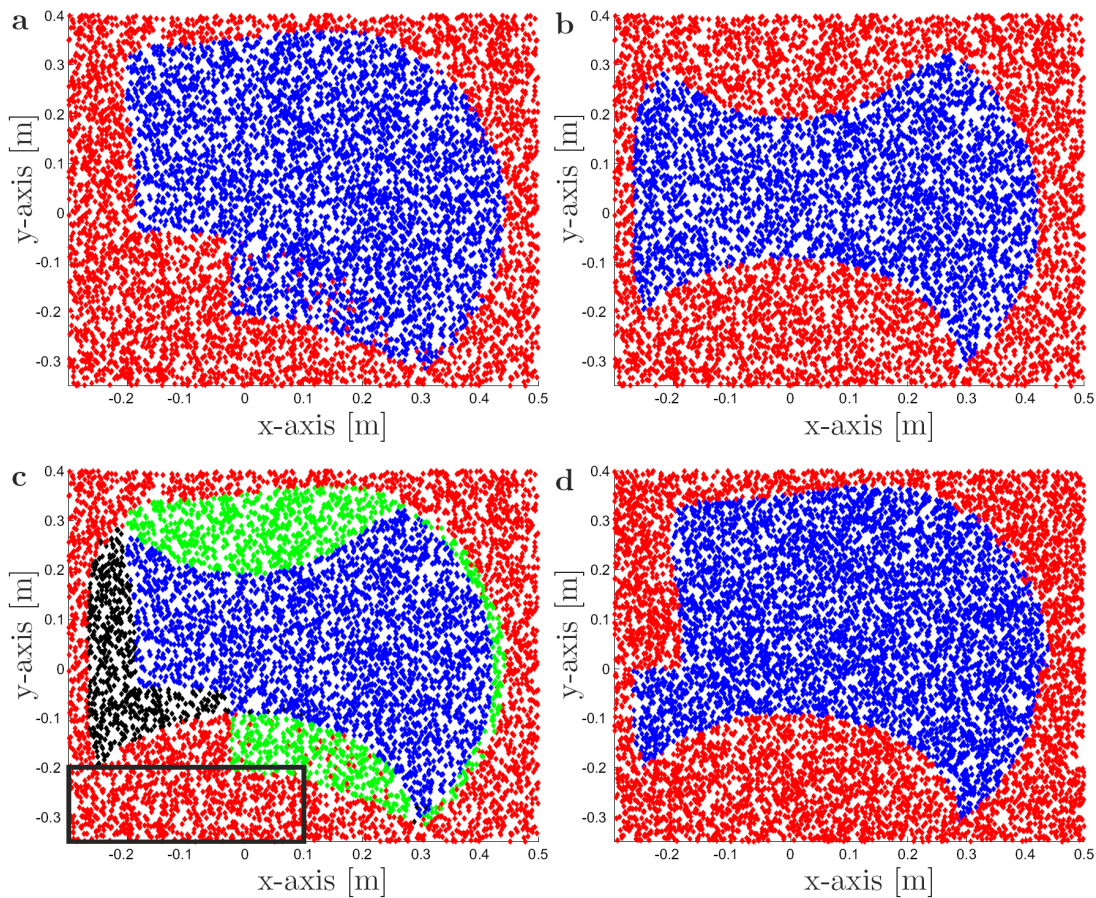


Figure 3.8: IK solutions for different spatial end-effector positions. The analyzed positions lie in the frontal plane at a distance of 0.35 m from the shoulder position. The red markers indicate end-effector positions which cannot be reached or for which no valid solution exists. (a) Kim inverse kinematics. (b) Inverse kinematics with constant  $10^\circ$  shoulder external rotation. (c) Overlay of the two inverse kinematics solutions. The black rectangle indicates the region which is occupied by the patient's legs. (d) Combination of the two IK's where the Kim IK is used for positive y-values and the constant external shoulder rotation IK for negative y-values.

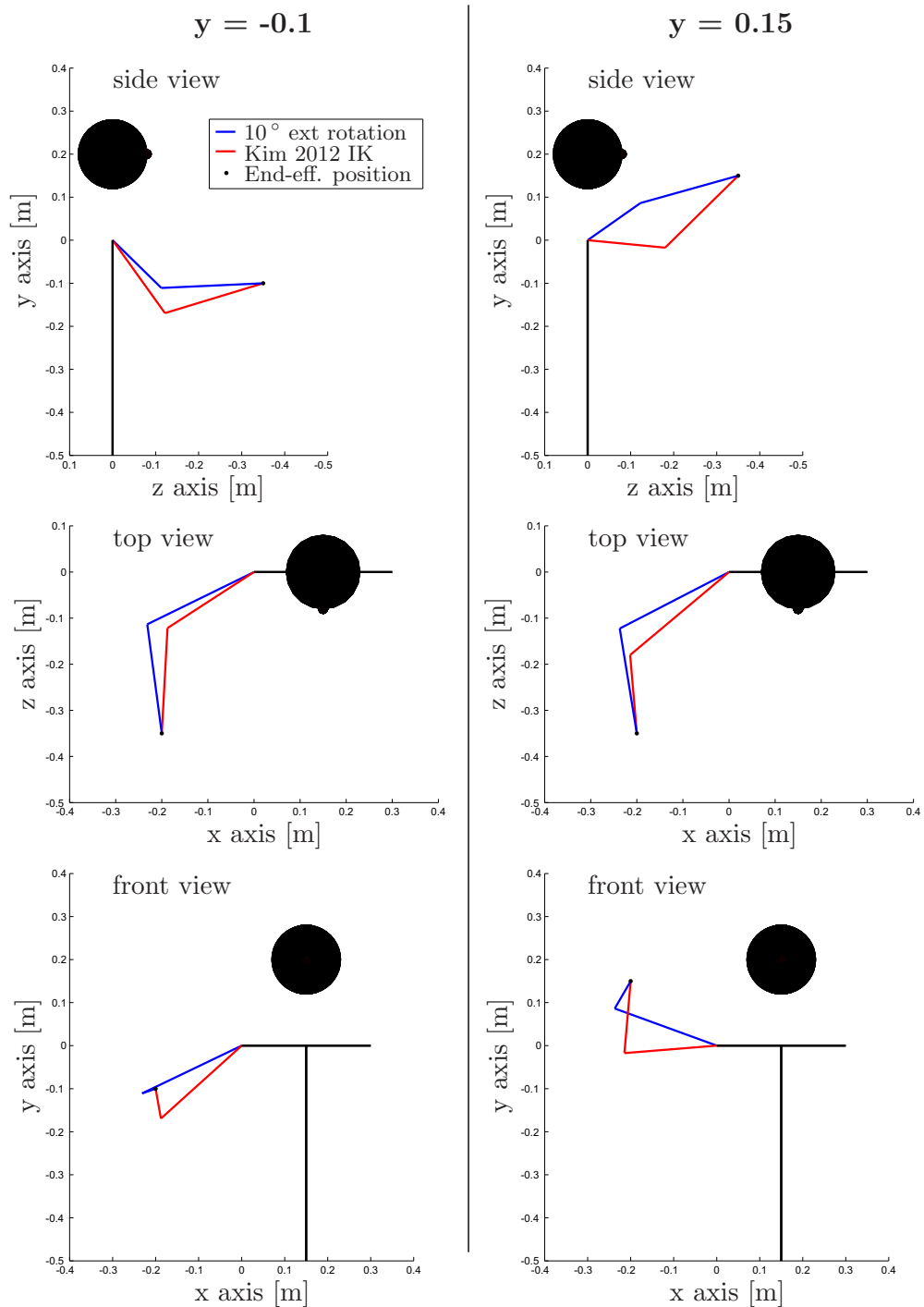


Figure 3.9: Two positions in the end-effector space and its inverse kinematic solutions according to Kim et al. 2012 and with a constant shoulder external rotation angle of  $10^\circ$  seen from three different sides. The black disc represents the head of the patient while the black lines indicate the trunk and the connection between the two shoulders.

### 3.2.2 Position Controller

Position controllers are used when an active device needs to follow a given reference trajectory. To improve this tracking, the robots control and mechanics are usually designed to behave very stiff. For a robot in interaction with a human, this means that no interaction torques between the robot and the patient are considered and the robot strictly follows a predefined trajectory. This kind of controller can be used for arm mobilization, for patients who need 100% guidance, to instruct a task, to lock single axes (e.g., during single axis games) or to move the robot to predefined positions (e.g., during assessments). The position controllers in ChARMin operate on joint-level, i.e., the controller receives the current joint angles of the robot and the desired joint angle trajectories and calculates the desired torques for the single axes (Fig. 3.1).

For the position controller, a proportional-derivative (PD) controller is used. For a first estimation of the position control gains, the Ziegler-Nichols method was used. It was applied by first setting the derivative part to zero and increasing the proportional gain until it reaches a level at which the robot joint becomes unstable and starts oscillating. This was investigated by applying a sinusoidal 0.2 Hz reference trajectory to the controller while increasing the proportional gain, as instabilities appear earlier in the moving joint. These critical gains ( $k_c$ ) and the corresponding oscillation period ( $T_c$ ) were measured (Tab. 3.4). Afterwards, the proportional gains ( $P_{ZN} = 0.8 \cdot k_c$ ) and derivative gains ( $D_{ZN} = k_c \cdot T_c/8$ ) were calculated. For some joints, these gains have to be slightly adapted. For this reason Tab. 3.4 also shows the manually adjusted values that are finally used in the position controller ( $P$ ,  $D$ ).

	$k_c$ [Nm/rad]	$T_c$ [ms]	$P_{ZN}$	$D_{ZN}$	$P$	$D$
Axis 1	8500	56	6800	59.5	6800·0.8	59.5
Axis 2	1800	77.4	1440	17.4	1440·1.5	17.4
Axis 3	400	117.8	320	5.9	320	5.9
Axis 4	900	172.4	720	19.4	720	19.4
Axis 5	200	147	160	3.7	160	3.7
Axis 6	300	120	240	4.5	240·0.65	4.5

Table 3.4: Ziegler-Nichols analysis and resulting position control gains for the small and large distal module.

To test the performance of the position controllers, the bandwidth was measured for the small distal module using a sinusoidal chirp position reference signal with an amplitude of  $5^\circ$ . The bandwidth of the position controller was then defined as the frequency at which the amplitude dropped below the -3 dB line ( $1/\sqrt{2}$ ). The position control performance can also be tested by measuring the position tracking of the robot. Therefore, the six joints of the robot were moved simultaneously with the position controller with 0.2 Hz and an amplitude of  $20^\circ$  for 5 s. The results for both tests can be found in Sec. 3.3.2.

### 3.2.3 Assist-as-Needed Path Controller

In the previous section, the position controller was introduced. For robots that interact with patients, a complete guidance of the arm is often not desired, as the user is not motivated to actively contribute to the arm movement. This section describes how the



path controller approach can be combined with various support features to support the patient arm during the exercise.

### Robot Setup

The herein presented assist-as-needed (AAN) path controller for the arm support in the ChARMin robot is end-effector based, i.e., the supporting forces act on the hand movement in space, while the elbow position is free to be moved, allowing the patient a multitude of postures to reach a given hand position. Therefore, the controller can be tested and evaluated with either the ChARMin exoskeleton robot or the PASCAL end-effector robot (Fig. 3.10). The development of the AAN path controller had started before the ChARMin robot was finished. Therefore, first path controller evaluations were performed with the PASCAL robot (Sec. 1.4.2). For these tests, PASCAL was decoupled from the Lokomat robot to focus on the upper extremity only. For the tests performed in the subsequent sections, the robot end effector was attached to the hand by replacing the cuff with an appropriate handle.

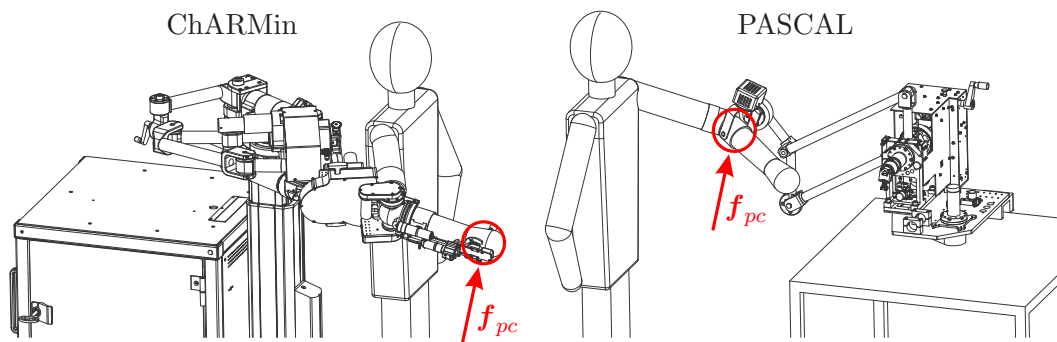


Figure 3.10: The AAN path controller is end-effector-based and can, therefore, apply the path control forces ( $f_{pc}$ ) to different robotic platforms, such as the exoskeleton robot ChARMin or the end-effector robot PASCAL. The two robots ChARMin and PASCAL robot are shown with a simplified body model of a 13-year-old child.

### Support Features

The PASCAL robot is used to support arm movements along a path in space. However, the patient may not be able to move actively along the given path. Therefore, the controller presented in this paper has four main features to help the patient's arm to move along the path:

- Virtual tunnel to stay close to the desired path
- Minimum and maximum speed restrictions
- Direction-dependent supportive flux along the path
- Gain-scheduling control to ensure that the target position is reached

These features will be discussed in the following subsections.

### Virtual Tunnel

In order to help the patient to stay close to a prescribed path in space, a virtual tunnel is rendered from the given start position  $\mathbf{p}_{start}$  to the desired target position  $\mathbf{p}_{target}$  of the path (Fig. 3.11) [191]. If the patient deviates from the given path, the tunnel wall will apply a force in the direction of the path and, therefore, push the patient's arm to stay close to the path. In close vicinity of the path, there is a dead band with constant radius  $R_w$ , where no tunnel forces are applied. This allows the patient to choose his individual trajectory without being assisted (patients with little or no remaining functions can be supported by the additional strategies introduced later). If the actual position  $\mathbf{p}_{act}$  is outside this radius, a tunnel force  $\mathbf{f}_{t,1}$  is applied to the end effector at position  $\mathbf{p}_{act,1}$  (Fig. 3.11) that points in the direction of the shortest distance to the path (Euclidean distance). Therefore, the patient's arm is forced to move towards the path.

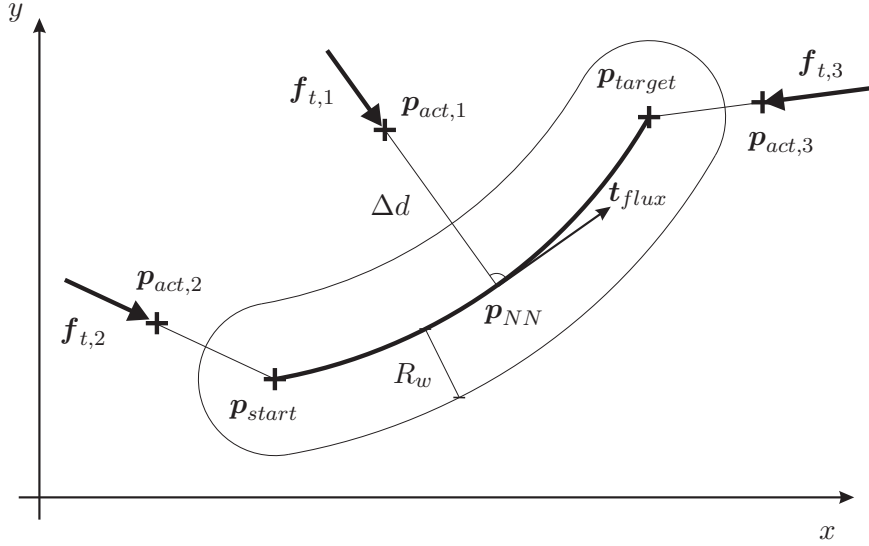


Figure 3.11: Concept of the virtual tunnel used in the path controller. Simplified to a planar case for better understanding.

The resulting force field for the tunnel can either be calculated by real-time differentiation of a potential field calculated beforehand (e.g., by using radial basis functions to build up a potential field [205]) or by directly calculating the force field in a given position. The approach presented in this paper requires that the force field can be changed during a movement (as described later by the changing path using minimum and maximum speed boundaries) and, therefore, the tunnel force applied to the arm is calculated online by using the following formula [64]:

$$\mathbf{f}_t = \begin{cases} \mathbf{K} \cdot (\Delta d - R_w) \cdot \frac{\mathbf{p}_{act} - \mathbf{p}_{NN}}{\Delta d}, & \text{if } \Delta d > R_w \\ 0, & \text{else} \end{cases} \quad (3.8)$$

where  $\Delta d = |\mathbf{p}_{act} - \mathbf{p}_{NN}|$ ,  $\mathbf{p}_{NN}$  is the nearest neighbor position on the path and  $\mathbf{K}$  is a diagonal matrix with the stiffness values for the tunnel wall. Both,  $\mathbf{K}$  and  $R_w$ , can be adapted during the therapy to adjust the controller to the needs of the patient. It can be seen from (3.8) that the tunnel force increases linearly with the distance to  $\mathbf{p}_{act}$  from the path. When the actual position is lying rearward to the start position

( $\mathbf{p}_{act,2}$ , Fig. 3.11),  $\mathbf{p}_{NN}$  is set to coincide with the start position. As a consequence, the tunnel forces  $\mathbf{f}_{t,2}$  point to the start position. In the case that the actual position is ahead of the target position ( $\mathbf{p}_{act,3}$ , Fig. 3.11),  $\mathbf{p}_{NN}$  is set to coincide with the target position and the tunnel forces point to the target.

The force calculation according to (3.8) will only produce a smooth force field over the whole workspace for end-effector positions  $\mathbf{p}_{act}$  that have only one single nearest neighbor. This is only true if the local radius of the path ( $r_{path}$ ) is longer than the distance between the actual position and its nearest neighbor position and, therefore, the necessary condition for the curvature  $\kappa$  of the path is:

$$\kappa < \frac{1}{|\mathbf{p}_{act} - \mathbf{p}_{NN}|} \quad \forall \mathbf{p}_{act} \in W,$$

where  $W$  is the set of the points that lie within the reachable workspace. As a consequence, it has to be ensured, that only reference paths are chosen that fulfill this condition for all possible end-effector positions within the workspace.

### Minimum and Maximum Speed Restrictions

A patient may not be able to move along the tunnel trajectory on his own. Here, the robot should adapt its support and start assisting along the path. For this purpose, a minimum speed reference trajectory is defined from the start to the target position. In case that the patient is slower than this minimum speed reference an additional force will help to move along the path. The idea to have a minimum speed was already introduced in 2003 by Krebs and his group [187] and was applied to the ARMin robot [64]. Based on this, a minimum speed trajectory  $\mathbf{p}_{min}(t)$  is defined using a minimum jerk profile. The minimum jerk paradigm is widely used in the literature [206]. However, for very slow movements, the speed trajectory should be changed to a constant velocity profile. This minimum speed trajectory can be considered as a moving wall in the back of the virtual tunnel, i.e., if the patient is not moving or his speed is too slow, the back of the tunnel will push the end effector towards the target position.

Another issue is that a patient can also move too fast, e.g., if a start position is above the target position. In this case the arm may fall down inside the tunnel due to the acting gravity, unless there is a braking force. In our project framework, this problem was solved by introducing an additional maximum speed trajectory  $\mathbf{p}_{max}(t)$  analogous to the minimum speed trajectory. This maximum speed trajectory defines the momentary end of the virtual tunnel, i.e., when the arm is moving too fast, the moving front end of the tunnel constrains the arm speed according to the maximum speed profile. Both speed boundaries superimposed lead to a virtual tunnel which is lengthening and contracting while the patient moves from the start to the target position. This is illustrated in Fig. 3.12.

### Direction-Dependent Supportive Flux

The minimum speed trajectory was introduced to help patients that cannot move their arm along the path. This approach can even be used for patients with severely affected arm functions or a completely passive arm. But patients with mildly affected arms may only need a little support to perform the movement on their own. Therefore, the concept of flux is introduced. The flux is an adaptable force that helps the patient

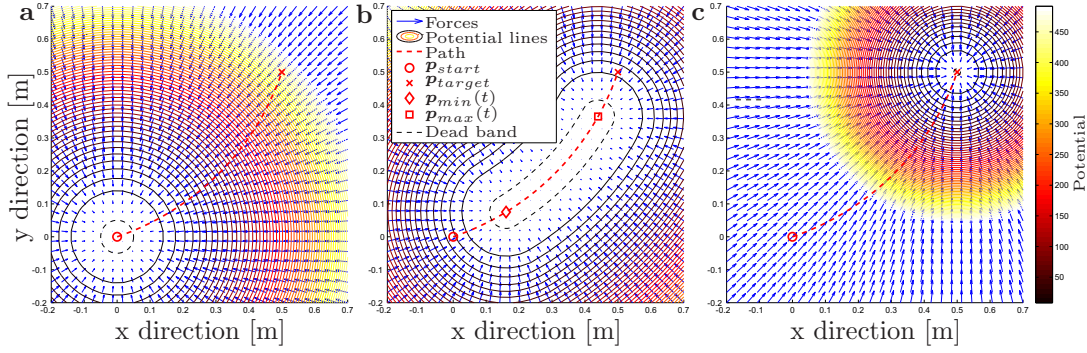


Figure 3.12: Development of the virtual tunnel towards the target position. The arrows are the calculated forces that point in the direction of the nearest neighbor on the path and the potential lines are shown for better understanding of the tunnel shape. Furthermore, the dead band is indicated by a dashed line. (a) Initial situation, an impedance controller keeps the hand at the start position. (b) As soon as the target position is shown, the minimum and maximum speed trajectories start spanning the virtual tunnel in which the patient can freely move. (c) An impedance controller attracts the end-effector to the target position.

along the virtual tunnel [64, 191, 207].

This supportive flux  $\mathbf{f}_{flux}$  can be calculated by the following formula:

$$\mathbf{f}_{flux} = k_{flux} \cdot \mathbf{t}_{flux} \quad (3.9)$$

where  $k_{flux}$  denotes the flux gain and can be adapted by the therapist and  $\mathbf{t}_{flux}$  is the direction of the flux which is parallel to the tangent of the path (Fig. 3.11). Generally, the total support applied by the path controller at the end effector is the superposition of the flux and the tunnel forces (As shown in Fig. 3.13):

$$\mathbf{f}_{pc} = \mathbf{f}_{flux} + \mathbf{f}_t \quad (3.10)$$

To account for different directions, the flux should be higher, when the inclination of the path from the horizontal is increased. The chosen solution to account for this is a direction-dependent flux factor  $k_{dd}$  that is used to calculate the flux:

$$\mathbf{f}_{flux} = k_{dd}(\mathbf{t}_{flux}) \cdot k_{flux} \cdot \mathbf{t}_{flux} \quad (3.11)$$

where  $k_{dd}(\mathbf{t}_{flux})$  is calculated using the scalar product of the tangent vector  $\mathbf{t}_{flux}$  and the unit vector in the vertical direction  $\mathbf{e}_y$ :

$$k_{dd}(\mathbf{t}_{flux}) = \frac{1}{2}(\mathbf{t}_{flux}^T \cdot \mathbf{e}_y + 1) \quad (3.12)$$

The direction-dependent flux factor is illustrated in Fig. 3.14 for the two dimensional case. The black arrows indicate the direction while its norm is given by  $k_{dd}$ . The red line is the envelope of all the possible directions. This allows to quickly see the amount of support which is generated in different directions.

With the new flux factor, the complete flux force is applied, when the path is pointing in the upward direction, half the flux, when the path is horizontal and no flux, when the arm is moving top down. An example of the calculated direction-dependent flux force field is shown in Fig. 3.15.

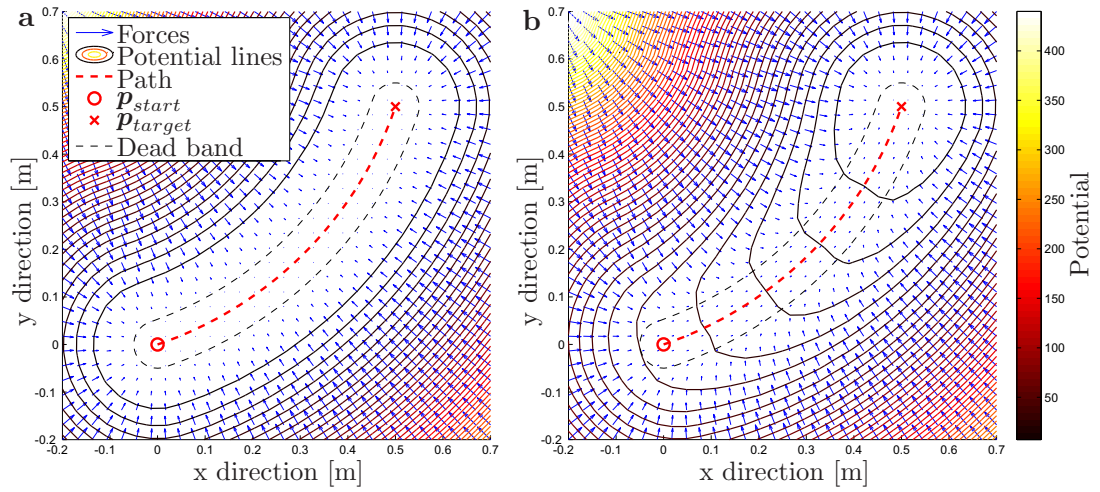


Figure 3.13: (a) Tunnel force field around the path from start position to target position (without minimum and maximum speed limits). (b) Tunnel- and flux force field applied to the end effector and according potential lines for better visualization of the tunnel and the flux.

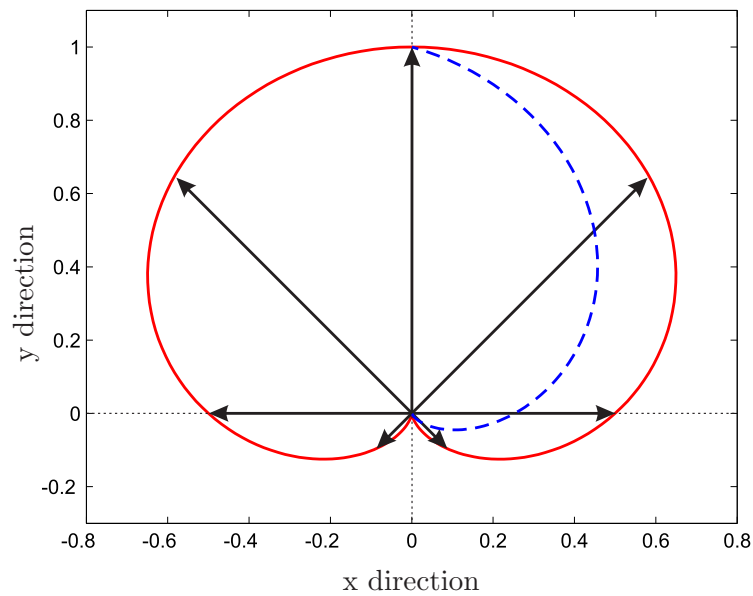


Figure 3.14: Illustration of the direction-dependent flux factor  $k_{dd}$ . The arrows point in direction of the  $t_{flux}$  while its length is  $k_{dd}$ . The dashed blue line gives an example of full support to the top direction and 25% of the support to the left and right direction.

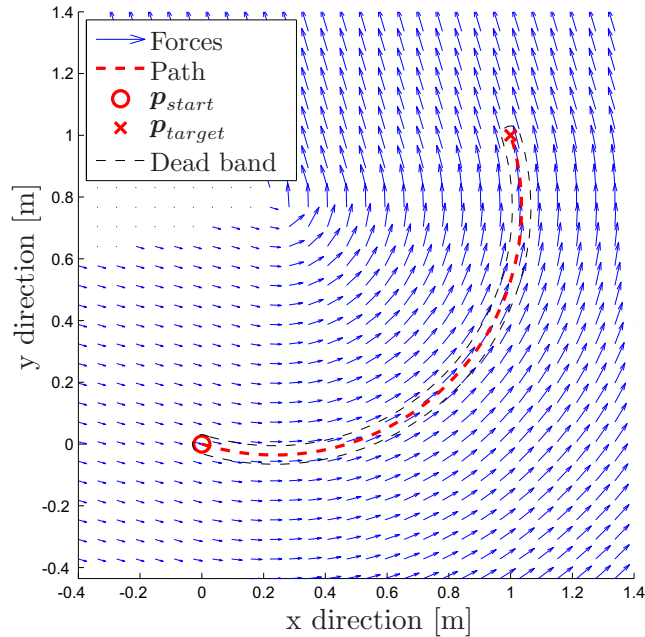


Figure 3.15: Force field of the direction-dependent flux to support the end-effector movement along the path. The force field is the highest for the upward direction. The tunnel force is set to zero for this visualization.

### Gain Scheduling

Depending on the stiffness of the tunnel wall, it may not be possible to reach the target, e.g., if the patient is completely passive or has a mild spasticity, the minimum speed wall will push the patient close to the target position and the impedance controller will keep the patient there, but the hand will deviate from the target position because of the arm's weight pushing into the wall of the impedance controller. In order to bring the hand closer to the target position, the stiffness of the impedance controller is continuously increased and the dead band radius  $R_w$  is decreased, until the hand is in the desired target region, or the predefined maximum stiffness is reached. This is indicated in Fig. 3.12 in panel C with the steeper potential around the target position (compared to panel A). In the currently implemented version, the algorithm first waits 2 seconds after the minimum speed wall reached the target and then starts increasing the stiffness. This allows the patient to first try to reach the target on his own.

### Implementation of the Path Controller

The adopted AAN path control strategy is implemented in MATLAB/Simulink, and the real-time code is executed on a desktop PC running xPC target (Mathworks). The sampling rate is 1 kHz. A simplified version of the control chart can be found in Fig. 3.16. On the right side is the PASCAL robot in interaction with the patient's arm ( $\tau_{int}$ ). Position sensors measure the actual angles  $\mathbf{q}_{act}$  in the kinematics structure. The forward kinematics of the robot is used to calculate the actual end-effector position  $\mathbf{p}_{act}$ , which is fed into the visual interface implemented in the Unity game engine (Unity Technologies). The interface gives visual feedback about the end-effector position as well as the start position  $\mathbf{p}_{start}$  and target position  $\mathbf{p}_{target}$  that define the current path.

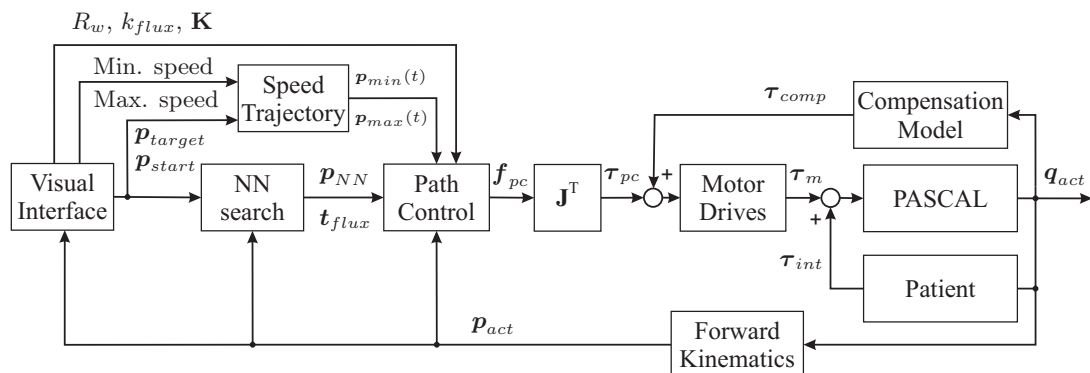


Figure 3.16: Control chart of the AAN path controller.

This information is used to calculate the nearest neighbor point  $\mathbf{p}_{NN}$  on the path and the tangential vector  $\mathbf{t}_{flux}$  by means of the end-effector position. Additionally, the minimum and maximum speed trajectories ( $\mathbf{p}_{min}(t)$ ,  $\mathbf{p}_{max}(t)$ ) are calculated using the minimal and maximal speed values defined by the therapist in the settings of the visual interface. The speed trajectories,  $\mathbf{p}_{NN}$ ,  $\mathbf{t}_{flux}$ , and the current position are used to calculate the path control forces  $\mathbf{f}_{pc}$  according to (3.10). The transposed Jacobian  $\mathbf{J}^T$  is used to derive the corresponding joint torques  $\boldsymbol{\tau}_{pc}$  that are used together with the torques from the compensation model  $\boldsymbol{\tau}_{comp}$  (consisting of friction, gravity, and spring compensation) as a reference for the torque-controlled motor drives (Maxon motor, Switzerland).

### Test Setup

A first test was performed with the AAN path controller by using a simple interface, where the end-effector position of PASCAL was represented as a sphere on the screen. The task was to move to one of eight different targets located at a distance of 10 cm around a starting position (Fig. 3.23). To avoid having gravity always act in the same direction with respect to the path, and for a better understanding of the test results, the targets and the starting position were placed in the vertical x-y plane (frontal plane) at a distance of 0.4 m from the subject's shoulder. Each of the eight targets had to be reached two times and the calculated reference path was a straight line from start to the target position. The robot safety features correspond to the criteria of the ethics committee of the Kanton of Zurich.

### Evaluation of the AAN Path Controller

The controller was tested for two extremal conditions, i.e., for a completely passive user, who needs full support and an active user who needs no assistance (results are given in Sec. 3.3.3). The performance of a patient is expected to be in between these extremal conditions. However, a few children with CP and a spastic arm may need full assistance from the different support features to reach a target. Furthermore, the passive condition can be used for arm mobilization or to instruct movement tasks. To test the full support condition, a subject was instructed to stay passive while the robot moves the left hand. Three passive arm conditions were used with different control parameter sets to show that the robot can perform the movement without any active

subject contribution and to investigate the influence of the different control parameters. The first condition tested whether the target can be reached when choosing a small tunnel wall stiffness and without flux. In this condition, the wall stiffness was 500 N/m, the minimum speed 0.03 m/s, the maximum speed 0.2 m/s, the maximum stiffness of the impedance controller at the target position 5000 N/m and the radius  $R_w$  was 0.01 m. In the second condition, the wall stiffness was increased to 3000 N/m and  $R_w$  decreased to 0.005 m, while the other parameters were unchanged, to test the influence of the tunnel wall stiffness and the minimum speed wall on the tunnel forces and the distance to the target. The third condition was used to show the influence of the flux on the forces that are applied by the virtual tunnel and on the movement timing. A flux gain  $k_{flux}$  of 12 N was used.

In a fourth condition, the subject was instructed to actively move to the target as straight as possible, in order to show, that the controller is only assisting if needed. Here, the flux gain was set to 0 N, while the other parameters were unchanged.

### 3.2.4 Single-Joint Controller

The AAN path controller can support complex multi-joint movements to a desired target position in spatial coordinates. For games which are played with a single joint, the path to the target is the movement of the joint to the target angle. Therefore, a simpler controller can be used for these games, i.e., the ball game and the whack-a-mole game.

#### Ball Game

The goal of the ball game is to hit the ball which is rolling downwards on an inclined plane with a bar on the bottom of the screen. The game can be played with one of the six available active joints. This game was similarly implemented in the ARMin robot already [168]. The robot supports the joint to reach the position, where the ball will hit the horizontal axis where the bar is (Fig. 3.17). The supporting joint torque  $\tau_{joint}$  is dependent on the normalized amount of support chosen by the therapist  $k_s$  (0 ... 1), the extremum range values  $q_{min}$  and  $q_{max}$  (can be changed in the patient settings), the desired joint position in radian  $q_{des}$  and the torque which is maximally applied in each particular joint  $\tau_{max}$ . Furthermore, the amount of support is incremented the closer the ball is to the bottom of the screen. The normalized ball height is used as a support incrementer ( $t_{inc} = 1 - h_{ball}$ ):

$$\tau_{joint} = \begin{cases} (q_{des} - q_{joint}) / (q_{max} - q_{min}) \cdot k_s \cdot \tau_{max} \cdot t_{inc}, & \text{if } \dot{h}_{ball} < 0 \\ -\dot{q}_{joint} \cdot d_{joint}, & \dot{h}_{ball} > 0 \end{cases} \quad (3.13)$$

The controller used is slightly different from the adult version. In the ARMin robot, the bar was supported to the current ball position and not to the target position. However, this behavior does not allow the patient to predict where the ball will hit and move to this position but will rather restrict the bar to the current ball position. Furthermore, a scaling was added with  $q_{min}$  and  $q_{max}$  which ensures that the robot support is not decreased when a smaller range is calibrated.



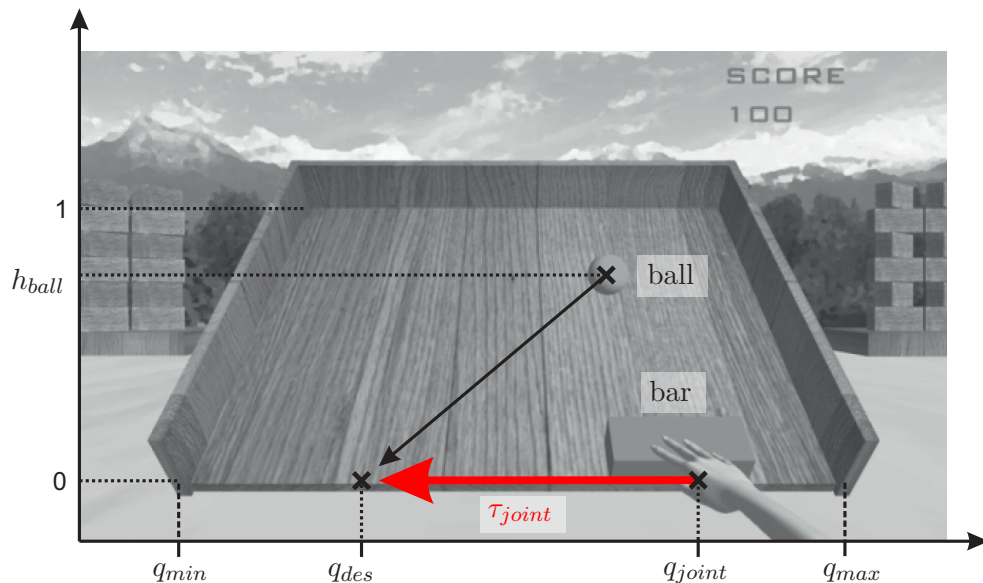


Figure 3.17: Visualization of the single-axis support during the ball game. The goal of this game is to catch the falling ball by moving the bar at the bottom of the screen with a predefined joint of the robot.

### Whack-a-Mole

The goal of the whack-a-mole game is to move the joint to the location where a mole is appearing in the virtual reality interface and hit it with a hammer. For this single-axis game, the support approach is slightly different from the ball game. There is no rolling ball which can be used as an incremter for the support, when the joint is not in the correct position. However, the mole is only showing up for a predefined time ( $t_{total}$ ) before it disappears again. Therefore, the time elapsed since the mole showed up ( $t_{elapsed}$ ) can be normalized with the total time and be used as an incremter ( $t_{inc} = 1 - (t_{total} - t_{elapsed})/t_{total}$ ) to increase the support up to a predefined amount of assistance (Eq. 3.13).

### 3.2.5 Control Stability

#### Passivity

A passivity-based approach was used to prove the stability of the different controllers implemented. Passivity is an inherent property of most of the real environments [208]. It is known that passivity is a necessary and sufficient condition for stability of a system when interconnected with another passive system (assuming that the user of the robotic system stays passive) [208, 209]. The reason is that passive elements can store or dissipate energy but do not increase the energy in a system and hence not destabilize it. Therefore, it is usually tried to make a robotic interface appear passive to the user, i.e., that the controllers are based on emulated passive mechanical elements of arbitrary complexity or its superposition ([205]). The stability is typically analyzed by verifying the passivity of the concept and a complex stability analysis is not necessary. In the following, the applicability of the passivity approach is discussed for the PD

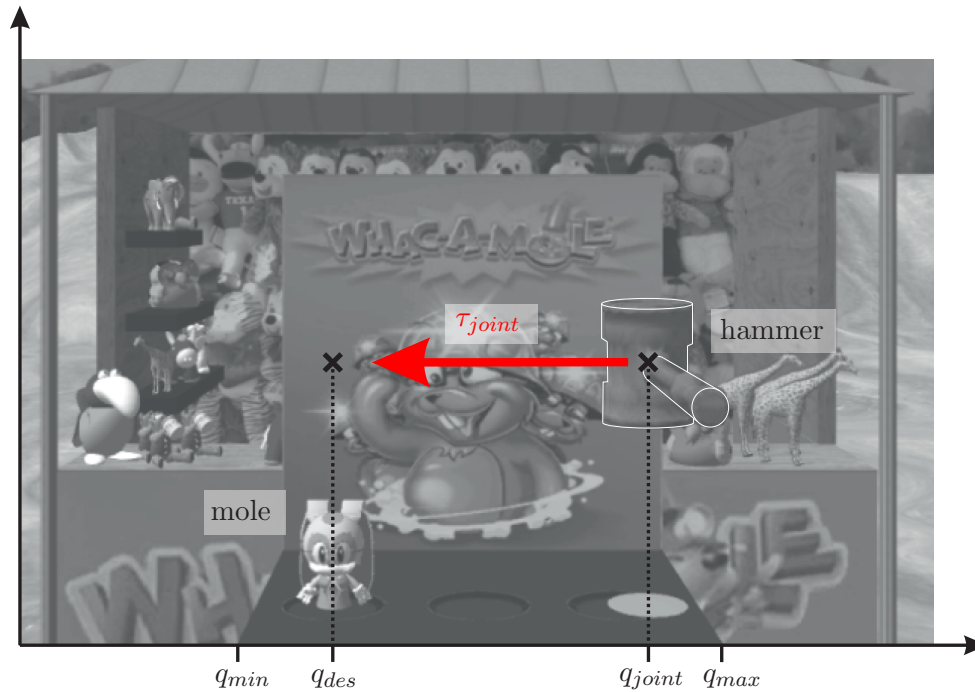


Figure 3.18: Visualizations of the single-axis support during the whack-a-mole game. The goal of this game is to hit the appearing mole by moving the hammer (highlighted with white contours in this figure) with the chosen joint of the robot.

position controller, the path controller, the virtual walls, and the learning controller which is based on a conservative force field [205].

**Position control** The PD controller consists of a constant gain and a differential part. It can, therefore, be interpreted as a passive viscoelastic element which is attached to a constant desired position. Given the passivity considerations above, the PD controller stays stable when interacting with a passive system, given that the control gains are not chosen too high. This was avoided by using the Ziegler-Nichols approach (Sec. 3.2.2) to tune the PD gains. With this methodology the system is intentionally brought into an unstable state in order to know the stability limit and to chose gains that are clearly below this stability limit.

**Path control** The path controller is characterized by a conservative force field that surrounds the path to a given target position. The passivity constraint is fulfilled as the force field is modeled as a linear elastic element and, therefore, the net energy provided to the user is unchanged.

**Gain scheduling** In the case of gain scheduling and the direction-dependent flux, the wall stiffness is increased to a maximum value of 2000 N/m, i.e the potential is increased for a given position and, therefore, the force pointing to the target position is increased.

Our system can be considered passive, as its user interface displays passive behavior.

Considering that the system is only stable because of a positive definite feedback gain ( $\mathbf{K}$  in Eq. 3.8), the system should be referred to as almost strictly passive (ASP) [210], i.e., the closed-loop system is strictly passive due to the stabilizing feedback gain. For an almost strictly passive system, it was previously shown that it maintains high-gain stability with any nonlinear nonstationary high gains [210]. It follows that the tunnel wall stiffness can be increased and stability maintained. A possible restriction is that the scheduling variable should "vary slowly" [211], which is assumed to be fulfilled by increasing the gain during 3s. The gains are increased linearly and continuously and the gain is restricted by a maximum value of 2000 N/m.

**Minimum and Maximum speed limits** In the case of the assist-as-needed path controller presented here, the robot is not only emulating the behavior of passive components, as there is the minimum and maximum speed walls that start moving the patient's arm and, therefore, the potential field is time-dependent and as a consequence nonconservative force and the traditional notion of passivity fails. Thus, it will occur that net energy is provided to the passive user, e.g., when the robot starts moving the stagnant arm. However, the speed changes are very low-dynamic and the forces that come from the minimum speed wall increase slowly. Furthermore, the introduced energy is restricted to the kinetic energy of the arm moving at minimum speed. A possibility to cope with dynamic virtual environments which increasing net energy is to use a passivity observer and to stabilize the system by dissipating the excessive energy [212]. In the presented controller, the added energy is bounded and no additional measures are planned to dissipate this energy.

**Virtual walls** Virtual walls were implemented on joint level to prevent hard impacts on the mechanical end stops. The virtual walls are modeled as virtual springs with linear stiffness starting about  $3^\circ$  before the mechanical stop. When leaving the virtual wall a damping component was added to brake fast impacting movements. The spring- and damper components of the virtual wall fulfill the criteria for passivity.

### Sample Frequency Dependent Stability

The passivity condition is sufficient for a continuous but not for a discrete time system. Here, energy may be generated because of the sampling process and cause instabilities. Diolaiti et al. [213] presented a methodology to analyze the achievable performance of a discrete time system. The analysis relates the dimensionless viscous friction ( $\beta$ ) and Coulomb friction ( $\sigma$ ) to stability properties. The consideration is for the worst case stability scenario with minimal damping, in which the user is not or barely touching the haptic device, thus adding negligible impedance to the system [213]. This approach allows to define the maximally renderable stiffness on joint- and end-effector level to achieve a locally stable system. Using the maximum joint velocity  $\dot{\xi}_{max}$  the  $(\beta, \sigma)$ -plane can be divided into different stability regions A to E (Fig. 3.19), where A is a globally stable region and E is a locally stable region (stable when the speed remains below  $\dot{\xi}_{max}$ ). In the paper, it is stated that most haptic devices rendering their maximum stable stiffness operate in region E. Their dissipation is dominated entirely by Coulomb friction, which works well at low speeds.

To analyze in which region ChARMin is operating the rendered stiffness, the encoder resolution, and the sampling interval had to be defined, which was done exemplarily

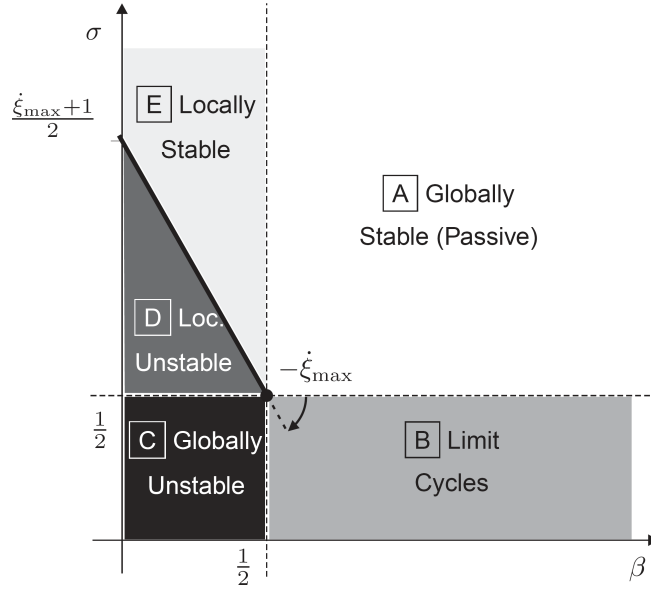


Figure 3.19: Stability regions according to Diolaiti 2006 [213]. On the x- and y-axis the dimensionless viscous friction ( $\beta$ ) and Coulomb friction ( $\sigma$ ) are plotted.  $\dot{\xi}_{max}$  is the maximum joint velocity.

for the first axis (Tab. 3.5). The resulting plots are listed in Fig. 3.25, Fig. 3.26, and Fig. 3.27) in the results section (Sec. 3.3.4). The sampling frequency in the previous ARMin control was 1 kHz. However, due to the CAN bus communication, which needs more computational time. The sampling time of the real-time controller had to be reduced to 500 Hz (Sec. 3.1). In order to analyze possible restrictions due to this reduction, the analysis was performed for both frequencies.

Parameter	Dimensionless value axis 1	Value
Spring stiffness $K^a$		6800 Nm/rad
Encoder resolution $\Delta$		$2\pi / 4000 / \text{gear}$
Sampling interval $T$		2 ms
Velocity $\dot{x}$	$\dot{\xi} = \frac{\dot{x}T}{\Delta}$	
Viscous friction $b^b$	$\beta := \frac{b}{KT}$	
Coulomb friction $c^b$	$\sigma := \frac{c}{K\Delta}$	

Table 3.5: Diolaiti parameters for axis 1. <sup>a</sup>The stiffness corresponds to the maximal position control gain found in Tab. 3.4. <sup>b</sup>Values from the friction compensation model (Tab. 3.3,  $b = 5.5 \text{ Nm rad}^{-1} \text{ s}^{-1}$ ,  $c = 3.3 \text{ Nm}$ ).

## 3.3 Results

### 3.3.1 Modeling

#### Equations of Motion

The analysis of the contributions of the different terms in the equations of motion revealed that Coriolis effects can be neglected for joint speeds relevant for therapy (i.e., approx. 0-50°/s) (Fig. 3.20). Hence, the equations of motion can be reduced to:

$$\mathbf{M}(\mathbf{q})\ddot{\mathbf{q}} + \mathbf{G}(\mathbf{q}) - \boldsymbol{\tau}_{spring} + \boldsymbol{\tau}_f = \boldsymbol{\tau}_{joint} \quad (3.14)$$

with  $\boldsymbol{\tau}_{joint}$  being the motor torques applied to the joints to compensate the robot.

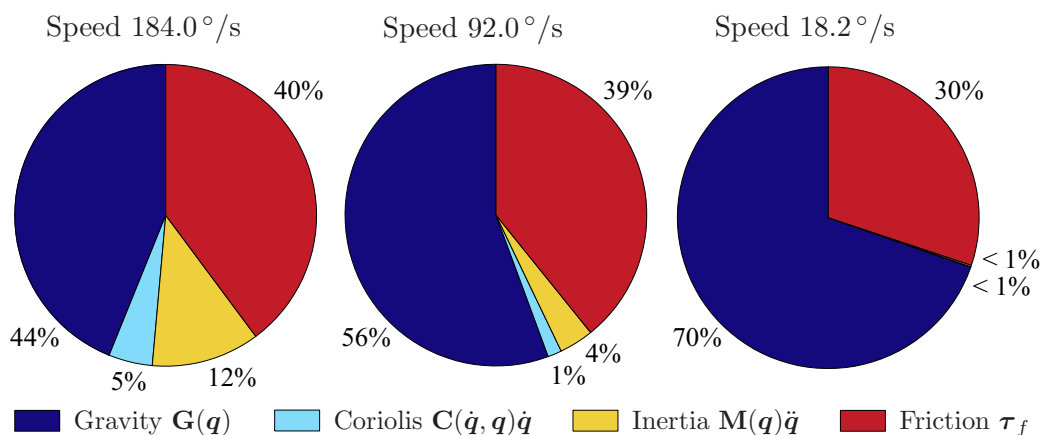


Figure 3.20: Contributions of different modeled effects (gravity  $\mathbf{G}(\mathbf{q})$ , Coriolis  $\mathbf{C}(\dot{\mathbf{q}}, \mathbf{q})\dot{\mathbf{q}}$ , inertia  $\mathbf{M}(\mathbf{q})\ddot{\mathbf{q}}$  and friction  $\boldsymbol{\tau}_f$ ) to the overall compensation torques applied to the robot for different speeds. For this analysis the robot joints were moved simultaneously and sinusoidally. The speed shown is the sum of all six RMS joint speeds. The gravity part also includes the torques that are later compensated by the spring.

The resulting compensation model is a good estimation of the real system. However, the model can never be a perfect match with the real system. Non-modeled aspects such as cables, plugs, cushions, etc. and imprecisions in the mass, inertia, and material estimations lead to under- and overcompensation of the exoskeleton. Therefore, the compensation model has to be further manually tuned. Mainly the gravitational and frictional gains have to be adapted. The correction factors for the gravitational model are given in Tab. 3.6.

#### Dithering

With the dithering approach, the joint torques needed to overcome the static friction were reduced by 32% (sinus: 5 Hz, 0.56 Nm), 42% (sinus: 15 Hz, 0.4 Nm), 12% (sinus: 5 Hz, 0.25 Nm), 54% (sinus: 12 Hz, 0.2 Nm) and 51% (sinus: 10 Hz, 0.1 Nm) in the joints 1, 3, 4, 5, and 6. For axis 2, dithering could not be applied as the passive gravity compensation mechanism with most of the static friction comes after the gear with the mechanical play. The results are shown in Fig. 3.21.

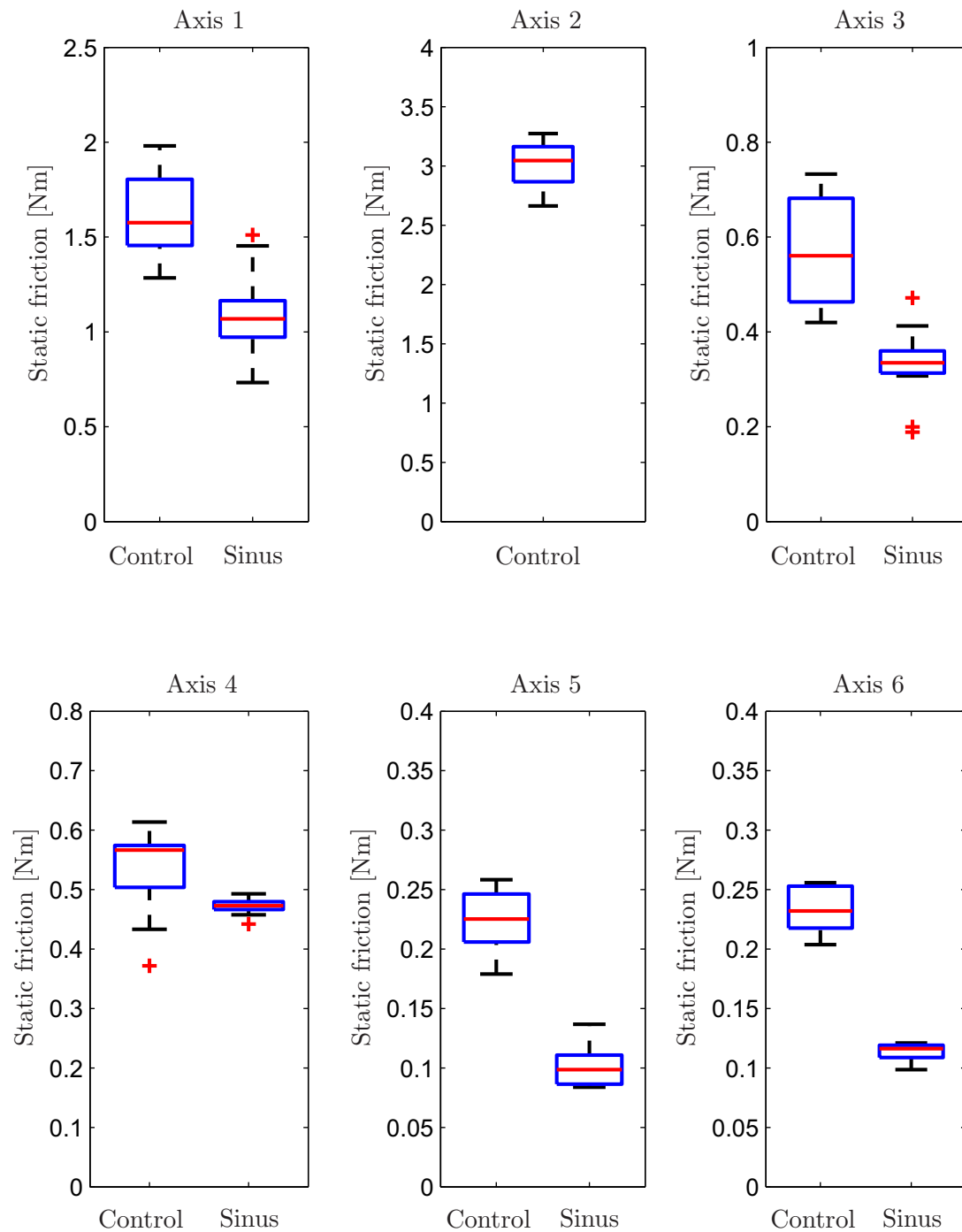


Figure 3.21: Comparison of the joint static friction with and without (indicated with 'Control' in the figure) the sinus dithering signal. In each condition, the static friction was measured 10 times by means of an externally applied 1 DoF Kistler force sensor. For axis 2, no dithering signal could be applied.

Axis	Correction factor small distal module	Correction factor large distal module
1	1.0	1.0
2	1.3	1.2
3	1.0	0.6
4	1.0	0.7
5	1.1	0.6
6	0.9	0.9

Table 3.6: Correction factors used for the compensation torques of the gravitational model.

### End-Effector Stiffness

Two different aspects influence the stiffness felt at the end-effector of the robot. Firstly, the mechanics of the exoskeleton which are not perfectly stiff. Secondly, the stiffness which can be rendered by the single joints (details in Sec. 3.3.4). The cumulated stiffness felt at the end-effector was measured by applying an external force with an AFG (Advanced Force Gauge) 1000N (Mecmesin, UK) force sensor at the robot end effector, while the robot holds the posture with a stiff position controller. The force applied in the positive and negative translational directions (according to the coordinate convention introduced in 2.3) was measured together with the deviation from the initial position. The robot length settings were set to the middle of the range and the robot was brought in a predefined posture  $[45\ 90\ 0\ 90\ 0\ 0]^T$ , according to convention introduced in Appendix A.2.4), which is considered to be in a normal working position. The resulting stiffness is listed in Tab. 3.7.

Direction	End-effector stiffness [N/mm]	
	Positive direction	Negative direction
X	1.0	1.1
Y	1.3	1.3
Z	2.4	2.9

Table 3.7: End-effector stiffness of the ChARMin robot. According to the coordinate system in Fig. 2.3.

While the end effector stiffness in X- and Y- direction is comparable, the end-effector stiffness in Z-direction is much higher, which is due to the selected posture, where forces in Z-direction produce less joint torques than in X- and Y-direction.

### 3.3.2 Position Control

The position control bandwidths for axis 1 to 6 are 2.1 Hz, 3.0 Hz, 5.3 Hz, 5.5 Hz, 6.0 Hz, and 5.0 Hz, respectively (Tab. 3.8). The test with axis 2 was stopped before crossing the -3 dB line due to strong vibrations (Fig. 3.22). The frequency at the end of the test was selected for the bandwidth. Under heavy load conditions, i.e., with an average arm weight of a 13-year-old (1.23 kg upper arm, 0.74 kg forearm, 0.28 kg hand, using the small distal module) the position control bandwidth was unchanged or reduced for axis 1 (1.9 Hz), axis 2 (2.9 Hz), axis 4 (3.7 Hz), and axis 6 (5.0 Hz). The bandwidth for axis 3 (7.8 Hz) and axis 5 (9.1 Hz) was markedly increased.

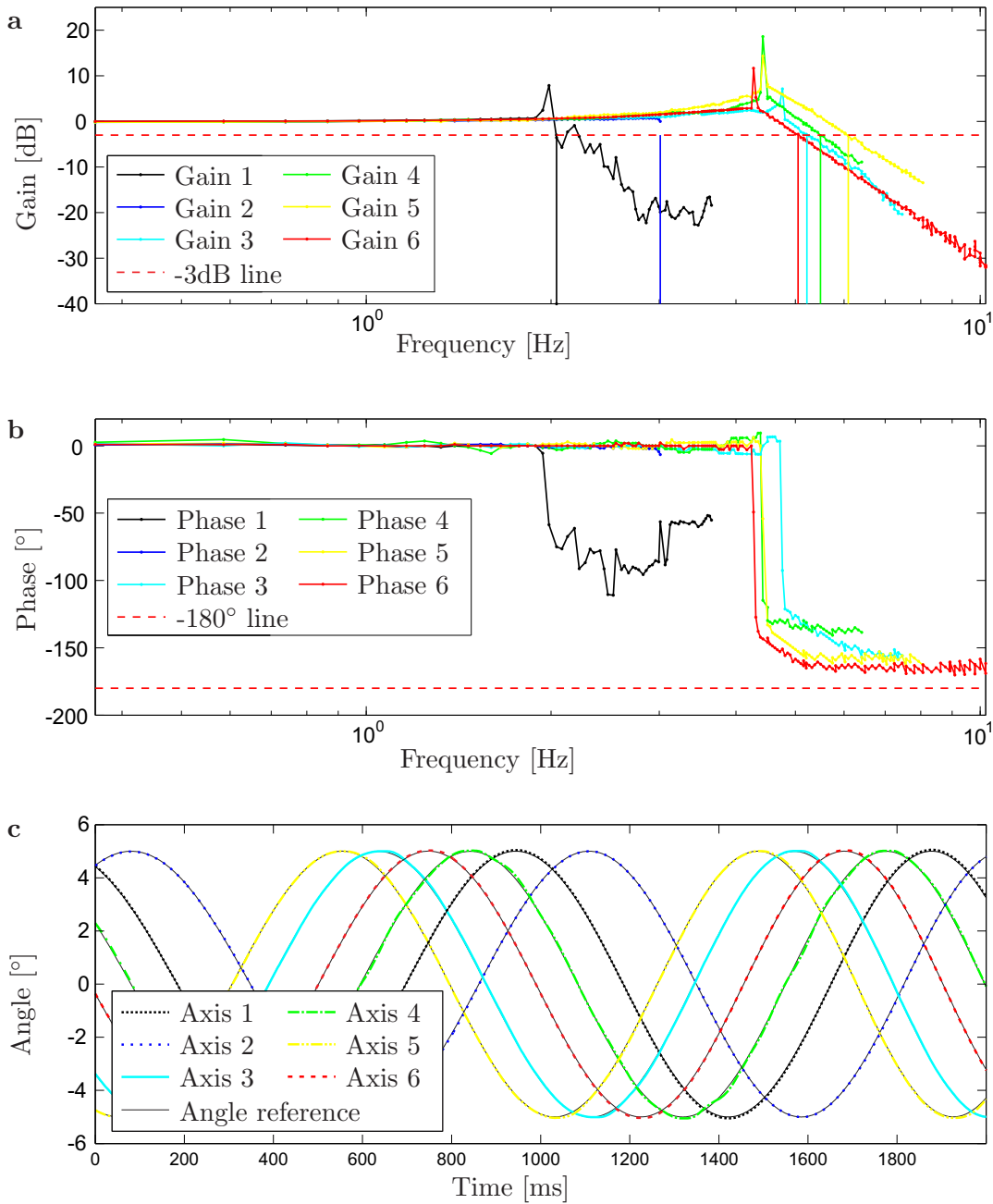


Figure 3.22: (a) and (b) show the position control Bode plots for axes 1 to 6 of ChARMin. The bandwidth was measured where the gain transfer function crosses the -3dB line (emphasized with the vertical lines in the gain plot). (c) Sample of the angular position control reference (black line) and the actual position for the axes 1 to 6 at a frequency of approx. 1 Hz and an amplitude of  $5^\circ$ .

For the position tracking test, the mean absolute error between the actual- and reference position was  $0.0116^\circ$ ,  $0.0521^\circ$ ,  $0.0408^\circ$ ,  $0.0465^\circ$ ,  $0.0743^\circ$ , and  $0.0147^\circ$  for axis 1 to 6, respectively. Fig. 3.22 c shows an example of the position tracking performance (bandwidth test at approx. 1 Hz and an amplitude of  $5^\circ$ ).



	Axis 1	Axis 2	Axis 3	Axis 4	Axis 5	Axis 6
Position bandwidth [Hz]	2.1	3.0	5.3	5.5	6.0	5.0

Table 3.8: Position control bandwidth for the ChARMin axes 1 to 6 (small distal module).

### 3.3.3 AAN Path Controller

The AAN path controller was first tested with a passive subject and two conditions with different path control parameters. The resulting end-effector paths can be seen in Fig. 3.23. All targets were successfully reached twice, while the deviation from the direct path was higher for the first condition (Fig. 3.23 a) due to the low wall stiffness. In the second condition (Fig. 3.23 b), the arm deviated less from the direct path. The deviation in position was highest for the horizontal movements where the weight of the arm is perpendicular to the path, which led to a deeper penetration into the wall.

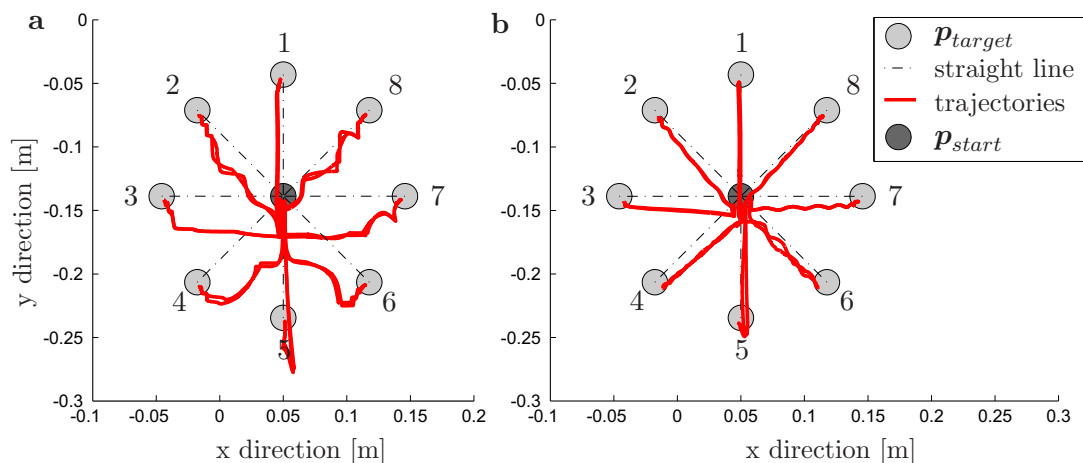


Figure 3.23: End-effector paths from the start position (center) to the 8 different target positions with the subject staying passive (movement back to start position not shown). The y-direction corresponds to the vertical direction; (a) Condition 1, tunnel walls with low stiffness lead to high deviation from the direct path; (b) Condition 2, increasing the tunnel wall stiffness and decreasing  $R_w$  brings the arm trajectories closer to the reference path.

For a more detailed analysis, the movements to target 8 (Fig. 3.23) were considered in more detail. Panel a in Fig. 3.24 shows the movement to target 8 for the first test condition described before (Fig. 3.23 a). As the arm was passive, the minimum speed wall started moving the arm towards the target position. This is indicated by the increasing tunnel forces and the decreasing distance to the target position. Once the minimum speed trajectory reached the target, the forces and position stayed constant. When the gain scheduling started, the tunnel forces increased and helped to reduce the distance to the target and finally the target position was reached. Panel b in Fig. 3.24 shows the second condition. Compared to the first condition, the increased stiffness kept the end-effector position closer to the path during the movement. Once the minimum speed trajectory reached the target, the distance to the target position is smaller than in condition 1. As a consequence, the target was reached quicker,

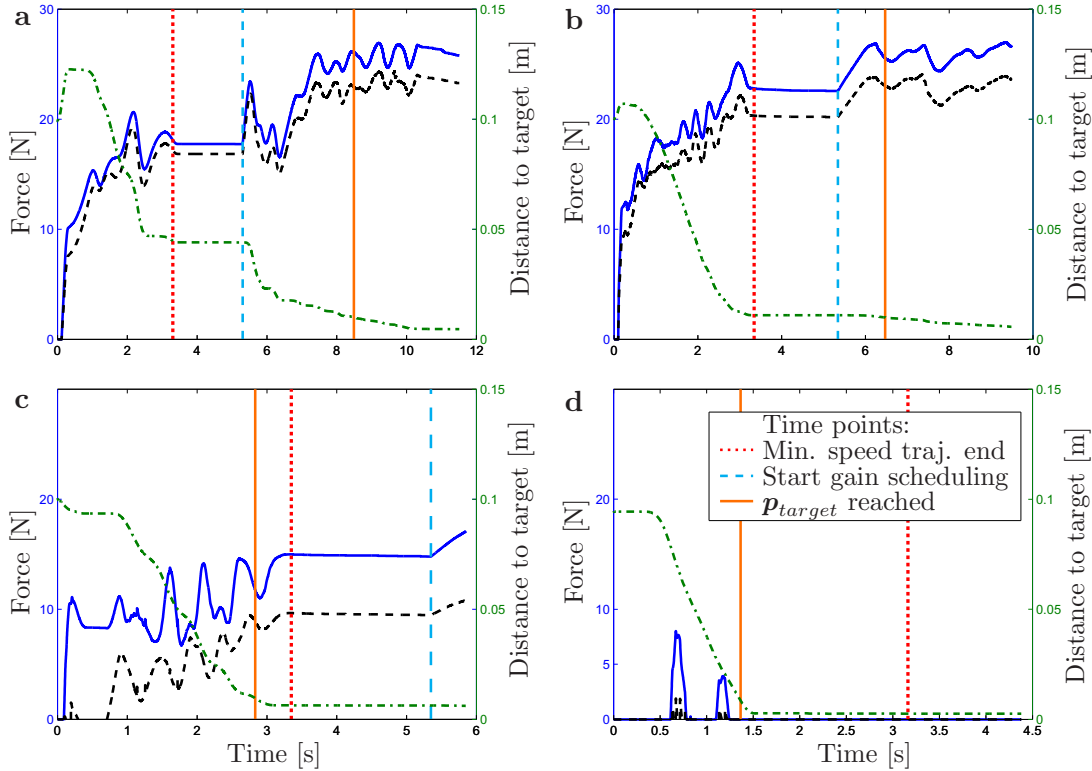


Figure 3.24: Detailed analysis of the arm trajectory to target number 8; (a) Condition 1, passive arm, low wall stiffness and no flux lead to high deviations from the direct path; (b) Condition 2, passive arm, high wall stiffness and no flux lead to decreased deviation from the path compared to a, tunnel forces similar to a; (c) Condition 3, passive arm, high wall stiffness and with flux lead to decreased tunnel forces and decreased tangential forces compared to a and b, target reached earlier; (d) Condition 4, active arm, high wall stiffness and no flux lead to nearly no tunnel forces supporting the movement; At time point 0 the target is shown. The solid line is the norm of the tunnel force  $f_t$ . The dash-dotted line shows the distance to the target. The dashed line displays the tangential contribution to the tunnel force. The dotted vertical line shows when the minimum speed trajectory reached the target position. The dashed vertical line indicates the onset of the gain scheduling, which starts 2 s after minimum speed trajectory reached the target. The solid vertical line shows when the target was reached, i.e.,  $p_{act}$  is closer than 0.01 m to the target position.

after the gain scheduling started. In the third condition (Fig. 3.24 c) with the flux, the tunnel force was decreased, and the tangential part of the tunnel force was much smaller compared to the previous conditions. The remaining tangential tunnel force resulted from the minimum speed wall. In this condition, the target position was reached slightly before the minimum speed trajectory reached the target position. In the last condition (Fig. 3.24 d), with active participation, the target was reached in a bit more than a second and, therefore, in half the time that the minimum speed trajectory needed to reach the target. As long as the subject moved in the dead band, there was no supporting force. At two times the arm left the dead band and touched the virtual wall, producing a small supporting force.

### 3.3.4 Control Stability

For the stability analysis, the passivity paradigm was applied. For the presented discrete-time control system, the stability was additionally analyzed using the methodology introduced by Diolaiti et al. [213]. First, axis 1 was considered. From the resulting plot (Fig. 3.25) it can be seen that the maximally renderable stiffness for axis 1 is 8500 Nm/rad (Tab. 3.9) in order to stay inside the stability region E for local stability. Therefore, a controller with constant gain stays stable as long as the joint speed does not exceed the maximum speed of  $\dot{\xi}_{max} = \pi/2$  rad/s ( $90^\circ$ /s) and the joint acceleration is below  $45^\circ$ /s<sup>2</sup>. Having a sample time of 1 kHz the limit for the renderable stiffness is higher at 13969 Nm/rad.

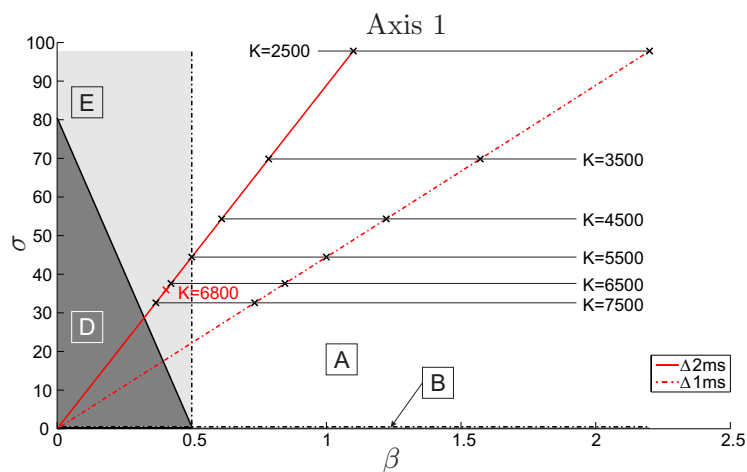


Figure 3.25: Diolaiti applied to ChARMin (equipped with the small distal module) to find the stability limit for axis 1. The analysis was performed with two different sampling times:  $\Delta$  1 ms and  $\Delta$  2 ms.

For the **path controller**, the maximally renderable stiffness at the end effector is relevant. Given the maximal joint stiffness, the maximal end-effector stiffness can be calculated, e.g., for axis 1 this corresponds to 20118 N/m (Tab. 3.9). The currently used end-effector stiffness in the path controller is 2000 N/m.

The **position controller** in ChARMin uses a PD-controller with a differential part. The considerations above are for proportional controllers only. However, the differential part as a dissipating element usually allows to increase the stiffness even further before

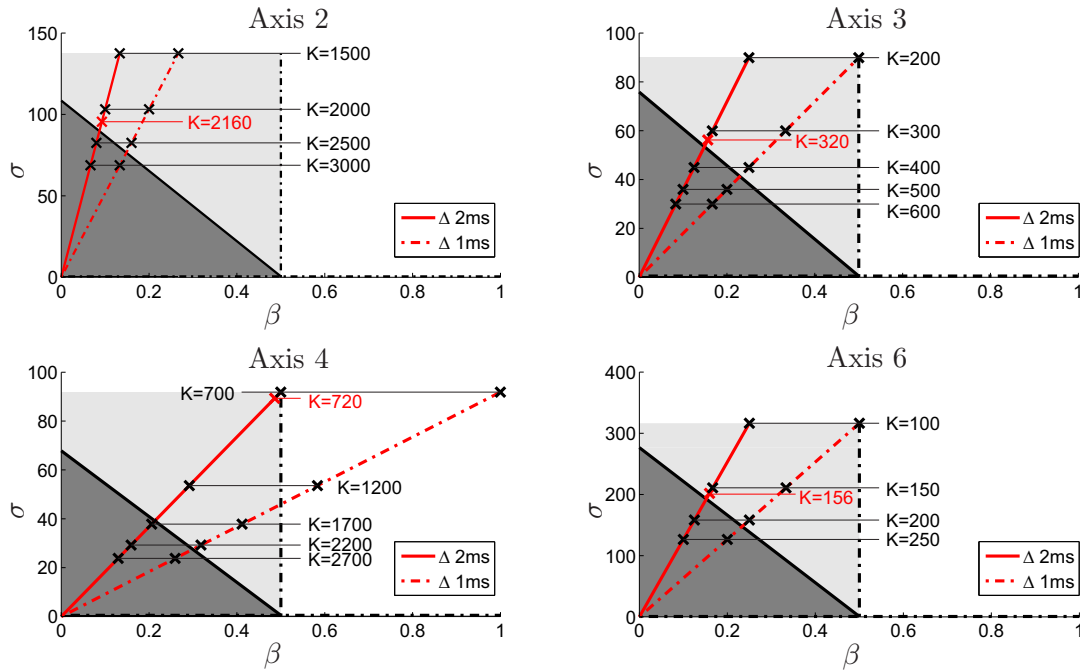


Figure 3.26: Diolaiti method applied to ChARMin (equipped with the small distal module) to find the stability limit for axes 2,3,4 and 6. The analysis was performed with two different sampling times:  $\Delta 1\text{ms}$  and  $\Delta 2\text{ms}$ .

getting unstable (Ziegler-Nichols method: P-controller:  $P = 0.5k_c$ ; PD-controller  $P = 0.8k_c$ , i.e., gains can be 60 % higher). Furthermore, for the position controller used in ChARMin, the maximal speed and maximal acceleration are slower, as defined minimal jerk trajectories for the reference trajectories are used. As a consequence, the situation in the Diolaiti plot (3.25) can be used as a conservative stability analysis of our position controller, i.e., the constant gain in the PD-controller should be smaller or equal to the 8500 Nm/rad. The constant gain which resulted from the Ziegler-Nichols analysis for the position controller is 6800 Nm/rad and was added in Fig. 3.25 in red.

This analysis was performed for axes 2, 3, 4, and 6 (Fig. 3.26). For axis 5 no analysis can be made for the path controller, as the forearm rotation has no effect on the end-effector position and, therefore, no desired stiffness can be calculated for this axis. However, the maximum renderable stiffness can be calculated and be used to define the stiffness of the virtual wall used for safety and for an estimation of the position controller constant gain (Fig. 3.27). The influence of changing the friction parameters on the maximally renderable stiffness can be seen for axis 5, as the parameters needed to be increased when replacing the ball bearings with plastic slide bearings. The Coulomb friction coefficient  $k_1$  was increased from 0.2 Nm to 0.6 Nm and the viscous friction coefficient  $k_2$  from 0.05 Nms/rad to 0.1 Nms/rad.

The maximally renderable stiffness also serves as a limit for the renderable stiffness of the virtual walls which are implemented on joint level to avoid a hard impact on the mechanical joint end stop (Tab. 3.9).

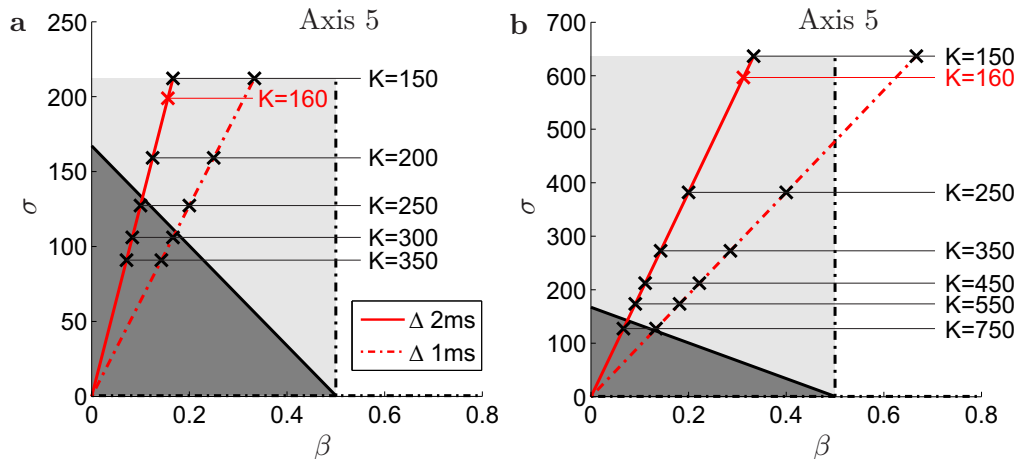


Figure 3.27: Diolaiti analysis applied to ChARMin (equipped with the small distal module) to find the stability limit for axis 5. Before (a) and after (b) replacing the ball bearings with plastic slide bearings.

## 3.4 Discussion

In this chapter the robot and human arm model, the different controllers and the control stability analysis was presented and are discussed in the following sections.

### 3.4.1 Modeling

Inertia, weight, and friction of ChARMin were modeled and feedforward compensated in the robot control. The Coriolis aspects can be ignored as they are negligible compared to the other effects (Fig. 3.20). Axes 1 and 2 have high joint inertias (Tab. 2.8). In order to compensate for inertial effects, the joint acceleration was estimated with dedicated Kalman filters.

Static friction, however, cannot be compensated with the friction model used (Eq. 3.4). A dithering approach was used to overcome the static friction at moving onset. While dithering reduced the static friction to about 50% for most of the axes, it could not be applied to axis 2 as the mechanical play of the gearing prevents the dithering signal from the motor to have an effect on the spring compensation mechanism which produces most of the static friction. However, in axis 6 with the largest mechanical play, static friction comes mostly from the gearing directly mounted on the motor (mainly from the 90° self-made gear). Therefore, the dithering can directly affect the mechanics with static friction and reduce it. Another approach to reduce static friction is to use force sensors in the interaction points between patient and robot. ChARMin is equipped with force sensor dummies, which can be replaced by 6 DoF force/torque sensors, in case that the robot is disturbing the arm movements and, hence, is not transparent enough. This approach was already tested in the ARMin IV robot [6].

The mathematical model of the robot dynamics is based on theoretical physical characteristics of the exoskeleton. This approach has the disadvantage that the different components have to be manually tuned afterwards. An alternative might be to estimate the parameters of the dynamic model, by using, e.g., the least squares approach

Axis	Maximally allowable stable stiffness [Nm/rad] <sup>a</sup> (500Hz)	Maximally allowable stable stiffness [Nm/rad] <sup>a</sup> (1kHz)	Position control gain [Nm/rad]	Reachable end-effector stiffness [N/m] <sup>b</sup>	Virtual wall stiffness [Nm/rad]
1	8500	13969	6800	20118	458
2	2299	2697	2160	5441	458
3(s)	336	436	320	4609	138
4(s)	1643	2337	720	22538	229
5(s)	240	290	160	-	92
6(s)	164	214	156	45556	128
3(l)	248	258	320	2100	92
4(l)	1130	1519	720	7062	138
5(l)	240	290	160	-	92
6(l)	186	186	156	18600	128

Table 3.9: Renderable stiffness for the different axes. <sup>a</sup>from Diolaiti plots above (Fig. 3.25, Fig. 3.26, and Fig. 3.27). (s) and (l) are referring to the small and large distal modules used. <sup>b</sup>Calculated by dividing the maximally allowable stable stiffness by the squared maximal distance of the end-effector from the joints (i.e., with maximal length settings). This transforms the joint stiffness in [Nm/rad] in [N/m]. For the small and the large module the maximal distances are [0.65, 0.65, 0.27, 0.27, -, -, 0.06]m and [0.77, 0.77, 0.4, 0.4, -, -, 0.1]m, respectively.

to fit of the dynamic model to measurements of the real system. This was previously done to estimate robot parameters, e.g., in a 4 DoF lower limb exoskeleton (BLEEX [214]) and by using 2 DoF of the ARMin robot [215]. To the best knowledge of the author, this approach has not been used yet for more degrees of freedom. Furthermore, the model needs to cover the different spring pretensions and length settings of the robot and cover the whole workspace, which makes it difficult to apply in our application.

### 3.4.2 Position Controller

The smallest bandwidths were found for axis 1 and 2. This is due to the high inertia of these axes. Furthermore, the motors were restricted to their nominal torque, which leads to lower bandwidth as the maximal torque applied is not enough to follow higher frequency movements. According to Howard et al. ([216], supplementary material), the mechanical structure needs a high mechanical bandwidth which should be greater than the bandwidth of the human arm. All the ChARMin bandwidths are higher than 2 Hz and are higher than what is usually required and trained during arm rehabilitation training. The reason for the increased bandwidth in axis 3 and 5 under load conditions may be due to the chosen water-filled segments for the loading (instead of solid weights). The position tracking experiment showed good performance with mean absolute position errors below  $0.1^\circ$

For haptic interfaces, the z-width is usually measured to define the bandwidth of the device [213, 217, 218]. In order to define the z-width a force tracking test has to be

performed using a force sensor. ChARMin is currently not equipped with force sensors and the position control bandwidth is used as a performance metric of the system. The position control gains for the position controller of the large distal module are identical with the small module. This set of control gains is inside the stability region of the discrete time stability analysis. Furthermore, the gains are high enough to hold the robot posture and follow a desired trajectory. Therefore, a systematic Ziegler-Nichols analysis of the large module was not performed.

### 3.4.3 AAN Path Controller

The results of the four different conditions show that the AAN path controller can be used to support the upper extremity during a reaching task. To adjust the assistance according to the patient's needs, the therapist can activate and change four different supporting features independent of each other. The influence of these features was tested in different conditions. Condition 1: The virtual tunnel helps the arm to stay in the vicinity of the desired path and the minimum speed trajectory was shown to bring the arm close to the target in a predefined time. Combined with the target gain scheduling the target could always be reached. Condition 2: Increasing the wall stiffness constrains the arm movement to closely follow the desired path. Condition 3: The direction-dependent flux force helps to move along the tunnel, which is indicated by the decreased tunnel forces and tangential forces. This support is mainly important for an arm movement with a speed higher than the minimum speed, i.e., for patients that actively contribute to the movement, but are not strong enough to complete the task without support. The presented direction-dependent flux factor presented here can be adapted to the desired amount by the therapist, i.e., patients may need more support to the left than to the right direction, or even resistance in a certain direction. Condition 4: Here we showed, when the subject is actively participating, there is only a small or no force that is helping along the path and there is no force from the minimum speed wall or the gain scheduling, i.e., the subject can freely move to the target position.

Upon completion of the ChARMin hardware, the AAN path controller was transferred and applied in different interface games, such as the diver game (Fig. 3.28).

For movements in space with several or no targets, where it is not known in advance where the patient wants to move, a directional support cannot be provided. Nevertheless, to provide support during a game such as the airplane game the free workspace is reduced to nine positions in space where the patient can move to and stay (Fig. 3.29), i.e., an impedance controller holds the hand of the patient in one of the nine positions. When a predefined position deviation threshold is overcome, the closest node out of the surrounding eight nodes is selected as the next target position. The AAN path controller or position controller is used to support the movement to the next position according to the therapist settings for the game. To better understand the game play, the airplane in the game is also restricted to stay on the nine positions.

For all the games available, the therapist chooses an appropriate difficulty level in the game interface in order to have the patient optimally challenged. The parameters which the therapist can adapt for the path controller are the tunnel wall stiffness, the dead band, the minimum and maximum speed and the flux force. While the therapists required the higher number of changeable parameters, the numerous settings do not seem to be very intuitive when starting to use the robot. For the first feasibility



Figure 3.28: Visualizations of the path control strategy for the diver scenario. The diver is walking on sea ground, collecting treasures and air bubbles while shooting pirate fishes and obstacles with his bubble shooter. The AAN path controller supports the hand (target of the bubble shooter) to reach the pirate fishes or the obstacles. Other objects are currently not supported. After shooting a pirate fish or obstacle in the supported mode, the free movement is chosen to let the patient shoot other objects, such as the treasures (e.g., in the left background of the figure) until a new obstacle or pirate fish appears.

trials (Chap. 5), all the settings were adjustable. The therapists stated that the settings could be changed intuitively. A more detailed analysis needs to be performed to understand which parameters were used and how they need to be changed. In a next step, this knowledge can be used to reduce the number of parameters or to use a learning controller to change the amount of support needed by the patient. A learning controller can be used to automatically change the amount of support needed by the patient or to automatically adapt the difficulty level of the task. Different rehabilitation robots already capitalize on the use of learning controllers. An iterative learning controller was used for the arm exoskeleton robot RUPERT IV and adaptive control algorithms were introduced in the MIT-MANUS and the ARM Guide (overview from [172]). For the ARMin robot, a learning path controller was developed to change the flux force when moving inside the virtual tunnel [219]. Metzger et al. [220] developed an automated routine that adapts the difficulty level to keep the patient challenged. Another area of application where a learning controller can be used is for non-targeted movements where no information is available about the direction in which the patient wants to move. In a semester thesis, Fabio Carrillo implemented a preliminary controller to learn a gravity- and direction-dependent force field to support the arm movement in space [221]. The idea was to define an initialization phase before the games were started. During this initialization, the patient should be instructed to move in six different directions in space and a dedicated algorithm calculates the support needed to perform these movements. Based on this information, a supportive force field can be computed for the whole workspace. A preliminary test was performed with the first 4 DoF version of the ChARMin robot.



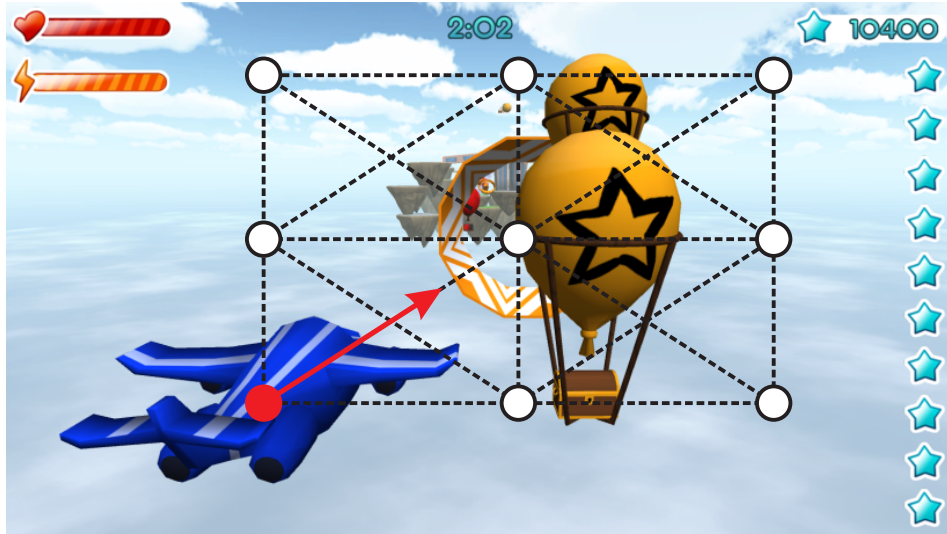


Figure 3.29: Visualization of the controller strategy for the airplane scenario. In the airplane game, balloons have to be collected while avoiding objects in the sky. The position- or path controller is used to support the hand (airplane) to nine discrete positions in space. The red circle shows the hand position represented on the screen while the red arrow symbolizes the supporting force towards the target position.

#### 3.4.4 Control Stability

For the stability analysis, a passivity-based approach was used. The stability of our controllers was analyzed by verifying the passivity of the chosen control concept. All the controllers described above, including the position controller, the AAN path controller and the virtual walls are based on passive mechanical elements, e.g., springs and dampers. To guarantee the stability for the discrete-time system an analysis of the maximally renderable stiffness was performed. All the position control gains and the chosen joint- and end-effector stiffness are at least locally stable.

For the passivity-based stability approaches, the assumption is made that the user behaves passive. This is a very strong assumption, however, it was previously stated that the user adds more damping to the system and reinforces the natural damping of the device, i.e., this effect enhances stability rather than destabilizing it [213]. Hence, the worst case scenario for stability is not the situation where the user is interacting, but when the robot is not touched by the user [213, 222]. Therefore, the focus of the stability considerations was on the robotic system.

Haptic devices are often characterized by the maximum virtual wall stiffness that can be stably displayed [223]. According to Tab. 3.9, the maximally renderable end-effector stiffness and, therefore, the performance quality of the ChARMin robot, is 2100 N/m for the large module and 5441 N/m for the small module (axis 5 is not contributing to the end-effector stiffness, therefore, axis 2 is the limiting factor). A tunnel wall stiffness of 2000 N/m is currently used for both modules as a maximum. This is stable according to the passivity analysis and seems to be stiff enough to make the child reaching the target position. The maximally renderable joint stiffness ranges from 186 Nm/rad (axis 6) to 13969 Nm/rad (axis 1) (Tab. 3.9).



# 4 ChARMin Assessments

The previous chapters highlighted the potential of rehabilitation robots to increase the therapy intensity by supporting arm movements and by motivating the patient to actively participate. Rehabilitation robots are advanced exercise tools to assist arm neurorehabilitation. Moreover, with their precise sensors, rehabilitation robots have the potential to provide an interface for objective, sensitive, and reliable measurements of the patient's arm motor function.

This chapter presents a set of robot-assisted assessments for the upper extremity which can be applied to the pediatric and adult target group. Before applying the assessments to the pediatric target group, the robot-assisted assessments were evaluated in a consideration of concept study with adult SCI patients. The first section introduces the different robot-assisted assessments and the results of this study with adult participants (based on a previous publication [5]). The second section focuses on the adaptations and extensions of the assessments for the pediatric target group.

## 4.1 Robot-Assisted Arm Assessments in Adult SCI Patients

### 4.1.1 Introduction

Patients who suffer from a neurological disorder such as SCI or stroke often face deficits in motor function. The global-incident rate for traumatic SCI is estimated to be 23 cases per million people (180'000) [224]. Stroke has a prevalence of approximately 795'000 people in the US (Centers of Disease Control and Prevention, 2010). These impairments due to stroke or SCI lead to a restriction of both independence and participation in daily life [225, 226]. An intensive rehabilitative intervention can help to improve motor function in stroke [227] and SCI patients [228] and, eventually, the patient's quality of life.

Plenty of clinical scores and assessments are available for different diseases, ages, movements and body parts to measure patient's motor functions. The assessments are often categorized using the international classification of functioning, disability and health (ICF) [229] to standardize the description of the health status. With this classification the scores can be grouped according to the disability they address, i.e., body functions and structure, activities and participation. Assessments covering these groups can be used for diagnosis of the patients' status, as a measurement of therapy progress or as feedback about patients' performance. However, clinical assessments often show deficits in terms of reliability, validity, sensitivity, duration of execution and potential ceiling effects [230–232].

Rehabilitation robots have the potential to provide an interface for objective, sensitive and reliable measurements. The prevalent use of robots for therapy and the positive findings of robot-assisted therapy contributed to an increased development of robot-assisted assessments in the last five years. Generally, two fundamental approaches can

be used to evaluate sensorimotor impairment using robot-assisted assessments: Using raw sensor data or feature extraction [230].

The first approach uses raw sensor data to directly extract information from sensors about body functions. Depending on the used sensors and parameters, different robot-assisted assessments have already been described. Several approaches focus on assessments of the upper extremity. In time-based assessments, the duration is usually measured that is needed to finish a given point-to-point movement or position adjustment of the hand or a joint (e.g., using the MIT Manus [232], the Delta robot [233], the REAplan [234] or the HapticKnob [235]) or by measuring the time needed for a given task (e.g., using the PHANTOM [141] or the MIT Manus [232]). With sensors that measure kinematic or kinetic information, assessments can be performed such as measuring the joint range of motion (ROM) or the workspace (work area) of the hand that can be reached (e.g., using the Lokomat [236], ACT<sup>3D</sup> [237], the ArmeoPower [111] or the Microsoft Kinect [238]) or the mean/peak/tangential speed (e.g., using the MIT Manus [232], the MEMOS [239], the IE2000 haptic joystick [240] or the REAplan [234]). An assessment device which can measure forces or torques can be used to measure the active joint strength. This can be done recording the maximum voluntary isometric forces or torques (e.g., using the ARMin [69], its commercial version the ArmeoPower [111] or the Lokomat [241]) or isokinetic forces and torques (e.g., using the Kin-Com Dynamometer [242]).

In the feature extraction approach, the sensor data is further processed, conditioned and characteristic properties are extracted. Using the time and position information during a movement, the quality of the corresponding joint or hand trajectory can be analyzed. Smoothness is a prominent metric to estimate the quality of a movement. Different metrics were used to calculate smoothness such as the ratio between mean speed and peak speed [234, 240, 243, 244], different jerk metrics [234, 235, 239, 243–246], tent metric [244], mean arrest period [244], peak metric [239, 244, 246], number of sub-movements [247], comparison with an idealized normal speed profile [248], number of directional changes [243] or the spectral arc length metric [246]. Another feature is the hand-path-ratio [232, 234, 240, 249], sometimes referred to as straightness or trajectory error, which measures the deviation from a given (often straight) trajectory that has to be followed. Moreover, the precision and accuracy [239, 248] of a given targeted movement or the shape accuracy [234, 250] are used as features to describe the quality of a movement. Patients with a neurological disorder often show abnormal synergy [251]. The assessment of abnormal synergies was previously performed using position information [250, 252] or isometric torque values during a motor task [253]. When kinetic information is available in an active device, the resistance to passive movement (RPM) can be extracted as a feature, which can be seen as a measure of spasticity in the measured joint. In this assessment, the patient is passive and moved by the isokinetic robot, often at different speeds, while the resistive torque is recorded [254–258]. Reaction time is a measure for the time the patient needs to initiate a movement. It is usually measured as the time needed between the moving instruction (visual cue, sound) and the movement onset, which is a predefined deviation from the starting position or a velocity threshold [249, 259].

A major challenge is that the robot-assisted assessments are clinically accepted. In clinical environments, there already exists a multitude of established clinical assessments and scores that are regularly used and well known by the therapist. A possible approach is, therefore, to reconstruct clinical scores based on the robotic assessment to

have an accepted measure understandable for therapists and physicians. Several publications evaluated the correlation between robotic assessments and accepted clinical scores, such as the Fugl-Meyer scale [232, 235, 240, 260], the Modified Ashworth Scale (MAS) [232, 235, 236], the Motor activity log [240], the Action Research Arm Test (ARAT) [240, 243], the Jebsen-Taylor Hand Function Test [240], the Graded and Redefined Assessment of Strength, Sensibility and Prehension (GRASSP) [243], Spinal Cord Independence Measure (SCIM) [243], Motor Status Score [232], Motor Power Scale [261], etc.

In this chapter, we evaluated a set of robot-assisted assessments for the upper extremity in healthy and SCI patients in a stage 1 consideration-of-concept study [262]. Five different assessment packages were implemented that include raw sensor data and feature extraction: ROM (active and passive joint range of motion), WORKSPACE (cubic arm reachable workspace), QOM (quality of arm reaching movements), STRENGTH (isometric joint torques) and RPM (resistance to passive joint movement). The assessments were tested in healthy subjects and SCI patients for applicability, safety, reliability and comparability with clinical scales. The assessments were implemented into the existing therapy robot ARMin III that, through its exoskeleton structure, allows not only for measurement of kinematic- and time-based parameters, but also for kinetic-based measures. The five different assessment packages were combined with a visual interface for an intuitive and standardized execution of the assessments. The implemented assessments are based on measurements used in other devices and are extended and adapted for the use of our robotic setup.

Up to now, most of the robot-assisted arm assessments were tested on stroke patients and the extension of the assessments to the SCI target group was rarely tested. An exception is Zariffa et al. [243] who tested different kinematic measures on SCI patients with the passive arm exoskeleton robot ArmeoSpring and Perell et al. [254] who investigated muscle tone in SCI patients with an isokinetic dynamometer. However, we are the first to offer a comprehensive measurement of patients' motor function within one single device.

We hypothesized that the ARMin assessment packages provide an applicable, safe, reliable, and comparable tool to measure arm motor functions in SCI patients. To evaluate the intra-rater reliability, data from ten healthy subjects was collected. To analyze correlations between clinical tests and ARMin assessments and to quantify the inter-rater reliability, a feasibility study on five SCI patients with two different testers was conducted. We believe that the robotic assessments are widely reliable and comparable to clinical scales for arm motor functions. Furthermore, they may offer a sensitive and objective measurement for more detailed insights in arm motor functions.

### 4.1.2 Method

To evaluate the five ARMin assessment packages - namely ROM, WORKSPACE, QOM, STRENGTH and RPM - healthy subjects and SCI patients participated in this study to investigate the four aspects intra-rater reliability, inter-rater reliability, comparison between healthy subjects and patients, and construct validity.

For the evaluation of the assessments, the ARMin platform is used (Fig. 4.1, more details in Sec. '1.3.2 ARMin Arm Rehabilitation Robot'). The implementation of

the assessments capitalizes on the different control modes available for the robot. The position controller is either used to move the passive patient arm during the RPM assessment or to fix the arm posture during single joint measurements such as ROM or STRENGTH assessment. The compensation mode is used for QOM and WORKSPACE assessments, where the robot should not interfere with the patient's movement and only follow the arm to record kinematic data.

With its exoskeletal structure, precise position sensors, mechanical transparency, and a visual display, ARMin is particularly useful to assess kinetic and kinematic arm functions on joint and end-effector level.

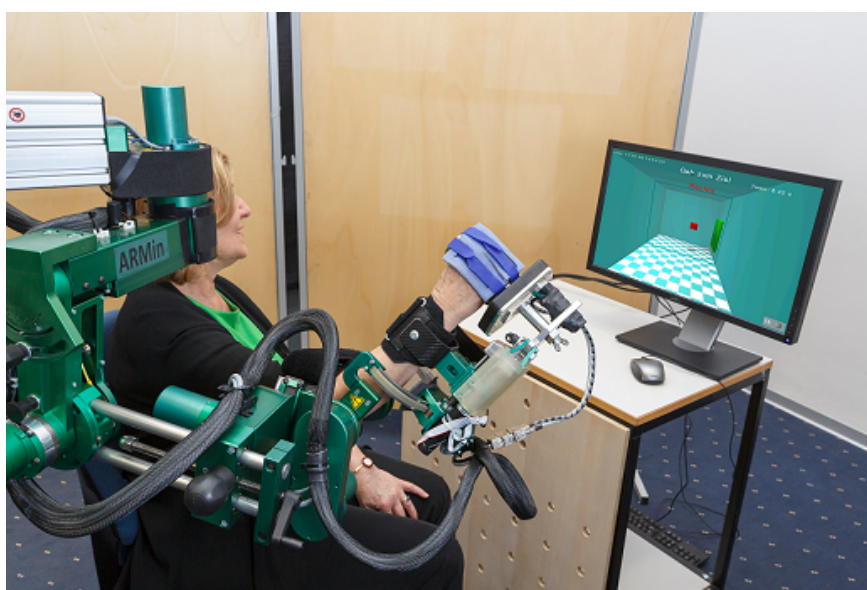


Figure 4.1: Subject performing assessments with the ARMin arm robot (courtesy of Dietmar Heinz). Published with written informed consent of the individual in the picture.

## Participants

Patients were recruited by contacting in- and out-patients of the University Hospital of Balgrist. This hospital located in Zurich, Switzerland, offers specialized treatment for SCI patients and treats about 230 inpatients and about 1'500 outpatients after SCI annually.

Eligibility criteria were i) cervical, complete or incomplete SCI with tetraparesis ii) no severe subluxation of the shoulder, iii) no severe shoulder pain on the tested side and iv) no other illness or incapability that could compromise the assessments. Five patients (aged 19 to 49, mean 33.8, Std 13.8; 4 male) were eligible to perform the five robotic assessments as well as clinical tests. Three patients were in the subacute (i.e.,  $\leq 6$  months) and two in the chronic (i.e.,  $> 6$  months) state post-SCI with different levels of severity (ASIA B to ASIA D) and arm dominance (four right-handed and one left-handed) (Tab. 4.1). As one out of the five patients reported severe shoulder pain on one side, the corresponding arm was excluded. As the SCI was incomplete in the five patients and their two arms were affected to different degrees, nine unrelated data sets were sampled for evaluation.

Eleven healthy right-handed subjects (aged 21 to 64, mean 35.4, Std 15.4; 6 male) were assessed on their dominant side to determine the intra-rater reliability. Thirteen healthy right-handed subjects (aged 20 to 68 years, mean 34.9, Std 15.7; 6 male) performed the assessments with their non-dominant arm to compare the performance with the patient’s non-dominant arm. This data was also used to define norm values. None of the subjects had experience with ARMin prior to the study onset.

**Ethic statement** All patients signed an informed consent; the study was approved by the responsible ethical committee (KEK, Zurich, Switzerland) and the Swiss Agency for Therapeutic Products (Swissmedic, reference number: 2011-MD-0002). The individual in Fig. 4.1 has given written informed consent (as outlined in PLOS consent form) to publish these case details.

ID	Status <sup>a</sup>	Level of lesion	Age [y.]	Sex	Seq. of arm side tested	Dominant hand <sup>b</sup>	Seq. of tester
1	subacute	sub C5, ASIA B	20	m	r, l	r	T1, T2
2	subacute	sub C5, ASIA B	19	m	l, r	r	T2, T1
3	chronic	sub C4, ASIA C	36	f	r, l	l	T1, T2
4	chronic	sub C6, ASIA B	47	m	r, l	r	T2, T1
5	subacute	sub C1, ASIA D	47	m	l	r	T1, T2

Table 4.1: Characteristics of patients. r = right, l = left. <sup>a</sup>Chronic (> 6 months) vs. subacute ( $\leq$  6 months post SCI). <sup>b</sup>Evaluated with the questionnaire of Chapman [263].

### Study Design

In this consideration-of-concept study (stage 1), we aimed to analyze the utility of the chosen assessment measurements and to evaluate how well they can be applied [262]. We tested for applicability, safety, reliability and validity. Forty minutes were scheduled for the performance of the assessment packages, including positioning and instruction of the subject.

**Intra-rater reliability with healthy subjects** The intra-rater reliability was tested with eleven right-handed healthy subjects. A set of norm values was determined. The subjects performed all ARMin assessments four times with their dominant right arm at intervals of one week. Hand dominance was evaluated with the questionnaire of Chapman [263]. No pretest was performed before starting the intra-rater measurement as only minor learning effects were expected. The settings of the robot (arm length settings, shoulder, and chair height and position) and the sequence of the ARMin assessments were held constant. Three trained testers performed the measurements, where each subject was always assessed by the same tester.

**Comparison between healthy subjects and patients** In order to complete a first set of norm values with data from non-dominant arms, 13 healthy subjects performed the assessments once with the non-dominant left hand. Again, three different testers performed the assessments. The acquired norm values for the non-dominant and the dominant arm (values from the first assessment session) were used to compare the assessment performance between the healthy subjects and the SCI patients.

**Inter-rater reliability and construct validity with patients** For evaluation, inter-rater reliability and correlation between ARMin assessments and common clinical assessments were tested in a cross-sectional study. To assess the inter-rater reliability of the ARMin assessments, two testers performed the assessments. Both trained the ARMin assessments procedure at least ten times and with at least two patients to gain experience with the robot. Tester was given a manual that described the handling of the robot and the instructions to be given to the participants was used. The order of testers and the order of measured sides of each subject were randomized by lots which the patient drew on day 1. The sequence of ARMin assessments and clinical tests was held constant.

Each patient participated in six sessions (one pretest session, four robotic assessment sessions, one clinical assessments session) that were arranged over a period of twelve days (Tab. 4.2). While robotic assessments were conducted by both testers (T1 and T2), all clinical assessments were performed by the same one tester for all patients.

Day 1	Day 4	Day 5	Day 7, Day 8 or Day 9	Day 11	Day 12
Pretest	ARMin test 1	ARMin test 2	Clinical tests	ARMin test 3	ARMin test 4
robot settings, first test, define tester and arm by lot	arm 1, T1	arm 1, T2	aROM, pROM, MAS, MTS, GRASSP, SCIM, VLT, MMT	arm 2, T1	arm 2, T2

Table 4.2: Study protocol for the patients.

## Outcome Measures

**Robotic assessments** A set of five assessment packages was implemented to evaluate various aspects of arm motor function. While the ROM and the STRENGTH assessment were purely based on raw sensor data, the WORKSPACE, QOM and RPM assessments calculated features that are extracted from the raw data (Tab. 4.3). For the QOM and the WORKSPACE assessment the robot is in compensation mode. While most of the gravitational and frictional effects are compensated there may still be forces disturbing the arm movement such as static friction or dynamical effects of the robot.

**ROM (range of motion) assessment** ROM measured active and passive ranges of motion (aROM and pROM) of the arm. During this assessment ARMin held the patient’s arm in a predefined posture while the assessed joint was free to move.



Assessment name	Assessment description	Parameters
ROM	Active and passive ranges of motion of seven joint movements	Active ROM [°] (aROM); Passive ROM [°] (pROM)
WORKSPACE	Actively achievable Cartesian workspace	Workspace levels [# reached levels]/ Cubic volume [dm <sup>3</sup> ]
QOM	Quality of hand movement while performing goal-directed reaching tasks	Distance-path ratio (D-P ratio to target) [ ]; Distance-path ratio (D-P ratio to start) [ ]; Time to target [ms]; Time to start [ms]; Precision (Deviation on target) [m]; Number of peaks to target [ ]; Number of peaks to start [ ]; Reaction time to target [ms]; Reaction time to start [ms]
STRENGTH	Isometric maximum torque for seven joints	Joint torques [Nm]
RPM	Resistance to passive movements for two different speeds in all seven joints	Joint stiffness [Nm/rad]

Table 4.3: Overview of implemented assessments and the measured parameters.

The patient (aROM) or the therapist (pROM) moved the free joint in both directions (e.g., flexion and extension), while the software recorded both achievable extreme positions. The order of joints measured was fixed. The predefined robotic postures depended on the joint measured and were chosen to be as similar as possible to the "standardized neutral-0-method positions" [264] (postures described in Tab. S1, Appendix A.4.2). Seven different joint movements were assessed: ShEx/ShFl, ShAb/ShAd, HSAb/HSAd, ShIR/ShER, ElEx/ElFl, ElPr/ElSu, and WrEx/WrFl.

**WORKSPACE assessment** WORKSPACE aimed to measure the reachable cubic workspace of the end effector (i.e., the hand). The starting position of the hand was 30 cm in front of the breast (i.e., the xiphoid process of the sternum). On the screen, a small cubic room (corresponding to an initial size of 20 cm x 20 cm x 20 cm in the real world) was presented (Fig. 4.2 a). Each wall in the room indicated a direction to move to (top, bottom, left, right, towards the body, away from the body). For simplification, more directions such as diagonals were not assessed. The aimed movement direction was indicated by a green cube on the wall in randomized order. After the patient had reached the indicated wall, the room grew 5 cm in this direction. If the subject missed an indicated wall the room did not grow in this direction and the direction was shown once more later. The number of discrete increases in a certain direction refers to as a level and was used as an outcome parameter (workspace level, in numbers). Furthermore, the achieved room size (cubic volume, in  $\text{dm}^3$ ) was calculated from the workspace levels reached. The maximal volume of the room was  $140 \text{ dm}^3$ , the initial size was  $8 \text{ dm}^3$  and the maximal distances to the given room walls were 35 cm for the left and right (five movements in each direction to reach maximum expansion), 30 cm for the top (four movements to reach maximum expansion), and 20 cm for the bottom direction, towards the body and away from the body (two movements in each direction to reach maximum expansion). This results in a total of 20 movements to discretely increase the room size to its maximum.

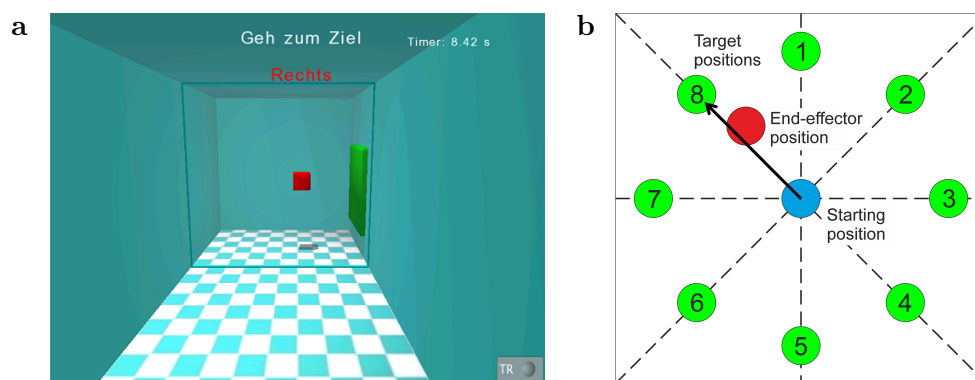


Figure 4.2: Visual representation of the WORKSPACE and QOM assessment packages. (a) Screenshot of the WORKSPACE assessment. A room was presented on the screen. The patient looked directly into this room. The end effector of the robot (the position of the patient's hand) was represented as a small red cube. In the shown situation the patient had to move to the green target position to the right. (b) Visualization of the eight targets (in green) in QOM that appeared successively on the screen around a given start position (in blue). The red disk represented the end-effector position.

**QOM (Quality of movement) assessment** QOM calculated accuracy and smoothness of a point-to-point movement. Eight target positions appeared successively around a starting position in the frontal plane (Fig. 4.2 b). The starting position was a circle that allowed some end-effector position variations in the range of 50 mm (rated as "on the start position"). The location of the target positions depended on the volume reached in WORKSPACE, i.e., the targets were at 80 % of the reachable distance. The patient was asked to move directly from the start to the target position as soon as it appeared, to rest on the target position until it disappeared (after 3 seconds) and then move directly back to the starting position. Output parameters were the distance-path ratio on the way to the target (D-P ratio to target), the standard deviation on the target position (precision), and the D-P ratio back to start (D-P ratio to start). Furthermore, the reaction time to initiate a movement (i.e., the time to leave a circle that was chosen 20 % wider than the starting position) and the time to target were calculated for each movement. For each movement the number of peaks of the end-effector speed (i.e., the zero transition of the end-effector acceleration) was counted as a measure of smoothness (using a peak detection threshold of 7.5 % of the maximum speed).

**STRENGTH assessment** STRENGTH recorded the maximum isometric torque of the arm (joint torques). ARMin moved the patient's arm to a predefined measuring posture similar to the one in ROM, but with the measured joint in the midrange (postures are described in Tab. S2, Appendix A.4.2). The posture was fixed during the joint torque measurement. For a baseline measurement the patient stayed passive for 5 s, and then applied the maximum possible torque in the measured joint for 5 s. A simple visual display showed the joint of interest and the timing. This procedure was repeated in both directions of each joint. The applied torque was estimated from the motor current. A moving average filter (window size 1 s) was applied to reduce the effect of single force peaks and the maximal joint torque was recorded.

**RPM (Resistance to passive movement) assessment** RPM quantified resistance of a single joint to passive movement within the prior measured pROM. ARMin moved the arm in a predefined start posture (identical to the postures in STRENGTH except for the measured joint which moves in the pROM, Tab. S2, Appendix A.4.2). The patient was instructed to keep the arm relaxed and passive while ARMin moved the joint of interest with two different speeds (30 °/s, 60 °/s). A calibration routine was used to identify the torque contributions that are caused by the robot arm mass (see also Fig. 4.7). This routine performed the same movements as the RPM assessment but without the patient. A 5<sup>th</sup> order Butterworth filter with 3 Hz cutoff was used to filter the calculated interaction torques. Knowing the torques applied by the patient the characteristic angle-torque relation could be used to calculate the resistance during the movement. It was assumed that this resistance is a combination of a constant offset torque and a stiffness contribution that changes when the joint angle increases or decreases. Therefore, a linear function was fitted into the data using the least squares method. Further analyzed for this paper was the joint stiffness using the slope of the linear fit.

**Clinical assessments** To evaluate the validity of the robot-assisted assessments the results were compared to clinical outcomes. The active and passive ranges of motion

were measured in a sitting position with a handheld goniometer. The measurement was accomplished according to the neutral-0-method [264]. For better comparison with the measurement of WORKSPACE, the arm reachable workspace (ARW) was calculated with a dedicated program as proposed by Klopčar et al. [265]. The ARW is based on the subject's body height, the maximal flexion/extension, abduction/adduction and internal/external rotation of the shoulder and the elbow flexion angle in standing position.

The modified Ashworth Scale (MAS) [266] and the modified Tardieu Scale (MTS) [267] rate the degree of spasticity and were measured for all relevant joints. For the MAS the joint is passively moved with a moderate velocity, for the MTS with high velocity. The tests use an ordinal scale in the range of 0 to 5 for the MAS and 0 to 4 for the MTS, where 0 is equivalent to 'no spasticity'.

The GRASSP [268] is an upper extremity assessment for patients after SCI and combines a muscle test for relevant upper extremity muscles, a Semmes-Weinstein-monofilament-test [24] and qualitative and quantitative grasping tasks. In addition to the muscle tests performed within the GRASSP, the Manual Muscle Test (MMT) [269] was performed on muscles that were not covered by the GRASSP but assessed with ARMin. The MMT was conducted in a sitting position. Arm positions were chosen according to the instructions of Daniels and Worthingham [270] and if necessary adapted to the sitting position.

Furthermore, the SCIM [271], a questionnaire for SCI patients that measures the independence in activities of daily living, was conducted to characterize the patients.

To measure functionality of the arm, the scientific or short version of the Van Lieshout Test (VLT) [272] and specific optional items for proximal function of the arm from the clinical or longer version of the VLT (wheelchair propulsion, transfers, push-ups while seated, stabilization of the arms, reaching low, reaching high) were conducted.

### Statistical Analysis

The feature extraction for the robotic assessments was performed using MATLAB (Mathworks, R2010b). The resulting parameters were exported to IBM SPSS Statistics for further statistical analysis. All the robotic measures were tested for normal distribution with histograms and Q-Q-Plots. The statistical methods used are summarized in (Tab. 4.4).

**Intra-rater reliability** Results of the four repeated assessments in healthy subjects were analyzed with the Friedman test against the null hypothesis that there are no differences. A significant difference ( $p < 0.05$ ) indicates a poor intra-rater reliability. Pairwise multiple comparisons were made by post hoc analysis with Wilcoxon signed-rank tests to determine where the differences between the repeated assessment measures occurred. To analyze the amount of variability between the four measurements, the mean difference between the maximum and the minimum value measured was calculated for the aROM, pROM, WORKSPACE, STRENGTH and RPM assessments. For QOM the standard deviation was calculated.

**Comparison between healthy subjects and patients** To analyze the differences between healthy subjects and patients, a qualitative approach was used calculating the ratio between mean values of the patients and mean values of healthy subjects. The

Analyzed aspect	Analyzed data		Statistical method
Intra-rater reliability	Parametric and nonparametric data		Friedman test with pairwise multiple comparison
Inter-rater reliability	Parametric data		ICC (two-way mixed model, single measure)
	Nonparametric data		Spearman
	Parametric and nonparametric data		Bland-Altman plot with one-sample Student's t-test
Construct validity	ROM	manual ROM	Spearman, Bland-Altman plot
	WORKSPACE	ARW, SCIM, GRASSP, VLT	Spearman
	QOM	VLT, SCIM, GRASSP	Spearman
	STRENGTH	MMT	Spearman
	RPM	MAS, MTS	Spearman

Table 4.4: Statistical methods for analysis of the intra-rater reliability, inter-rater reliability, and construct validity.

hypothesis was that patients would show a lower performance compared to healthy subjects. Accordingly, for the assessments that produce ascending scores for better performance, the ratio was expected to be less than 1 in patients. The dominant and non-dominant arms were analyzed independently. For the ROM, rather than comparing the minimal and maximal values of the joint range (e.g.,  $-5^\circ$  and  $130^\circ$ ) the full ranges (for this example,  $135^\circ$ ) were calculated and compared to healthy subjects.

**Inter-rater reliability** For evaluation of the inter-rater reliability, nine patient arms were measured. The Spearman's rank correlation coefficient was calculated for those ARMin assessments which were nonparametric. For parametric data, the intraclass correlation coefficient (ICC) was used (two-way mixed model, single measure). A significant correlation in either of these tests indicates a good inter-rater reliability for the assessment.

The differences between the two testers were further analyzed with Bland-Altman plots. The difference of two measurements was plotted against the mean of the two measurements. The one-sample Student's t-test was used with the null hypothesis that the mean difference between the testers is zero. A significant Student's t-test ( $p < 0.05$ ) indicates a significant difference between results of testers 1 and 2. The Bland-Altman plots were calculated without outliers (rejected by visual inspection; number of outliers: ROM: 20/252, WORKSPACE: 0/63, QOM: 31/514, STRENGTH: 7/128, RPM: 4/184).

**Construct validity** The construct validity was analyzed by comparing ARMin assessment parameters of the patient arms with clinical measurements, using the Spearman's rank correlation coefficient. The ARMin assessments and corresponding clinical tests are listed in Tab. 4.4. Mean values of the ARMin assessment parameters of

Assessment	Significant differences between the parameters from the four assessment tests
ROM <sup>a</sup>	pROM in pronation (p=0.03)
WORKSPACE <sup>b</sup>	No significant differences
QOM	D-P ratio to start for target 1 (p=0.003) (test 1 → test 3/4); D-P ratio to target 2 (p=0.033) (test 1 → test 2); Precision on target 1 (p=0.008) (test 1 → test 3/4); Reaction time to target 2 (p=0.041) (not sign. post hoc); Reaction time to target 7 (p=0.045) (not sign. post hoc); Reaction time to start for target 6 (p=0.048) (test 2 → test 4)
STRENGTH	Hand opening (p=0.013) (test 1 → test3 )
RPM	Shoulder external rotation 60 °/s (p=0.001) (test 2 → test 4) Elbow flexion 60 °/s (p=0.018) (not sign. post hoc)

Table 4.5: Summary of the significant differences found in the Friedman test of the intra-rater reliability. <sup>a</sup>As healthy subjects almost exclusively reached the mechanical limits ROM values correspond in most cases to the mechanical end limit. <sup>b</sup>The maximal workspace levels and, therefore, the maximal cubic volume were reached for the evaluated subjects for all the directions (p=1.00).

testers 1 and 2 were used. Values which were rated as outliers by visual inspection in the reliability analysis were excluded from validity analysis as well. A correlation of 0.0-0.5 was considered as weak, 0.5-0.75 as moderate and 0.75-1.0 as strong correlation. Correlations with a significance level  $p < 0.05$  are marked with \*, correlations with significance level  $< 0.01$  with \*\* in the text.

### 4.1.3 Results

Only STRENGTH values were normally distributed. Nonparametric methods were used for analysis in the other assessments.

#### Intra-Rater Reliability

Intra-rater reliability was calculated from four complete assessment sessions performed in eleven healthy subjects. The results are summarized in Tab. 4.5. The amount of variability between the four tests can be seen in Tab. S4 in Appendix A.4.2.

#### Comparison Between Values of Healthy Subject and Patients

The different assessment parameters were compared in the dominant (n=5) and non-dominant (n=4) arms. The results are listed in Tab. 4.6. The results for age and age/gender matched (only male patients and subjects) comparisons are similar. For better visualization of the differences between patients and healthy subjects in the RPM assessment, the average joint stiffness parameters for all joint movements are plotted in Fig. 4.3.

Assessment	Patients in comparison with healthy subjects
ROM	<b>Dominant arm:</b> aROM: 81 %; pROM: 95 %. <b>Non-dominant arm:</b> aROM: 67 %; pROM: 90 %.
WORKSPACE	<b>Dominant arm:</b> cubic volume: 79 %. <b>Non-dominant arm:</b> cubic volume: 73 %.
QOM	<b>Dominant arm:</b> D-P ratio to target: 102 %; D-P ratio to start: 101 %; time to target: 129 %; time to start: 125 %; number of peaks to target: 115 %; number of peaks to start: 168 %; precision: 85 %. <b>Non-dominant arm:</b> D-P ratio to target: 93 %; D-P ratio to start: 99 %; time to target: 84 %; time to start: 107 %; number of peaks to target: 69 %; number of peaks to start: 72 %; precision: 88 %.
STRENGTH	<b>Dominant arm:</b> Joint torques between 23 % (hand opening) and 97 % (elbow flexion). <b>Non-dominant arm:</b> Joint torques between 8 % (hand closing) and 97 % (supination).
RPM	<b>Dominant arm:</b> The difference between joint stiffness in the patients' arms (mean: 0.49 Nm/rad) and the healthy subjects (mean: 0.34 Nm/rad) is 0.15 Nm/rad. <b>Non-dominant arm:</b> The difference between joint stiffness in the patients' arms (mean: 0.72 Nm/rad) and the healthy subjects (mean: -0.08 Nm/rad) is 0.80 Nm/rad.

Table 4.6: Summary of the comparison between data of patients and healthy subjects. For D-P ratio, time to start/target, number of peaks and precision a value below 100 % indicates a better performance of the patients while for ROM, cubic volume, and joint torque a value below 100 % indicates a better performance of the healthy subjects.

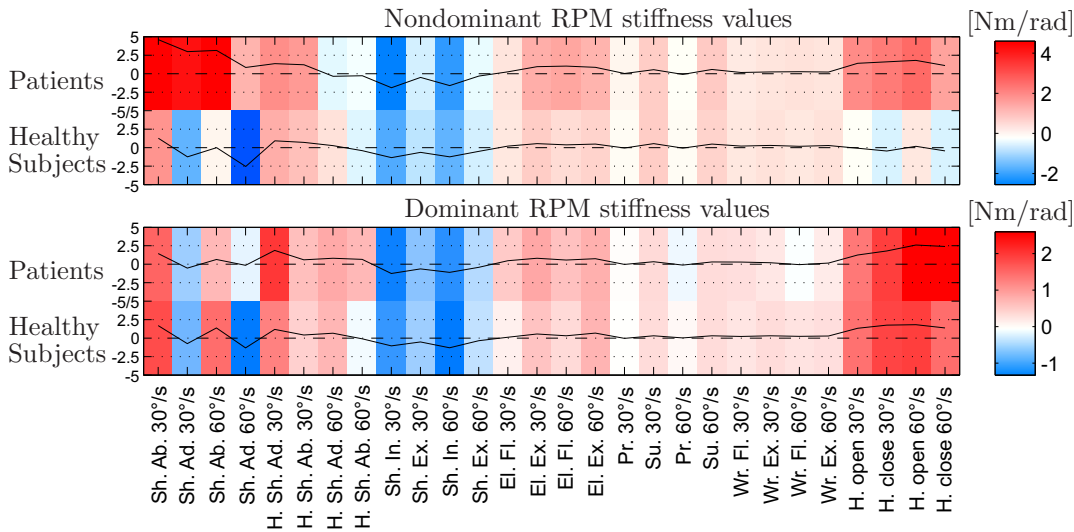


Figure 4.3: Visualization of joint stiffness measurements within the RPM assessment for the non-dominant and dominant arms of healthy subjects and patients. The more a joint counteracted the robot movement over the angle, the higher and more intense in color (red) the value. The color gradient ranges from minimal (blue) to maximal values (red) and is different for the non-dominant (-2 to 4) and dominant arms (-1 to 2).

### Inter-Rater Reliability

The inter-rater reliability was analyzed using the Spearman’s rank correlation coefficient and the Bland-Altman plot. In Fig. 4.4 an exemplary Bland-Altman plot for the wrist flexion is shown. The analysis of the WORKSPACE and QOM parameters is shown in more detail in Tab. S3 (Appendix A.4.2). The mean cubic volume was  $107.5 \text{ dm}^3$ . Fig. 4.5 is an example of a patient’s hand movements to the eight different targets in the QOM assessment package. The summarized results for the inter-rater reliability between testers 1 and 2 are summarized in Tab. 4.7.

### Construct Validity

**ROM** Spearman’s rank correlation coefficient between the clinical ROM measurement and the robot’s ROM was significant for aROM in lateral shoulder abduction, elbow flexion and wrist flexion/extension, and showed a moderate but not significant correlation for shoulder flexion ( $0.59, p=0.06$ ). The other correlations were not significant ( $p=0.1$  to  $p=0.43$ ). Regarding pROM, only lateral shoulder abduction and horizontal abduction were significant. The results are shown in Tab. 4.8.

Bland-Altman plots were generated to evaluate the degree of agreement between clinical and robotic measurements. The mean difference between the two measurement methods were significantly different regarding aROM for 6 out of 12 measurements (lateral shoulder adduction, shoulder extension, internal and external rotation, supination and wrist flexion) and regarding pROM for 10 out of 12 measurements (lateral shoulder adduction, shoulder extension, horizontal ab-/adduction, internal and external rotation, elbow flexion, pronation and wrist flexion/extension). This difference results from predominantly higher clinical ROM values compared to the ranges measured in



Assessment	Spearman correlation, ICC, Bland-Altman analysis
ROM	Spearman: aROM: Shoulder flexion/extension (0.95/0.85); lateral shoulder ab-/adduction (0.83/0.96); horizontal shoulder ab-/adduction (0.78/0.83); shoulder internal rotation (0.87); supination (0.92); wrist flexion/extension (0.72/0.85). pROM: Lateral shoulder adduction (0.98); shoulder extension (0.92); horizontal shoulder ab-/adduction (0.77/0.90); internal rotation (0.80); wrist flexion (0.67). Bland-Altman: aROM: No significant differences; pROM: Shoulder extension (p=0.047), internal-/external rotation (p=0.033/p=0.028).
WORKSPACE	Spearman: Workspace levels (between 0.75* and 1.0**); cubic volume (0.77*). Bland-Altman: Workspace levels downwards (p=0.035); cubic volume (p=0.025).
QOM	Spearman: Number of peaks to start: 0.71*. Bland-Altman: No significant difference between testers.
STRENGTH <sup>a</sup>	ICC: Between 0.80** and 0.98** (except for supination joint torque: 0.38). Bland-Altman: Wrist extension (p=0.01).
RPM	Spearman: Shoulder flexion at speed 30°/s and 60°/s; Shoulder internal rotation at 30°/s. Bland-Altman: Elbow flexion at 60°/s (p=0.019).

Table 4.7: Summary for the inter-rater reliability analysis. The numbers show the significant Spearman correlation coefficients, the significant ICC values and the significant differences from 0 in the t-test for the Bland-Altman analysis. \*= $p < 0.05$ . \*\*= $p < 0.01$ . <sup>a</sup>Data of testers 1 and 2 were normally distributed for STRENGTH.

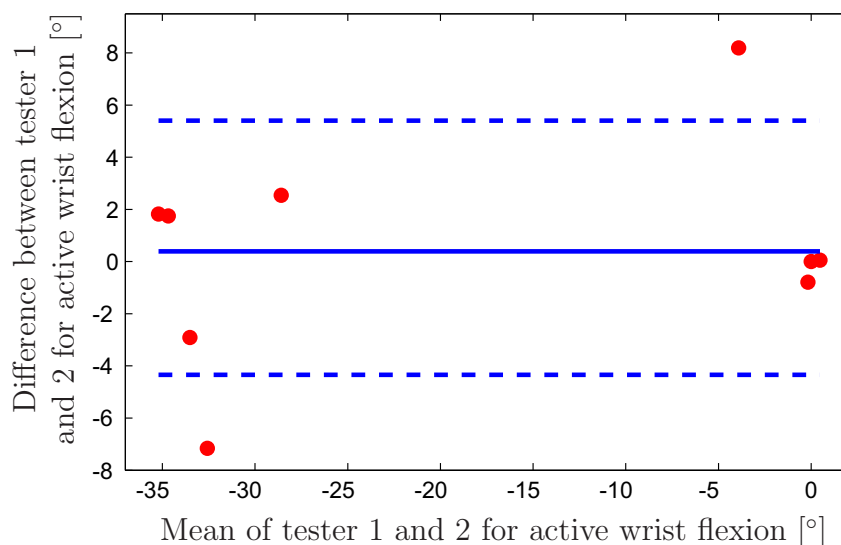


Figure 4.4: Example of an aROM Bland-Altman plot regarding wrist flexion for the nine patient arms. The limits of agreement (dashed lines for lower  $-4.3^\circ$  and upper  $5.4^\circ$  limit) and the mean difference (solid line at  $0.5^\circ$ ) are shown. The x-axis shows the mean values of the two measurements of tester 1 and 2 (negative values indicate flexion, positive values stand for extension), while the y-axis shows the measurement difference between tester 1 and 2.

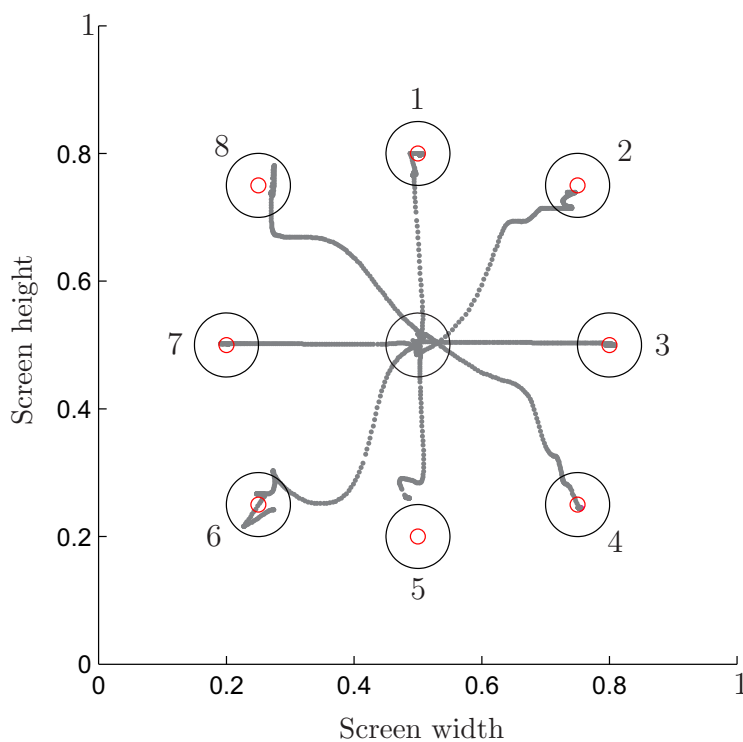


Figure 4.5: QOM: The hand paths of a patient moving to the 8 different targets.

Robotic assessment	Clinical assessment	Spearman correlation
ROM	Manual ROM	aROM: Lateral shoulder abduction (0.63, $p=0.034^*$ ), elbow flexion (0.81, $p=0.004^{**}$ ) and wrist flexion/extension (0.78, $p=0.007^{**}/0.67$ , $p=0.035^*$ ); pROM: Lateral shoulder abduction (0.78, $p=0.006^{**}$ ) and horizontal abduction (0.64, $p=0.031^*$ ).
WORKSPACE	ARW	Cubic volume significantly correlates with ARW (0.69*).
	VLT, GRASSP, SCIM	Cubic volume correlates moderately with the test score of GRASSP (0.53), VLT (0.54) and SCIM (0.51). The workspace levels correlate on a 0.7* level with the VLT and GRASSP items.
QOM	VLT, GRASSP, SCIM	Particularly D-P ratio to start (GRASSP: -0.700*, VLT: -0.644*) and reaction time to start (GRASSP: -0.667*, VLT: -0.636*) show moderate correlations with the clinical scores.
STRENGTH	MMT	The correlations between STRENGTH joint torque and MMT range between 0.69* and 0.91** (except for shoulder extension).
RPM	MAS, MTS	No analysis due to lack of data.

Table 4.8: Summary of the results for the construct validity. The table shows the significant correlations between the robotic and clinical assessments.  $^*=p<0.05$ .  $^{**}=p<0.01$ .

the robot. This was also reflected in correlations between the assessment differences and the mean values in the evaluation of the Bland-Altman plots, i.e., the difference was higher, for higher mean values.

**WORKSPACE** The ARW was calculated from ROM values measured with a goniometer. Spearman's correlation coefficient between cubic volume and the ARW was 0.69\*. The cubic volume was approximately half the size of the ARW. Cubic volume correlates on a 0.5-0.6 level with VLT and the single prehension items of the GRASSP but not with the sensibility items of GRASSP. The correlation of cubic volume was 0.53 for the GRASSP, 0.54 for the VLT and 0.51 for the SCIM. The workspace levels in the different ARMin directions correlated on a 0.7\* level with VLT and GRASSP items, and on a 0.8\* level with the targets in the "up" direction, but not for the sensibility items.

**QOM** Overall, results regarding correlations of QOM with GRASSP, VLT and SCIM were inconsistent, but there was a tendency that patients with higher values in GRASSP, VLT and SCIM got better results in QOM values (Tab. 4.9). Particularly, D-P ratio to start and reaction time to start showed moderate correlations with the clinical scores.

QOM metric (Mean values)	GRASSP	VLT	SCIM
D-P ratio to target	-0.450	-0.326	-0.441
D-P ratio to start	-0.700*	-0.644*	-0.653*
Precision	0.217	0.209	0.314
Number of peaks to target	0.233	0.142	0.144
Number of peaks to start	0.000	-0.050	-0.059
Reaction time to target	-0.350	-0.293	-0.398
Reaction time to start	-0.667*	-0.636*	-0.687*
Time to target	0.400	0.427	0.373
Time to start	-0.017	0.000	0.008

Table 4.9: Correlations between the QOM assessment and the clinical GRASSP, VLT, and SCIM scores. Negative values result when scales have diametric changes with improvement. \*= $p < 0.05$ .

**STRENGTH** The Spearman’s correlation coefficients between STRENGTH and the manual muscle test of corresponding joints were very high and ranged between 0.69\* and 0.91\*\*. The corresponding data for all joints is plotted in Fig. 4.6. Only for shoulder extension there was no significant correlation (0.54,  $p=0.066$ ).

**RPM** Only one single patient showed a Tardieu and/or Ashworth Scale value higher than 0 (for shoulder extension, internal rotation, elbow flexion, supination, and wrist extension), all other patients had no clinically detectable spasticity. Therefore, no further statistical analysis was possible to calculate the correlations. An example of RPM is shown in Fig. 4.7. It represents both the elbow flexion data of a patient with a Tardieu score of 2 and a patient with a Tardieu score of 0.

#### 4.1.4 Discussion

Despite the small sample size, first conclusions could be drawn regarding applicability, reliability, validity and limitations of the single assessment packages. All subjects and patients were able to understand and perform the different assessment packages.

#### ROM

**Assessment evaluation** The mechanical joint limits of the robot were reached by the healthy subjects and sometimes by the patients, leading to a saturation effect of the range values. Therefore, ROM showed good intra-rater (except for pROM pronation) and inter-rater (except for shoulder extension and internal-/external shoulder rotation) reliabilities. The aROM and pROM values of the patients were both smaller compared to healthy subjects. Furthermore, the comparison of the aROM and pROM values with the manual ROM test was good for several joints (active lateral shoulder abduction, elbow flexion, wrist extension, shoulder flexion and passive lateral shoulder abduction). We assume that this correlation is better for severely and moderately affected patients, who do not reach the robot joint ranges. The results support our use of the ROM values as a basis for exercises or assessments (such as the RPM assessment) to define the usable and safe region.

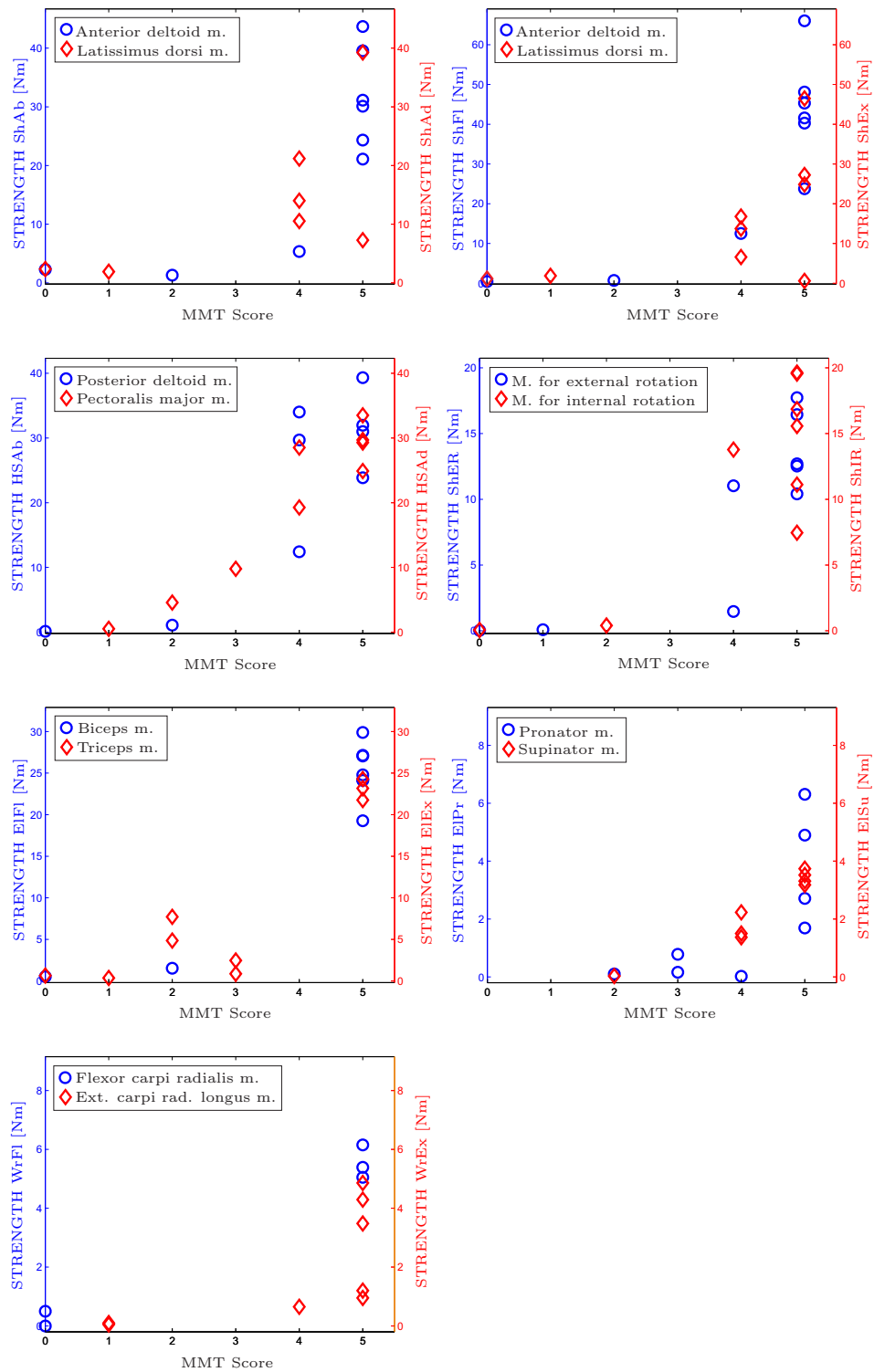


Figure 4.6: Plots of the patient joint torques from STRENGTH vs. MMT scores for all joints and in both directions. (x-axis = MMT score, y-axis = joint torque from STRENGTH).

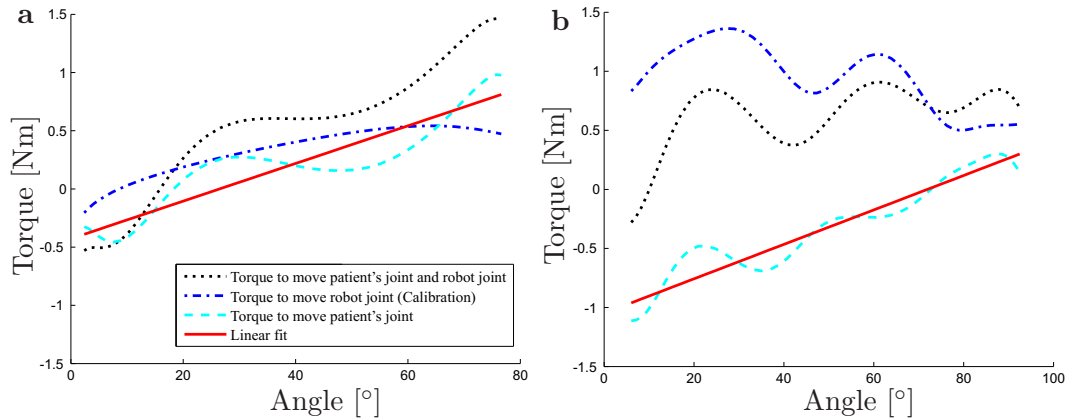


Figure 4.7: Example RPM plot for elbow flexion ( $60^\circ/\text{s}$ ) of two patients (**a** and **b**). The black dotted line shows the torque progression measured during the assessment. The blue dash-dotted line is the data from the calibration routine without the patient. The dashed cyan line is the estimated torque progression of the patient's joint. The red line is the linear least square fit for the patient's joint torques. (**a**) The movement in the left picture was rated a 2 on the Tardieu scale. (**b**) The movement on the right example was rated a 0 on the Tardieu scale. The measured stiffness by the robot assigned  $0.93 \text{ Nm/rad}$  to the left and  $0.84 \text{ Nm/rad}$  to the right movement.

**Limitations** The mechanical limits of the robot are not only due to kinematic constraints but also chosen for safety reasons and, therefore, do not cover the whole range that can maximally be reached by a healthy subject (e.g., in [273]). This was reflected by the significant differences between tester 1 and 2 found in the Bland-Altman plot and the strong correlation between the differences and the mean of clinical and robotic results. As most patients in the sample got higher ROM values in the clinical measurements with the goniometer, a goniometer has to be preferred to robots (with similar ROM) for the measurement of joint range.

**Applicability** The chosen robot postures for measuring the range were applicable for all patients. Even patients sitting in a wheelchair could be measured in the predefined positions. The discrepancy between clinical and robotic ROM in wrist extension was mainly due to an offset between the zero position of the robot (i.e., grasping the hand module leads to an initial dorsal extension) and the zero position measured by the therapist (straight hand with stretched fingers and no dorsal extension).

## WORKSPACE

**Assessment evaluation** The subjects reached the maximum cubic workspace, therefore, intra-rater reliability was good regarding cubic volume and workspace levels. The comparison with the patients showed that their cubic volume was around 70 - 80 % of healthy subjects (Tab. 4.6). Furthermore, a good inter-rater reliability was found for workspace level and cubic volume. However, the Bland-Altman plot showed significant differences between the two testers for cubic volume. A closer look at the values revealed that the volume assessed by tester 2 was always equal (4 out of 9 tests) or higher (5 out of 9 tests) as compared to tester 1. The actual source for this difference could

not be identified. Possibly, the difference came from discrepancies in how the patient was motivated to reach in the different directions. The cubic volume correlated well with the ARW and moderately with the VLT/ GRASSP items. As WORKSPACE is reliable, it can be used for calibration of exercises (e.g., to place objects in the virtual environment, so that the patient can reach them) or as a basis for further assessments (e.g., as we did in QOM). More parameters might be extracted from this assessment to analyze the movements in more detail, such as the interjoint coordination. However, changing distances to the room walls have to be taken into account.

**Limitations** WORKSPACE should only be used for assessment of severely affected patients, who do not reach the maximum cubic volume. The inter-rater reliability was poor in the downward direction for workspace level. The reason may be that downward movements were limited by the legs and depending on the robot forearm posture the robot could be moved more or less in this direction. A solution would be to fix the pro-/supination in a predefined position during this measurement such that the conditions stay the same for each patient.

Another limitation related to the clinical validity was that the absolute values of the workspace volume were much higher for the clinical assessment than in WORKSPACE, the reason being that WORKSPACE did not calculate the real workspace volume (e.g., as shown in [238]) but a cubic volume in front of the patient.

**Applicability** No problems with the applicability of the assessment. The workspace was assessed in several steps reaching walls of discretely increasing distance. It could be simplified by continuously moving the walls away from the center position.

## QOM

**Assessment evaluation** The QOM assessment had mainly good intra-rater reliability. The only values that changed significantly over the course of the four ARMin sessions were almost exclusively due to different results for the first targets of the first session pointing to a learning effect. The comparison between patients and healthy subjects revealed that the patients performed similar or better than healthy subjects with the non-dominant arm. Currently, we have no explanation for this trend. In the dominant arm, the healthy subjects gained better results (as expected, Tab. 4.6). The inter-rater analysis showed neither significant correlation between the testers (except for number of peaks to start) nor could differences be detected in the Bland-Altman analysis. The reason is in our opinion the small sample size. The precision metric showed a tendency to moderately correlate between the testers. The construct validity analysis revealed moderate but significant correlations comparing D-P ratio to start and reaction time to start with GRASSP and VLT.

**Limitations** The fact that specifically the movements to the first target in the first test showed significant differences to later tests indicates that the first couple of movements should not be included in the assessment as it is likely influenced by learning factors or inattention in the beginning. The results of the comparison and the inter-rater reliability showed clear differences between movements to the target and start position. This effect may be caused by a clear knowledge about the direction in which the start position will appear and, therefore, the movement could be planned before

the start position showed up. For the target positions the direction was not known beforehand and the reaction and the movement may have been influenced by where the target appeared.

The results of the peak metric from the comparison between patients and healthy subjects were very ambiguous. It is known from the literature that the peak metric performs fairly well for stroke patients, but is insensitive and nonrobust and unsuitable for healthy subjects [246] and insensitive to brief resting periods [245]. Although our assessment was performed in the frontal and not in the transverse plane as described therein, conclusions from the number of peaks metric should be drawn carefully. Further metrics, such as the spectral arc-length metric for smoothness [246] should be considered for evaluation in a next assessment version.

Reaction time would be more reliable, when measuring the time to overcome a certain distance from the real starting position, rather than measuring the time to leave a starting circle, where the real starting position inside this circle was unknown. Therefore, the distance that had to be moved until the reaction time was measured changed in each trial.

The location of the targets in the frontal plane without a restriction for the distance to the body may have been a source of higher variability in the assessed parameters, as the patient could choose slightly closer or more distant targets in different trials. An additional assessment package covering the quality of movement could be a tracking task of a figure e.g., a circle [234] or a Lissajous figure [274].

**Applicability** No problems with the applicability of the assessment.

## STRENGTH

**Assessment evaluation** The STRENGTH assessment had a good intra-rater and inter-rater reliability (except for wrist extension which showed a significant difference between the two testers in the Bland-Altman analysis). All the six valid comparisons for wrist extension showed slightly higher values in the assessments of one tester. The reason for this effect is unclear and we assume that it comes from the small number of valid samples in this joint and the normal variability in the force data. Furthermore, the construct validity showed a very good correlation with the MMT. The STRENGTH measurement detected even small changes in torques applied which cannot be detected with the MMT score. Moreover, the MMT scores showed a clear ceiling effect (Fig. 4.6) which was not present in the STRENGTH assessment (i.e., a maximum MMT score of 5 can still be continuously graduated with the STRENGTH measurement). The MMT is the standard assessment to measure muscle forces. Cuthbert et al. [275] reported an inter-rater-reliability from 0.63 to 0.98 with very well trained testers. As the STRENGTH assessment reached ICC scores for the inter-rater reliability from 0.80\*\* to 0.98\*\* the robotic assessment is comparable with the MMT score. Further aspects that could potentially be investigated in a later version are endurance or fatigue.

**Limitations** The measurement of the mid-hand closing forces may not be reproducible in other robots without knowledge of the exact design of the specific hand module.



**Applicability** The interface was used to show the currently assessed joint and in which direction the torque has to be applied. However, difficulties in understanding the indicated direction and the correct timing were reported sporadically.

## RPM

**Assessment evaluation** The RPM assessment aimed to measure the torque that was needed to move single joints of the arm. The stiffness portion of the arm resistance may be used as an indicator for arm stiffness or spasticity. The patients participating in this assessment study had almost no clinical relevant spasticity and, therefore, the interpretability of the results is very vague. Accordingly, the joint stiffness values were rather noisy with a trend for an increased resistance in patients. Mainly for shoulder ab-/adduction, elbow flexion/extension and hand opening/closing, Fig. 4.3).

If further investigations proof the validity of RPM assessments this would be a very good alternative for clinical scales such as MTS and the MAS which are neither reliable measurements for the upper extremity [231] nor have a rational scale with an appropriate resolution to measure subtle changes in the arm stiffness.

Similar robot-assisted RPM measurements were already performed by other groups with the therapist moving the arm and measuring force and angle with sensors achieving promising results [257]. Therefore, we hold to this approach and plan more tests with patients with spasticity or biomechanical stiffness in the arm.

**Limitations** The variation between ARMin tests on different days were high, this could be due to a real variation of the spasticity over time. Furthermore, clinical tests and the ARMin assessments were not performed on the same day or during the same time, which also influences the measured stiffness. For further studies, the clinical investigation of spasticity has to be short before or after the RPM measurement.

Higher joint speeds would be desirable for measuring aspects of speed-dependent stiffness (as in [254] or [276]). However, the ARMin robot is not powerful enough to reach higher speeds than roughly  $60^\circ/\text{s}$  over a sufficient joint range (after subtracting the joint region for acceleration and deceleration of the joint).

**Applicability** For the RPM measurements in this paper there was a calibration routine of the robot necessary in order to know the torques without the patient. An accurate dynamic model of the robot would make the calibration redundant and it could be skipped.

## General Remarks

In this consideration of concept study, only mean values for all directional movements were used (QOM and WORKSPACE). However, in a later study when there is more patient data available, specific directions, sectors or quadrants of the workspace should be grouped for a more detailed direction-dependent analysis.

Although the presented assessment packages were implemented in the ARMin robot, the methods can be applied to other exoskeleton robots. However, for STRENGTH the actuators and the robot structure have to be strong and stiff enough to counteract the torques applied by the patient. WORKSPACE and QOM can also be applied to end-effector robots, as both assessments only need the hand position as an input. The

robot as a measuring tool may produce unwanted interaction forces with the patient. These were reduced by active compensation of both gravity and friction. However, the arm dynamics may still be influenced, e.g., by additional inertia or non-modeled gravitational and frictional effects. This makes it more difficult to compare the assessment outcomes with other platforms or measurements (e.g., a free arm movement outside the robot) or with a platform with different inertial properties. This is mainly an issue for the assessments with free end-effector movements (QOM and WORKSPACE).

Furthermore, we cannot exclude that small imprecisions in the modeling of the non-linear spring compensation may have led to a systematic bias for a certain direction in the shoulder flexion/extension joint. However, this effect could not be observed from the recorded assessment data.

Besides these modeling factors of the robot, the therapist as well has some influence on the outcome. Even though the recordings are performed by the robot (except for the pROM) the positioning, instruction and motivation of the patient - though unintended - can influence the performance during the assessment and is reflected in the observed inter-rater reliability. This influence could further be reduced by using standardized audio-instructions or self-aligning exoskeleton axes [106]. In pROM the range measurement is directly affected by the therapist's (and also patient's) rating of how strong and far the joint can be moved before the resistance gets too high or the movement causes pain. The different assessments can be used independently from each other. Therefore, single assessment packages can be used to assess changes on daily basis, i.e., before or after the robotic arm therapy session. Considering the duration to perform all assessments successively, the complete assessment package may only be used for admission and discharge measurements or for outcome tests in research studies.

Finally, concerning the concurrent validity which was calculated by comparing each single robot-assisted assessment with one clinical assessment, the use of linear models or mixed models based on several robotic metrics [232] may have led to better reconstructions of the clinical scores and should be applied in a next validity analysis.

## 4.2 Robot-Assisted Assessments in ChARMin

### 4.2.1 Introduction

The availability of adequate arm assessments for diagnosis, measurement of therapy outcomes and improvements, for adaptation of the rehabilitation treatment and to gain insights in motor learning, is equally important for adults and children. A variety of clinical assessments are available for measuring pediatric arm function. Some assessments are specifically developed for the pediatric target group, e.g., the Assisting Hand Assessment (AHA), Melbourne Assessment 2, Quality of Upper Extremities Skills Test (QUEST) or the Pediatric Arm Function Test. Others are used likewise for children and adults, such as the Box and Block Test (BBT), Manual Muscle Test (MMT) or the modified Tardieu scale. A more extensive overview is given in the review of Gerber et al. [61]. For the pediatric target group the psychometric properties of these clinical assessments have not been extensively investigated and the assessments are not well tolerated by the young patients. Therefore, trials on upper limb rehabilitation in children and adolescents risk being biased by insensitive measurement tools lacking reliability [61].

Adult rehabilitation already capitalizes on repeatable, sensitive, and objective robot-

assisted assessments as mentioned in the literature overview in Sec. 4.1.1. In some of the previously mentioned robotic platforms for children, assessments are already included. Namely, the Pablo measures the range of movement of the arm with its integrated position sensors as well as hand force and pincers grip force [145]. The ArneoSpring Pediatric measures the active range of motion in the 3D workspace, the active and passive range of motion on joint level and the precision of hand movements in space. The Amadeo robot allows to assess the finger ROM and finger force.

In the study using the NJIT-RAVR system for children with hemiparetic CP [141], movement duration, smoothness of the end-point trajectory and reaching trajectory length were measured. In the study using the REAPlan [147], children with CP performed four different tasks (namely free amplitude, target, square and circle) which allowed measuring the amplitude (distance reached to the front) as well as the coefficient of variation of the straightness, the jerk metric and the speed metric (as previously presented in [234] for stroke patients). These examples show that robot-assisted arm assessments can be applied to children. However, there is currently no evidence for the reliability of these tools. Here, five robot-assisted assessments were developed to investigate the applicability, reliability, validity and responsiveness of robotic assessments in pediatric rehabilitation. In a first consideration of concept study, these assessments were applied to adult SCI patients with the ARMin robot as described in the previous section (Sec. 4.1). Based on the results of this study, the assessment packages were adapted for the ChARMin robot where needed. These assessments include the ROM assessment where the robot holds the arm in a predefined position and the assessed joint can actively or passively be moved to the minimal and maximal joint angles. The WORKSPACE assessment measures the cubic volume that the patient can reach in front of the trunk by showing alternately different directions to move to. The QOM package is used to assess the quality of goal-directed movements in space such as smoothness, time for the movement, speed, reaction time or distance-path ratio. In the STRENGTH assessment ChARMin holds the child's arm in a predefined posture to measure the isometric joint torques that the patient can apply. The RPM assesses the resistance to passive movement in the different joints. Furthermore, the existing assessments were extended by the CIRCLE package which measures the tracking capabilities of the child (such as the summed deviation from the target circle, smoothness, variability or the circularness of the resulting circle). The resulting six assessment packages were again combined with a visual interface for an intuitive and standardized execution of the assessments.

### 4.2.2 Method

#### **Adaptations from the Robot-Assisted Assessment Packages in Adults**

A first set of five robot-assisted assessment packages was tested on the ARMin platform with SCI patients [5] and are described in more details above (Sec. 4.1). This consideration of concept study showed different aspects that should be improved before the five packages were transferred and tested with the ChARMin robot. The adaptations performed on the algorithms, the evaluation software, and the interface are subsequently listed.

**General adaptations** The evaluation routine for the assessments was extended to increase the user-friendliness, the number of assessment parameters assessed and the

field of application of the software.

- A user interface was implemented for the evaluation routine for a user-friendly operation by therapists and other users of the robot (Fig. 4.8). The interface allows to choose the assessment which should be evaluated, to insert the assessment-specific parameters selected, the user profile (to know which files to evaluate), the source folder and the target folder, where the assessment parameters are saved.
- Additionally to the assessments, the games can also be evaluated with the same user interface (Fig. 4.8). Examples for the game evaluation are given in the results section (Sec. 5.3) of the ChARMin feasibility chapter.
- New output plots are generated and new parameters calculated for a more detailed analysis of the patient's arm motor function (maximum speed, average speed, etc.).
- The assessment software is directly embedded in the software interface (as shown in Fig. 2.18), compared to ARMin, where it was an additional software.

**ROM** A major issue with the ROM assessment was the fact that the patients often reached the mechanical end stop. The range of motion of the ChARMin robot is comparable to the ARMin robot. Therefore, we expect similar problems for mildly to moderately affected children who perform the ROM assessment.

**Interface** The interface mainly stayed the same. Each joint is represented on the screen by a horizontal bar. When moving the joint actively, the range is shown in blue. When the joint is moved passively by the therapist, the range is colored in green (Fig. 4.10 a).

**Algorithm** The ROM assessment starts with shoulder flexion/extension. When 90° flexion cannot be reached, all the other joints which use robot postures which are at this height (horizontal shoulder ab-/adduction, shoulder internal/external rotation and elbow flexion/extension) are skipped for safety reasons. The starting position for the elbow measurement was adapted from 0° to 45°.

**WORKSPACE** The tests with adult SCI patients showed that the WORKSPACE takes quite some time and that a continuous increase of the workspace volume is desirable (Sec. 4.1.4). Therefore, the WORKSPACE was extended with a continuous mode where the walls of the cubic volume can be moved continuously.

**Interface** The continuous mode was introduced to increase the walls of an initial room continuously by moving towards instructed room walls indicated with a green wall (Fig. 4.10 b). Further new settings for the assessment are the initial room size, the time that the patient needs to stay on the wall before the room is increased (for the discrete mode) and the possibility in the evaluation interface to choose which target movement should be plotted and analyzed in more detail. An example is given in the ChARMin feasibility chapter (Fig. 5.7 d).

**Algorithm** The evaluation algorithm was extended for the continuous mode. Parameters such as mean speed, maximal speed, reaction time, etc. are calculated for further analysis of the targeted movements. However, the instruction is not to

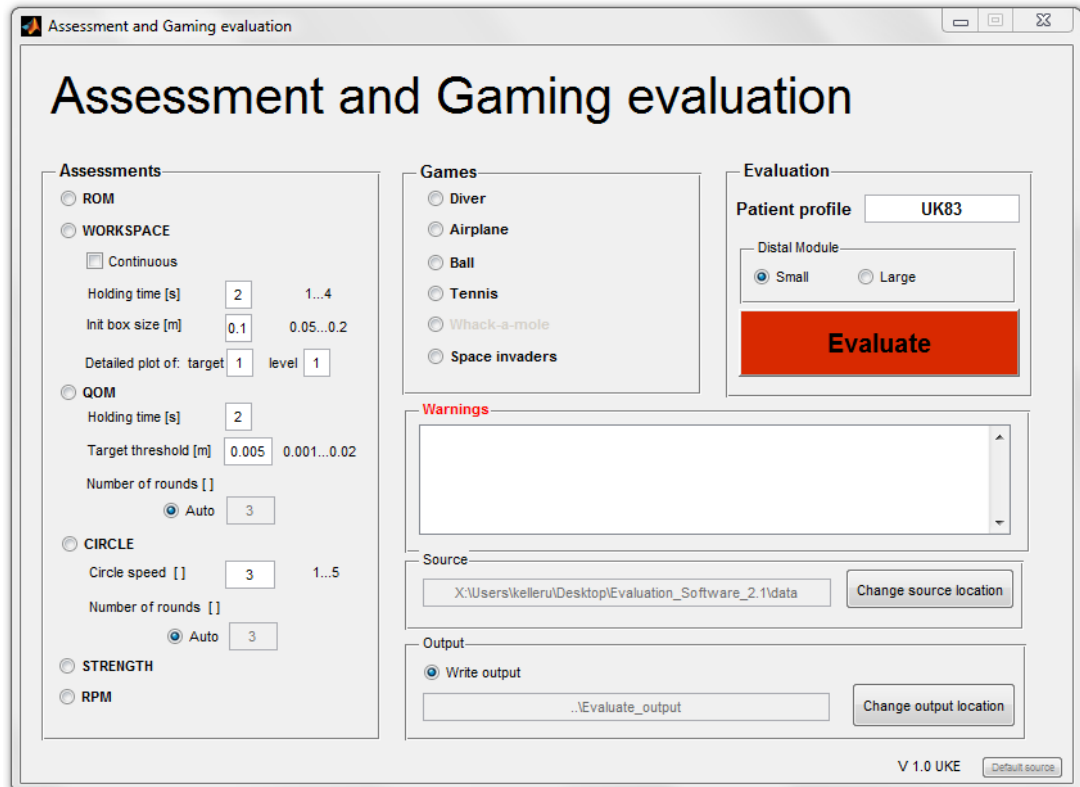


Figure 4.8: Interface for the evaluation of the recorded assessment and gaming data. In the left 'Assessments' panel, the user chooses the assessments to be evaluated and the settings which were used together with the assessments. The middle 'Games' panel allows to chose the games which should be evaluated. On the bottom right are the settings for the source folder of the assessment files and the output folder for the generated files with the assessment parameters. A warning panel informs about missing files, about files which are present several times, etc. On the top right, the patient profile and the distal module are specified and the evaluation can be started.

move as fast as possible to the target wall indicated and, therefore, these parameters have more informative content and should not be used as an assessment outcome.

**QOM** The QOM assessment and evaluation were mostly transferred to the ChARMin robot. More settings were added to adjust the assessment to the patient.

**Interface** In the assessment trials for adults, the distance of the targets from the start position depended on the previously assessed WORKSPACE levels. In the new assessment software, this distance can be fixed when desired. Further new settings are the time that the patient needs to hold the target position, the distance from the target which is rated as 'being on the target' and the number of rounds which should be evaluated. An example of the QOM assessment screen is shown in Fig. 4.10 c.

**Algorithm** The evaluation algorithm was slightly adapted to take the new settings into consideration.

**STRENGTH** The STRENGTH assessment was largely copied from the ARMin version.

**Interface** The posture for the elbow measurement was changed to get closer to the neutral-0-method position and get rid of the 90° shoulder flexion position. Furthermore, the therapist chooses the time point for the recording with a button on the interface (Fig. 4.10 d). For adults, this assessment was fully automated with predefined baseline and recording intervals. For children, in contrast, the therapist decides when the child is ready for the recording, as it may temporarily be distracted or some instructions may be needed in between to visualize the direction in which the force has to be applied.

**Algorithm** The evaluation algorithm remained unchanged.

**RPM** The RPM assessment was slightly adapted from the ARMin version.

**Interface** The interface looks similar to the previous version (Fig. 4.10 e). An additional feature allows reading previous pROM values to be able to run the calibration at a later time point and not directly after the assessment session.

**Algorithm** The lower speed for measuring the resistance was set to 10°/s compared to the ARMin measurement which measured at 30°/s. As the slow movement should be 'as slow as possible' (according to [267]) to not trigger a spastic reaction to the movement, but high enough to finish the assessment in reasonable time, the speed was chosen to be 10°/s, which was confirmed by the therapists. The rest of the evaluation algorithm remained unchanged.

### **CIRCLE Assessment**

In the conclusions of the adult assessment evaluation, the idea was raised that a tracking task could give additional information about the quality of the arm movement of the patient (Sec. 4.1.4). Gilliaux et al. [234] successfully used this concept for robot-assisted assessments with children suffering from CP. Therefore, a CIRCLE tracking

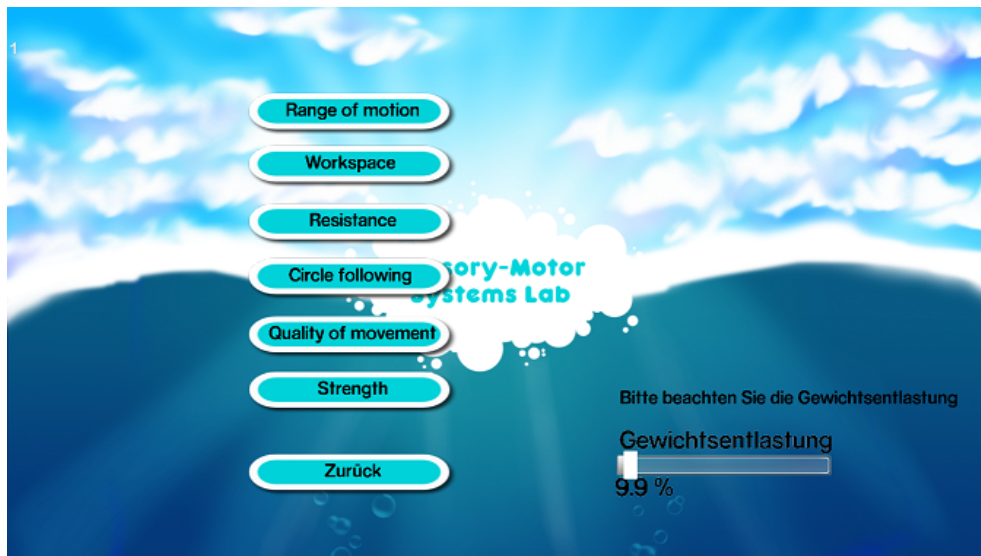


Figure 4.9: Assessment screen with the six different assessment packages available.

assessment was newly introduced for the ChARMin assessments. For this assessment, the patient's hand is represented as a red disk on the screen. A green reference disk moves circularly on the screen and the patient needs to follow this disk as closely as possible (Fig. 4.10 f). The assessment settings allow to select five different speeds (speed 1: 60 s/round, speed 2: 30 s/round, speed 3: 20 s/round, speed 4: 15 s/round, speed 5: 12 s/round) for the reference circle to adapt the assessments to the patient, when needed.

The assessment parameters extracted from the raw end-effector data are the summed difference between the current position and the reference disk, the percentage of the time that the patient was in front of the reference disk and the ellipse ratio, which is the ratio between the minimal and the maximal radius of the least-squares fitted ellipse. Further parameters, such as the smoothness of the end-effector movement are currently not calculated for the CIRCLE assessment.

### Implementation

The assessments software is directly integrated into the main menu of the user interface (Fig. 2.18). When the assessment is chosen in the main menu, the six different assessment packages can be selected on the screen (Fig. 4.9). Each assessment has a supportive interface showing the joint ranges, joint torques or targets that have to be reached or followed (Tab. 4.10).

For the integration of the assessments in the ChARMin robot, the software platform changed from the GIANTS engine software to the Unity game engine software. This is why the interface for all the assessments looks slightly different from the adult version. However, the conceptual ideas and the arm movements performed during the assessments remained mainly unchanged.

<p style="text-align: center;"><b>(a) ROM</b></p> <p>Range of Motion</p> <p>Leertaste für nächstes Gelenk</p> <p><input type="checkbox"/> Aktiv <input checked="" type="checkbox"/> Passiv</p> <table border="1"> <thead> <tr> <th>Joint</th> <th>Start Angle</th> <th>End Angle</th> </tr> </thead> <tbody> <tr> <td>Schulter Flex-Extension</td> <td>65.6°</td> <td>127.9°</td> </tr> <tr> <td>Horizontale Schulter Ab-Adduktion</td> <td>12.9°</td> <td>93.7°</td> </tr> <tr> <td>Schulter Innen-/Aussenrotation</td> <td>-30.1°</td> <td>66.1°</td> </tr> <tr> <td>Ellbogen Flex-Extension</td> <td>4°</td> <td>115.9°</td> </tr> <tr> <td>Pro-Supination</td> <td>-78.4°</td> <td>83.9°</td> </tr> <tr> <td>Handgelenk Flex-Extension</td> <td>-62.6°</td> <td>62.4°</td> </tr> </tbody> </table> <p>Fertig</p>	Joint	Start Angle	End Angle	Schulter Flex-Extension	65.6°	127.9°	Horizontale Schulter Ab-Adduktion	12.9°	93.7°	Schulter Innen-/Aussenrotation	-30.1°	66.1°	Ellbogen Flex-Extension	4°	115.9°	Pro-Supination	-78.4°	83.9°	Handgelenk Flex-Extension	-62.6°	62.4°	<p style="text-align: center;"><b>(b) WORKSPACE</b></p> <p>Nach rechts</p> <p>2</p> <p>current size of box = 0.32</p>
Joint	Start Angle	End Angle																				
Schulter Flex-Extension	65.6°	127.9°																				
Horizontale Schulter Ab-Adduktion	12.9°	93.7°																				
Schulter Innen-/Aussenrotation	-30.1°	66.1°																				
Ellbogen Flex-Extension	4°	115.9°																				
Pro-Supination	-78.4°	83.9°																				
Handgelenk Flex-Extension	-62.6°	62.4°																				
<p style="text-align: center;"><b>(c) QOM</b></p> <p>Quality of movement</p> <p>Trial Num: 1</p> <p>Bitte gehen Sie zum Ziel</p> <p>9</p> <p>Mit Leertaste zum Menü</p> <p>Schulterpositionierung</p>	<p style="text-align: center;"><b>(d) STRENGTH</b></p> <p>Strength</p> <p>Baseline Extension</p> <p>Record</p> <p>Press Record button to start measurement</p> <table border="1"> <thead> <tr> <th>Joint</th> <th>Min Value</th> <th>Max Value</th> </tr> </thead> <tbody> <tr> <td>Horizontale Schulter Ab-Adduktion</td> <td>-11.051</td> <td>16.067</td> </tr> <tr> <td>Schulter Flex-Extension</td> <td>-10.546</td> <td>17.042</td> </tr> <tr> <td>Schulter Innen-/Aussenrotation</td> <td>-11.739</td> <td>10.582</td> </tr> <tr> <td>Ellbogen Flex-Extension</td> <td>-10.767</td> <td>8.895</td> </tr> <tr> <td>Pro-Supination</td> <td>-10.515</td> <td>6.295</td> </tr> <tr> <td>Handgelenk Flex-Extension</td> <td>-1.387</td> <td>4.067</td> </tr> </tbody> </table> <p>Fertig</p>	Joint	Min Value	Max Value	Horizontale Schulter Ab-Adduktion	-11.051	16.067	Schulter Flex-Extension	-10.546	17.042	Schulter Innen-/Aussenrotation	-11.739	10.582	Ellbogen Flex-Extension	-10.767	8.895	Pro-Supination	-10.515	6.295	Handgelenk Flex-Extension	-1.387	4.067
Joint	Min Value	Max Value																				
Horizontale Schulter Ab-Adduktion	-11.051	16.067																				
Schulter Flex-Extension	-10.546	17.042																				
Schulter Innen-/Aussenrotation	-11.739	10.582																				
Ellbogen Flex-Extension	-10.767	8.895																				
Pro-Supination	-10.515	6.295																				
Handgelenk Flex-Extension	-1.387	4.067																				
<p style="text-align: center;"><b>(e) RPM</b></p> <p>Resistance</p> <p>Resistance assessment läuft</p> <p>Passiver ROM für Schulter Abduktion muss grösser als 90° sein</p> <p>Calibration</p> <table border="1"> <thead> <tr> <th>Joint</th> <th>Start Angle</th> <th>End Angle</th> </tr> </thead> <tbody> <tr> <td>Horizontale Schulter Ab-Adduktion</td> <td>13</td> <td>93.6</td> </tr> <tr> <td>Schulter Flex-Extension</td> <td>65.6</td> <td>127.6</td> </tr> <tr> <td>Schulter Innen-/Aussenrotation</td> <td>-29.8</td> <td>65.9</td> </tr> <tr> <td>Ellbogen Flex-Extension</td> <td>4</td> <td>115.8</td> </tr> <tr> <td>Pro-Supination</td> <td>-78.21</td> <td>83.7</td> </tr> <tr> <td>Handgelenk Flex-Extension</td> <td>-62.5</td> <td>62.4</td> </tr> </tbody> </table> <p>Fertig</p>	Joint	Start Angle	End Angle	Horizontale Schulter Ab-Adduktion	13	93.6	Schulter Flex-Extension	65.6	127.6	Schulter Innen-/Aussenrotation	-29.8	65.9	Ellbogen Flex-Extension	4	115.8	Pro-Supination	-78.21	83.7	Handgelenk Flex-Extension	-62.5	62.4	<p style="text-align: center;"><b>(f) CIRCLE</b></p> <p>Circle Following</p> <p>Speed level: 3</p> <p>Number of rounds: 1</p> <p>Mit Leertaste zum Menü</p> <p>Schulterpositionierung</p>
Joint	Start Angle	End Angle																				
Horizontale Schulter Ab-Adduktion	13	93.6																				
Schulter Flex-Extension	65.6	127.6																				
Schulter Innen-/Aussenrotation	-29.8	65.9																				
Ellbogen Flex-Extension	4	115.8																				
Pro-Supination	-78.21	83.7																				
Handgelenk Flex-Extension	-62.5	62.4																				

Table 4.10: Six different robot-assisted assessment packages were implemented for the ChARMin robot to describe the patient's arm motor function with kinematic, kinetic, and timing parameters.



### Technical Validation

A technical validation of the ChARMin assessments is necessary to characterize the suitability of ChARMin as a measurement tool. The measurements recorded during the assessments are the isometric joint torques, the joint angles, and the end-effector position. The technical validation allows to understand the assessment parameters with respect to the measurement precision, i.e., to judge what parameter uncertainty is introduced by imprecisions of the robot sensors.

**Torque estimation from motor current** For STRENGTH, a measurement of the patient's joint torques is needed. ChARMin is not equipped with force or torque sensors to measure this joint torque directly. However, ChARMin uses DC electric motors for each actuated joint. In DC motors, the torque is proportional to the motor current. The motor current is known, as the innermost control loop in our application is a current controller. As a consequence, the joint torque can directly be computed from the motor current.

For the isometric strength measurement, the robot is held in place by the robot actuators. When the patient applies a joint torque to the robot, the controller produces a counter torque to hold the position. Unfortunately, the motor torques and the torques applied by the patient are usually not identical, as friction decreases the torques which the motor needs to apply to counteract. Therefore, the relation between torques applied and torques measured has to be calibrated and its validity needs to be tested.

To calibrate the torque measurement, a hand-held AFG (Advanced Force Gauge) 1000N (Mecmesin, UK) sensor was used to apply forces to the different joints of the robot. The forces measured with the Mecmesin sensor and the robot joint torques were recorded simultaneously and compared to each other. From the AFG force measurements, the applied torques can be determined by multiplication with the distance from the measured joint to the attachment point of the AFG. For each joint, the two joint directions were measured twice.

**End-effector measurement repeatability and precision** For the assessments which instruct to move to a point in space, such as the WORKSPACE, QOM or CIRCLE, it is important to know how precisely a target position in space can be measured, e.g., when the patient moves his hand exactly to the same position during the WORKSPACE assessment, will the robot repeatedly measure the same end-effector position, also when recalibrating the robot in between?

To test the measurement repeatability and precision, the end-effector was moved manually to the same position in space for ten times. For this reason, a pin was attached to the end-effector of the robot with the peak lying on the axis of rotation of the forearm. This peak was moved to the peak of another stationary fixed target pin in space. In each target position, the end-effector position calculated by ChARMin was recorded. To account for errors which can be introduced by the robot calibration, the control model was started again after each single movement to the target and the sensors were newly calibrated. Furthermore, different robot postures were applied to reach the target position. The tested postures varied around  $[20, 65, 5, 55, 30, 0]^\circ$  for the six axes. The large distal module was used with an upper arm length of 5.5, forearm length of 5.5 and a hand length of 3.

**Achievable end-effector accuracy for a virtual target** Another important measure is the achievable accuracy of the end-effector position when moving to a target position shown on the screen. In the QOM and CIRCLE assessment, a target position has to be reached on the screen. To understand how accurately this position can be reached with the robot, a virtual target position was manually reached for ten times as accurately as possible. Similarly to the measurement repeatability test, the control model was started again before each measurement and the postures were varied. As the virtual target is only shown in the frontal plane, the third translational axis was also varied when reaching for the target. The virtual target was on the x-y-coordinates (0, 0). The z-coordinate was varied between -0.58 m and -0.28 m.

**Repeatability, precision, and accuracy of the joint angle measurement** For the ROM measurement, the repeatability of the joint angle measurement is important. Therefore, each robot joint had to be moved to a mechanically predefined position. The mechanical end stops were used to guarantee that always the same position is measured. In each of the angular positions, the joint angles were recorded ten times. To test the repeatability between different assessment sessions, the control model was restarted between the single joint measurements.

### 4.2.3 Results

**Torque estimation from motor current** The motor torques which were produced to counteract an externally applied torque by the Mecmesing AFG sensor were measured. This revealed a large hysteresis in the ChARMin force estimation due to joint friction (Appendix A.4.1). However, when measuring the maximally applied isometric torque, only the loading phase, where the torque is increased is of interest. The unloading can be ignored. The accordingly cut data without the unloading is shown in Fig. 4.10 for the large distal module. The results for the small module are given in Fig. A.16 (Appendix A.4.1). The figures show the diagonal (blue line) which can be seen as the perfect mapping if the joint was frictionless (i.e., Mecmesin is equal to the motor torque). The linear fit which was finally used for the calibration is shown in black. The slope of the linear fit is between 0.35 and 0.81 of the diagonal (Tab. 4.11). The linearity of the robot force estimation is between 2.38 % and 5.69 % for the small distal module and between 1.86 % and 5.24 % for the large module (Tab. 4.11).

**End-effector measurement repeatability and precision** Ten end-effector positions were recorded after reaching to a fixed spatial position. For the ten positions, the posture was varied and the control model restarted. The mean values, standard deviations (Std) and coefficients of variation (COV) of the recorded target positions are listed in Tab. 4.12. The Std and COV can be understood as a measure for precision (measuring the same position) as well as repeatability (after restart) of the measurement. The COV sets the Std in relation to the x-, y- and z-range which can be reached (1.01 m, 0.96 m and 0.72 m, with the large distal module and maximal range settings). The positions recorded are plotted in Fig. 4.11 a.

**Achievable end-effector accuracy for a virtual target** The resulting mean values, standard deviations, and COV for reaching a virtual target are listed in Tab. 4.13. The ChARMin positions recorded are plotted in Fig. 4.11 b.

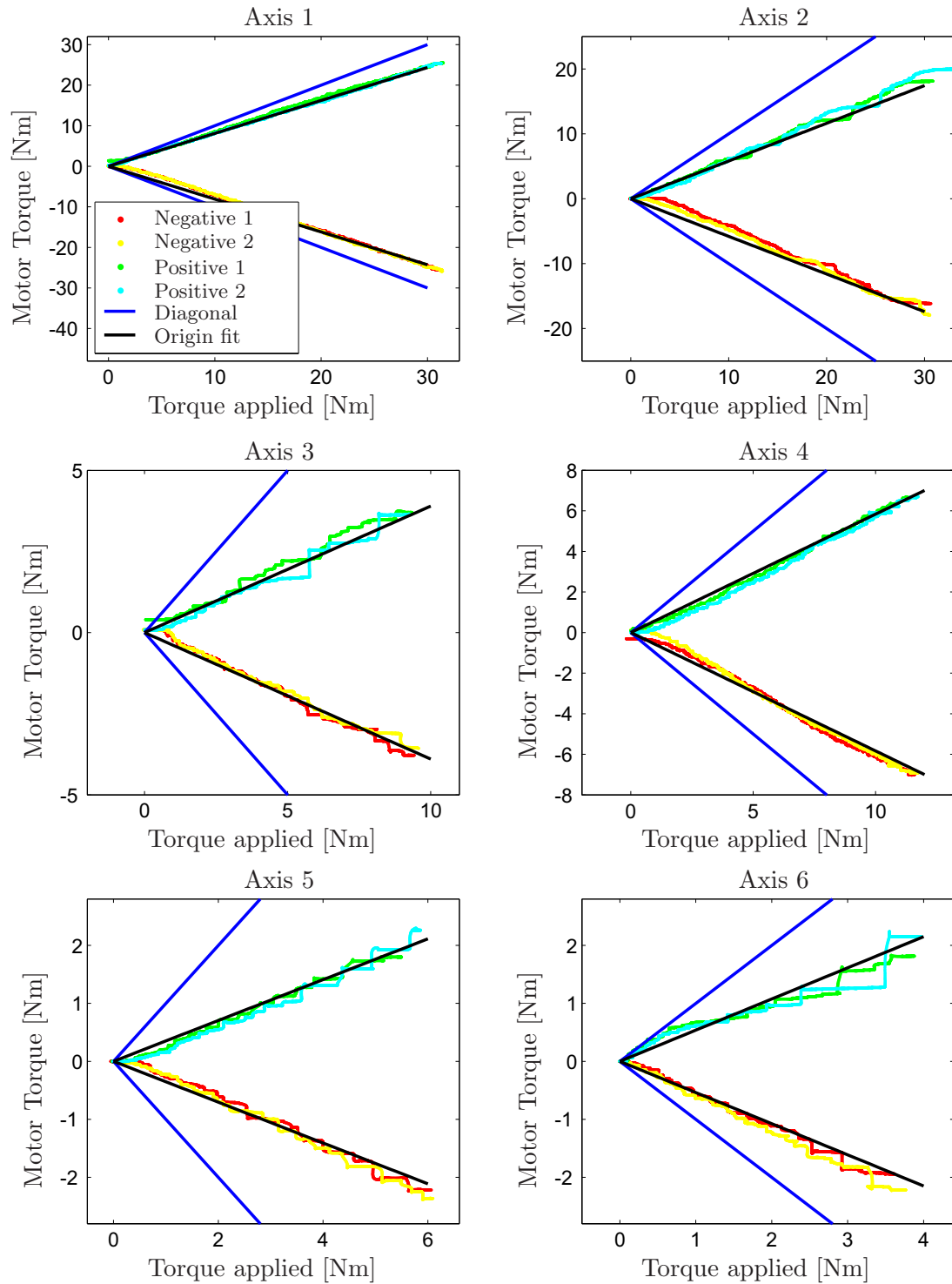


Figure 4.10: Isometric torque validation for the six axes of ChARMin equipped with the large distal module. Only the loading of the robot is shown, i.e., without hysteresis. On the x-axes are the torques applied by the Mecmesin AFG sensor and on the y-axes are the motor torques applied to the robot joint by the motors to counteract the external forces. The blue line is the diagonal which can be seen as the perfect mapping if the joint was frictionless. The black line is the linear fit of the cut data.

	Axis 1	Axis 2	Axis 3	Axis 4	Axis 5	Axis 6
<b>Small distal module</b>						
Slope of the linear fit	0.81	0.64	0.58	0.78	0.55	0.44
Linearity FS [%]	2.38	3.41	5.58	4.33	5.31	5.69
Max deviation FS [%]	9.20	13.57	21.97	12.53	15.00	25.05
<b>Large distal module</b>						
Slope of the linear fit	0.81	0.58	0.39	0.58	0.35	0.54
Linearity FS [%]	1.86	3.53	3.52	3.18	3.33	5.24
Max deviation FS [%]	7.41	12.19	17.70	15.13	13.79	25.97

Table 4.11: Correction gains and linearity of the ChARMin force estimation. 'Linearity FS' is the mean value of the absolute difference between measured value and linear fit with respect to the full-scale value (FS). Here, the FS corresponds to the maximally measured torque. The 'Max deviation FS' gives the maximal deviation of the measured force from the linear fit with respect to the FS value.

Mean x [mm]	Mean y [mm]	Mean z [mm]
-50.4	-170.9	-476.1
Std x [mm]	Std y [mm]	Std z [mm]
2.0	3.6	2.0
COV x [%]	COV y [%]	COV z [%]
0.20	0.37	0.28

Table 4.12: Measured end-effector repeatability and precision for reaching a fixed point in space. Std = Standard deviation. COV = Coefficient of variation.

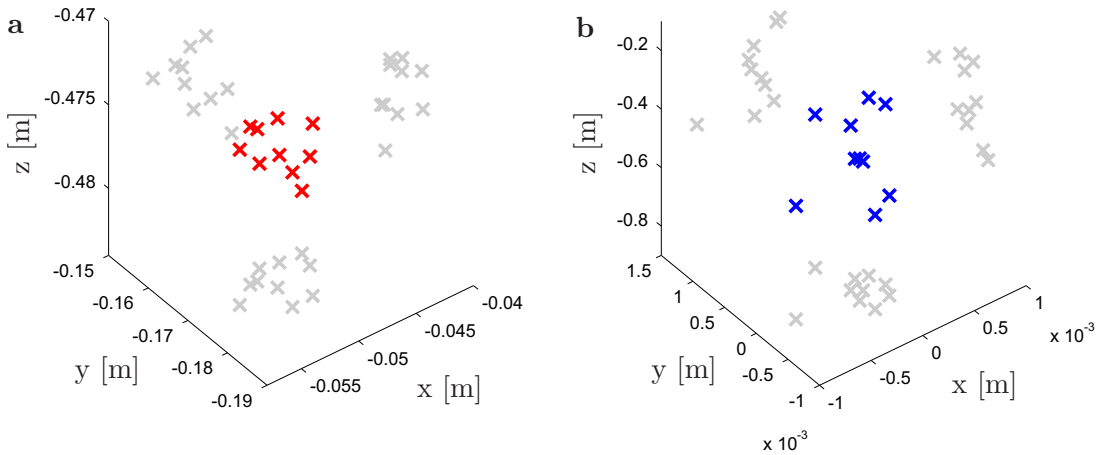


Figure 4.11: Measured end-effector positions and its projections (gray) to the xy-, yz- and xz-plane for (a) the end-effector repeatability and precision for reaching a fixed point in space and (b) the achievable end-effector accuracy for reaching a virtual target.

Mean x [mm]	Mean y [mm]	Std x [mm]	Std y [mm]	COV [%]	COV [%]
0.08	0.07	0.22	0.23	0.021	0.024

Table 4.13: Measured achievable end-effector accuracy for a virtual target. Std = Standard deviation. COV = Coefficient of variation.

**Repeatability, precision, and accuracy of the joint angle measurement** The mean values, standard deviations, and COV for the two directions of the six joints are given in Tab. 4.14.

Axis direction	Mean [°]	Std [°]	COV [%]
1 min	-11.72	0.26	0.25
1 max	97.77	0.27	0.26
2 min	51.93	0.29	0.36
2 max	130.87	0.29	0.36
3 min	-31.22	0.36	0.36
3 max	73.15	0.31	0.31
4 min	-0.04	0.17	0.15
4 max	122.32	0.16	0.14
5 min	-89.18	0.12	0.07
5 max	88.95	0.17	0.09
6 min	-64.54	0.42	0.30
6 max	65.39	0.53	0.38

Table 4.14: Repeatability, precision, and accuracy of the joint angle measurements. Std = Standard deviation. COV = Coefficient of variation.

#### 4.2.4 Discussion

Five different robot-assisted assessments packages were previously tested with adult SCI patients using the ARMin rehabilitation robot. The different assessment packages were adapted and implemented in the ChARMin robot. Only minor changes had to be applied to the single assessment packages. The interface was newly programmed on a different platform, but the assessment procedure was only changed minimally. In general, more settings are provided to test different assessment configurations (e.g., speed of the circle reference, time to stay on the target in QOM and target region in QOM), the handling was improved (e.g., by adding the recording feature in STRENGTH and more instructions on the screen) and the safety increased (e.g., adapting the measurement positions, skip certain measurements when the patient cannot flex the shoulder more than 90°). For the WORKSPACE assessment, a new continuous mode was added. The evaluation software was extended and a user interface added for a more intuitive evaluation of the assessments and games. Lastly, a new assessment package, CIRCLE, was added to measure the tracking skills of the patient. With this set of six assessments we believe to have an objective, reliable, and valid tool to measure the therapy outcome as it was required by Sakzewski et al. [32].

A supplementary way to capture and quantify skill at the level of motor execution is the speed-accuracy tradeoff function, which refers to the relationship between movement speed and accuracy for a particular task. Subjects tend to make more errors at higher movement speed and, conversely, to slow down for more accuracy. It can be concluded that an increase in accuracy alone does not indicate improved skill and that true skill acquisition can only be described with the learners speed-accuracy tradeoff function [37]. The CIRCLE assessment has the potential to measure this speed-accuracy tradeoff, however, the instruction should be changed, such that the patient chooses his own speed to follow the target circle, rather than following a target which performs a pre-

defined circular movement. The moving reference could be a switchable feature, such that both assessment variations can be tested.

In the technical validation, the ChARMin torque measurement was evaluated. The ChARMin joint torques, derived from the motor current by means of the linear motor-specific characteristic between current and torque, shows a large hysteresis<sup>1</sup>. This hysteresis comes from the mechanics between the motor and the human arm and inaccuracies in the current and motor torque measurements. However, for the isometric torque measurement, only the loading phase of the joint is of interest. A linear model was used to explain the difference between the torque induced by an externally applied force sensor and the corresponding motor torques derived from the motor current. The slope of the linear fit ranges between 0.35 and 0.81 (Tab. 4.11). The calibrated force estimation using the motor current showed an acceptable linearity between 1.86 % and 5.69 % (Tab. 4.11). The maximally observed deviations from the linear model range between 7 % and 15 %. The deviations for axis 3 and axis 6 for both distal modules are even higher, which can also be observed in Fig. 4.10. These higher differences come from more distinct stick and slip effects at higher loads. In general, the joint torque estimation can be used to measure isometric torques. However, the measurement accuracy has to be mentioned when using the robot as an assessment tool. A repeated measure (e.g. performing the STRENGTH assessment two times) will improve the accuracy of the joint torque measurement.

The ten measurements for the end-effector positions showed a small variability and, therefore, a good repeatability and precision (Tab. 4.12). As the robot was restarted between each single measurement, the variability is a measure for the precision and repeatability. To analyze the precision alone, the recordings have to be performed without restarting the system. However, given that the combined Std and COV are very small, the precision is expected to be at least in the same range or better. The Std for the y-axis (upwards and downwards direction) is higher compared to the x-, or y-direction. The reason probably is the mechanical play in axis 2 which, combined with the distance to the end-effector, leads to a higher measurement uncertainty for this direction.

The achievable end-effector accuracy for a virtual target (Tab. 4.13) is very high. The virtual target was at the position (0 mm/ 0 mm) and the mean of the robot end-effector positions (when being on the target) was (0.08 mm/ 0.07 mm), which is a position error of about 0.11 mm. Moreover, the precision and repeatability which can be inferred from the Std and COV are very high.

The precision and repeatability of the joint angle measurement were very high with a standard deviation between  $0.12^\circ$  and  $0.53^\circ$ . As in the measurement for end-effector precision and repeatability, the precision alone was not measured, but is in the same range or better than the measurement of both effects. The accuracy can be given by considering the difference between the measured absolute joint angle and the position of the mechanical end stop. The differences are  $-1.72^\circ$  and  $2.77^\circ$  (axis 1),  $1.93^\circ$  and  $0.87^\circ$  (axis 2),  $-1.22^\circ$  and  $3.15^\circ$  (axis 3),  $-0.04^\circ$  and  $2.32^\circ$  (axis 4),  $0.82^\circ$  and  $-1.05^\circ$  (axis 5) and  $0.46^\circ$  and  $0.39^\circ$  (axis 6). These differences show a rather good accuracy.

---

<sup>1</sup>That is also the reason why it is impossible to use the motor current force estimation for the controller, e.g., for an admittance controller or to reduce interaction forces between the robot and the patient.

The reasons for the differences between the measured and real end stop might come from a unprecise calibration of the sensor or an unprecise position of the mechanical end stop.

A measurement of the absolute end-effector accuracy is missing. This is mainly important for the WORKSPACE assessment to know whether the reached positions and, therefore, the reached volume are correct. This measurement could be performed with a visual tracking system with a marker on the end-effector and calibrated to have the origin in the shoulder position. This measurement was not performed. However, the absolute end-effector accuracy can be roughly estimated from the joint angle accuracy above and the robot length settings. For the x-direction and y-direction this is maximally 21 mm and 26 mm, respectively. This accuracy can be increased by improving the sensor calibration. Additionally, there is the mechanical play which also adds up to about 0.4 mm in the x-direction and 4 mm in the y-direction.





# 5 ChARMin Feasibility

## 5.1 Introduction Feasibility

Upon finishing the robot, controllers, and assessments, ChARMin was ready for a preliminary feasibility test with young patients. After receiving approval from the ethical committee (KEK, Zurich, Switzerland) on the 12<sup>th</sup> June 2015 and the Swissmedic (Swiss Agency for Therapeutic Products) on the 25<sup>th</sup> June 2015, the first feasibility trials could be started with in- and outpatients from the Rehabilitation Center for Children and Adolescents, Affoltern am Albis, Zurich, Switzerland. For first feasibility considerations, five children and adolescents were recruited and the games and assessments tested.

## 5.2 Method

### 5.2.1 Participants

Patients were recruited by contacting in- and outpatients of the Rehabilitation Center for Children and Adolescents, Affoltern a. A. Switzerland. Eligibility criteria for the ChARMin therapy are children between 5 and 18 years with a neurological diagnose or other (non-neurological) diagnoses and an impairment of the upper extremity requiring an intensive training of the upper extremity. Exclusion criteria are among others:

- Strong adiposity, which makes it not possible to adjust the cuffs and orthoses to the anthropometries of the participant
- Instabilities of bones or joints, fractures or osteoporosis/osteopenia
- Open skin lesions of the upper extremity that should be positioned in ChARMin
- Luxation or subluxation of joints of the upper extremity that should be positioned in ChARMin
- Strong pain
- Injuries or lesioned nerves of the upper extremity that should be positioned in ChARMin
- Strong spontaneous movements like ataxia, dyskinesia, myoclonus
- Instable vital functions like pulmonary or cardiovascular conditions
- Implanted pace maker, defibrillator of the heart
- Severe cognitive deficits
- Inability to signal pain or discomfort
- Severe visual impairment (inability to see the screen)
- Severe spasticity (Ashworth 4)

- Severe epilepsy
- Insufficient head stability
- Infections requiring isolation of the patient

For the first case trials, five patients (aged 5.9 to 17.1 years, mean 12.1, 3 male) were eligible to perform a feasibility test with the ChARMin robot. Two patients suffered from CP, two patients from a stroke, and one patient from a TBI (Tab. 5.1). Four patients used the right arm for the ChARMin training. Three of the patients also performed the six robotic assessments and the clinical tests. Three therapists were educated in advance in the use of the robot and an elaborated manual was provided which described the robot in detail.

Patient ID	Age [y]	Sex (f=female, m=male)	Diagnose	Time since incident [y]	Affected side (r=right, l=left)	Arm side tested (r=right, l=left)	Inpatient (in)/ outpatient (out)
1	16.17	m	TBI <sup>a</sup>	1.70	l	r <sup>b</sup>	in
2	5.92	f	Stroke	0.16	l/r	r	in
3	17.08	f	CP	-	l/r	r	out
4	6.08	m	Stroke	0.61	l	l	in
5	15.08	m	Ataxic CP	-	l/r	r	in

Table 5.1: Characteristics of the patients. <sup>a</sup>Traumatic brain injury (TBI) following an accident. <sup>b</sup>The feasibility trial was started with left (mobilization, spaceship and tennis) but the patient was weary of using his left arm after 10 min and could not be motivated to continue.

**Ethic statement** All parents signed an informed consent; the study was approved by the responsible ethical committee (KEK, Zurich, Switzerland, KEK-ZH-Nr. 2015-0239) and Swissmedic (Swiss Agency for Therapeutic Products, reference number: 2015-MD-0009). The parents of the individuals in Fig. 5.5 and Fig. 5.6 gave written informed consent to publish the pictures.

### 5.2.2 Study Design

With the five case trials, a preliminary feasibility test of the ChARMin was performed to investigate the applicability of the robot to the pediatric target group. Two sessions were scheduled for the test with the robot.

### Session A: Robot Settings, Handling, Comfort and Game Testing

In session A, the applicability of the robot to the pediatric arm, the robot handling, the games, and the arm support were evaluated. The following protocol was used as a guideline for conducting this session:

**Setup** Welcome the patient and introduction of ChARMin. Measure the patient’s arm length. Adjust the robot and settings to the patient. Perform a short mobilization sequence to familiarize the patient with the active robot support mode.

**Gaming** Play the ball game with a single joint chosen by the therapist and support chosen according to the assistance needed. Subsequently, test more of the remaining five games when possible (dependent on time and child motivation). Adapt the support and difficulty of the games to optimally address the impairment of the patient.

**Questions child** The patient answers questions about the motivation, comfort, and gameplay.

**Questions therapist** After the test session, the therapist answers a couple of questions to analyze the feasibility and handling of the robot.

Session A - Duration 60 min			
Setup	Gaming	Questions child	Questions therapist
15 min	20 min	5 min	20 min
Measure patient’s arm length, adapt robot settings, mobilization	Play single-axis and multi-axis games	Patient answers questions about motivation and comfort	Therapist answers questions about the applicability and handling of the robot

Table 5.2: Protocol for session A. In 60 min, the robot was adjusted, games were played, and the session was evaluated with a questionnaire.

### Session B: Robot Settings and Robot-Assisted Assessments

In session B, the applicability of the six different assessment packages were tested with the patient. To measure the intra-rater reliability of the assessments, session B was performed twice by the same tester. Session B was always performed after session A. The following protocol was used as a guideline for conducting session B:

**Setup** Positioning of the patient and adjustment of the robot.

**Assessments** Performing the six different assessment packages including the calibration of the RPM assessment. The sequence for the assessments is ROM - WORKSPACE - RESISTANCE - CIRCLE - QOM - STRENGTH for all the patients.

**Questions therapist** After the assessments, the therapist fills out a questionnaire to analyze the feasibility of the assessments.

Session B - Duration 45 min		
Setup	Assessments	Questions therapist
5 min	30 min	10 min
Robot settings and adjustments	Perform the six robot-assisted assessments	Questionnaire for the therapist about the feasibility of the assessments

Table 5.3: Protocol for session B. In 45 min, the robot was setup and the six robot-assisted assessment packages were performed with the young patient.

### 5.2.3 Outcome Measures

#### Questionnaires and Settings

For the first feasibility tests, a case report form questionnaire was used which covered the following aspects:

**i. Patient information** The patient information included the age, sex, body height, body weight, diagnose, time since the incident, affected side, arm side tested, arm length (upper arm, forearm, carpus, finger), arm circumference, and the information whether it was an in- or outpatient.

**ii. Positioning** The positioning comprised the time needed to sit the patient down and adjust the robot hardware and settings as well as the seating chosen (e.g., a chair, an active or passive wheelchair). It captures whether a good positioning is possible, whether the patient is sitting stable, how well the positioning of shoulder joint/upper arm/forearm/hand is, whether the lasers are useful, the comfort of the robot, robot parts which are close to the patient, the gravity compensation and the need for position adaptations during the test or between the test sessions.

**iii. Robot settings and handling** All the robot length settings were recorded (upper arm scale, forearm scale, hand scale, lifting column height, chair height). The questions related to the handling of the robot collected information about the change-of-side mechanism and the exchange of the distal module and the time needed for these operations.

**iv. Therapy aspects** The questions which addressed the training were: What are the most important therapeutical goals for the current patient and what movements can best be addressed with the ChARMin therapy? Which parts or components of ChARMin are restricting the therapy? Can the patient profit from active support? Should more movements be supported, or the support be changed? Which is the most motivating game for the patient, which is the most suitable according to the therapist? Are more handles for the therapist needed to hold and interact with the robot? Were there complications with the hardware? Is the robot easy movable? Did the robot perform any undesired or unexpected movements?

**v. Interface** The interface user-friendliness was described with these questions: Were there any software errors? Can the support be changed intuitively? Are more

adjustments/settings needed? Is the safety foot pedal restricting the training? Is the emergency button within reach? What were the direct interactions with the exoskeleton and why?

**vi. Assessments** The assessment questions addressed the usefulness of the robot-assisted assessments. The different assessments were rated regarding understandability, duration, and applied robot posture.

### **Robot Parameters**

**Games** During the games, the game score and the end-effector position, as well as the joint angles, were recorded. This data allows extracting various parameters describing the training performed. For a first analysis, the duration that the game was played, the amount of support which was chosen by the therapist, the joint range (for single-axis games) or workspace (for multi-axis games) and the mean end-effector speed during the games were measured.

**Assessments** With the set of six robot-assisted assessment packages, various aspects of arm motor function were evaluated (as described in Sec. 4.1.2 and Sec. 4.2). While the ROM and the STRENGTH assessment were purely based on raw sensor data, the WORKSPACE, QOM, RPM, and CIRCLE assessments calculated features that were extracted from the raw data.

### **Clinical Scores**

The clinical scores that are standardly applied to the child in the rehabilitation center are Nine-hole-peg test (NHPT), Box and block test (BBT), manual muscle test (MMT), pinch grip strength, power grip strength, range of motion (ROM), and modified Ashworth scale (MAS). To compare the robot-assisted assessments to the clinical assessments, the two tests should be performed within seven days.

## **5.3 Results**

### **5.3.1 ChARMin Applicability and Settings**

For the analysis of the ChARMin applicability, the case report form was evaluated and the results listed according to the aspects mentioned above (Sec. 5.2.3).

#### **i. Patient Information**

The general patient characteristics were already summarized in Tab. 5.1. At the beginning of session A, the anthropometric parameters of the patient's arm were measured. The body height and weight are usually assessed in the standard clinical routine. The collected data is listed in Tab. 5.4.

ID	Body height [cm]	Body weight [kg]	Upper arm length [cm]	Forearm length [cm]	Hand-MCP [cm]	MCP finger tip [cm]	Upper arm circumference [cm]	Forearm circumference [cm]
1	164.0	75.0	32.0	25.0	8.0	10.0	35.0	21.0
2	117.0	19.0	19.0	17.0	5.0	7.0	16.0	17.0
3	159.0	55.0	29.0	23.0	9.0	9.0	27.0	18.0
4	121.0	21.7	20.0	17.0	8.0	7.0	-	15.0
5	171.0	46.8	30.0	27.0	10.0	9.5	21.0	19.0

Table 5.4: Weight and arm anthropometry of the five patients measured. MCP = Metacarpophalangeal Joint.

## ii. Positioning

The positioning in the robot took about 5-10 min (ID1: 5 min, ID2: 8 min, ID3: 5 min, ID4: 10 min, ID5: 10 min). The robot could be adjusted to the arm sizes of the five different patients. Patient ID1 and ID2 were transferred from a wheelchair to a chair and an active wheelchair, respectively. The therapists rated the lasers to be useful for the shoulder positioning (in four out of five questionnaires). However, the patients had to be reminded from time to time to sit upright and to adjust the shoulder position. The positioning of the upper arm, forearm, and hand was without any problems, except for ID5 who needed additional foam material inside the cuff for a good alignment with the robot. For patients with little strength in the hand and fingers, the forearm can slide in the direction of the elbow, leading to a misalignment between robot axis and patient joint (observed in ID4). ID1, ID3, and ID5 needed no additional stabilization. ID2 was fixed with a chest strap and the hand position needed to be adjusted during the test session. The trunk stability of ID4 could have been improved with a chair featuring pelottes for the thorax and/or the pelvis. The positioning was comfortable for all five patients.

In general, the patient was first seated in front of the screen. Then the robot was positioned with respect to the patients' shoulder by means of the lasers. In the following, the arm was placed in the exoskeleton and the upper arm scale, forearm scale, and hand scale were adjusted to the patient. When needed additional foam material (adjusting the upper arm position in ID5) or cushions (additional cushions for the elbow joint in ID4) were provided.

Collisions were detected with the chair of ID1 during the ROM assessment of joint 5 and 6 and the robot elbow was very close to the patient's trunk when the patient was sitting slightly too close to the exoskeleton. During the gameplay with patient ID2, a collision with the arm rest of the wheelchair occurred, however, the test session did not need to be stopped. Examples for the positioning of the patients in the exoskeleton in front of the screen can be found in Fig. 5.5 and Fig. 5.6.

## iii. Robot Settings and Handling

For all the patients, the robot could be adjusted such that the robot axes were aligned with the anatomical joint axes of the patient. The patients ID1, ID3, and ID5 used the large distal module, while the patients ID2 and ID4 used the small distal module.

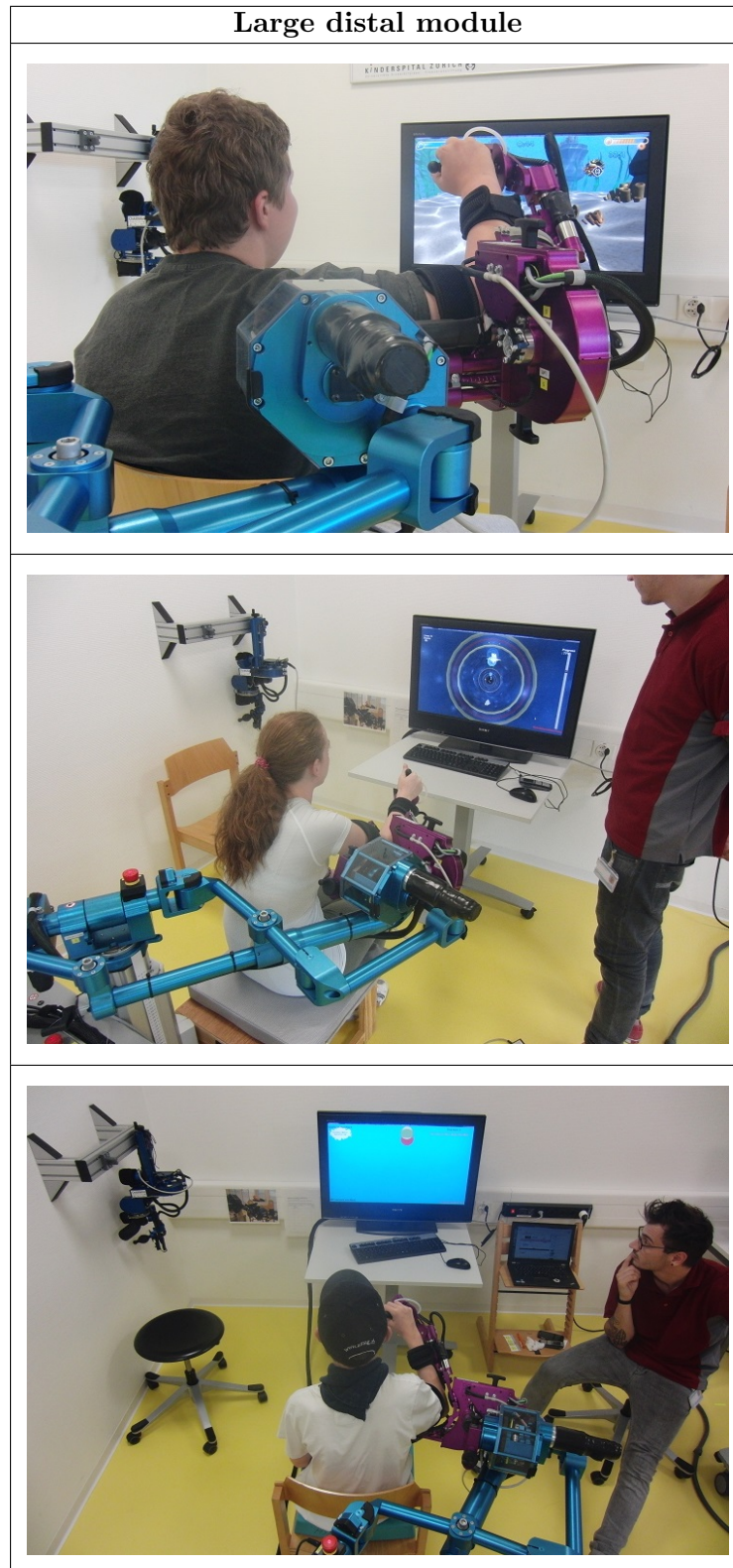


Table 5.5: Patients ID1, ID3, and ID5 of the ChARMin feasibility trials who trained with the large distal module. The patients in the pictures play the spaceship game and perform the CIRCLE assessment (from top to bottom). Published with written informed consent of the parents and individuals in the picture.

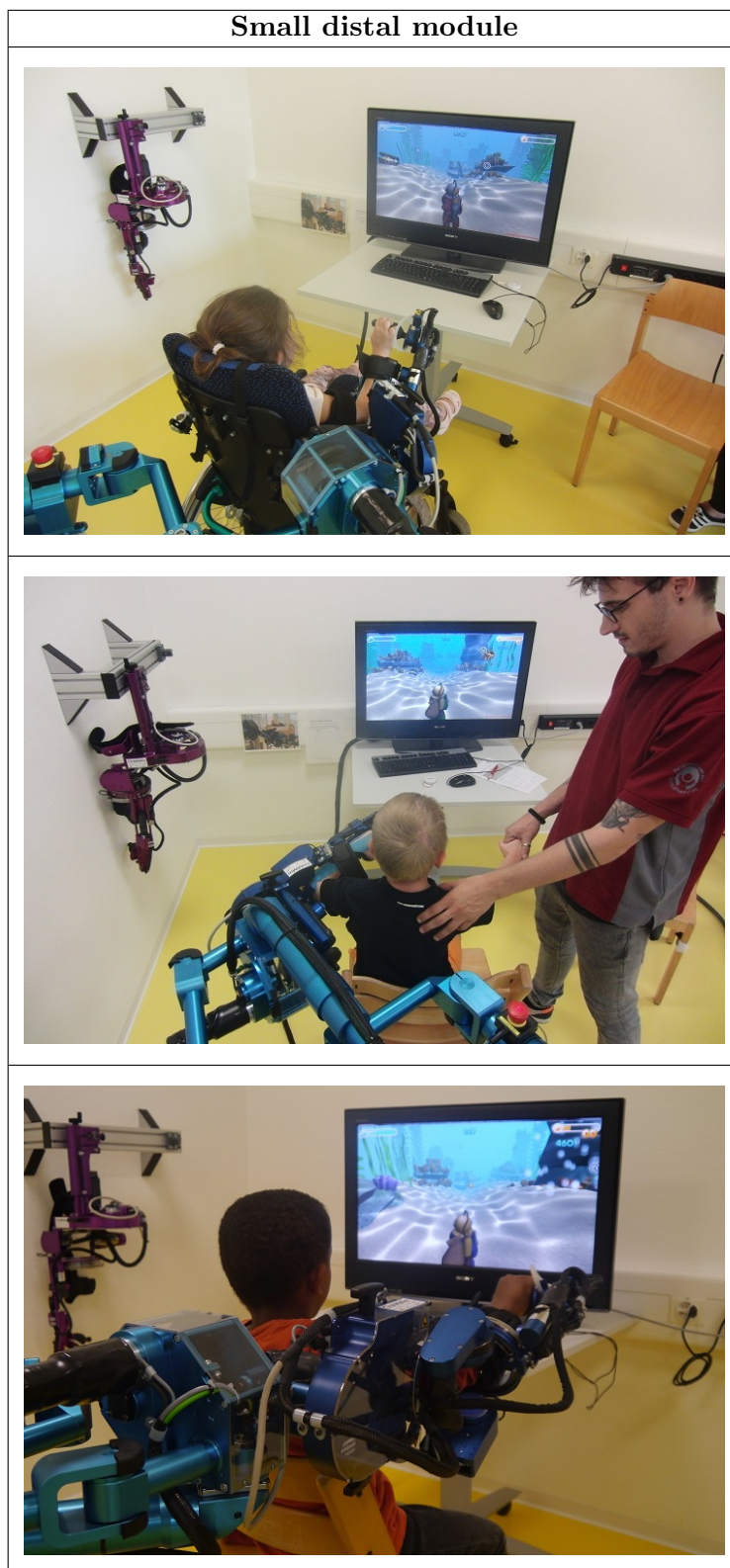


Table 5.6: Three participants of the ChARMin test session. The first two pictures show patient ID2 and ID4 of the ChARMin feasibility trials who trained with the small distal module. All of them are playing the diver game. The third picture shows a healthy 6-year-old child (bottom). Published with written informed consent of the parents and individuals in the picture.



With a body height of 117 cm, the anthropometrics of the youngest patient (ID2) approached the limits of the robot. This can be seen from the robot length scale settings with the hand scale and the lifting column at their minimum and the upper arm scale and forearm scale close to the minimum (Tab. 5.7). For comparison, the total range settings for the robot scales are listed in Tab. 5.8. For patient ID4, aged 6 years, the scales are close to the minimum but not at the limit. For the three patients using the large distal module, the length scales were in the lower range of the scales.

Patient ID	Sitting on a chair (y = yes, n = no)	Distal module (s = small, l = large)	Upper arm scale [ ]	Forearm scale [ ]	Hand scale [ ]	Lifting column scale [ ]	Support [%]	Spring pretension [ ]	Chair height [cm]
1	y	l	5.5	4	2	6	5	90	44
2	n <sup>a</sup>	s	2	3	0	1	0	70	61
3	y	l	5.5	4	2	5	5	90	46
4	y	s	2.5	2.5	1	14	7	70	54
5	y	l	3	3.5	3	6	5	90	50

Table 5.7: Robot settings for the five patients. <sup>a</sup>Patient ID2 was sitting in an active wheelchair.

For almost all the patients, a small gravity support was added to not have to lift the own arm weight during the whole session (5.2%, 0%, 4.7%, 6.8%, 4.7%).

During the test session of the patient ID1, the change-of-side of the robot was performed and took approximately 2 min. For the other sessions, the robot was always prepared before the arrival of the patient. The estimated time for the exchange of the distal module is approx. 3 min and approx. 2 min for the change of side for a trained user. The exchange of the distal module requires some training for the user but could be performed by all the three therapists trained so far.

Distal module	Upper arm scale [ ]	Forearm scale [ ]	Hand scale [ ]	Lifting column [ ]
Small	1 ... 13	0 ... 7	0 ... 2.5	1 ... 41
Large	1 ... 14	0 ... 10	0 ... 5	1 ... 41

Table 5.8: Maximum range values for the ChARMin length scales.

#### iv. Therapy Aspects

A short mobilization was conducted with all the patients. The movements could intuitively be recorded and replayed and no difficulties were pointed out. Mobilization was stated to be an important therapeutical goal in the patients ID1, ID2, and ID4. Other therapeutical goals for the patients focused on improving the range of motion of ShEx or ShFl (in 5 patients), HSAb or HSAc (in 4 patients), ShER or ShIR (in 2

patients), ElFl or ElEx (in 4 patients), ElSu or ElPr (in 2 patients), WrEx or WrFl (in 3 patients), wrist ulnar- or radial flexion (in 1 patient), thumb (in 3 patients), and finger (in 3 patients). The questionnaire revealed that with the ChARMin robot mostly shoulder and elbow movements can be trained well (rated between 7 and 10 out of 10). For ElPr and ElSu the suitability had a good rating as well (8, 8, and 10 out of 10). The wrist was only mentioned twice with a rating of 6 each. The thumb and fingers cannot be addressed very well, except for finger flexion which was rated with a 3, 5, and 8. The pressure bulb was mentioned twice to restrict the training, because the hand can slip of the bulb (ID1) and because it can not support an active extension of the fingers (ID4).

According to the therapists, the patients ID1, ID2, and ID4 profited from the active support. For the patients ID3 and ID5, the support was not helpful. More support was required for the whack-a-mole game, which had no support features included.

Asking the patients which game was the most motivating, the diver (3x), whack-a-mole (2x), spaceship (2x), and ball game (1x) were mentioned. However, not all the games were played by each patient. The airplane game was rarely played, because there was no support feature. When asking the therapist which game was most suitable for the patient, spaceship (4x), diver (3x), and the ball game(1x) were named.

During the session with ID4 (small distal module), the therapists mentioned that an additional handle at the forearm of the robot could be useful. The therapists stated that a larger elbow cushion is necessary (ID1 and ID4) and that the robot collided with the chair (ID2 and ID3). An illustration which shows possible collisions between a wheelchair and ChARMin is given in Fig. A.25 (Appendix A.5.6).

The therapists and patients reported that the robot can be moved well without resistance and that the robot made no undesired or unexpected movement, except for ID3 where the patient wanted to target another object than the robot supported to, leading to a 'forced' movement to the target chosen by the robot.

## **v. Interface**

During the test session, software errors occurred from time to time (approx. two times in each session). The errors were 'end-effector speed too high' when the patient moved faster than expected, 'wrong side selected', when another distal module was selected in the settings than actually mounted, 'motor current mismatch' when a software end stop was hit strongly, 'foot pedal pressed during startup', when the foot pedal was pressed while starting the software, and 'position control error', when pressing or releasing the foot pedal. While the first two errors can just be confirmed and the therapy can be continued, the others force a restart of the software.

No problem was reported in the understanding and use of the interface and the adaptation of the arm support. The safety foot pedal had to be pressed continuously and restricted the radius of operation of the therapist during the test session and an alternative solution was desired. Therefore, an additional hand-hold switch solution was recently added. When using the ChARMin prototype, the foot pedal and the switch are critical safety features and either of it has to be pressed continuously to ensure that the therapist can stop the robot immediately at any point in time.

The main reason for interaction with the robot was to hold the robot in place when the foot pedal was released and to avoid that the robot impacts the mechanical end stops, furthermore, to instruct movements during the session.

## vi. Assessments

The total duration of the assessments was 30 min, 25 min, and 40 min, including the RPM time for the calibration of the robot and the restarts which were sometimes necessary after an error occurred (e.g., 'end-effector speed too high' during ROM, 'current mismatch error' during STRENGTH).

The understandability for the six different assessments was rated between 4 and 10 out of 10. RPM, CIRCLE, and QOM were always rated a 10. STRENGTH was rated 4, 8, and 8, as the sequence of joints and the visual representation was not always clear. WORKSPACE was rated with 6, 7, and 8 because of the visual representation which was not completely intuitive for the patient. Especially the movement to the trunk and the start position were difficult because of the depth perception needed to navigate in the room on the screen. ROM received 8, 8, and 10 out of 10 as rating.

The duration of the single assessments was rated between 8 and 10 out of 10, with ROM, STRENGTH, RPM, and WORKSPACE having the lower values. CIRCLE and QOM were rated a 10.

The robot postures were given numbers between 8 and 10 out of 10. ROM was rated between 8 and 10. RPM was rated with 5, 10, and 10. It was mentioned that the forearm should be supinated while abducting the shoulder. STRENGTH was rated 8 and 10. It was suggested to change the posture for measuring isometric elbow torque to be closer to the neutral-0-method position.

### 5.3.2 Games

After the positioning of the patient and an arm mobilization to familiarize with the robot, different games were played with the patient. With most of the patients, the ball game was chosen first. Following this, as many other games as possible were played, dependent on the patient's motivation and the time available. An overview of the games played by the different patients is given in Tab. 5.9.

#### Ball Game

The ball game was chosen in the beginning of the session because of its single-axis character. It is not very complicated to understand and gives a first impression of how the robot interacts with the gaming environment. The ball game was often played with the ElEx/ElFl (ID1, ID2, ID3, and ID4) and the HSAb/HSAc (ID1, ID4, and ID5). Patient ID3 also played with the ShIR/ShER axis. The support was mostly chosen to be around 50%. For patient ID3, it was reduced to 15% (Tab. 5.9). For a more detailed analysis of the ball game, the assessment evaluation software (presented in Sec. 4.2.2) generated plots which show the end-effector movement in space while playing the game (Fig. 5.1). While the plots for ID1, ID4, and ID5 only show a singular end-effector path, for ID3 (and ID2, which is not shown in the figure) the posture of the robot was adapted during the ball game, leading to two different curved trajectories (Fig. 5.1 b).

The score development during the ball game is given in Fig. 5.2, first column. It shows that the patients usually hit most of the balls. A missed ball can be seen by a delayed increase in the score, e.g., in the plot for ID1 in the beginning (Fig. 5.2 a). The second column in Fig. 5.2 shows the joint angle of the patient (blue line) and the desired angle where the ball will hit the bottom of the inclined plane (black line). The time point

ID	Ball	Whack (multi)	Diver	Airplane	Tennis	Space
			<b>Duration [s]</b>			
1	60-a1 / 60-a4 / 60-a4 / 60-a4	11 / 43	115	ts	ts (1) <sup>b</sup>	103 (1)
2	30-a4	(110-a3-a4 / 76-a4) <sup>e</sup>	54 / 62	ns	np	np
3	75-a3 / 63-a4	22 / 76 / 98	ns	ns	93	132
4	110-a1 / 96-a4	(49-a1 / 49-a1) <sup>e</sup>	53	np	52 / 83 / 87 / 74	31
5	107-a1	65	49 <sup>a</sup> / 341	52	89 / 65	96
			<b>Support [%]</b>			
1	54 / 63 / 45 / 80	70 / 70	70	ts	ts	70
2	53	(100 / 100) <sup>e</sup>	71 / 71	ns	np	np
3	15 / 15	0 / 0 / 0	ns	ns	0	25
4	50 / 50	(100 / 100) <sup>e</sup>	60	np	100 / 100 / 80 / 60	60
5	46	0	0 / 0	0	21 / 21	0
		<b>Joint range [°], Workspace [m<sup>3</sup>]</b>				
1	52 / 44 / 48 / 43	0.0093 / 0.039	0.0142	ts	ts	0.0040
2	49	(51-95 / 101) <sup>e</sup>	0.0068 / 0.013	ns	np	np
3	79 / 76	0.039 / 0.062 / 0.041	ns	ns	0.0045	0.0027
4	66 / 69	(56 / 55) <sup>e</sup>	0.0027	np	0.0001 <sup>e</sup> / 0.0018 <sup>d</sup> / 0.0018 / 0.0012	0.0001
5	69	0.040	0.0024 / 0.029	0.015	0.015 / 0.040	0.006
		<b>Mean speed [m/s]</b>				
1	0.024 / 0.015 / 0.026 / 0.014	0.12 / 0.106	0.100	ts	ts	0.024
2	0.063	(0.021 / 0.030) <sup>e</sup>	0.051 / 0.074	ns	np	np
3	0.067 / 0.043	0.099 / 0.091 / 0.11	ns	ns	0.052	0.033
4	0.039 / 0.029	(0.066 / 0.065) <sup>e</sup>	0.020	np	0.012 / 0.021 / 0.027 / 0.027	0.020
5	0.067	0.082	0.054 / 0.069	0.076	0.080 / 0.082	0.070

Table 5.9: Overview of the games played by the five patients and their performance in terms of duration, support, workspace, and mean speed. Numbers separated with a slash indicate that the game was played several times, e.g., with different support. For the ball game the joint range was measured while for the others the workspace is listed. The affix -a defines which axis the game was played with (e.g., 60-a1, when played with axis 1). <sup>a</sup>First run without support mode on (support mode freezes the scene when a pirate fish or obstacle is close). <sup>b</sup>First game played on the left side and stopped left arm training a couple of seconds later. <sup>c</sup>Ball positions were all lying on the same height and the movements were almost exclusively on this line. <sup>d</sup>After therapist increased the workspace. <sup>e</sup>Whack-a-mole played in single-joint mode, the robot is moved by therapist and the patient is only pressing, joint range in [°]. ns = data not saved (software problem). np = not played. ts = game duration too short (< 10 s).

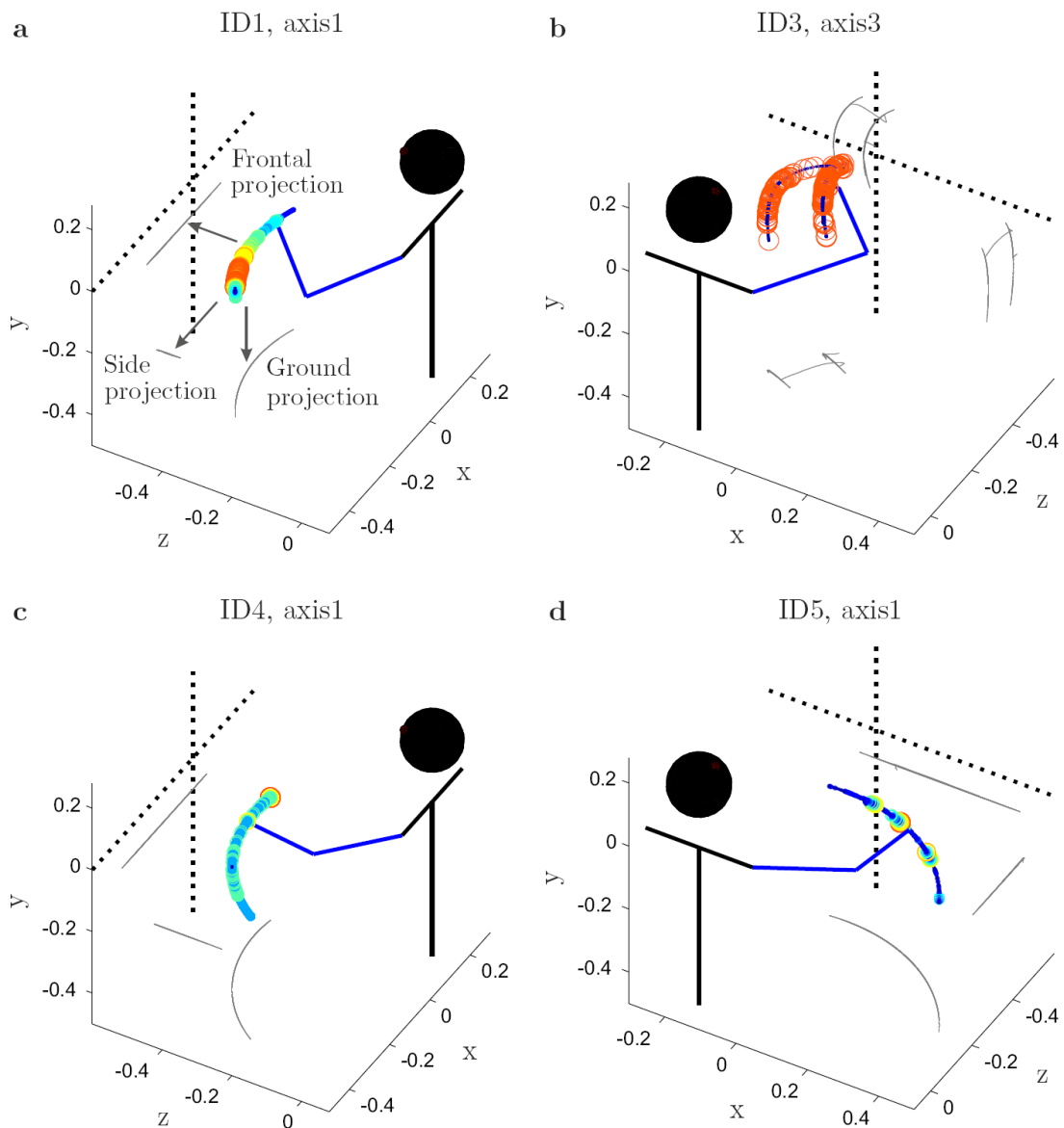


Figure 5.1: Example of the ball game play for the patients ID1, ID3, ID4, and ID5. The figures show the end-effector paths (colored circles) together with a simple human head and trunk model and the arm posture at recording onset (blue line). (a) The gray lines show the 3 projections of the end-effector path onto the xy-plane (frontal projection), yz-plane (side projection) and xz-plane (ground projection). (b) The plot of patient ID3 shows an adaptation of posture during the test session. The pressure is color-coded from blue to red, where red is always the maximum pressure which was applied. Patient ID3 was applying no pressure to the handle and only small noise was measured. The discretization of the noise values resulted in either a red or a blue circle. For a better understanding of the frontal projection, the shoulder position is projected to the frontal plane as well. The shoulder position lies on the intersection point of the dotted horizontal and vertical line in the frontal plane. (c) Patient ID4 and (d) patient ID5 played the ball game with axis1. The HSA<sub>b</sub>/HSA<sub>d</sub> movement leads to a curved ground projection while the side and front projections are only lines.

when the ball hits the bottom is indicated by a black circle. The red line represents the ball height. The ball starts falling from 1 and decreases the height till it hits the bar at 0. When the ball height is further decreasing to the negative region, the ball was missed.

### **Whack-a-mole**

The whack-a-mole game was played by patient ID1, ID3, ID4, and ID5. The robot was not providing support to the patient's arm movement. Detailed plots for the patients playing the whack-a-mole game are shown in Fig. 5.3. Patient ID1, ID3, and ID5 played the game with nine holes on the table where a mole can appear. This pattern can be detected in the locations where the pressure handle was pressed by patient ID3 (Fig. 5.3 b). For the other patients who played the game with nine holes (Fig. 5.3, a and d). The game was tested in the single-axis mode with patient ID4 (Fig. 5.3 c), assuming that the patient might be able to generate enough force to play in a small range. Finally, the therapist moved the joint and the patient tried to hit the mole by pressing the pressure bulb. For analyzing the score development, it is important to know that the software allowed to hit the mole several times when the handle stayed pressed. Therefore, patient ID4 reached a high score (Fig. 5.3 c) even though she was not hitting more moles than, e.g., patient ID3 (Fig. 5.3 b).

### **Diver**

All the patients played the diver game. The support varied from 0 % to 71 % (Tab. 5.9). The detailed end-effector paths are shown for Patient ID1, ID2, and ID5 (Fig. 5.4 a - c). The score can be increased by shooting treasures (500 points) and bonus objects (1000 points) appearing on the screen or by shooting pirate fishes (150 points), air bubbles (100 points) and obstacles (250 points). However, only shooting the pirate fish and the obstacle is actively supported. When the support mode is switched on, the diver and the scenery stop when a pirate fish or obstacle are getting close and the robot supports towards the target. Collecting the treasure or shooting the pirate fish is performed by applying pressure to the hand bulb. This can be seen well for patient ID1 (Fig. 5.4 a) with the distinct regions where pressure is applied (red circles). Patient ID2 could not apply a lot of force on her own. The robot mostly moved the arm leading to smooth arm movements (Fig. 5.4 b).

### **Airplane**

The airplane game was played by patient ID1, ID3, and ID5. However, the recording for patient ID1 was too short. The measurement for ID3 was not saved correctly. Patient ID2 and ID4 have not played the game as there was no support provided. Detailed plots of the end-effector movements of patient ID1 can be found in Fig. A.21 (Appendix A.5.2).

### **Tennis**

The tennis game was played by patient ID3, ID4, and ID5. For patient ID1 the measurement was too short. Dependent on the patient different amounts of support were used. While patient ID4 sometimes had full guidance with 100 % support, patient



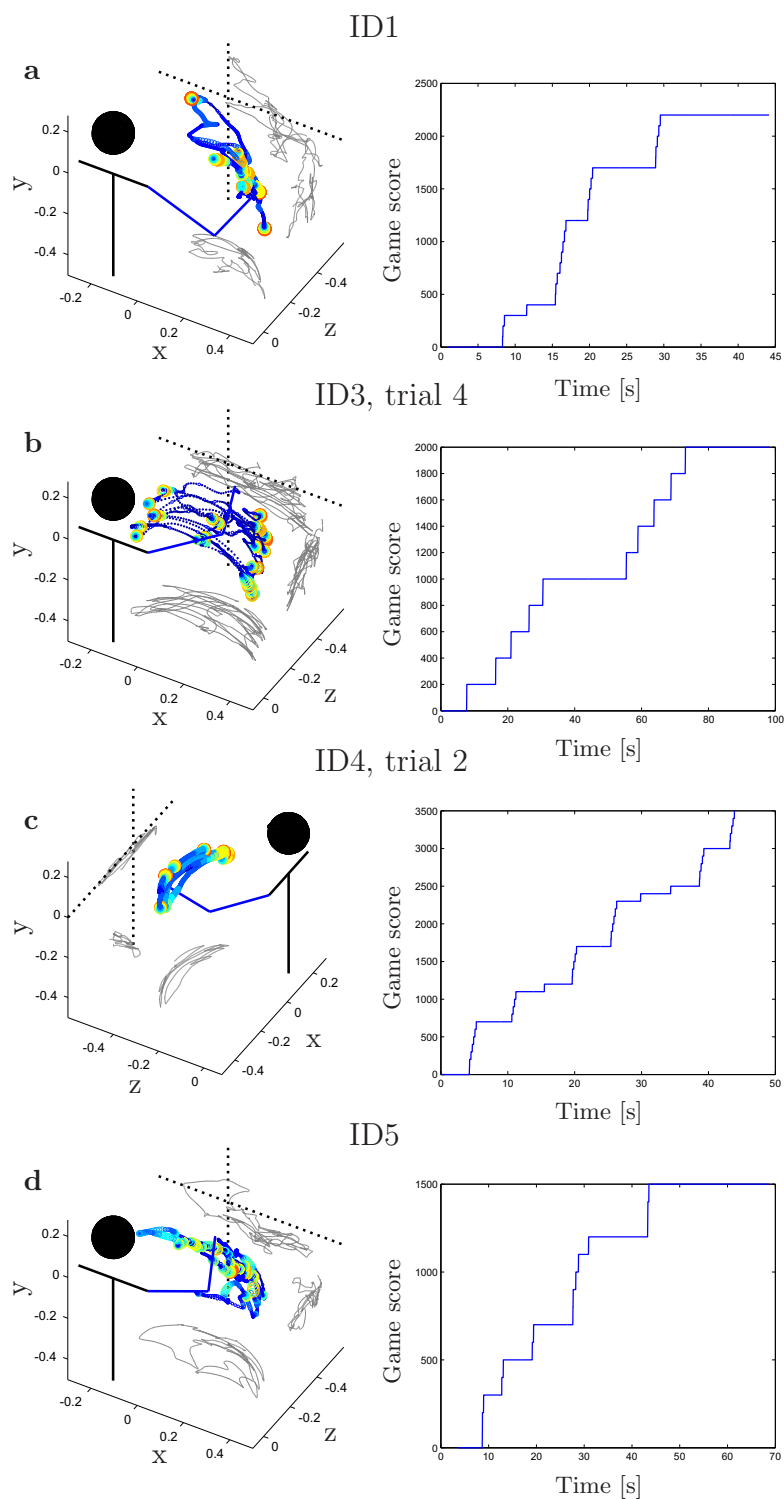


Figure 5.3: Example of the whack-a-mole gameplay for ID1, ID3, ID4, and ID5. **(a)** The first plot shows the end-effector path of patient ID1. The locations where the patient pressed the handle are shown with the red circles. **(b)** The second plot shows the end-effector path of patient ID3 (trial 4). **(c)** Patient ID4 played the game in the single-axis mode. The therapist mostly moved the joint. **(d)** Patient ID5 showed less distinct pressure spots and hit fewer moles as seen from the score development.



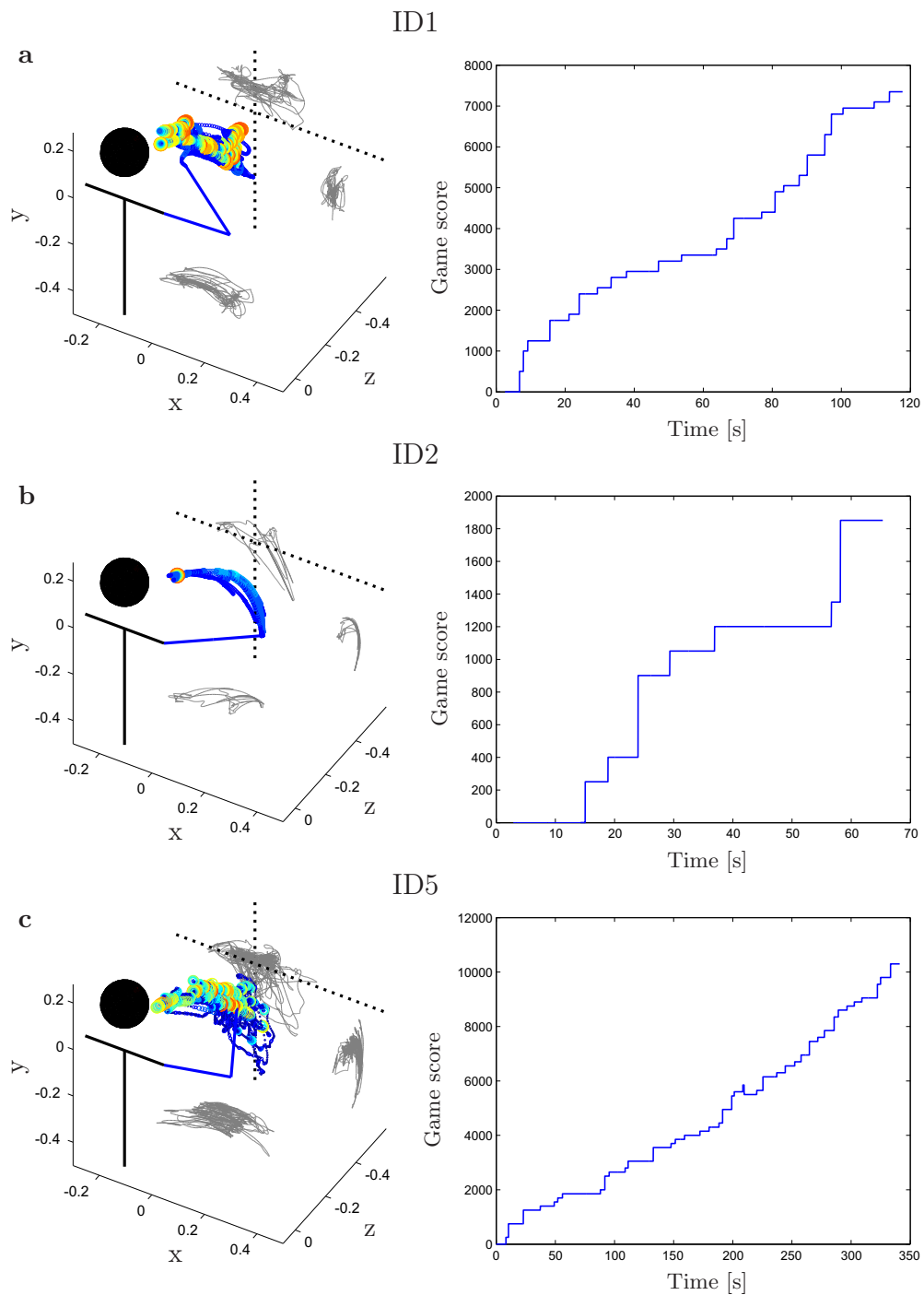


Figure 5.4: Example of the diver game played by ID1, ID2, and ID5. **(a)** The first plot shows the end-effector path of patient ID1 during the diver game with 70 % support. Objects are collected or shot in the game by applying pressure to the handle. This can be seen by the single red circles in the plot. **(b)** The second plot shows the trajectories of patient ID2 with 71 % support. This patient had a problem applying pressure to the handle and the movements are mostly performed by the robot, leading to the smooth trajectories. **(c)** The last plot shows the end-effector path of patient ID5 with 0 % support playing for quite long time (341 s).

ID5 only needed 21 % support, and patient ID3 played without support. The effect of the different amounts of support on the movement can be seen in the end-effector path figures (Fig. 5.5). Patient ID4 first played the tennis game with 100 % support (Fig. 5.5 a). The robot was completely guiding the movement to hit the approaching tennis ball. After the therapist had realized that the movements are rather small, he increased the workspace. The resulting movements covered more workspace (Fig. 5.5 b). To provoke an active participation, the position controller was changed to the AAN path controller with 60 % support. This led to higher variations in the end-effector movements (Fig. 5.5 c). For patient ID5, the AAN path controller was used with 21 % support allowing quite high variations in the performed movements (Fig. 5.5 d).

### Spaceship

All the patients played the spaceship game except for patient ID2. The support chosen varied between 0 % and 70 %. The task is to collect blue objects in space while flying with a spaceship. The spaceship flies with constant speed and is controlled by the robot end-effector position. Obstacles in space increase the difficulty of the game. Detailed plots of the end-effector movements and the score development can be found in Fig. A.22 (Appendix A.5.2). Compared to the other games the workspace is smaller. The game was usually played with the standard settings where the targets to be hit are quite close together leading to a lot of short movements.

In summary, the patients mostly liked the games played with the robot. Especially the diver, whack-a-mole, and spaceship game were enjoyed. The diver and the spaceship game were also rated as suitable for the patient. The airplane and the whack-a-mole game were not actively assisted by the robot. The therapists required that the support is extended to these games.

### 5.3.3 Robot-Assisted Assessments

Three out of the five patients who participated in the feasibility trials performed session B, i.e., the robot-assisted assessments. For patient ID4, it was planned to do the pROM and resistance measurements of the robot. However, the patient could not be motivated. For the other participants, the six assessment packages were performed twice. The assessments were all carried out by a single occupational therapist. The applicability of the assessments was rated by the therapist who conducted the assessments. The ratings ranged between 0 and 10 and are given in the following sections in brackets for the three different patients (ID1, ID3, ID5).

#### ROM

**Applicability** No problems were reported during the application of the ROM assessment. The understandability (8, 10, 8), duration (8, 8, 8), and robot posture (7, 10, 8) were rated quite good by the therapist performing the assessments. No specific adaptations of the ROM assessment were yet required by the therapists.

**Parameters assessed** The three patients who performed the assessments had only mildly affected arm functions and, therefore, almost exclusively reached the mechanical limits of the robot during the aROM assessment. Passively the same range was covered.

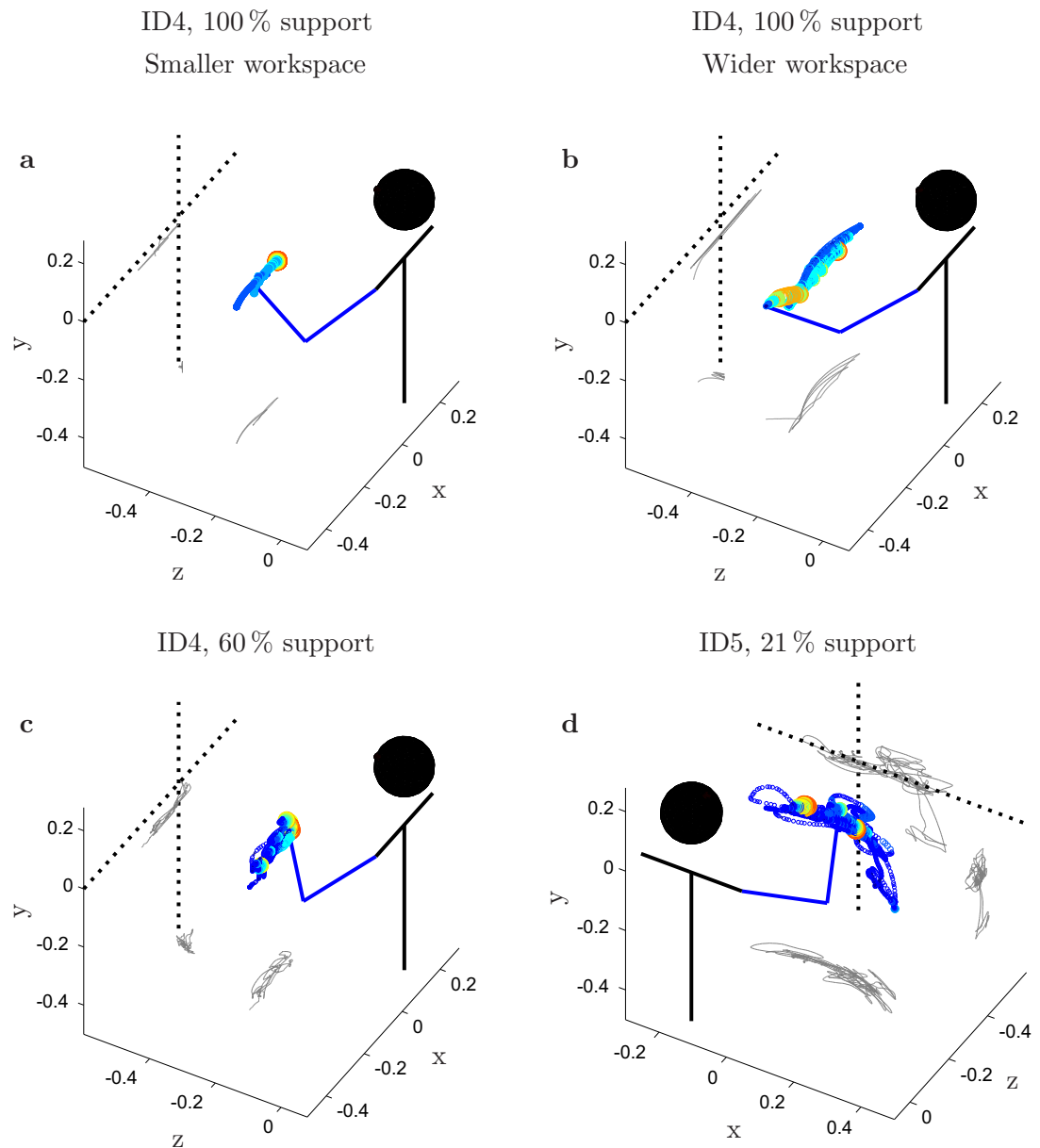


Figure 5.5: Example of the tennis game played by the patients ID4 and ID5 with different amounts of support. The first two plots show the end-effector path of patient ID4 during the tennis game with complete guidance in (a) a small workspace and (b) a wider workspace. (c) End-effector path of patient ID4 using the AAN path controller with 60% support. (d) Patient ID5 played with 21% support leading to more variations in the end-effector movement.

Except for the ElPr and WrEx range, which were slightly higher in the passive mode compared to the active condition. The aROM and pROM of the three patients are summarized in Tab. 5.10. An example of the evaluation plot is given for ID1 for the first test (Fig. 5.6).

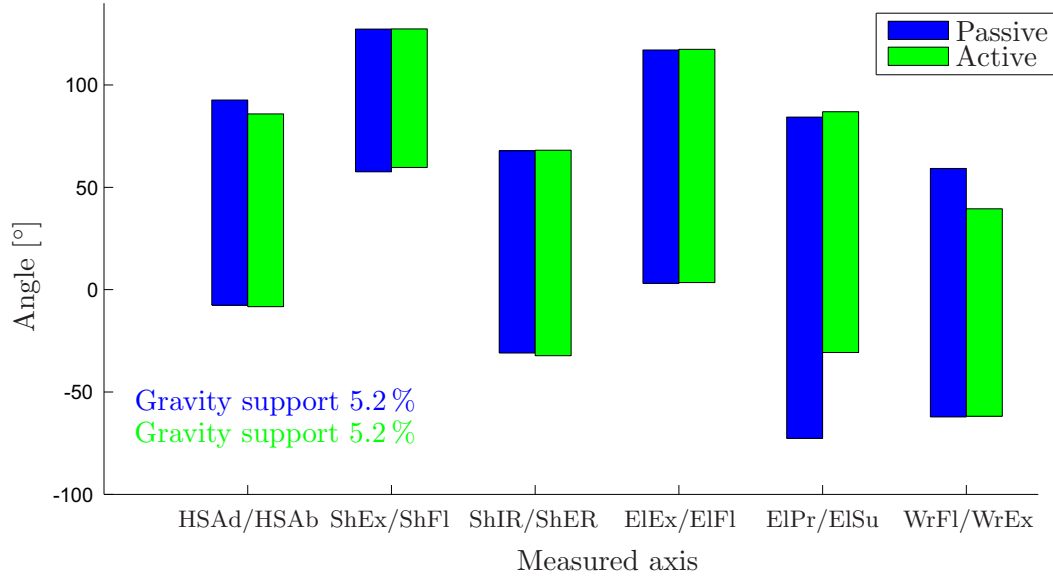


Figure 5.6: Exempry ROM plot from the first assessment of patient ID1. The mechanical limits of the robot were mostly reached. The active and passive ROM are almost identical except for ElPr and WrEx.

	ID1		ID3		ID5		ID1		ID3		ID5	
	t1	t2	t1	t2	t1	t2	t1	t2	t1	t2	t1	t2
	Active ROM [°]						Passive ROM [°]					
HSAb	86	92	93	94	93	94	93	93	93	93	93	92
HSAd	-8	-9	0	-8	-8	-9	-8	-8	1	-8	-8	-7
ShFl	127	128	128	129	128	129	127	128	128	128	128	128
ShEx	60	55	58	58	65	57	58	56	58	57	65	57
ShIR	-32	-32	-30	-31	-31	-29	-31	-29	-29	-30	-31	-29
ShER	68	68	67	68	67	66	68	66	66	66	67	66
ElEx	3	5	4	4	5	9	3	4	4	4	5	4
ElFl	117	117	116	116	116	116	117	116	116	116	116	116
ElPr	-62	-15	-33	-36	-50	-28	-73	-47	-43	-56	-50	-68
ElSu	87	84	84	86	84	54	84	84	84	84	84	84
WrFl	-62	-63	-63	-67	-62	-62	-62	-61	-63	-62	-62	-62
WrEx	40	30	63	65	27	21	59	40	62	62	27	34

Table 5.10: Active and passive ROM of the three measured patients (ID1, ID3, and ID5). For each patient, the assessments were performed twice (t1 and t2).

## WORKSPACE

**Applicability** Before testing the three patients, the decision was taken to measure only the continuous WORKSPACE to reduce the total time for the assessments, as the discrete WORKSPACE assessments can take up to 5 min. No problems were reported during the application of the continuous WORKSPACE assessment. The understandability (6, 7, 8), duration (-, 8, 8), and robot posture (-, 10, 10) were rated by the therapist performing the assessments. The lower ratings in the understandability are attributed to the visual representation of the assessment where it happened that the target wall disappeared when moving too far in a certain direction. However, this has not changed the fact that the patient had to move as far as possible to the indicated range. In a next release, this needs to be improved.

**Parameters assessed** The main outcome of the WORKSPACE assessment is the cubic volume achieved after reaching in all the six different directions. The resulting volumes are given in Tab. 5.11 and the detailed output parameters are plotted in Fig. 5.7 for the second test of patient ID1. While the assessment primarily measures the workspace, the other parameters such as the number of peaks, maximum speed etc. were recorded for further analysis of the movements performed.

	ID1		ID3		ID5	
	t1	t2	t1	t2	t1	t2
WORKSPACE assessment						
Volume [m <sup>3</sup> ]	0.177	0.179	0.099	0.102	0.073	0.095

Table 5.11: Continuous WORKSPACE (for both tests) of the three measured patients (ID1, ID3, and ID5). For each patient, the assessments were performed twice (t1 and t2).

## QOM

**Applicability** No problems were reported during the application of the QOM assessment. The understandability (10, 10, 10), duration (10, 10, 10) and robot posture (10, 10, 10) were all given the best rating by therapist performing the assessments. The target distance was fixed to a distance of 0.1 m from the starting position. The start position was chosen to be at (x=0, y=0, according to the convention in Fig. 3.2) which is in front of the shoulder joint. For patient ID3, the target region was increased to 0.03 m instead of 0.01 m as it was difficult to impossible for him to stay steadily and precisely on the target position because of his ataxic CP. ID1 reached the end-effector speed limit two times, however, the assessment could be continued.

**Parameters assessed** The parameters assessed encompass the D-P ratio, the precision on the target position, the number of speed peaks, the time needed to move to the target, and the reaction time to leave the start position (Tab. 5.12). The movement paths to the target and start position are illustrated in Fig. 5.8. The paths to and from the different targets are shown in different colors to better differentiate the paths when several are overlapping. A detailed analysis of patient ID3 (test 1) can be found in Fig. A.24 in Appendix A.5.3.

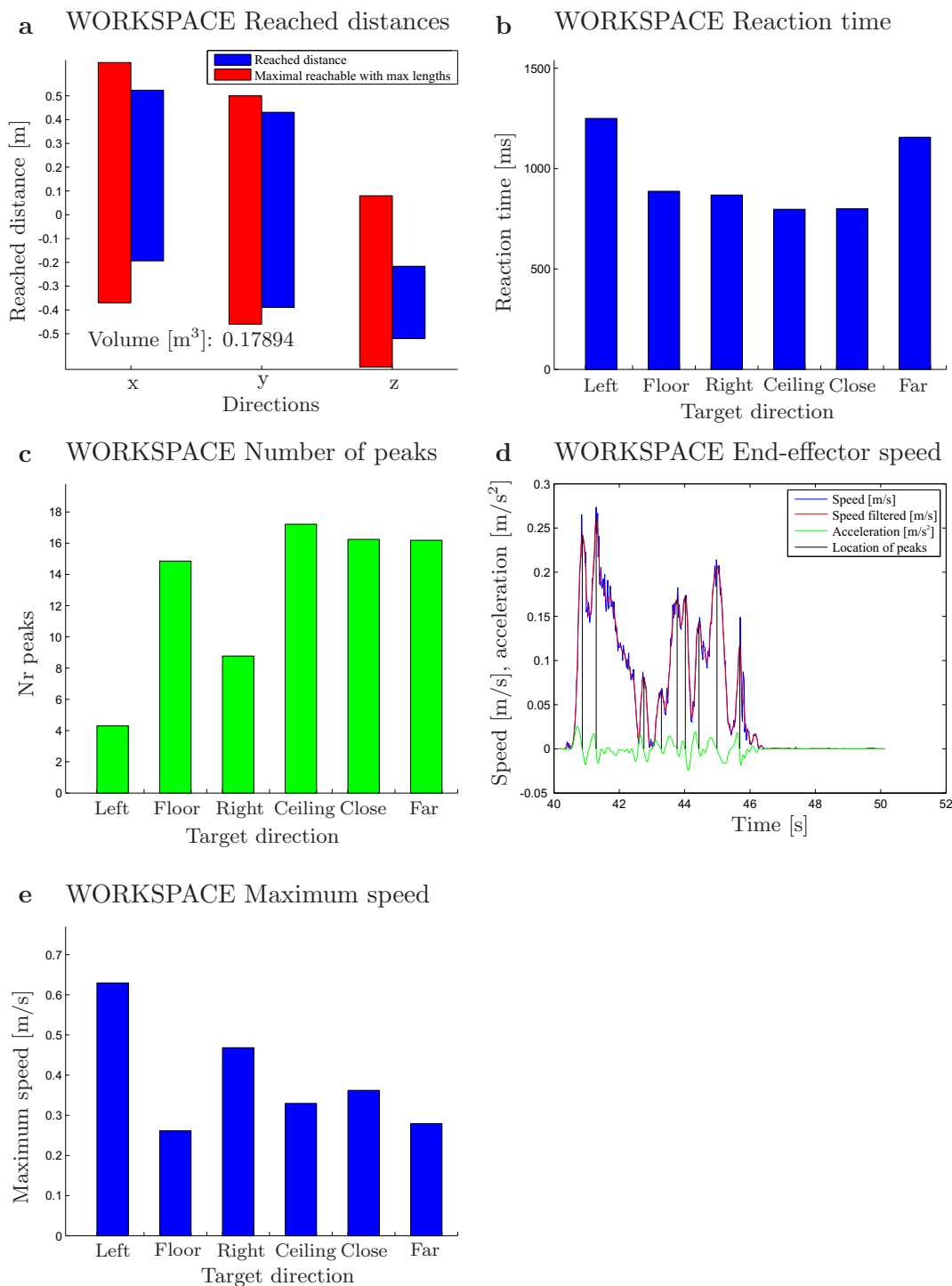


Figure 5.7: Results for the continuous WORKSPACE assessment for the second test of patient ID1. (a) The range in the different translational (x-, y- and z-direction) are plotted with respect to the maximally reachable workspace. (b) The reaction time describes how long it took to leave the start position. (c) The number of speed peaks in the different directions. (d) Example of the end-effector speed (filtered and unfiltered) and acceleration in the floor direction with the locations of the speed peaks indicated. (e) Maximal speed to the different walls indicated on the screen.

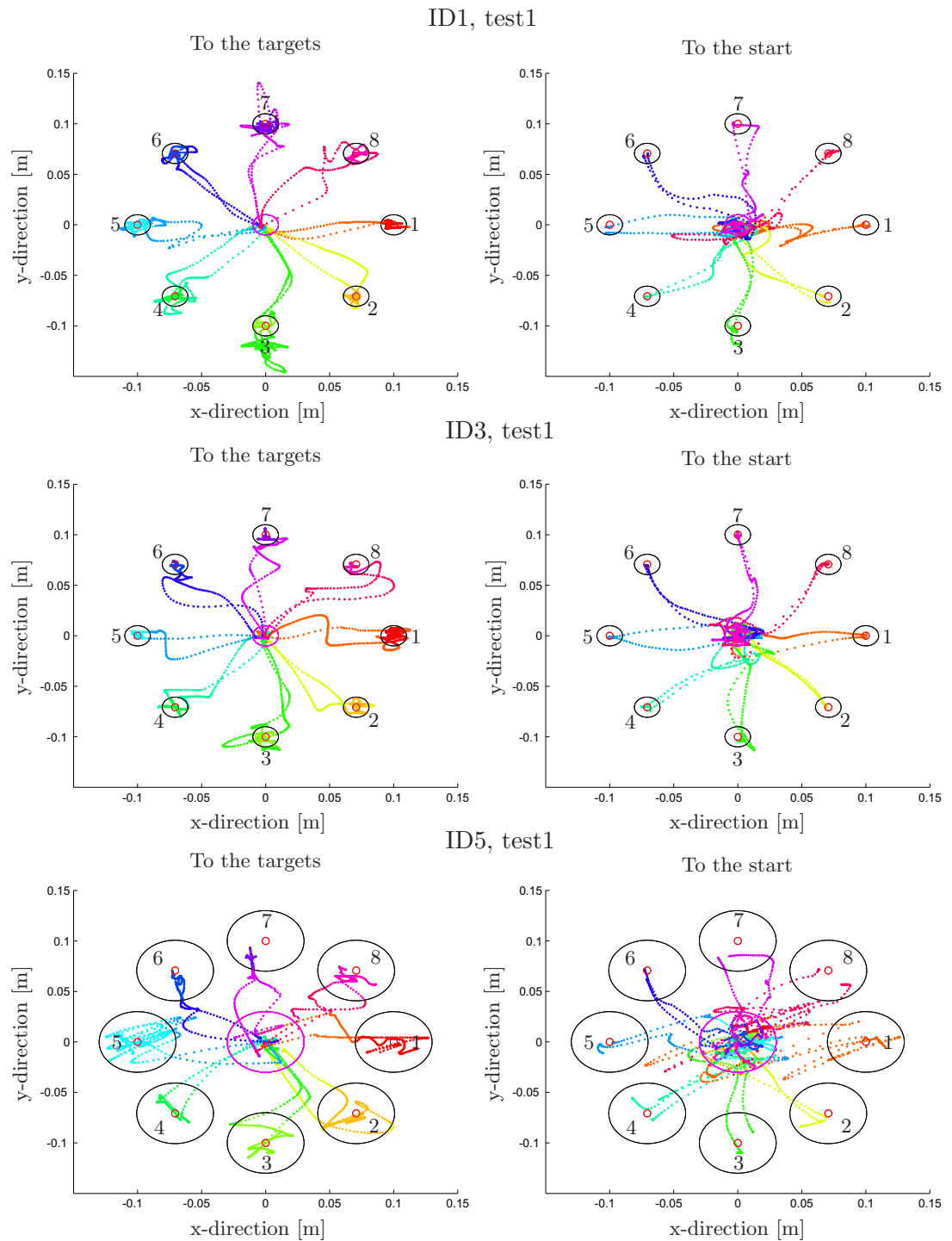


Figure 5.8: Comparison of the end-effector paths to the eight target positions (left column) and back to the start position (right column) for the three patients ID1, ID3, and ID5. The target positions are at a distance of 0.1 m. Each target position was reached twice.

	ID1		ID3		ID5	
	t1	t2	t1	t2	t1	t2
QOM assessment values						
D-P ratio to target [ ]	1.24	1.50	1.41	1.20	1.48	1.93
D-P ratio to start [ ]	1.40	1.30	1.36	1.24	1.63	1.85
Precision [m]	0.010	0.009	0.007	0.007	0.016	0.017
Number of peaks to target [ ]	32.9	30.5	33.7	36.9	24.6	28.7
Number of peaks to start [ ]	25.4	29.1	27.9	30.5	19.8	28.3
Time to target [ms]	1634	2000	1902	1568	1646	1881
Time to start [ms]	1681	1735	1604	1503	1411	1747
Reaction time to target [ms]	611	598	613	573	772	846
Reaction time to start [ms]	615	606	668	673	748	1086

Table 5.12: Mean values for all the 8 targets and both rounds. QOM assessment (for both tests) of the three measured patients (ID1, ID3, and ID5). For each patient, the assessments were performed twice (t1 and t2).

## STRENGTH

**Applicability** No major issues were reported for the STRENGTH assessment. The understandability (8, 4, 8), duration (8, 8, 9), and robot posture (-, 8, 10) were rated by the therapist performing the assessments. The reason for the lower ratings is the understandability of the assessment interface, which needs some time to be understood correctly. For patient ID3 and ID5, the assessment could be performed without problems. Patient ID1 was performing the assessments with his mildly affected, strong right arm. Two times a software error forced a restart of the interface. The exoskeleton withstood the forces applied, but the forces seem to be at the higher end of what the robot can handle. Especially the parallel kinematics of axis 3 and axis 6 seemed to start bending at these high forces. The torques of the motors were high enough to hold the position. For the strength assessment, the motors can currently apply a short-time double overload for all the axes. For the large distal module, this results in roughly 36 Nm, 45 Nm, 24 Nm, 18 Nm, 16 Nm and 13 Nm for the axes 1 to 6, respectively (based on the values for the large distal module, Tab. 2.4). These limits show that the elbow torque which can be resisted was already exceeded. However, the robot joint was not moving. Therefore, the joint friction and the short-time application of the torque by the patient may have prevented a joint movement.

**Parameters assessed** The parameters assessed during the STRENGTH measurement are listed in Tab. 5.13. A detailed plot for the STRENGTH measurement of patient ID1 in all the six joints in the two directions is shown in Fig. 5.9. The green blocks show the recording windows in which the maximum of the filtered joint torque was taken as STRENGTH measurement, indicated with a red cross in the plots.



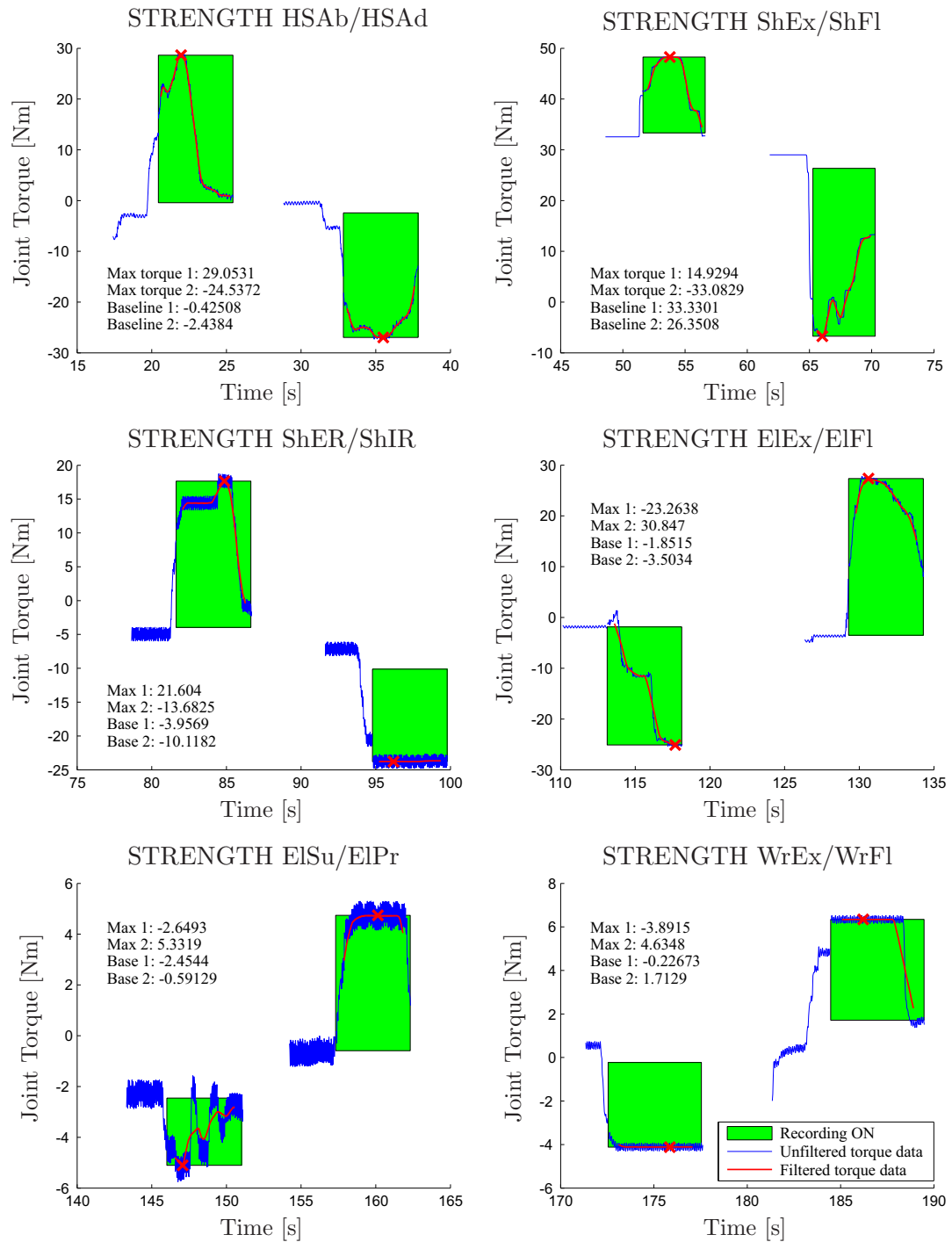


Figure 5.9: STRENGTH assessment results for patient ID1. The blue lines show the noisy joint torque signal. This torque signal was filtered for further processing (plotted in red). The green squares indicate the recording blocks where the maximal joint torque was measured (red cross). The developed evaluation tool directly plots the baseline values and maximal values into the plots for visual checking of the recorded data.

	ID1		ID3		ID5	
	t1	t2 <sup>a</sup>	t1	t2	t1	t2
STRENGTH joint torques [Nm]						
HSA <sub>b</sub>	29.05	22.34	13.40	13.68	29.88	19.79
HSA <sub>d</sub>	-24.54	-22.75	-25.65	(-2.58) <sup>c</sup>	-20.36	-20.49
ShEx	14.93	10.61	(16.76) <sup>b</sup>	20.57	16.51	17.93
ShFl	-33.08	-17.29	-34.28	-33.88	-35.93	-32.11
ShER	21.60	12.93	11.50	13.24	(6.38) <sup>c</sup>	13.17
ShIR	-13.68	-7.42	-20.89	-18.03	-8.59	-7.51
ElEx	-23.26	-24.87	-15.06	-16.34	-12.91	-12.36
ElFl	30.85	24.55	15.69	21.18	(12.93) <sup>c</sup>	22.17
ElSu	-2.65	-3.72	-1.92	-1.92	- <sup>d</sup>	-2.12
ElPr	5.33	4.29	1.82	1.16	(1.64) <sup>c</sup>	0 <sup>e</sup>
WrEx	-3.89	-1.69	-2.69	-3.34	- <sup>d</sup>	(-1.96) <sup>c</sup>
WrFl	4.63	5.61	2.67	2.68	(3.42) <sup>c</sup>	(2.57) <sup>c</sup>

Table 5.13: ChARMin STRENGTH torques for the three patients ID1, ID3, and ID5. <sup>a</sup>The measurement was conducted in the afternoon after the patient felt over in the morning and suffered a femoral neck fracture (which was diagnosed later). <sup>b</sup>Force applied too late when the recording was almost over. <sup>c</sup>Corrupted baseline measurement because of the torque being applied too early. <sup>d</sup>Force applied in the wrong direction. <sup>e</sup>No force applied. For each patient, the assessments were performed twice (t1 and t2).

## RPM

**Applicability** No problems were reported during the application of the RPM assessment. The understandability (-, 10, 10), duration (-, 8, 10), and robot posture (5, 10, 10) were rated by the therapist performing the assessments. The lower values for the robot posture were because of the shoulder abduction movement which should be improved such that the movement is attended with an elbow supination. The RPM software needed to be restarted because of different software error messages (e.g., 'end-effector speed too high', 'current mismatch'). The calibration was performed immediately after conducting the RPM assessment to ensure the calibration is done with the same robot settings and in the previously assessed pROM. For this, the patient was quickly released from the robot and a pause of 5 min was taken while the robot performed the calibration run.

**Parameters assessed** The ChARMin moved the arm at two different constant speeds (10°/s and 60°/s) and the patient was instructed to stay passive. The resulting resistance values are listed in Tab. 5.14. In Fig. 5.10, the calculated patient torques during the joint movement are plotted for the slower speed in both movement directions.

	ID1		ID3		ID5	
	t1	t2	t1	t2	t1	t2
RPM [Nm/rad] @ Speed 10°/s						
HSAb	-3.83	-3.27	0.46	0.35	-0.16	-0.11
HSAd	0.26	6.01	2.14	-0.45	-0.32	0.54
ShFl	-4.50	-0.60	-0.70	-1.84	-2.02	3.36
ShEx	-1.07	-0.09	-1.84	-1.47	-0.91	1.92
ShER	-0.71	-1.08	-0.48	-0.26	-0.10	-0.25
ShIR	0.36	0.01	-0.07	0.06	0.23	0.21
ElEx	-0.57	-1.44	-0.19	-0.21	-1.32	-0.73
ElFl	0.54	0.86	0.31	0.62	0.16	0.93
ElSu	-0.16	-0.25	-0.03	-0.14	-0.26	-0.04
ElPr	0.21	0.24	0.10	0.13	0.28	0.12
WrEx	-0.33	-0.70	-0.15	-0.10	-0.78	-0.93
WrFl	0.07	0.21	0.05	0.03	0.22	0.59
RPM [Nm/rad] @ Speed 60°/s						
HSAb	-1.15	-4.90	-0.70	-1.13	-2.24	-1.69
HSAd	0.61	5.01	1.37	-0.01	0.21	-0.81
ShFl	-5.98	-8.14	-4.65	-9.21	-10.85	-8.31
ShEx	0.79	-0.20	-2.19	2.11	2.07	0.56
ShER	1.59	0.84	0.62	0.54	0.17	-0.43
ShIR	-0.10	0.37	-0.02	-0.09	0.12	0.23
ElEx	-1.91	-2.55	-1.09	-1.63	-1.81	-1.62
ElFl	-0.21	0.40	0.19	0.10	-0.06	0.42
ElSu	-0.65	-0.86	-0.63	-0.80	-0.83	-0.69
ElPr	0.16	0.25	0.03	0.11	0.21	0.14
WrEx	-0.47	-0.59	-0.17	-0.02	-0.57	-1.01
WrFl	0.20	0.28	0.00	-0.00	0.32	0.69

Table 5.14: ChARMin RPM measures for the three patients ID1, ID3, and ID5. Negative RPM values indicate a resistance where the patient counteracted the movement of the robot while a positive resistance value is measured when the patient supports the movement of the robot. For each patient, the assessments were performed twice (t1 and t2).

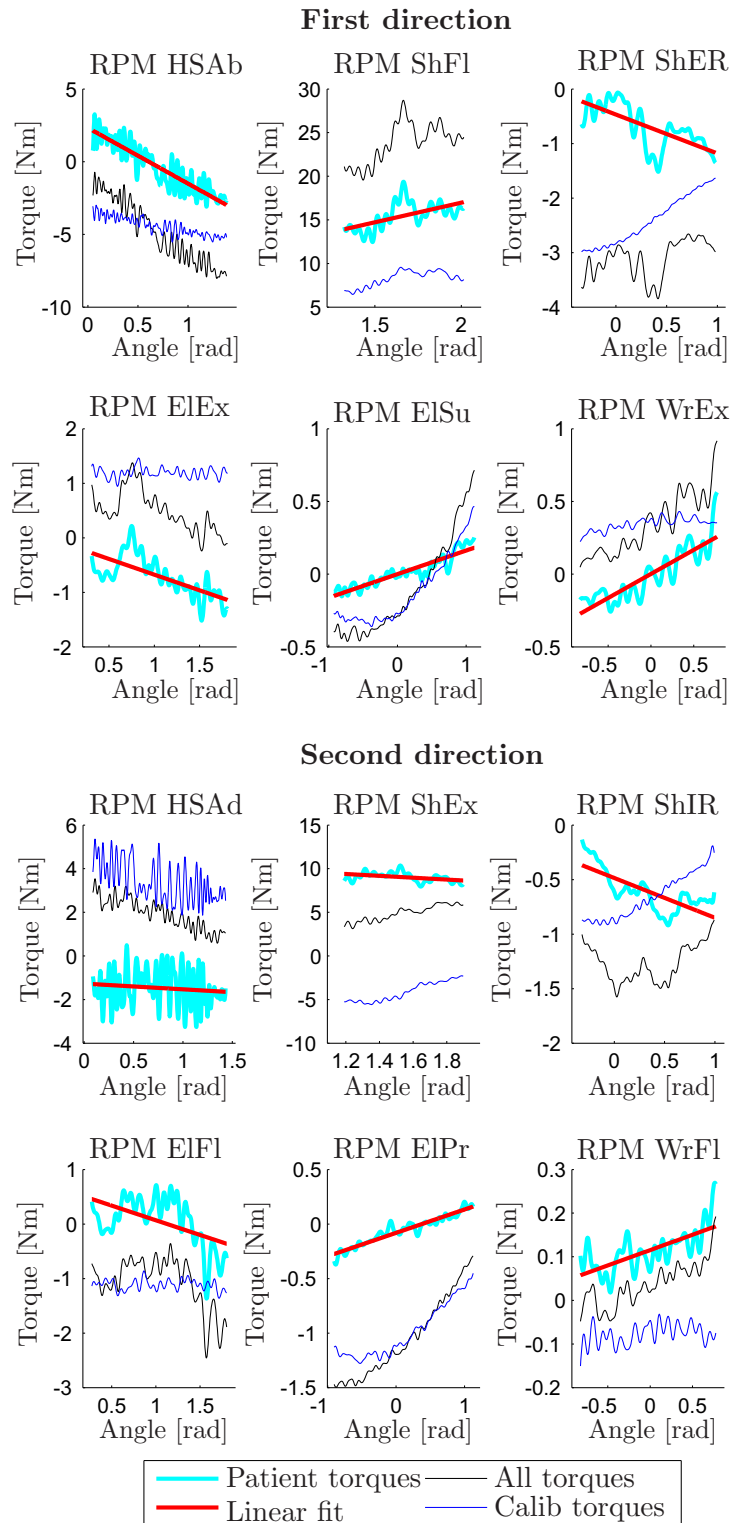


Figure 5.10: RPM results for patient ID1, test 1, at  $10^\circ/\text{s}$ . The plots show the joint torque measured with ('All torques') and without ('Calib torques') the arm of the patient. The difference is plotted in bold cyan ('Patient torques'). A linear model ('Linear fit') was fitted to this difference and the slope was used as a measure of arm resistance.

## CIRCLE

**Applicability** No problems were reported during the application of the CIRCLE assessment. The understandability (10, 10, 10), duration (10, 10, 10), and robot posture (10, 10, 10) had the best rating given by the therapist performing the assessments. For all the three assessments, the same target speed 3 was chosen which corresponds to 20s per round.

**Parameters assessed** The resulting circle end-effector paths for patient ID1, ID3, and ID5 are shown in Fig. 5.11. The parameters measured by the CIRCLE assessment were the 'summed difference' which is the sum of the differences between the current end-effector position and the moving reference position, the 'percentage in front' which states how often the patient moved in front of the reference position, and the 'ellipse ratio' which is the ratio between the shortest and the longest radius of the ellipse which is fitted to the recorded data points. These parameters are listed in Fig. 5.15 for the three patients. A more detailed analysis of patient ID1, test 1, is presented in Fig. A.23 (Appendix A.5.3). These plots correspond to the output plots of the evaluation software provided for the feasibility study.

	ID1		ID3		ID5	
	t1	t2	t1	t2	t1	t2
CIRCLE round 1						
Summed difference [m]	0.25	0.24	0.24	- <sup>a</sup>	0.65	0.48
Percentage in front [%]	58	56	43	- <sup>a</sup>	60	39
Ellipse ratio [ ]	0.962	0.914	0.977	- <sup>a</sup>	0.919	0.908
CIRCLE round 2						
Summed difference [m]	0.29	0.25	0.20	0.23	0.53	0.44
Percentage in front [%]	48	58	40	26	6	27
Ellipse ratio [ ]	0.923	0.958	0.957	0.918	0.911	0.884
CIRCLE round 3						
Summed difference [m]	0.25	0.27	0.24	0.23	0.37	0.70
Percentage in front [%]	48	59	41	26	26	90
Ellipse ratio [ ]	0.941	0.934	0.989	0.943	0.894	0.732
CIRCLE Mean values						
Summed difference [m]	0.26	0.26	0.23	0.23	0.51	0.54
Percentage in front [%]	51	58	41	26	31	52
Ellipse ratio [ ]	0.942	0.935	0.974	0.930	0.908	0.842

Table 5.15: ChARMin CIRCLE parameters for the three patients ID1, ID3, and ID5. The reference ellipse ratio is 1. <sup>a</sup>The patient was not on the target position when the circular movement started. For each patient, the assessments were performed twice (t1 and t2).

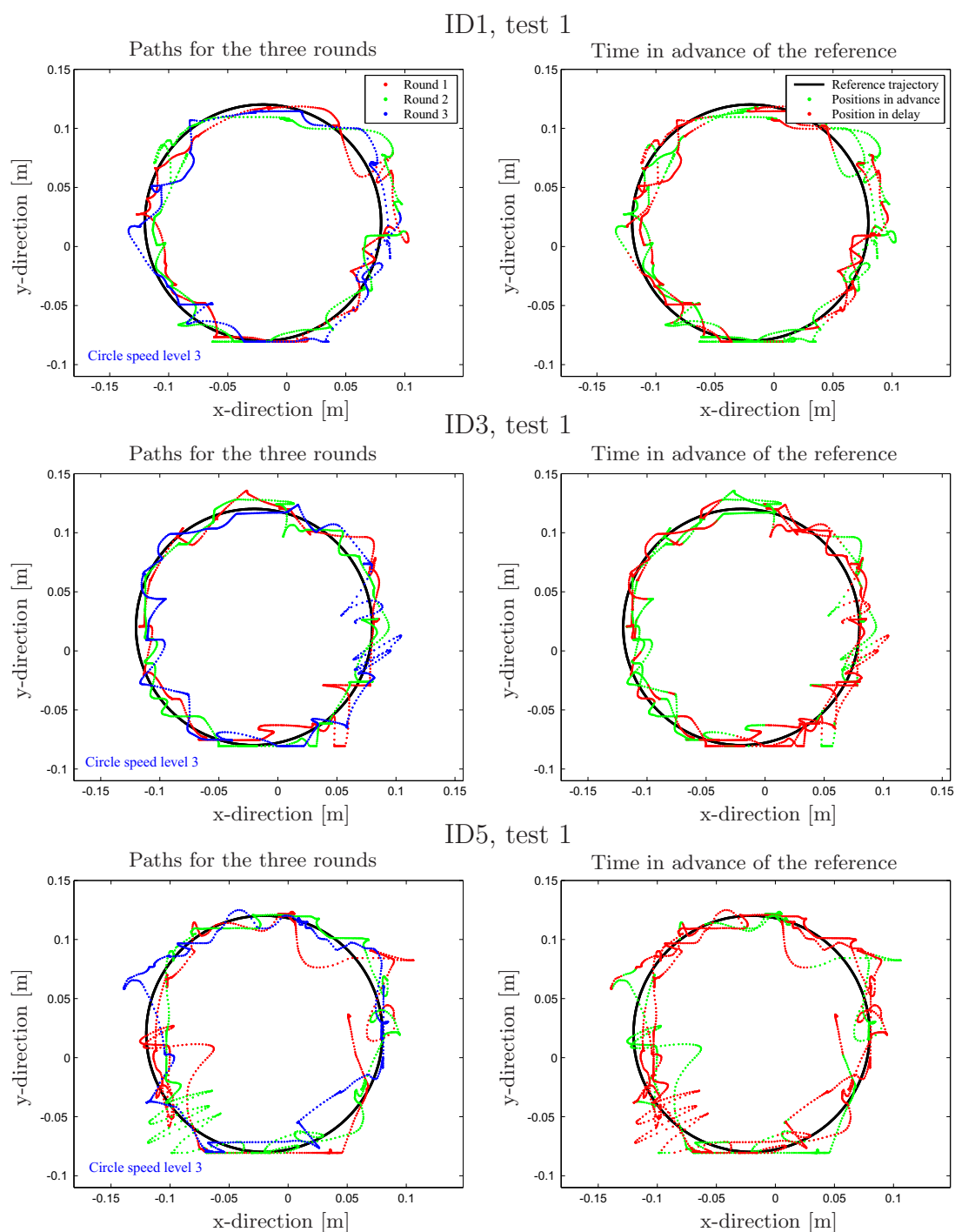


Figure 5.11: CIRCLE results for patient ID1, ID3, and ID5 for the first assessment session. The left column shows the three rounds which were measured while the patient tried to follow a moving target on a circle. The right column shows whether the patient was in front (green) or behind (red) the target reference position.

### 5.3.4 Clinical Assessments

For all the patients, the clinical assessments were performed within the 7 days following the robot-assisted assessments. The measured scores are listed in the Tab. 5.16.

		ID1	ID3	ID5
NHPT	Time for moving the pegs [s]	30.15	16.18	- <sup>a</sup>
BBT	Number of blocks moved [ ]	49	72	30
MMT	Shoulder flexion [ ]	4-5	5	3-4
	Shoulder abduction [ ]	4-5	5	3-4
	Shoulder external rotation [ ]	5	5	3-4
	Elbow flexion [ ]	5	5	3-4
	Elbow extension [ ]	4-5	5	4
	Skapula [ ]	3	5	3-4
Strength	Power grip (Jamar) [kg]	27.7	19.5	8.3
	Pinch grip [kg]	7.3	6.7	4.1
ROM	Shoulder flexion [°]	130	140	130
	Shoulder abduction [°] <sup>b</sup>	90	90	90
	Shoulder ex rotation [°]	50	90	65
	Elbow flexion [°]	130	140	140
	Elbow extension [°]	10	0	0
	Elbow pronation [°]	70	80	80
	Elbow supination [°]	80	100	90
MAS	Ashworth elbow ex [ ]	- <sup>c</sup>	0	1+
	Ashworth wrist ex [ ]	0	0	0

Table 5.16: Results of the clinical assessments for the right arm side of the patients ID1, ID3, and ID5. <sup>a</sup>Not assessed because of strong ataxic movements. <sup>b</sup>The shoulder abduction is not measured higher than 90° by the therapists in the robotic group, Affoltern a. A. <sup>c</sup>Not measured because the patient was not able to keep his arm passive.

## 5.4 Discussion

The aim of these preliminary trials was to show the feasibility of the ChARMin robot. Five patients participated in session A (Robot settings, handling, comfort and game testing) and three patients in session B (Robot settings and robot-assisted assessments). For patient ID2 and patient ID4, the robot-assisted assessments were not testable (child not compliant to perform tests). In general, all the children and youths could be successfully positioned in the robot and were able to use the different training modes.

### 5.4.1 ChARMin Applicability and Settings

The target group of ChARMin is 5- to 18-year-old children. The five patients who tested the ChARMin robot were aged 5.9 to 17.1 years and were, therefore, optimal to test the limits of the approved range.

The five patients could be well positioned in the ChARMin robot in an acceptable time. The initial positioning took 5-10 min. This time is further reduced once the robot length settings are known. The time needed for the change-of-side and the exchange of the distal module was also rather short (for a trained user). The youngest patient reached the lower limit for the shoulder height and the hand scale and was close to the possible minimum. The older patients were still in the lower range of the length settings. The reason is that the large distal module covers the range up to the 95th percentile of the arm anthropometry of an 18-year-old healthy subject. No patient was measured who was close to the anthropometric region where the distal module has to be exchanged (i.e., approx. 10 to 13 years of age). Hence, more data on robot settings and corresponding arm lengths has to be collected before a criterion can be defined which determines the distal module that has to be applied for a given patient. This criterion could depend on age, gender, arm anthropometries, or other markers and will probably decrease the time for the patient positioning by simplifying the choice of the correct distal module.

The first tests with the therapists and the patients revealed that, for patients with enough trunk stability, a standard chair with small back can be used for therapy with ChARMin without collisions. However, for wheelchair-bound children, collisions can occur between the robot and the wheelchair (as illustrated in Fig. A.25, Appendix A.5.6). Therefore, it is planned to adapt the backrest and armrest of two differently sized wheelchairs (for younger and older children) to avoid collisions (unmodified wheelchairs shown in Fig. 5.12 a). As a consequence, the wheelchair-bound child has to be transferred from its wheelchair to the adapted ChARMin wheelchair. While some patients are regularly transferred to a specialized chair for upper extremity therapy anyway, for other children this transfer will produce additional effort for therapist and patient.

It was observed that the shoulder position had to be corrected several times during the ChARMin test session. The added sensor-based feature to detect wrong shoulder positioning (indicated with a warning prompt in the bottom right corner of the screen, Fig. 2.18) was currently not used as a feedback feature. Mostly, because the therapists were too focused on the game and assessments, the settings, the patient's movements, the motivation of the child, the observation of the robot movement, etc. However, the therapists think that the feature will be used, once the therapists are more familiar



with the robot and have more capacity to focus on this feedback.

Patients with little grasping force or spastic hands could be correctly positioned with the handle, however, had problems with the hand slipping off the rubber bulb during the test session (e.g., patient ID1 and ID4). This slipping off can occur either in the direction of the elbow (e.g., when retracting the shoulder) or to the top of the handle. An occupational therapist had the idea to add a disk on top of the pressure handle to avoid slipping off the handle when flexing the elbow (Fig. 5.12 for the (b) large and (c) small distal module). The concept will have to be tested with patients.

The questionnaire revealed that the ChARMin robot covered the therapeutical goals to train shoulder and elbow in the five patients. Mobilization of the arm was rated to be important in three patients. The pressure handle restricts finger training (except finger flexion) and the hand can not be fixed. Here, an active module for opening and closing the hand might be a good solution (a first prototype was designed earlier, Appendix A.2.1).

For the patients ID3 and ID5, the active support from ChARMin was not helpful, because these patients had enough function to perform the games on their own. ChARMin could still be used for the test session, but without support or only gravity support. However, this can also be trained with other less complex rehabilitation robots such as the YouGrabber or the ArmeoSpring.

The transparency of the exoskeleton is crucial to not disturb the patient's arm movement during the robot-assisted assessments, but also to move the arm while using the AAN path controller. This performance depends heavily on the quality of the compensation model of the robot. In the feasibility trials, stick-slip effects were observed (e.g., during the CIRCLE assessment in Fig. 5.11). These effects are very difficult to model reliably. If this turns out to have a bad influence on the quality of the assessments or the movement of the patient, force/torque sensors need to be mounted (dummies already foreseen) to measure even small interaction forces and, therefore, to increase the robot's transparency.

The usability of the ChARMin interface was considered good. The number of software errors occurring needs to be further decreased before the extensive feasibility study will start.

The interface would benefit from an avatar in the mobilization mode. A virtual reality interface showing the avatar arms could trigger the mirror neuron system by imagination [277] and imitation [278] of the arm movement and, as a consequence, increase the activity in the motor control areas.

### 5.4.2 Games

The five patients who tested the ChARMin robot built a trial group with male and female children, affected on the left and/or the right arm and with different severity of arm impairment. Thanks to this very heterogeneous group, the different settings and limits of the games and the assist-as-needed controllers could be tested. The patients ID2 and ID4 needed a lot of support and tested amongst others the complete guidance while the others played the games with less or no support. In general, the game difficulty and the active arm assistance could be adapted well to the capabilities of the different patients. Furthermore, the children and adolescents enjoyed playing the games. The movement mean speed showed a tendency to be higher for less supported movements. The highest speeds were achieved for the whack-a-mole game with no

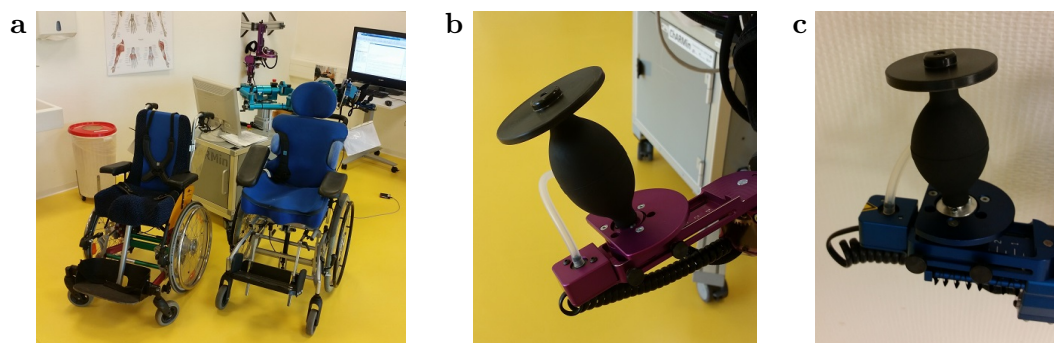


Figure 5.12: Addressing the ChARMin shortcomings by (a) adapting wheelchairs and (b) adding a slide-off protection disk to the handle of the large and (c) the small distal module.

support (in the patients who did not need a lot of support). The lowest speeds were reached during the completely guided tennis game. However, the mean speed also depends on the workspace chosen.

**Ball game** The ball game was played by all the children with different joints, dependent on the therapy goals of the individual patient. The range could be well adjusted using the calibration routine and ranged from  $43^\circ$  to  $79^\circ$  (Tab. 5.9). The support was adapted from 15% to 80% for the different patients. The posture to play the game was chosen by the therapist and was adapted during the game when desired (e.g., for patient ID3 in Fig. 5.1). The therapist required no changes with respect to the interface or the provided single-axis support.

**Whack-a-mole** The whack-a-mole game was played by all the patients (Tab. 5.9). For the patients with more severely affected arm function (patients ID2 and ID4), the therapist moved the robot and the patient pressed the handle to hit the mole. The patients enjoyed the game very much. However, active support for the arm movement is required and needs to be implemented before the ChARMin feasibility study starts. Potentially, a haptic table could be used to slide on and prevent that the patient gets tired. The game scoring algorithm needs to be improved to make it comparable between the patients.

**Diver** All the children played the diver game and liked it a lot. The support could be adapted intuitively, however, active support should be available for more targets. Currently, only the movements towards the pirate fishes and the obstacles (stone) are supported. Additionally, the reaching for the air bubbles (to refill the air tanks and extend the gameplay) could be supported. This would increase the covered workspace for more affected children. The reaching for the treasures is not actively supported for now as they are seen as motivational bonus objects to provoke active participation.

**Airplane** The airplane game was only played by two patients (ID3 and ID5). The two patients liked the game. It was stated by the patient and the therapist that the game is visually rather challenging to understand how the obstacles can be avoided. The saving of the log files needs to be improved as several files were not saved correctly.

The active robotic support needs to be extended to this game. The snap-grid controller is a possible concept which could be implemented and tested (discussed in Sec. 3.4.3).

**Tennis** The tennis game was played by four patients and support ranging from 0 % to 100 % (Tab. 5.9). The game can be played with nonstop complete guidance where the patient's arm is moved to the position where the racket has to hit the next tennis ball (compared to, e.g., the diver game where the complete guidance is only switched on when a pirate fish or stone is appearing). This feature was used for patient ID4. The movements are mostly in a horizontal workspace (Fig. 5.5) and do not intensively train movements in shoulder flexion and extension.

**Spaceship** Four patients played the spaceship game with support ranging from 0 % to 70 %. The spaceship game is the second game which can be performed with nonstop complete guidance of the arm by ChARMin. However, 100 % support was not chosen during the first trials. The movements only covered a small workspace in front of the patient (Fig. A.22). The problem is, that the standard settings for the game place the targets very close together. This setting was not adapted to the patients. Widening the distance between the objects on the screen would increase the workspace and the mean speed of the arm movements.

### 5.4.3 Robot-Assisted Assessments

The six different robot-assisted assessment packages were applied to three patients (ID1, ID3, and ID5). The patients were mildly to moderately affected. This led to saturation effects in the ROM assessment and challenged the hardware during the STRENGTH assessment. However, all the assessments were conducted twice with each patient with only minor issues concerning the understanding of the assessment and a couple of software errors.

#### ROM

The three patients, who only had minor impairments of their arms, almost exclusively reached the software end stops of the robot in both, the active and passive, ROM (Tab. 5.10). The very small differences in the angle measurement originate from the impact on the elastic virtual joint wall which happened at various speeds for the different patients. Differences between the aROM and pROM could only be detected for elbow pronation and wrist extension. This matches the findings from the adult ROM assessments stating that the ROM is only useful for moderately to severely affected patients who do not reach all the mechanical limits (Sec. 4.1.4).

#### WORKSPACE

For all the three patients, the WORKSPACE assessment was applied in the continuous mode. This is based on the adult assessments suggesting that the continuous increase of the room decreases the assessment time (Sec. 4.1.4). Patient ID1 reached the largest workspace volume with a mean of  $0.178 \text{ m}^3$ . The average workspace volume for the other patients was much smaller with  $0.101 \text{ m}^3$  and  $0.084 \text{ m}^3$ . The assessment outcomes from the two sessions are close together for all the three patients, pointing out a good repeatability of the measurement. The absolute workspace measurement is

dependent on the arm length of the patient, i.e., a patient with longer arms can reach a larger volume while having the same joint range as a patient with shorter arms. A possible standardization would be to output the volume in percentage of the reachable volume (i.e., the volume which potentially can be reached with the given arm length and the maximum joint range of the robot). For this, the ARW measurement could be a possible tool to calculate the maximally reachable volume (as used for the adult robot-assisted assessments).

The ratings for the understandability revealed that the visual representation of the assessment should be improved to make it more intuitive. Possible changes are arrows indicating the direction to move to or an improved depth perception to reach the start position.

Lastly, the patient's movements to the bottom target wall have to be supervised by the therapist, as the patient can hit the chair or the leg when moving downwards in front with a completely stretched arm.

## QOM

In the adult robot-assisted QOM assessment, the position of the targets was dependent on the previously assessed workspace levels. For the three youths, the target distance was fixed to a distance of 0.1 m for better comparison between the patients. The understandability, duration, and robot posture had the best possible rating for all the patients.

The parameters are difficult to compare to each other as patient ID5 had an increased target radius to be able to perform the assessment. Patient ID1 and ID3 had similar values for D-P ratio, time to target and reaction time. The precision was slightly better for ID3 and the number of peaks was slightly higher. No conclusions can be drawn, or trends be seen for the repeatability of the measurements.

More parameters could be computed from the raw sensor values such as the mean speed, peak speed or other smoothness metrics.

For reaching target number 3 at the bottom, a problem was observed for patient ID1 as visually the target and the current position could be superimposed, but the end-effector was not on target, because of the end-effector position being saturated at the screen frame. This needs to be improved for the future assessments.

For the first three patients, the QOM, as well as the CIRCLE recording, were always started from the beginning of the assessment. In order to improve the assessment, the first round (CIRCLE) or the first targets (QOM) should be excluded from the evaluation.

## STRENGTH

The STRENGTH assessment was applied to all three patients. The measurements of the patients seem to be mostly repeatable (Tab. 5.13). The three patients were all very strong and applied joint torques close to the limit of the robot exoskeleton (especially patient ID1 during elbow flexion and extension). In the possible case that even stronger patients use the robot's STRENGTH assessment, a torque limit should be defined where the robot saturates the resisting torque for the measured axis to protect the robot mechanics.

A problem occurred with patient ID1, who did not feel very well at the second STRENGTH testing after a fall he had in the morning. Later, a femoral neck fracture

was diagnosed. The data was listed anyway. It shows that most of the STRENGTH values are decreased compared to the day when he felt good, indicating that the assessment potentially can detect a change in the test condition and pointing to a sensitive assessment.

The force measurement of patient ID5 showed shortcomings with the understanding of the direction the force needs to be applied. Moreover, the timing of the assessment needs to be further improved. For the assessments the therapist used an interface button to start the recording of the measurement. The time window between 3 s and 1 s before the recording was taken as the baseline. However, some patients were not completely passive during this period (e.g., WrFl or ShIR of patient ID1 in Fig. 5.9) or during the elbow and wrist measurements in patient ID5 (Tab. 5.13). The instruction for the patient should possibly be improved.

### **RPM**

The RPM assessment is performed in the pROM of the patient. Therefore, the RPM covered the almost identical range for the three patients measured. The assessment is rather intuitive as the robot performs all the movements for all the joints consecutively while the patient is instructed to keep the arm passive. No problems occurred during the assessment.

The RPM measurements of the two assessment sessions varied a lot for the three patients. Some joints show better repeatability than others (e.g., WrEx/WrFl for the lower speed or ElPr/ElSu for the fast speed) but no further conclusions can be drawn from this preliminary set. The patients had to be remembered to stay passive several times during the RPM assessment. A possible explanation of the variability could, therefore, be a non-passive patient.

It can be observed from the resistance data (Tab. 5.14) that the values for extensor movements were permanently higher than the ones for the flexor movements for the higher joint speed. However, no explanation was found for this trend.

The calibration routine was always run immediately after the RPM assessment to use the same pROM for both measurements. The software needs to be improved to be able to load old pROM settings and to perform the calibration later after the therapy session.

### **CIRCLE**

The CIRCLE assessment was by far the shortest assessment. Furthermore, it received best ratings for the understandability and the robot postures.

The summed difference values show a good repeatability for the two tests performed. For the other values, the variability is higher. Patient ID5 had the most affected arm motor functions with ataxic movements. This is reflected in the much larger summed difference and the reduced ellipse ratio. The 'percentage in front' parameter had high variability in patient ID5 but this effect was averaged in the mean values. Analyzing the variation of the time in front and back of the reference could offer more information about the patient status.

More assessment parameters for inter-joint coordination could be assessed, e.g., by analyzing the contribution of the different joints to the resulting circle movement at the end-effector. As the depth coordinate is not restricted, the assessment could be performed with shoulder only or with elbow and shoulder internal/external rotation

only. The contribution of the different joints to the end-effector movement could give more insights into the coordinative motor functions.

### General Comments

Currently, the assessments took 25 - 30 min which is rather long and the patients might become unmotivated. The assessment time for the patient might be reduced by performing the RPM calibration after the therapy, by improving the procedure of the single assessments, by increasing the speed in which different postures are reached or by skipping joint measurements which are not clinically relevant. The latter will have to be further analyzed after testing more patients with the ChARMin robot.

Two arm postures were required to be adapted (feedback from the therapists). The forearm needs to be supinated when abducting the shoulder higher than  $90^\circ$  during the RPM assessment. Furthermore, the exoskeleton posture during the elbow STRENGTH measurement has to be closer to the neutral-0-method.

CIRCLE, QOM, and WORKSPACE are played in the compensation mode. While most of the gravitational and frictional effects are compensated there may still be forces disturbing the arm movement such as static friction or dynamical effects of the robot. Even though the questionnaire pointed out that the robot could be moved well, there are certain effects in the resulting plots which look like stick-and-slip effects which may come from interaction torques with the robot.

For patients who are aged between 10 and 13 years, both distal modules can potentially be applied. Here, it would be interesting to evaluate the assessments with both distal modules to analyze the influence of the hardware on the assessed parameters and could help to decide, whether the device needs to be more transparent.

### Comparison to Clinical Assessments

In this feasibility trial, the robot-assisted assessments and clinical assessments were only tested with three patients. This low number does not allow for a powerful analysis between the two assessment groups. Nevertheless, some aspects and trends shall be considered in the following.

STRENGTH and MMT had a very good correlation in the ARMin assessments with SCI patients (4.1.3). No patterns could be observed in the three youths measured. The group was too small and diverse. However, the group of children measured with ChARMin will probably always be very heterogeneous in terms of impairment, age, and sex. For the MMT, the therapist measures the arm strength with respect to the patient impairment, age, and sex and the assumed maximum force of the measured patient. In contrast, the STRENGTH measurement is an absolute measure of the arm torque. Therefore, a score of 5 in MMT (e.g., in elbow flexion for ID1, ID3) can correspond to quite different torques in STRENGTH (27.7 Nm and 18.4 Nm). This effect was not further analyzed for the adult robot-assisted assessments, as there were mostly men (4/5) with similar impairments. To turn the STRENGTH assessment in a relative measurement, norm values are needed for patients of different impairment, age, and sex. ChARMin has the potential to provide a first set of norm values after the planned feasibility study.

The assessment scores for the BBT and NHPT show a first trend to correlate with the 'summed difference' from the CIRCLE assessment, as well as with the QOM precision and QOM D-P ratio. These trends have to be considered cautiously, as the assessment was slightly different for patient ID5 with the increased target size.

The elbow extension of patient ID5 was scored a 1+ on the MAS. The RPM assessment showed a clear resistance in the elbow extension joint. However, the other patients showed similar resistance (Fig. 5.14, @ 60°/s) and were not rated to have a stiffness in this joint (only ID3 could be measured with the MAS for elbow extension). More norm values from healthy subjects and patients are needed to analyze the measured resistance values.

The measured volume in the WORKSPACE assessment shows a trend to correlate with BBT and NHPT. However, the two assessments do not measure the same arm function. While the WORKSPACE measures the reachable cubic volume in front of the patient, the BBT measures grasping and transportation skills. The NHPT measures fine-motor manipulation, selective finger movements, and transportation. The only assessments which has traits of the same arm function as in WORKSPACE is the 'Schürzengriff' (patient is asked to place their hand behind their back) and the 'Nackengriff' (patient is asked to place their hand at the back of the neck) which are measured in the standard clinical routine. These tests only give categorical data of the successful performance of the movement. All the three patients who took part in the robot-assisted assessments were able to fulfill both tasks. Therefore, no conclusions can currently be drawn from the comparison of the WORKSPACE assessment with the clinical scores.





# 6 Conclusion and Outlook

## 6.1 General Conclusion

This thesis presented the development and first clinical implementation of the new pediatric arm rehabilitation robot ChARMin. The robot was developed to provide an intensive, activity-based, and task-oriented exercise tool for neurorehabilitation training that optimally challenges children with moderately to severely affected arm motor function aged 5 years and older. Different aims were stated in the introduction (Sec. 1.5.2) and were subsequently addressed in the four different main chapters of this thesis. Here, the four chapters are listed again together with the according aims and concluding remarks on whether they were reached.

### 6.1.1 ChARMin Robot

**Aim: Design and realization of an active child-specific arm rehabilitation robot hardware which is safely applicable to the anthropometric range of the pediatric target group and an audiovisual interface to motivate an active participation of the child during the therapy.**

In the ChARMin chapter, the development and realization of the ChARMin arm robot was described. The robot was built according to the clinical and technical requirements stated in the beginning of this thesis. The challenging requirements could be met with a modular design which includes serial and parallel kinematic structures to achieve a highly adjustable and safe exoskeleton robot design which can be applied to pediatric arm rehabilitation and covers the anthropometric range of children aged 5 years and older with arm motor impairments. An immersive game-like audiovisual interface was integrated into the ChARMin system to provoke active participation, to feedback information to the therapist and the patient and to instruct and visualize the assessments.

### 6.1.2 ChARMin Control

**Aim: Implementation of a patient-cooperative support strategy to assist children with different levels of impairment and with different therapy goals during the robotic rehabilitation session.**

Different controllers were introduced and discussed in this chapter to address the requirements for single-joint and multi-joint movement support ranging from free arm movements to complete guidance dependent on the impairment level of the user and to support different therapy modes, games, and assessments. A position controller was used to impose desired movements on the patient's arm during the mobilization, for completely guided movements in games or to hold postures during the assessments. To support target-oriented movements in space, a new assist-as-needed path controller was developed. For games on joint-level, an adaptive single-joint controller was introduced. The single-joint controller and the AAN path controller cover the support range from a

passive patient arm that needs full assistance to a completely active movement, where the support is unnecessary. For movements with little or no support, the robot has to be as transparent as possible. Therefore, an accurate compensation model was derived for the controller which not only compensates for inertia, weight, Coriolis- and viscous friction, but also reduces the static friction of the joints with a dithering approach.

### 6.1.3 ChARMin Assessments

**Aim: Development of robot-assisted assessments to measure various kinematic, kinetic, and timing aspects of arm motor function.**

Different robot-assisted assessment packages were developed and integrated into the ChARMin interface. A first set of five assessment packages was tested in adults with 24 healthy subjects and five SCI patients using the ARMin robot. Very good reliability and validity for the joint torque measurements was found despite the small number of patients. Furthermore, the measurements for the reachable cubic workspace and different quality of movement metrics showed tendencies for good intra-rater and inter-rater reliability as well as validity. To our knowledge, this was the first study integrating a comprehensive set of assessment packages in a single actuated robotic platform to measure kinematic, kinetic, and timing parameters on joint and end-effector level. Furthermore, this study presented for the first time the application of an actuated arm robot for assessment of SCI patients. With this consideration of concept study, the feasibility of the assessment packages could be shown. Based on the knowledge acquired during this study, the assessment packages were adjusted and transferred to the ChARMin robot for children. A sixth assessment package was added to assess the tracking possibilities of the child. The developed assessment packages are a new opportunity to measure the patient's arm function and cannot only replace clinical assessments but offer a sensitive, objective, and reliable measurement for more detailed insights in arm motor functions.

### 6.1.4 ChARMin Feasibility

**Aim: Test of the resulting robotic hardware, control paradigms, and assessments in first feasibility case trials with children and youths with affected arm motor function.**

First clinical feasibility trials with ChARMin were conducted in the Rehabilitation Center for Children and Adolescents (Affoltern am Albis, Switzerland). A small and heterogeneous group of five patients aged between 6 and 17 years, different disabilities (stroke, CP and TBI) and sex (3 male, 2 female) tested the applicability of the ChARMin robot in a clinical setting on different arm sides (4 right, 1 left). The robot could be safely applied and adjusted to all the patients' arms with the different distal modules and was mostly rated as comfortable. The therapists consider the handling of the robot as intuitive but it needs some experience. The difficulty of the games and the arm support could be intuitively adapted. Depending on the impairment of the patient, the support was adjusted from completely guided to a free arm movement. For each patient, the mobilization, ball game, and several other games were tested and the patients enjoyed the training. The assessments were performed with three patients. All the patients finished the assessments twice which took about 25-30 min for each session. First weak trends point to repeatable assessment outcome values and to potential correlations with the clinical assessments. The trials revealed only minor

shortcomings which need to be addressed before the start of an enlarged ChARMin feasibility study.

The results of these feasibility trials demonstrate a high potential of the ChARMin robot to be used as an active arm rehabilitation tool for moderately to severely affected children aged 5 years and older.

## 6.2 Contribution of this Thesis

ChARMin is the pediatric version of the adult arm rehabilitation robot ARMin. The two robots differ in various aspects concerning the hardware, interface, control, and assessments. A comparison of the two arm exoskeletons is given in Appendix A.2.6.

To the best of the authors knowledge, ChARMin is the first actuated exoskeleton robot for pediatric arm rehabilitation. With the robotic technology, control methods, and assessment strategies, this thesis can contribute to the establishment of rehabilitation robotics in clinics as an assisting and assessing tool to complement conventional therapy for children. Although ChARMin was specifically designed and built for arm rehabilitation of children, based on the requirements from the pediatric target group, the herein developed exoskeleton hardware, control approaches, and robot-assisted assessments can also be transferred to other robotic platforms, including robots for adult rehabilitation, or other robotic fields.

**ChARMin robot** The kinematic approach to increase the safety by moving robotic parts further away from the user and the consequently developed change-of-side mechanism and passive spring compensation mechanics are novel designs for a safe and a user-optimized robot structure. To our knowledge, it is further the only exoskeleton which capitalizes on a modular design with decentralized motor control boards to easily exchange parts to adapt the robot to the user. The developed user interface is used to access the calibration, assessments, games, mobilization, and patient settings and exemplifies a comprehensive and intuitive solution to operate a rehabilitation robot. The developed games and concepts can be transferred to other platforms and robots, e.g., the interface with the games was already tested with an ArmeoSpring and the PASCAL robot.

**ChARMin control** The extended path controller was successfully tested during the feasibility trials and provides a powerful and stable algorithm to support arm movements during targeted hand movements in space. The controller can be applied to exoskeleton as well as end-effector robots. The different control modes need to be further evaluated to understand which patient profits most from which kind of support. Even in adult rehabilitation studies the differential effects of a specific control mode were rarely tested [74]. The benefits of using force/torque sensors to reduce interaction torques between the patient and the robot was shortly discussed. When no force/torque sensors are available, the dithering approach was presented as a feasible solution to reduce static friction in rehabilitation robots. The presented Kalman filter approach gives good estimates for the acceleration for robots with encoder position sensors only.

**ChARMin assessments** It was the first time that a set of extensive arm assessments was tested within a single robotic tool. Its applicability to adult and pediatric

children could be shown. The described methods have the potential to be generalized and transferred to other robotic exoskeleton platforms (e.g., the commercial version of the ARMin robot, the ArmeoPower) or other patient groups. WORKSPACE and QOM assessments can also be applied to end-effector robots, such as the ACT<sup>3D</sup> [237], the GENTLE/G [279] or the PASCAL robot [152]. By giving detailed precise instructions for conducting the assessments, we offer a reproducible guidance for future assessment implementations into rehabilitation robots.

### 6.3 General Outlook

The novel robotic technology and methods developed for ChARMin, ARMin IV, and PASCAL open doors for new innovative, promising and visionary future directions of research.

The first feasibility case trials with ChARMin revealed promising results for the use of the robot as an advanced exercise tool for neurorehabilitation. The first application to children also showed several shortcomings which will have to be addressed to achieve a robotic system which can be used in a clinical setting with high acceptance by the therapists who use it.

Since 1997, there have been more than 60 clinical trials reporting the use of two dozen different robots for neurorehabilitation [74]. Most of these studies were only pilot studies and no larger studies were performed [74]. To the best knowledge of the author, for children, there is only a single study available which investigated robot-assisted therapy in children on a larger scale [147]. The ChARMin feasibility study will be conducted over the next five years and covers different subprojects (Appendix A.5.1). This large study and the close teamwork between the therapists and researchers in the Rehabilitation Center Affoltern am Albis, provides an optimal framework to investigate the feasibility of the ChARMin therapy, to add substantially to the understanding of the benefits and shortcomings of robotic therapy in children and potentially to provide evidence of the efficacy of robotic rehabilitation training in children.

# A Appendix

## A.1 Appendix of Introduction

### A.1.1 Degrees of Freedom of the PASCAL Kinematics

PASCAL is an end-effector robot to support arm movements in space. The robot is attached to the combined center of mass of the arm. The degrees of freedom at the arm attachment point of the robot are calculated to analyze which DoFs at the interaction point are mechanically constrained, which DoF are controllable by the robot and which DoF are unconstrained and can be freely moved by the user.

PASCAL consists of an axis rotating the robot around the vertical axis and a four-bar linkage (pantograph kinematics) which consists of links which are connected in a loop. At the attachment point two more passive degrees of freedom are added (Fig. 1.9).

The Grübler's formula can be used to calculate the number of degrees of freedom at the arm attachment point. Therefore, the degrees of freedom of the parallel kinematics are first calculated. All five joints from the parallel kinematic structure are one degree of freedom joints. The parameters needed are the number of links ( $N = 5$ , including the base), the number of joints ( $j = 5$ ) and the degrees of freedom of the joints ( $f = 1$ , as all joints are hinge joints). It follows from the Grübler's formula

$$M_{parallel} = 3 \cdot (N - 1 - j) + \sum_{i=1}^j f_i = 2 \quad (\text{A.1})$$

that the parallel kinematic structure has 2 degrees of freedom. In the next step, the parallelogram structure is included in a simple open kinematic chain with the active vertical axis and the two passive DoFs of the robot:

$$M = M_{parallel} + \sum_{i=1}^k f_{active,i} + \sum_{i=1}^l f_{passive,i} = 5 \quad (\text{A.2})$$

where  $k$  is the number of active joints (here  $k = 1$  with one degree of freedom  $q_3$ ) and  $l$  is the number of passive joints (here  $l = 2$  with one degree of freedom for each passive joint). Therefore, the arm attachment joint has 5 degrees of freedom. Three DoF are actuated and can be controlled by PASCAL, i.e., forces can be transmitted to the arm of the patient. The other two DoF are passive rotational DoF. The only DoF, which is restricted, is the rotation of the forearm (pro-/supination of the arm). It follows that PASCAL can apply translational forces but not torques to the arm attachment point. The patient is restricted in his forearm rotation, however, is free in the other two rotational DoF. In other words, there is no control from the robot over the pointing-direction of the forearm. This is illustrated in Fig. A.1.



Figure A.1: Visualization of different arm postures that can be reached in a steady robot posture.

## A.2 Appendix of ChARMin Robot

### A.2.1 Design of an Active Hand Module for ChARMin

The first prototype of the ChARMin robot is equipped with a pressure-sensitive rubber bulb to detect grasping forces applied. This training can increase grasping forces and finger flexion in the patient's hand, however, it lacks the possibility to train finger extension and range of motion (Sec. 5.4.1). Here, a possible design for a hand grasping module was elaborated by Daniel Dörig in his semester thesis [174]. The hand module was conceptualized for the smaller distal module, e.g., for children aged 5 to 13 years. The main requirements for the active hand module were a compact, lightweight, and safe hand module which can be applied to both hands. The module should allow a simple hand fixation, natural hand movements, and be adjustable to the pediatric hand sizes<sup>1</sup>. Individual finger training is no primary requirement. In accordance with the therapists from the Rehabilitation Center for Children and Adolescents, Affoltern a. A., Switzerland, the trained hand movement should be a power-grip like movement. First, existing hand modules were analyzed (A summary of active hand modules is given in Tab. 1.1, Sec. 1.3.1). A comprehensive overview of existing hand rehabilitation technologies can be found in the review of Heo et al. [280]. No active hand

---

<sup>1</sup>A detailed overview of the different requirements can be found in the semester thesis of Daniel Dörig [174].

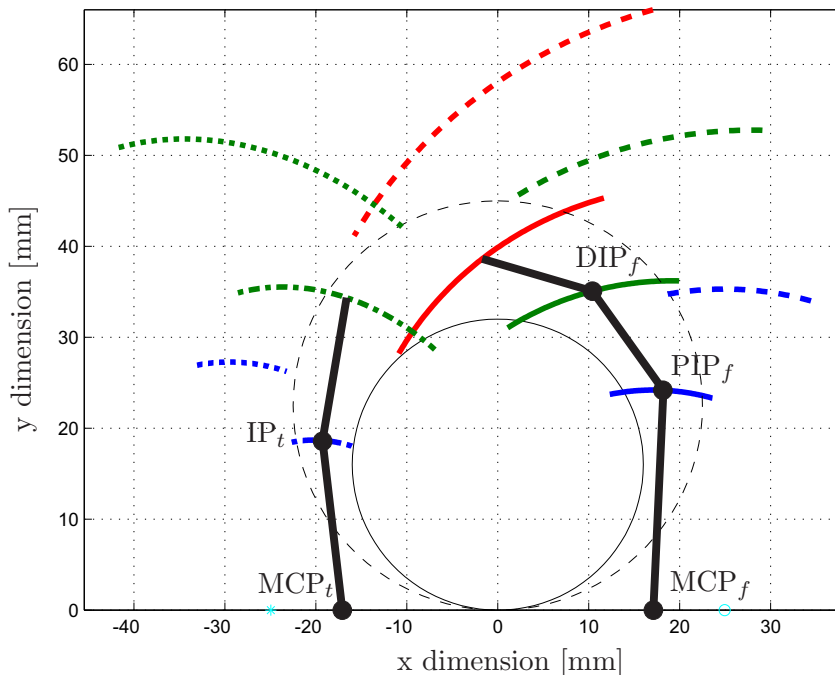


Figure A.2: Trajectories of the fingers during hand opening, mapped onto a plane. Solid and dash-dotted line describe the motion of the index finger and the thumb of a five-year-old. The dashed and the dotted lines refer to a thirteen-year-old. As an example, the fingers of an five-year-old were included into the figure. IP = Interphalangeal Joint (thumb); MCP = Metacarpophalangeal Joint; PIP = Proximal Interphalangeal Joint; DIP = Distal Interphalangeal Joint.

module was found specifically designed for children. The literature review showed that there are two fundamental concepts used already which are potential candidates for a ChARMin hand module. While the 'extending handle' pushes the hand open from the inside the 'finger guidance' concept opens the hand by moving the fingers, e.g., by using a finger exoskeleton. The two concepts were further analyzed with respect to the pediatric requirements given. This evaluation concluded with the decision to use an extending handle concept for the hand module.

### Concept of the Hand Module

**Modeling of the finger movements** The patient should be able to train a power grip with the hand module. To train a physiological movement, it is critical to know the trajectories of the joints during a power grip. A literature review revealed that there is no complete mathematical description of the power grip. A mathematical model of the finger movements during hand opening and closing was derived from literature data about finger lengths and range of motion (ROM) of the finger joints [281]. For simplification, it was assumed that the Metacarpophalangeal Joint (MCP) of the index finger and thumb were static during the opening of the hand. Together with a second assumption that the joint angles change linearly, the finger trajectories could be plotted in Fig. A.2.

Additionally, two circles are integrated into the plot. They describe the diameter when

the thumb touches the index- or middle finger for a 5- and a 13-year-old child. It can be seen as a minimum position for a power grip because at this point no force can be applied on the object hold in the hand anymore.

**Handles** For the 'extending handles' concept, the hand module consists of different handles which push the hand open. From the mathematical model of the power grip the optimal trajectories of these handles were derived, such that the hand is opened in a physiological manner.

The found solution has five handles that move along linear trajectories. The handles are arranged symmetrically. More handles are nearly impossible because of the limited size of the inner circle. Fewer handles guide the fingers too inaccurately. A disadvantage of this arrangement is that the thumb is not activated over the full functional range of motion.

**Cam disc design** To have a lightweight and compact design the handles should be moved by a single actuator. The idea was the use of a cam disc which is rotated by the actuator and slits in the disc move the handles along linear guides. The challenge is to design the cam disc such that its rotation moves the single handles continuously and linearly from the innermost position to the outermost position. After several iterations, a solution was found. This solution is sketched in Fig. A.3. The handles (blue disk) move on the linear guides (orange line) by a rotation of the cam disc. The slits in the cam disc are shown with the curved lines, e.g., the green curve with the triangles moves the blue disk upwards while rotating the cam disc.

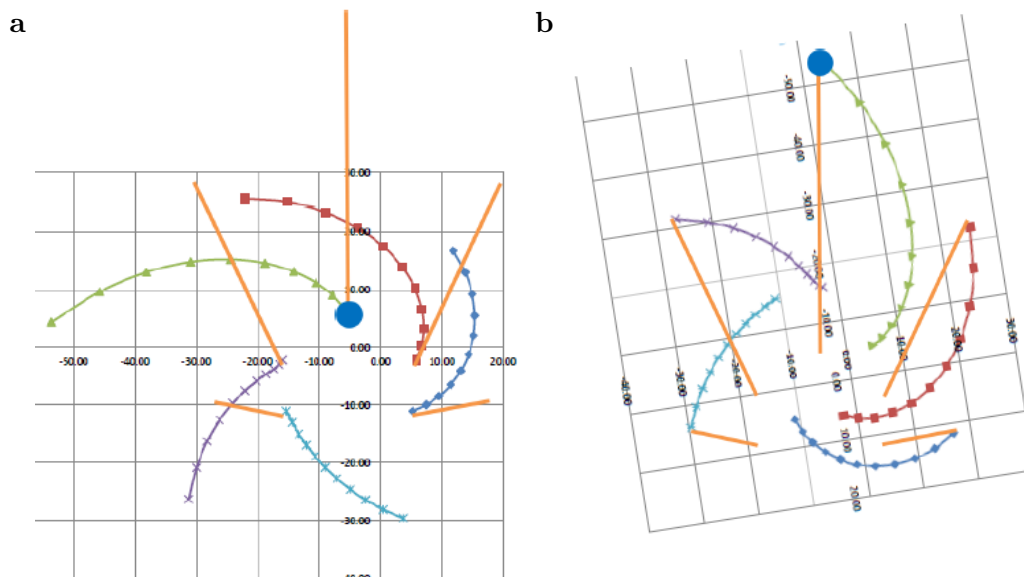


Figure A.3: Combination of the linear guides (orange lines) for the handles (blue disks) and the cam disc (coordinate system with the curved lines). The rotation of the cam disc moves the handles. (a) Closed hand position. (b) Opened hand position.

**Final design** The movement trajectories of the handles defined are defined by the cam disc. The handles are moving in the slits of the cam disc and, therefore, when



the cam disc is turning, the handles start moving outside or inside depending on the rotational direction of the disc.

The hand module was built in a multi-layer design. At the bottom is the base plate on which the linear guides are mounted. The fixation for the handles is screwed on the slide of the linear guide. Above the linear guides, the cam disc is mounted which is connected to the base plate over its axle. The cam disc is driven by the motor (black cylinder) over an involute gear (Fig. A.4 **a**).

The inner moving parts are hidden under a cover to protect the patient's hand. Above the cover the five handles can be seen which are driven by the cam disc (Fig. A.4 **b**). To avoid that the fingers can be clamped between the moving handles a soft tissue should span the handles. To avoid high forces by the extending surface of a tissue fixed around the handles, the idea was to use one of the handles (the one at the top) as a coil which acts as a material reservoir. When the handles open the reservoir releases tissue and when the handles close the coil collects the material with the help of a spring.

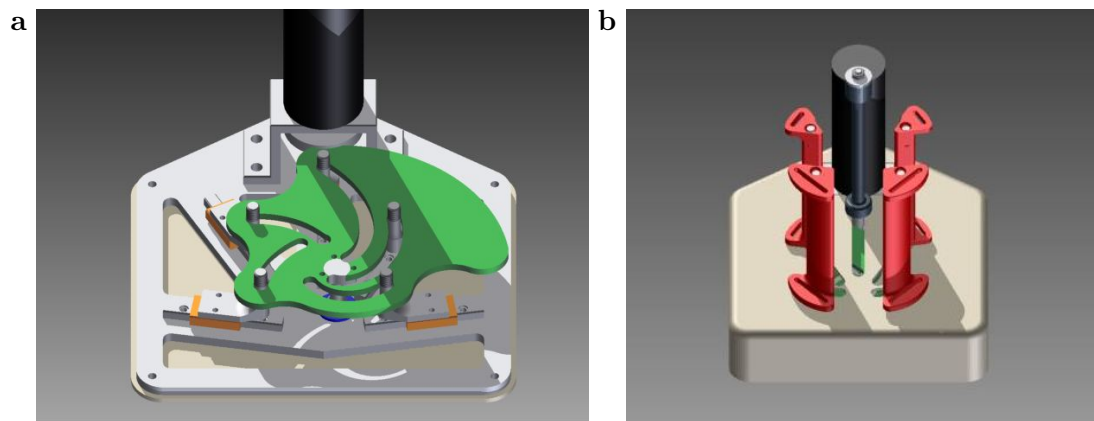


Figure A.4: (a) Inner parts of the hand module in opened position, (b) Hand module fully assembled in open position.

The resulting design is still quite large and it is unclear whether the cam disc can move the handles, whether the soft tissue can protect the fingers from being squeezed, and whether the handles would withstand a spastic hand. The next step would be to analyze the feasibility of the concept once more and to realize a functional prototype which could answer these questions risen.

### A.2.2 List of ChARMin Errors

To guarantee the safe operation of the system, several software-, sensor-, electronic- and handling errors can be detected. A list of the detectable errors is given in Tab. A.1 and the subsequent Tab. A.2.

Error	Error name	Description
0	Force sensor overload	Indicates an overload on the force/torque sensors. Currently, no force/torque sensors are mounted.
1-7	Limit reached axis x	A wrong joint angle position of axis x was detected due to incorrect sensor value or a joint which is out of range (e.g., missing mechanical end stop). Joint angle of axis 7 is a dummy placeholder.
8-14	Redundant sensor error x	The difference between the redundant absolute potentiometer value and the digital encoder value is more than $10^\circ$ because of a faulty calibration or incorrect sensor values.
15	48 V supply error	Shows under- or overvoltage ( $\pm 10\%$ ) of the 48 V supply.
16	- not in use -	- not in use -
17	Connection error	Connection to the interface software lost.
18	Motor drives not ready	Maxon drives or ChAxis drives are not ready for control.
19	Position control error	The reference signal for the controller has a step of more than $15^\circ$ .
20	Endeffector speed too high	The end-effector speed is higher than 1 m/s. This error is resettable in the software interface and therapy does not have to be stopped.
21	Force sensor no noise	When force sensors are used, this error supervises whether the sensors are connected.
22	Food pedal pressed during startup	During the first 2 seconds the robot calibrates the sensors. During this time the robot should not be powered which is checked and this error is prompted when the foot pedal is pressed.

Table A.1: List of the errors 1 - 22 which can be produced by the Simulink control software.

Error	Error name	Description
23	Motor temperature exceeded	This error is produced when the motor housing temperature is higher than 70 °C (for the motors on the distal module).
24	5V Supply error	The software supervises whether the 5 V supply voltage is in range.
25	No distal module or touching motor 3	This error occurs when the REED sensor detects no distal module or when the proximity sensor on the small distal module detects that an object is close to the clamping zone.
26	Computers are too hot	Supervision that the temperature in the electronic box is not higher than 60 °C
27	48 V supply error	Checks whether the 48 V supply is initially on 0 V to guarantee that the power supply can be switched off.
28	Jump in encoder	Checks for encoder position increments larger than 0.5 °.
29	Position control error	Checks that no step higher than 15 ° is applied to the position controller.
30	IK has no solution	- not in use -
31	Wrong side selected	Detects when the module chosen in the software does not match the one mounted on the robot.
32	CtrlModeError	Checks that all axes are in the same control mode for controllers which use all axes.
33	PositionErrorMobi	Checks that no step higher than 15 ° is applied to the mobilization position controller.
34	Error_board_1	This error is prompted when the ChAXIS current control board 1 is in error mode.
35	Error_board_2	This error is prompted when the ChAXIS current control board 2 is in error mode.
36	Current_mismatch	Checks whether the current required from the ChAXIS board is equal to the one measured on the board ( $\pm 1$ A).
37	Emergency button hit	Prompts when one of the two emergency buttons is hit.
38	Wrong orientation of the emergency button	Detects whether the mobile emergency button is placed horizontally.

Table A.2: List of the errors 23 - 38 which can be produced by the Simulink control software.

### A.2.3 Comparison with US Patent 2008-0304935

The Patent US 2008/0304935 A1 shows similarities with the ChARMin remote center of rotation (RCoR) design of the first axis (horizontal shoulder ab-/adduction). In order to compare both, the ChARMin illustration is drafted according to the representation in the patent (Fig. A.5).

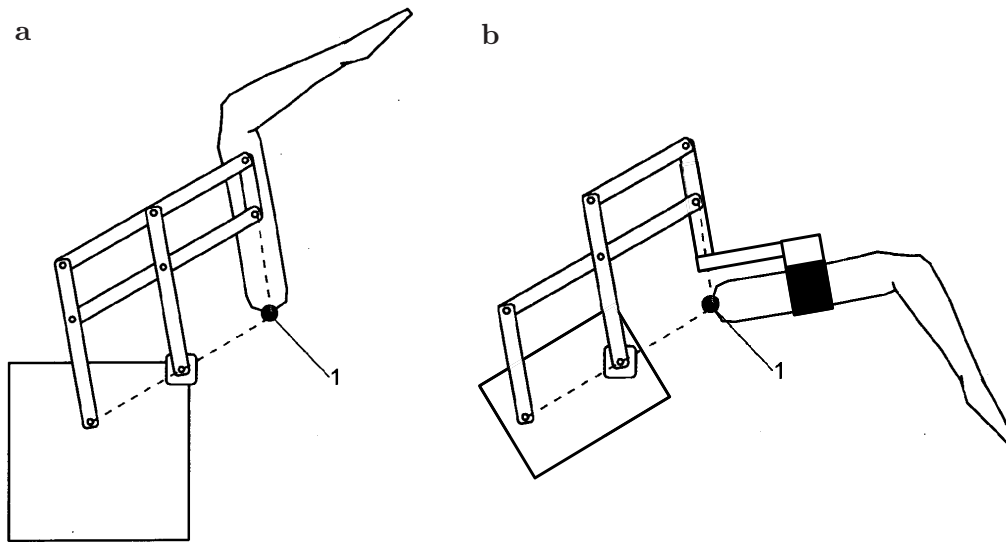
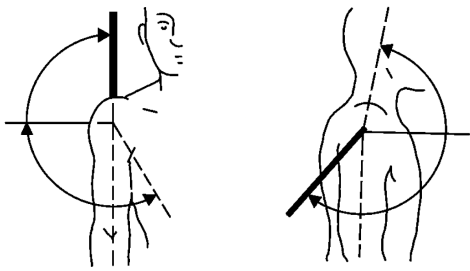
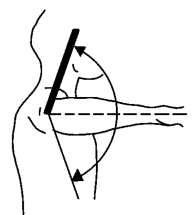
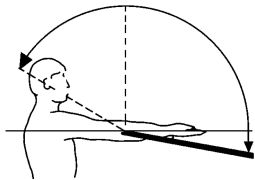
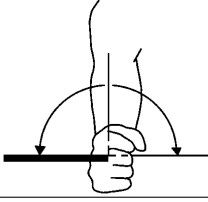
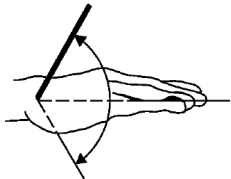


Figure A.5: Comparison between (a) the Patent US 2008/0304935 A1 and (b) the ChARMin kinematics of axis 1 (horizontal shoulder ab-/adduction). The glenohumeral joint is numbered with 1.

### A.2.4 Angle Convention of ChARMin

The ChARMin joint angles are defined in accordance with the "standardized neutral-0-method positions" [264] used by therapists.

<b>Axis 1: HSAb/HSAd - Horizontal shoulder ab-/adduction</b>	
This joint is usually not defined by the therapists. For the definition which is used, the joint angle starts at zero when the arm is stretched to the front.	
<b>Axis 2: ShAb/ShAd - Shoulder ab-/adduction</b>	
The shoulder ab- /adduction movement and shoulder flexion/extension movement are both actuated with axis 2 in ChARMin. The zero position is the position shown in the figure on the right (arm straight down) and the angle is increasing when flexing/abducting the shoulder.	
<b>Axis 3: ShIR/ShER - Shoulder internal/external rotation</b>	
The shoulder internal/external rotation is defined to be zero in the posture shown on the right (arm horizontal with elbow flexed). The angle is increasing when rotating the shoulder externally.	
<b>Axis 4: ElEx/ElFl - Elbow extension/flexion</b>	
The elbow angle is defined to be zero when the arm is completely stretched. The angle is increasing when the elbow is flexed.	
<b>Axis 5: ElPr/ElSu - Elbow pronation/supination</b>	
The pronation/supination angle is zero in the posture on the right. The angle is increasing when supinating the elbow.	
<b>Axis 6: WrEx/WrFl - Wrist extension/flexion</b>	
The wrist angle is zero when the forearm and hand are straight as shown in the figure. Further extending the wrist will increase the angle.	

## A.2.5 ChARMin History and Conceptualization

### First Sketches

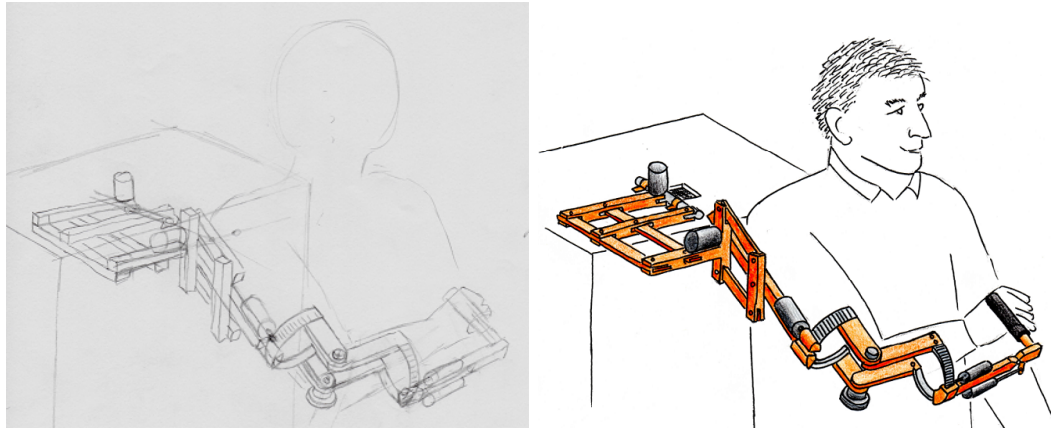


Figure A.6: First sketch of the ChARMin system.

### Conceptual Model

The first concept of the robot was roughly modeled in CAD (Fig. A.7) for further discussion and as a basis for the more detailed and correctly dimensioned model.

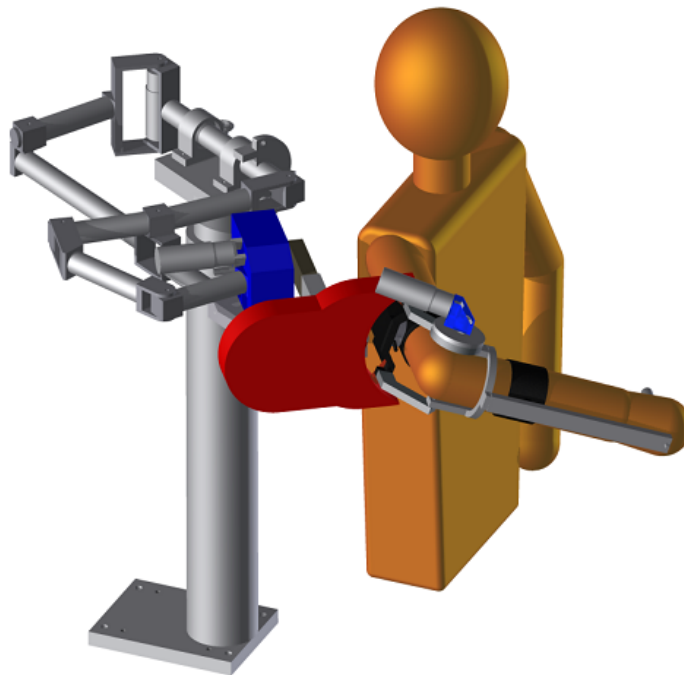


Figure A.7: First conceptual CAD model of the ChARMin robot.

**First Version with 4 DoFs**

The first ChARMin prototype had 4 DoF, i.e., 3 DoF for the shoulder and 1 DoF for the elbow (Fig. A.8 a, b). It was equipped with a distal module for children from 5 to 13 years. A length-adaptable arm rest with a cuff for the forearm was provided as well as a pressure sensitive stick that could be grabbed by the subject.

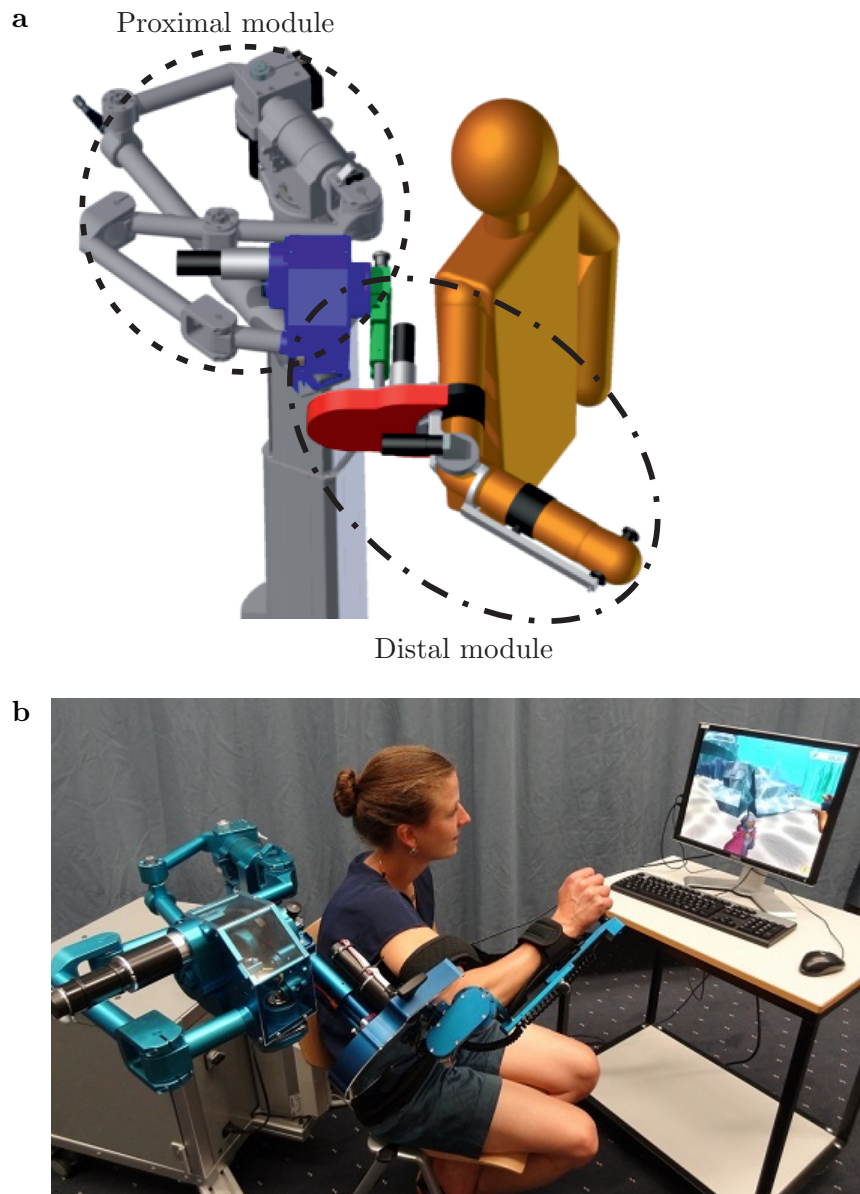


Figure A.8: First ChARMin prototype with four DoF. (a) Modular design of ChARMin with 4 DoF and with the distal module for younger patients, shown with the upper body of a 13-year-old child. (b) Healthy subject fixed in the ChARMin robot in a typical setup with the audio-visual display for the therapy. The axis control boards were not mounted in the picture.

## A.2.6 Comparing ChARMin and ARMin

### Differences Between ChARMin and ARMin

As mentioned earlier, the ARMin hardware and software could only partially be used for the pediatric version. Here, the main differences of the ChARMin robot compared to the ARMin robot are listed.


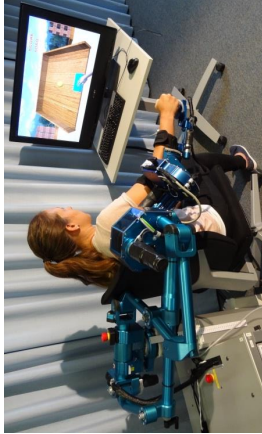
**Robot** i) Adjustable for children aged 5 years and older, ii) Modular approach to exchange the four distal DoF, iii) Two parallel remote center of rotation kinematics to move the robot away from the patient, iv) New change-of-side mechanism, v) Adapted passive spring compensation mechanism, vi) Electronics with current control boards directly on the exoskeleton to reduce cabling and improve exchange of distal module, vii) Activities of daily living replaced with game-like scenarios for more immersion and a motivational and playful training, viii) Non-actuated pressure-sensitive angled hand module, ix) New mechanics for the curved guidance moving the elbow pro-/supination joint (eccentric gears), x) Different wrist actuation (no spindle drive).

**Control** i) Extended path controller, ii) Changed inverse kinematics, iii) Dithering approach to reduce static friction, iv) Kalman filter to estimate the joint accelerations, v) All the joints can be controlled independently, e.g., axis 1 holds the position, axis 2 is freely movable, axis 3 applies a sinus reference signal to a position controller while the elbow is in single-axis control mode, vi) Adapted single-axis support to the predicted target position instead of the current ball position.

**Assessment** i) Continuous mode for the WORKSPACE assessment added, ii) CIRCLE following assessment added, iii) Assessments are more adaptable (e.g., QOM: Time to hold target position, CIRCLE: Speed of the target, QOM: Sequence of the targets shown, etc.), iv) Improved evaluation tool for the assessments and games with an intuitive user interface.



Comparing the Specifications for ChARMin and ARMin

	ARMin	ChARMin
		
	<b>Small module</b>	<b>Large module</b>
<b>Impairment</b>	Stroke (ARMin III, ARMin IV) and SCI patients (ARMin IV) with arm motor impairments	Children with neurological and orthopedic deficits and arm motor impairments, focus mainly on cerebral palsy (CP)
<b>Age</b>	18 - 99y	5-13y 11-18y
<b>Interaction</b>	3 interaction points (upper arm, forearm, handle)	3 interaction points (upper arm, forearm, handle)
<b>Mass</b>	100kg (Whole robot) / 20kg (orthosis)	110kg (Whole robot) / 5.7kg – 7.2kg (Exchangeable part)
<b>Features</b>	Left/right arm use Passive gravity compensation Backdrivable	Left/right arm use Passive gravity compensation Backdrivable
<b>Type</b>	Exoskeleton	Exoskeleton
<b>Kinematics</b>	Serial kinematics	Modular design with serial and parallel kinematics
<b>Degrees of freedom</b>	7 DoF	6 DoF
<b>Actuated joints</b>	Horizontal shoulder ab-/adduction Shoulder flexion/extension Shoulder internal/external rotation Elbow flexion/extension Forearm pro-/supination Wrist flexion/extension Hand opening and closing	Horizontal shoulder ab-/adduction Shoulder flexion/extension Shoulder internal/external rotation Elbow flexion/extension Forearm pro-/supination Wrist flexion/extension
	<b>Target group</b>	<b>Target group</b>
	Stroke (ARMin III, ARMin IV) and SCI patients (ARMin IV) with arm motor impairments	Children with neurological and orthopedic deficits and arm motor impairments, focus mainly on cerebral palsy (CP)
	18 - 99y	5-13y 11-18y
	<b>Robot general</b>	<b>Robot general</b>
	3 interaction points (upper arm, forearm, handle)	3 interaction points (upper arm, forearm, handle)
	100kg (Whole robot) / 20kg (orthosis)	110kg (Whole robot) / 5.7kg – 7.2kg (Exchangeable part)
	Left/right arm use Passive gravity compensation Backdrivable	Left/right arm use Passive gravity compensation Backdrivable
	<b>Kinematics</b>	<b>Kinematics</b>
	Exoskeleton	Exoskeleton
	Serial kinematics	Modular design with serial and parallel kinematics
	7 DoF	6 DoF
	Horizontal shoulder ab-/adduction Shoulder flexion/extension Shoulder internal/external rotation Elbow flexion/extension Forearm pro-/supination Wrist flexion/extension Hand opening and closing	Horizontal shoulder ab-/adduction Shoulder flexion/extension Shoulder internal/external rotation Elbow flexion/extension Forearm pro-/supination Wrist flexion/extension

Upper arm length [cm]	23.5 – 40.5	21.1 – 33.6	23.3 – 36.3
Forearm length [cm]	24.0 – 31.0	13.8 – 20.4	17.8 – 28.8
Hand length [cm] (Wrist-handle)	4.5 – 8.5	4.6 – 7.1	5.2 – 10.2
<b>Range of motion</b>			
Horiz. Sh. ab-/adduction	-40° ... 140°	-10° ... 95°	
Sh. flexion/extension	40° ... 140°	50° ... 130°	
Sh. Int./ext. rotation	-90° ... 90°	-70° ... 70°	
Elbow flexion/extension	0° ... 120°	0° ... 120°	
Forearm pro-/supination	-90° ... 90°	-90° ... 90°	
Wrist flexion/extension	-40° ... 40°	-70° ... 70°	
Hand opening/closing	0° ... 32°	-	
<b>Interface</b>			
Hardware	22" LCD screen, stereo speakers	32" LCD screen, stereo speakers	
Software	Mobilization 1 Single-joint games (Ball) 2 Multi-joint games (Labyrinth, Ping-pong) Assessments (not in standard software) 8 ADL tasks	Mobilization 1 Single joint game (Ball) 5 Multi-joint games (Airplane, diver, tennis, spaceship, Whac-a-mole) Assessments (in standard software) No ADL tasks	
<b>Nominal joint torques</b>			
Horiz. Sh. ab-/adduction	22.4 Nm	18.0 Nm	18.0 Nm
Sh. flexion/extension	10.5 Nm	22.7 Nm	22.7 Nm
Sh. Int./ext. rotation	12.7 Nm	8.6 Nm	11.8 Nm
Elbow flexion/extension	10.5 Nm	6.3 Nm	9.1 Nm
Forearm pro-/supination	2.5 Nm	5.0 Nm	8.3 Nm
Wrist flexion/extension	6.6 Nm	4.7 Nm	7.5 Nm
Hand opening/closing	2.2 Nm	-	-
<b>Electronics</b>			
Power consumption	1290 VA	346 VA	
Drives	Maxon drives	Maxon drives/Axis control boards (in-house)	
Cabling	Parallel cabling for each motor/sensor	Parallel cabling for axis 1-2, Serial cabling for axis 3-6 using motor current controllers on the robot. Communication is established with two CAN buses.	

## A.2.7 ChARMin Technical Specifications

### 1. ChARMin robot hardware

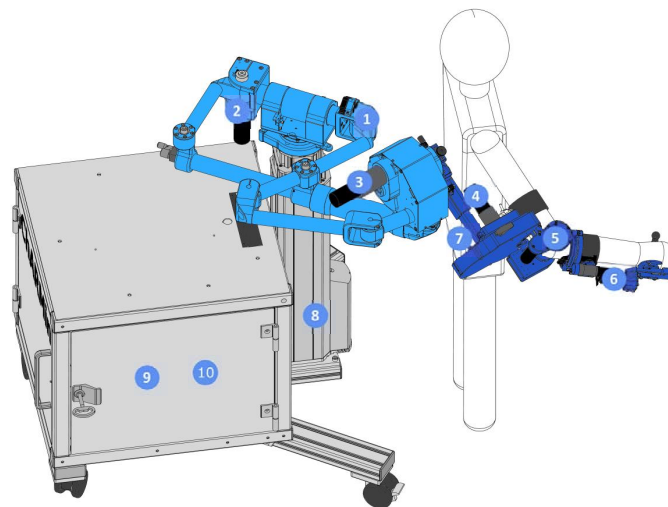


Figure 1 ChARMin robot with lifting column, an avatar for a 13-year-old child and the electronic cabinet

- |   |  |
|---|--|
| 1) Laser to mark the center of the glenohumeral joint | 6) Axis 5/6: Shown in more detail below (Figure 2)       |
| 2) Axis 1: Horizontal shoulder ab-/adduction          | 7) Upper arm length adjustment                           |
| 3) Axis 2: Shoulder flexion/extension, ab-/adduction  | 8) Lifting column to raise the height of the exoskeleton |
| 4) Axis 3: Shoulder internal/external rotation        | 9) Real-time computer xPC target (inside cabinet)        |
| 5) Axis 4: Elbow flexion/extension                    | 10) Host computer (inside cabinet)                       |

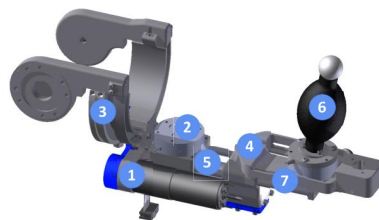


Figure 2 ChARMin forearm module

- |                                    |   |
|------------------------------------|---|
| 1) Laser                           | 5) Forearm length adjustment                                  |
| 2) Forearm cuff attachment         | 6) Pressure ball for game input and grip strength measurement |
| 3) Curved guidance for axis 5      | 7) Wrist-hand length adjustment                               |
| 4) Axis 6: Wrist flexion/extension |   |



## 2. Power

The main power supply for ChARMin is 230V/4A. The power is connected via the main switch to a medical approved transformer (Thalheimer ERT 230/230/6G). All the electric components of the system are connected to the transformer.

- 1) **Main power supply:** 230V/4A
- 2) **Motor power supply:** 48V/600W (Traco Power, TSP 600-148)

## 3. Computer

### 3.1. Real time xPC target (commercial PC)

Component	Type
CPU	Intel Core 2, 2.13 GHz, 32bit
Chipset	975X
RAM	2 GB
Network	IntelPRO/1000 GT
HD	150 GB
DAQ	Humusoft MF624
CAN card	Softing CAN-AC2-PCI

### 3.2. Host (commercial PC)

Component	Type
CPU	Intel Core i7-3770, 3.4GHz, 64bit
Chipset	Intel C216
RAM	4 GB
Network	Intel PRO/1000 GT
HD	500 GB
Graphic	Intel HD Graphics 4000
Audio	Realtek High Definition Audio

## 4. Robot hardware

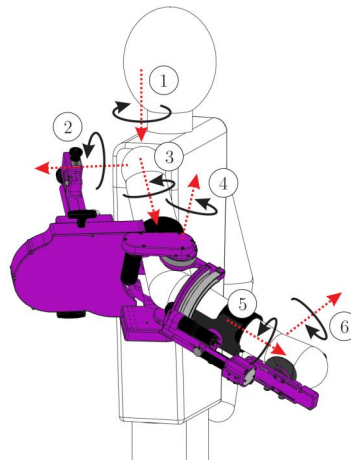


Figure 3 Definition of the six actuated ChARMin joint axes. Shown with the large distal module and the avatar of an 18-year-old child.

### 4.1. Kinematics

#### 4.1.1. Robot length adjustments

	Small distal module	Large distal module
Shoulder height [cm]	ca. 85.0 - 125.0	ca. 85.0 - 125.0
Upper arm length [cm]	21.1 - 33.6	23.3 - 36.3
Forearm length (elbow to wrist) [cm]	12.9 - 20.4	18.7 - 28.8
Hand length (wrist to handle) [cm]	4.6 - 7.1	5.2 - 10.2

#### 4.1.2. Joint range of motion (ROM) and achievable nominal joint torques

Joint	ROM	Nominal torque small module [Nm]	Nominal torque large module [Nm]
Axis 1: Shoulder horizontal ab-adduction	$-10^\circ < \theta_1 < 95^\circ$	18.0	18.0
Axis 2: Shoulder flexion/extension	$50^\circ < \theta_2 < 130^\circ$	22.7	22.7
Axis 3: Shoulder int./ext. rotation	$-30^\circ < \theta_3 < 70^\circ$	8.6	11.8
Axis 4: Elbow flexion/extension	$0^\circ < \theta_4 < 120^\circ$	6.3	9.1
Axis 5: Forearm pro/supination	$-90^\circ < \theta_5 < 90^\circ$	5.0	8.3
Axis 6: Wrist flexion/extension	$-70^\circ < \theta_6 < 70^\circ$	4.7	6.5

## 4.2. Mechanics

### 4.2.1. Friction

#### Static friction

The static friction has been measured as user driven breakaway torque with a 1DOF Kistler force sensor. The measurements were taken in the assembled robot with the feedforward gravity and friction compensation on.

Axis	Static friction [Nm]
1	1.6
2	3.0
<b>Small distal module</b>	
3	0.6
4	0.5
5	0.2
6	0.2

#### Coulomb and viscous friction

The coulomb and viscous friction was measured by moving each of the axes at different speed while measuring the torque needed. The overall torque was approximated with the following equation.

$$\tau_f = k_1 \cdot (1 - e^{-k_3 \cdot |v|}) \cdot \text{sign}(v) + k_2 \cdot v$$

Axis	Coulomb friction coeff. $k_1$ [Nm]	Viscous friction coeff. $k_2$ [Nms/rad]	Exponential rise coeff. $k_3$ []
1	3.3	5.5	50
2	3.0	0.4	5
<b>Small distal module</b>			
3	0.25	0.1	30
4	0.9	0.7	60
5	0.65	0.13	10
6	0.12	0.05	30
<b>Large distal module</b>			
3	0.3	0.03	20
4	0.8	0.4	60
5	0.3	0.05	10
6	0.15	0	15

### 4.2.2. Mass

Whole device: 110 kg

Exchangeable part (small module): 5.7 kg

Exchangeable part (large module): 7.5 kg

#### 4.2.3. Inertial properties CAD

Reflected joint inertia (including motor rotor inertia). Completely horizontal and stretched robot posture. Midrange for length scales.

	Reflected inertia	Comments
Axis 1	2.45 kg·m <sup>2</sup>	Inertia proximal part estimated with dynamic measurement and a least square fit and CAD inertia for the distal part.
Axis 2	0.82 kg·m <sup>2</sup>	CAD
Axis 3	0.11 kg·m <sup>2</sup>	CAD
Axis 4	0.058 kg·m <sup>2</sup>	CAD
Axis 5	0.090 kg·m <sup>2</sup>	CAD
Axis 6	0.090 kg·m <sup>2</sup>	CAD

#### 4.2.4. Spring

Durovis pull spring (25/4/3)  
Spring stiffness: 3300 N/m  
Spring constant effective: 4900 N/m  
Min. length: 157 mm (including adapter)  
Lengthening while moving: 91mm  
Possible pretension (crank): 50mm  
Rope: LIROS- D-PRO, Ø4mm

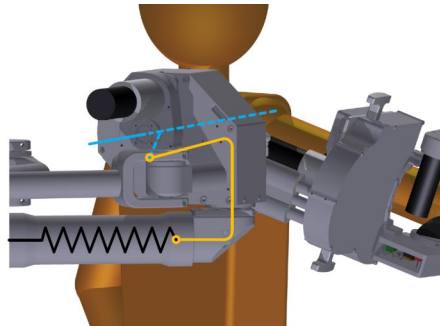


Figure 4 Spring for passive gravity compensation

#### 4.2.5. Mechanical play

	Mechanical play	Comment
Axis 1	0.05°	Harmonic Drive with no known mechanical play
Axis 2	0.63°	Tested with the robot sensors <sup>a</sup>
Axis 3	0.45°	Tested with the robot sensors <sup>a</sup>
Axis 4	0.03°	Harmonic Drive with no known mechanical play
Axis 5	0.1°	Tested with the robot sensors <sup>a</sup>
Axis 6	1.39°	Tested with the robot sensors <sup>a</sup>

<sup>a</sup>Tested by comparing the digital with the analog sensor (mechanical play is between these sensors)



### 4.3. Actuators

Axis	Motor	Gear	Ratio	Speed <sup>a</sup> [°/s]
1	MX RE40 (DC)	HD CSG-17-120-2UH	1:120	373
2	MX RE40 (DC)	Custom gear and PG MX GP52C	1:162 (1:2 and 1:8)	278
<b>Small distal module</b>				
3	MX RE35 (DC)	PG Maxon GP 42 C	1:113	185
4	MX RE30 (DC)	HD HFUS-14-100-2SO	1:101	481
5	MX RE25 (DC)	PG MX GP26A & belt	1:249.7 (1:19 and 1:13.14)	212
6	MX DCX22S (DC)	PG MX GPX22	1:138*3	164
<b>Large distal module</b>				
3	MX RE35 (DC)	PG MX GP 32 HP	1:159	135
4	MX DCX32L (DC)	HD HFUS-14-100-2SO	1:101	264
5	MX RE25 (DC)	PG MX GP26A & belt	1:362.9 (1:19 and 1:19.1)	150
6	MX RE25 (DC)	PG MX GP26A & 90° gear	1:278 (1:139 and 1:2)	192

<sup>a</sup>Theoretically achievable speed (with 5Nm load). MX = Maxon. HD = Harmonic Drive. PG = Planetary Gear.

### 4.4. Electronics

#### 4.4.1. Sensors

##### Angular position

ChARMin is equipped with optical incremental encoders at each joint (1000 impulses per rotation, except for axis 4 on the large distal module). With the four quadrant amplifier of the encoders, the resolution of the axes is around a per mill degree range. All the axes have additional, absolute analog sensors for redundancy (foil potentiometers, hollow shaft potentiometer, magnetic encoders).

Axis	Angular resolution (encoder incl. gear)	Sampling rate
1	0.00075°	2 ms
2	0.00056°	2 ms
<b>Small distal module</b>		
3	0.00080°	2 ms
4	0.00089°	2 ms
5	0.00036°	2 ms
6	0.00032°	2 ms
<b>Large distal module</b>		
3	0.00057°	2 ms
4	0.0035°	2 ms
5	0.00025°	2 ms
6	0.00033°	2 ms



**4.4.2. Axis current control board (ChAXIS)**

In order to reduce cabling and to make the distal part easily exchangeable, the motors on the distal part are not controlled with motor drives in the electronic cabinet, but with current controllers directly on the distal part. This reduces the cabling between the proximal and the distal part to 4 CAN bus wires (2 buses à 2 wires) and 2 power lines for 48V supply for the boards. The ChAXIS board was developed and built inhouse and encompasses the interface for two actuators with corresponding analog and digital sensors.

Feature	Number
Current controller	2 (for controlling 2 actuators)
Encoder input	2 (20bit)
Digital input	1 (5V TTL)
Digital output	2 (5V TTL)
Analog input	3 (10bit)
Communication	CAN 2.0 B
Dimension	52x63x18 mm
Board supply voltage	48V
Data transfer rate	1 Mbit/s
Max output current	5.5 A
Output voltage	-48 ... +48V
Sample rate current controller	22.05 kS/s

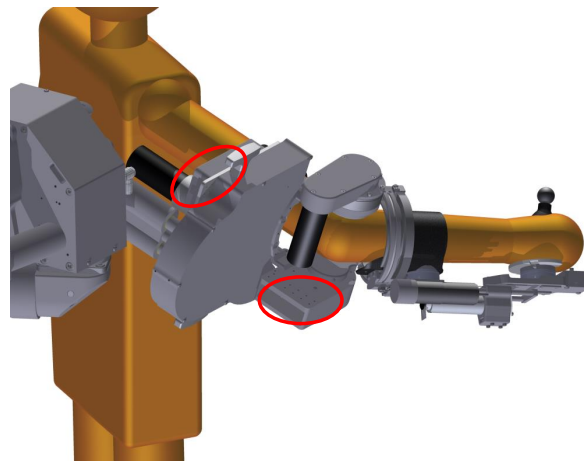


Figure 5 Location of the two ChAXIS control boards on the distal module of ChARMin.

## 5. Safety

### Passive

- Mechanical end stops at all joints and length adjustments
- Spring ensures that in case of a power loss the exoskeleton does not fall down on the patient
- No sharp edges
- Skin biocompatible cuffs

### Active

- Redundant position sensors
- Dead-man's switch has to be pressed to turn on the actuators.
- Watchdog for supervision of the real-time controller
- Surveillance of electronic voltage (48V and 5V levels)
- Check for left/right settings configuration using a tilt sensor
- Check for proper fixation of the distal module using a REED proximity sensor
- Surveillance of range of motion
- Surveillance of communication with ChAXIS boards
- Observation of the end-effector speed (not allowed to exceed 1m/s)
- Monitoring of the motor temperatures for the motors 3-6 (using a NTC sensor)
- Supervision of position-control errors
- Comparison between desired current requested from ChAXIS board and actual current
- Supervision of ChAXIS board drive temperature, undervoltage, drive shutdown, heartbeat, successful sending, general firmware error (queue overload, etc.)

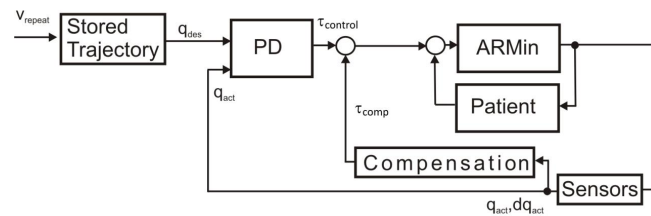
## 6. Control

### 6.1. Position control

The control parameters for the PD-Controller used during the repetition in the mobilization mode, the holding of positions during patient fixation or assessments as well as the 100% support mode in the games can be found in the table below.

**Table 1 : PD controller gains for mobilization and 100% support in games. The values are identical for the small and large distal module**

Axis	$K_p$ [Nm/rad]	$K_D$ [Nms/rad]
1	5440	59.5
2	2160	17.4
3	320	5.9
4	720	19.4
5	160	3.7
6	156	4.5



**Figure 6** Example of the position controller used in the mobilization mode (identical to mobilization in ARMin)

#### 6.1.1. Position control bandwidth

Measured position control bandwidth using a constant amplitude (5°) and increasing frequencies. The -3 dB amplitude was used as a measure for the bandwidth.

**Table 2** Position control bandwidth measured for the small distal module.

	Position control bandwidth	Comments
Axis 1	2.1 Hz	
Axis 2	3.0 Hz	Measurement up to 3 Hz and then stopped because of mechanical safety reason.
Axis 3	5.3 Hz	
Axis 4	5.5 Hz	
Axis 5	6.0 Hz	
Axis 6	5.0 Hz	

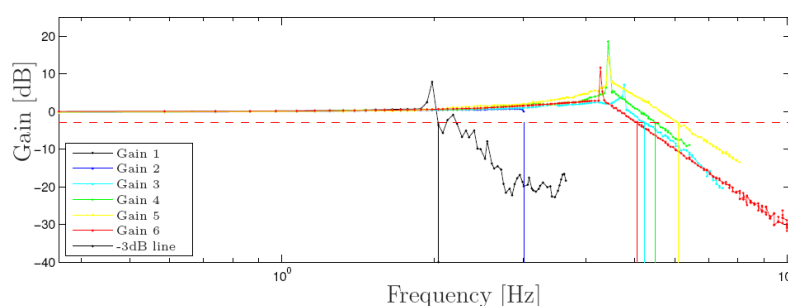


Figure 7 Position control bandwidth for the 6 axes of ChARMin equipped with the small distal module.

### 6.1.2. End-effector stiffness

The end-effector stiffness is anisotropic, i.e. it varies in different directions. The stiffness at the end effector was measured by applying an external force with a Kistler force sensor at the end-effector of the position-controlled exoskeleton. The measured forces and the displacements at the end effector were measured and the stiffness calculated as the ratio between these values. The posture was chosen in the middle of the workspace in front of the patients solar plexus. The stiffness was measured 5 times in each direction.

	End-effector stiffness
X positive	1.0 N/mm
X negative	1.1 N/mm
Y positive	1.3 N/mm
Y negative	1.3 N/mm
Z positive	2.4 N/mm
Z negative	2.9 N/mm

### 6.2. Adaptive ball game control

The adaptive support during the ball game is defined as:

$$\tau_{joint} = (q_{des} - q_{joint}) / (q_{max} - q_{min}) \cdot k_s \cdot \tau_{max} \cdot t_{inc}$$

where  $q_{des}$  is the desired joint angle in radian,  $q_{joint}$  is the current joint angle in radian,  $q_{max}$  and  $q_{min}$  are the extremum joint range values (can be changed in the patient settings),  $k_s$  is the normalized amount of support chosen by the therapist,  $\tau_{max}$  is the torque which is maximally applied in each particular joint,  $t_{inc}$  is an incrementation variable (e.g.  $(1 - h_{ball})$  where  $h_{ball}$  is the normalized ball height in the ball game or the normalized time since a target appeared on the screen in the whack-a-mole game).



### 6.3. Path control

The assist-as-needed path control strategy is used for the games that have a clearly defined target to move to (e.g., tennis game, the spaceship game or the diver game).

A virtual tunnel is rendered around the path from the given start position  $p_{start}$  to the desired target position  $p_{target}$  (Figure 7 Example of the position controller used in the mobilization mode (identical to mobilization in ARMin) Figure 7). If the patient deviates from the given path, the tunnel wall will apply a force towards the path and, therefore, push the patient's arm to stay close to the path.

In close vicinity to the path, there is a dead band with constant radius  $R_w$ , where no tunnel forces are applied. This allows the patient to choose his individual trajectory without being assisted. If the actual position  $p_{act}$  is outside this radius, a tunnel force is applied to the end effector. Inside the tunnel a direction-dependent adaptable flux force assists the patient along the tunnel direction.

The back of the tunnel and the front of the tunnel are moving according to a predefined minimal and maximal speed trajectory in order to provide additional support for the patient. A gain scheduling approach in the target position increases the wall stiffness  $K$  and decreases  $R_w$  in order to reach the target position [2].

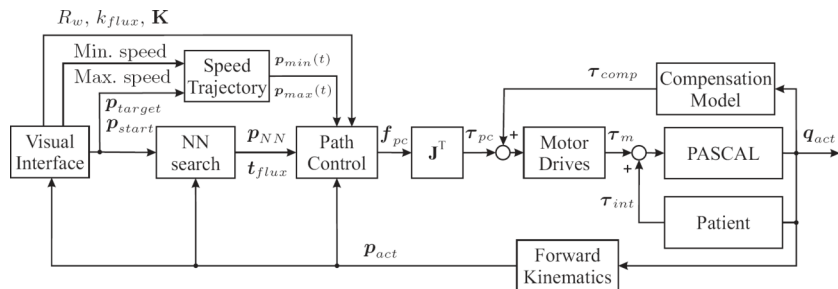


Figure 7: Control chart of the AAN path controller used in ChARMin

### Literature

- [1] U. Keller, V. Klamroth, H. van Hedel, and R. Riener. *ChARMin: A robot for pediatric arm rehabilitation*, IEEE International Conference on Robotics and Automation (ICRA), 2013, 3908-3913
- [2] U. Keller, G. Rauter, and R. Riener. *Assist-as-needed path control for the PASCAL rehabilitation robot*, IEEE International Conference on Rehabilitation Robotics (ICORR), 2013

## Appendix A - Order numbers

### Motors

Axis	Motor	Distributor	Order Nr.
1	Maxon RE 40	Maxon	148877
2	Maxon RE 40	Maxon	148877
<b>Small distal module</b>			
3	Maxon RE 35	Maxon	273759
4	Maxon RE 30	Maxon	310009
5	Maxon RE 25	Maxon	339155
6	Maxon DCX22S	Maxon	B716F657CED5
<b>Large distal module</b>			
3	Maxon RE 35	Maxon	273759
4	Maxon DCX32L	Maxon	B72D7EEAC8CC
5	Maxon RE 25	Maxon	339155
6	Maxon RE 25	Maxon	339155

### Gears

Axis	Gear	Distributor	Order Nr.
1	Harmonic Drive CSG-17	ASS	CSG-17-120-2UH
2	Planetary gear Maxon GP 52 C/	Maxon/Maedler	223093
<b>Small distal module</b>			
3	Planetary gear Maxon GP 42 C	Maxon	203126
4	Harmonic Drive HFUS-14	ASS	HFUS-14-100-2SO
5	Planetary gear Maxon GP26A	Maxon	406762
6	Planetary gear Maxon GPX22 / Maedler spur gears	Maxon/Maedler	B716F657CED5/ 350 277 00 and 350 276 000
<b>Large distal module</b>			
3	Planetary gear Maxon GP32HP	Maxon	326671
4	Harmonic Drive HFUS-14	ASS	HFUS-14-100-2SO
5	Planetary gear Maxon GP26A	Maxon	406770
6	Planetary gear Maxon GP26A / Maedler spur gears	Maxon	406770/350 557 00 and 350 556 00



### Sensors

#### Digital:

Axis	Encoder	Distributor	Order Nr
1	Maxon MR 1000 imp/rot	Maxon	228456
2	Maxon MR 1000 imp/rot	Maxon	228456
<b>Small distal module</b>			
3	Maxon MR 1000 imp/rot	Maxon	228456
4	Maxon MR 1000 imp/rot	Maxon	228456
5	Maxon MR 1000 imp/rot	Maxon	225780
6	Maxon ENX16 EASY 1024 imp/rot	Maxon	B716F657CED5
<b>Large distal module</b>			
3	Maxon MR 1000 imp/rot	Maxon	228456
4	Maxon MR 256 imp/rot	Maxon	ENX16 EASY
5	Maxon MR 1000 imp/rot	Maxon	225780
6	Maxon MR 1000 imp/rot	Maxon	225780

#### Analog:

Axis	Analog Sensor	Distributor	Order Nr
1	Contelec GL60 10KM354, Winkelaufnehmer	Distrelec	715766
2	Angle sensor 360°, RFA 4001-636-211-401, Novotechnik with NdFeB magnet 8x4x3mm	Distrelec/Supermagnete	242800/ Q-08-04-03-N
<b>Small distal module</b>			
3	Angle sensor 360°, RFA 4001-636-211-401, Novotechnik with NdFeB magnet 8x4x3mm	Distrelec/Supermagnete	242800/ Q-08-04-03-N
4	Angle sensor 360°, AKM Semiconductor Inc. (on elbow ChAXIS)	Digikey	974-1044-1-ND
5	ThinPot 170mm foil potentiometer	Mouser Electronics Inc	TSP-L-0170-103-3%-ST
6	Bourns, 12mm rotary position sensor	Digikey	3382H-1-502-ND
<b>Large distal module</b>			
3	Angle sensor 360°, RFA 4001-636-211-401, Novotechnik with NdFeB magnet 8x4x3mm	Distrelec/Supermagnete	242800/ Q-08-04-03-N
4	Angle sensor 360°, AKM Semiconductor Inc. (on elbow ChAXIS)	Digikey	974-1044-1-ND
5	ThinPot 300mm foil potentiometer	Mouser Electronics Inc	TSP-L-0300-103-1%-RH
6	Bourns, 12mm rotary position sensor	Digikey	3382H-1-502-ND

## A.3 Appendix of ChARMin Control

### A.3.1 Increased Transparency with Force Sensors in ARMin IV

*(This section is based on a previous conference publication of the author [6])*

#### Introduction

In the last seven years, different consecutive generations of the arm rehabilitation robot ARMin were developed at the Sensory-Motor Systems (SMS) Lab in Zurich. The last version, ARMin III, is an actuated exoskeletal structure with seven degrees of freedom (DoF) and is being used for therapy with stroke patients in four different clinics in Switzerland [171]. This year, ARMin III was transferred to the industry, with Hocoma AG (CH) building a commercial version of the device, available under the name Armeo®Power. In parallel a new generation, ARMin IV (Fig. A.9), was developed at the SMS Lab and optimized for the use with spinal cord injured (SCI) patients. A leveling caster system was attached to the base frame of the robot to adjust its position to the patient (especially for patients with electronic wheelchair) and the software was extended. New assessments were implemented to measure patient's range of motion, movement smoothness, joint stiffness, isometric force, reaction time, etc. and the training of the tenodesis function of the hand (passive finger flexion in response to wrist extension) was enabled, which is common in tetraplegic SCI patients. Furthermore, new force/torque (F/T) sensors were mounted to improve the measurement accuracy of direct interaction between robot and patient, and thus, also allow the inclusion of rather weak patients. In the following, the focus will be laid on these sensors and particularly the associated models and force control algorithms which increase the sensitivity of the device and, therefore, improve the transparency.

#### Methods and Materials

**Measuring interaction** To measure interaction forces and torques in the ARMin IV, three 6-DoF F/T sensors (Mini45, ATI Industrial Automation) were added in the cuffs of the upper arm and forearm, as well as in the hand module for precise measurements of patient interaction (Fig. A.10). This has the advantage that even small forces, which are below the static friction of the gears and joints, can be detected.

**Force sensor placement** Basically, two possibilities to place a force sensor are differed. The two positions are sketched in Fig. A.11. Either the sensor is close to the robot axis to measure the force directly after the motor (Sensor 1) or as close as possible to the patient to measure the interaction torques between the robot and the patient (Sensor 2). To understand which position to choose for the ARMin IV robot design, a simplified model was introduced (Fig. A.12).

The model is assumed to move in the horizontal plane, i.e., gravitational effects can be ignored. Furthermore, the sensors are assumed to be massless and no friction-, damping- or Coriolis effects are considered. Given the simplified model the equation of motion can be derived:

$$\boxed{(m_{robot} + m_{arm})\ddot{x} = F_{human} + F_{motor}} \quad (\text{A.3})$$



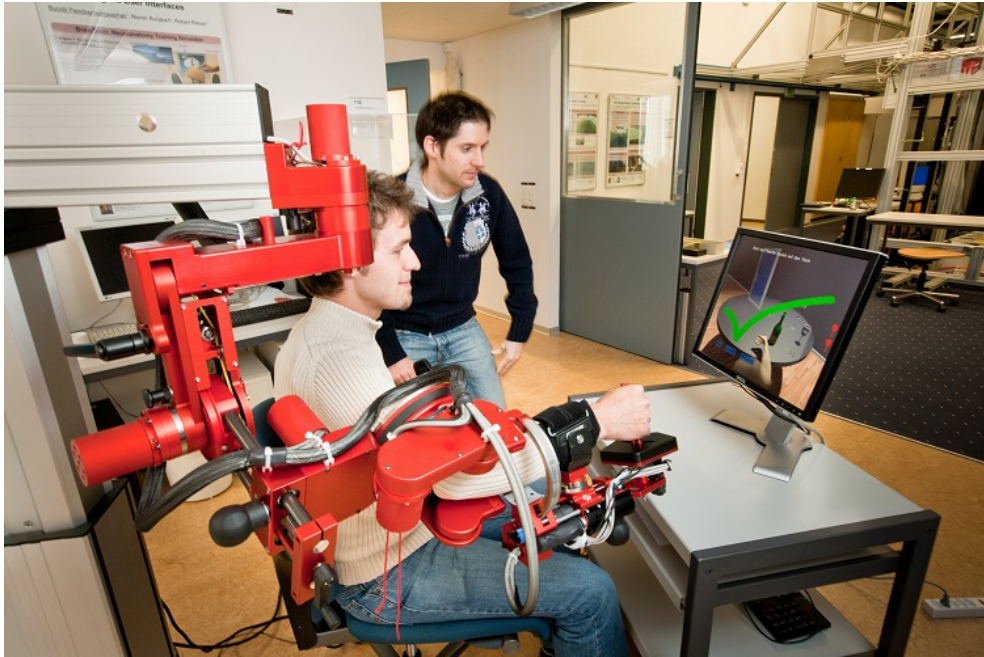


Figure A.9: ARMin IV - Arm rehabilitation robot optimized for the use with SCI patients

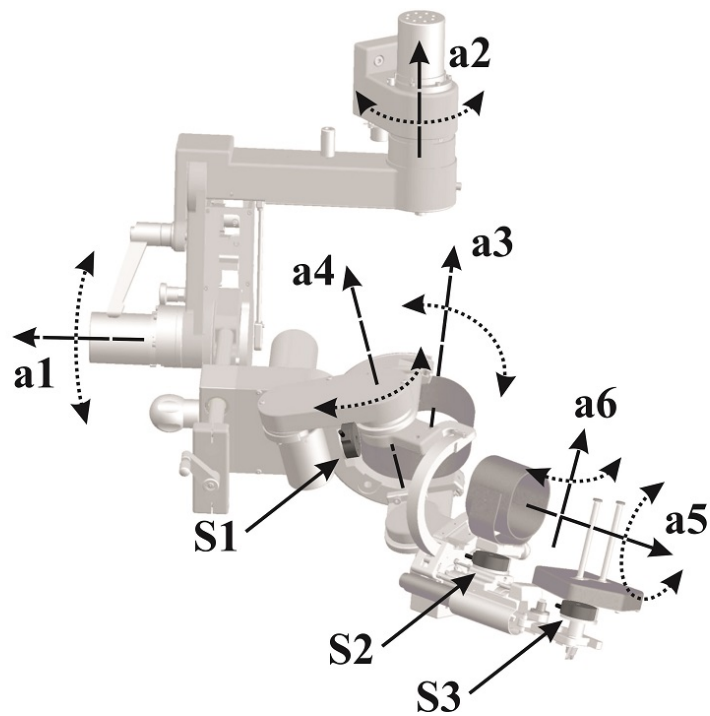


Figure A.10: Positions of the three F/T sensors on the exoskeleton (S1...S3) and axis numbering (a1...a6).

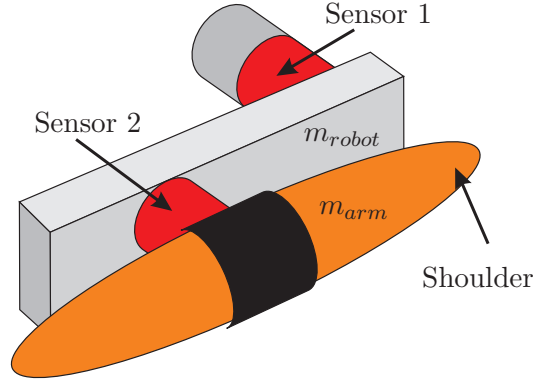


Figure A.11: Simplified upper arm and robot representation to illustrate the possible positions for a force sensor on the robot exoskeleton.

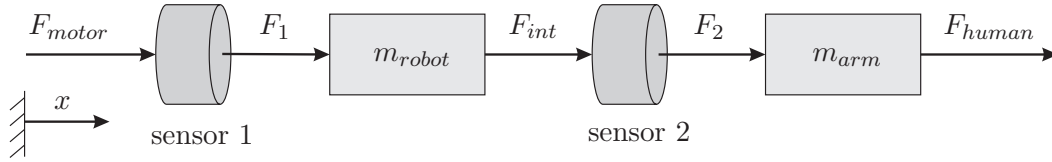


Figure A.12: Simplified model derived from the representation in Fig. A.11. For simplification the movement analyzed was a linear instead of a rotational model.

These terms can be rearranged to get the forces acting on the two sensors:

$$\text{Sensor 1:} \quad F_1 = F_{motor} = \underbrace{m_{robot} \cdot \ddot{x}}_{\text{robot dynamics}} + \underbrace{m_{arm} \cdot \ddot{x} - F_{human}}_{\text{interaction forces}}$$

$$\text{Sensor 2:} \quad F_2 = -F_{motor} + m_{robot} \cdot \ddot{x} = \underbrace{-m_{arm} \cdot \ddot{x} + F_{human}}_{\text{interaction forces}}$$

From these relations, it is clear that sensor 1 measures the interaction force  $F_{human}$  as well as the robot and arm dynamics. In order to calculate the interaction forces, the arm dynamics have to be subtracted from the measurement. However, the acceleration is hard to derive from the position sensor and an accurate model of the robot arm is usually difficult to achieve. Sensor 2 measures the interaction forces  $F_{human}$  only. Therefore, the decision was to choose the sensor position as close to the patient arm as possible.

**Control** To be able to use these new force/torque measurements for the joint-level torque control, the sensor information is mapped to the joints that are actuated in the robot. This mapping is described by the Jacobian  $\mathbf{J}$ . The Jacobian relates the speed of the sensor position to the according angular joint speeds, but is also the position-dependant relation between the externally applied forces  $\mathbf{f}_{Si}$  and torques  $\boldsymbol{\tau}_{Si}$  (measured in the sensors) and the joint torques  $\boldsymbol{\tau}_{joints}$  that need to be applied to have the robot in a static equilibrium.

The Jacobian for a specific point P on the robot can be found by calculating the speed of a point P on the exoskeleton and then splitting this speed into the contributions of each single joint.

$$\mathbf{v}_P = \mathbf{J}_P \dot{\mathbf{q}} + \text{rest} \quad (\text{A.4})$$

where  $\dot{\mathbf{q}}$  is a vector with the different joint speeds  $\dot{q}_1$  to  $\dot{q}_6$ .

Considering all the forces and the torques in each sensor the joint torques can be written as:

$$\boldsymbol{\tau}_{joints} = \sum_{i=1}^3 (\mathbf{J}_{f_{Si}}^T \mathbf{f}_{Si} + \mathbf{J}_{\tau_{Si}}^T \boldsymbol{\tau}_{Si}) \quad (\text{A.5})$$

These six Jacobians ( $\mathbf{J}_{f_{Si}}^T, \mathbf{J}_{\tau_{Si}}^T, i = \{1, 2, 3\}$ ) can be merged to one large Jacobian  $\mathbf{J}_{tot}$ , which is then multiplied by a vector  $\mathbf{f}_{tot}$  which consists of all the force and torque components received from the three sensors:

$$\boldsymbol{\tau}_{joints}^{6 \times 1} = \mathbf{J}_{tot}^{6 \times 18} \cdot \mathbf{f}_{tot}^{18 \times 1} \quad (\text{A.6})$$

The seventh DoF for the hand opening can not be detected with the new sensors and is, therefore, excluded here.

For the control loop, the data from the sensors is first filtered with a 2nd-order 8 Hz Butterworth low-pass filter before being processed through the previously calculated Jacobian, together with the robot angles  $\mathbf{q}_{act}$ . The resulting joint torques  $\boldsymbol{\tau}_{joints}$  are then used in a closed-loop force controller (Fig. A.13) with underlying current control.

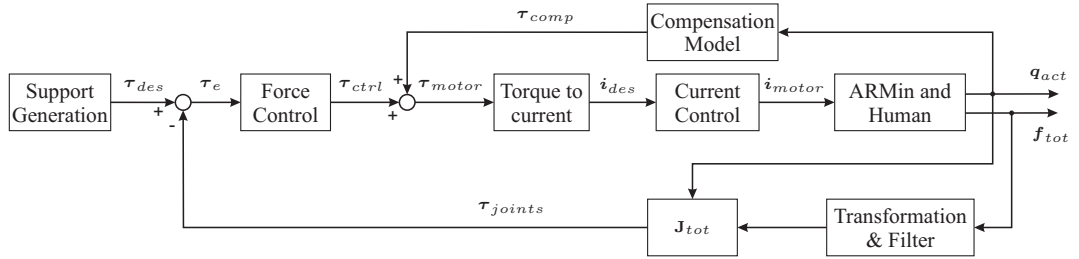


Figure A.13: Force control scheme for ARMin IV

The 'Compensation Model'-block acts as a feedforward control component and includes a model for the influence of friction  $\boldsymbol{\tau}_f$ , gravity  $\boldsymbol{\tau}_g$  and springs  $\boldsymbol{\tau}_s$  on the exoskeleton ( $\boldsymbol{\tau}_{comp} = \boldsymbol{\tau}_f + \boldsymbol{\tau}_g + \boldsymbol{\tau}_s$ ) [64]. These compensation torques and the control torques are then applied to the motors of ARMin ( $\boldsymbol{\tau}_{motor}$ ). For the subsequent test of the force controller, a PI- and a P-controller were used, which were designed by using the Ziegler-Nichols method [282]. To test the performance of the force controller the scheme (Fig. A.13) was reduced to a zero-force controller by setting the reference force to zero ( $\boldsymbol{\tau}_{des} = \mathbf{0}$ ). In this condition, the interaction forces/torques are maximally reduced by the controller.

## Results

In a first single case study, a healthy subject was fixed in the ARMin and then asked to follow, joint by joint, a minimal jerk reference trajectory displayed on the screen. As an example the trajectories for elbow flexion/extension and shoulder internal/external

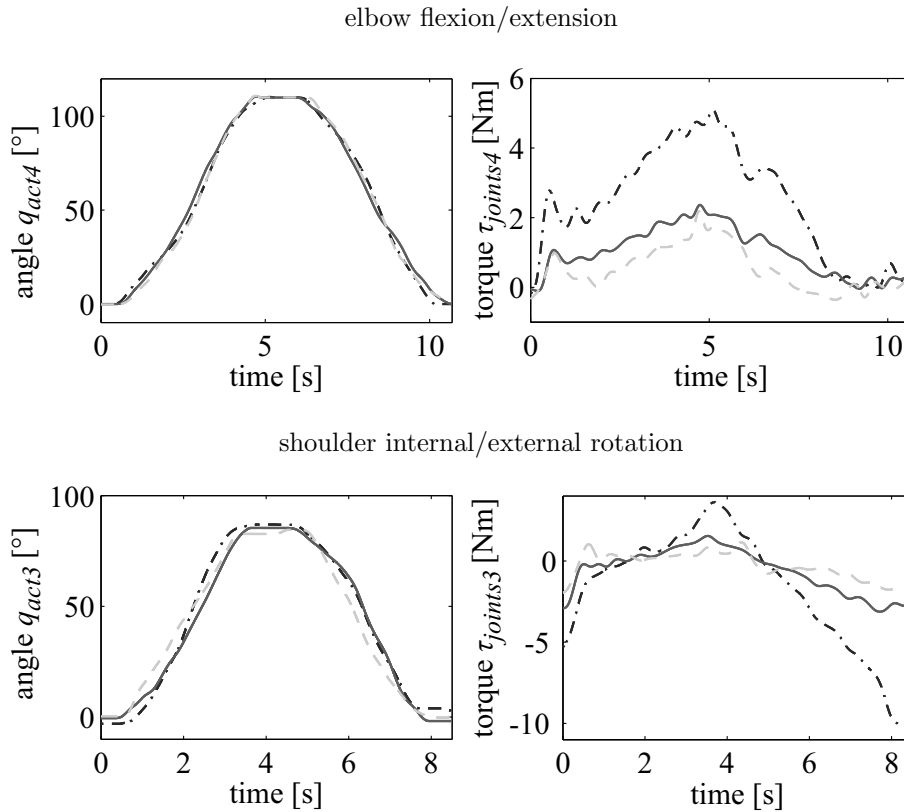


Figure A.14: Angle trajectory and corresponding interaction torques for the elbow and shoulder. Dash-dotted: Compensation, solid: PI-controller, dashed: P-controller

rotation are shown (Fig. A.14, left). The corresponding ARMin axes (axis 3 and axis 4) can be found in Fig. A.10.

The movement was performed for all joints in three different randomized conditions with either the feedforward compensation only (as test reference) or with additional PI- or P-controller. The calculated interaction torques during the movements are exemplarily displayed for the elbow and shoulder rotation (Fig. A.14, right).

To compare the different conditions, the integral over the torque course was calculated. This comparison showed a reduction of interaction torques of 58 % for the elbow flexion/extension (61 % for shoulder internal/external rotation) for the PI-controller and 78 % for the P-controller (77 % for shoulder internal/external rotation) compared to the compensation model.

## Discussion

The results show that the F/T sensors mounted in the cuffs improve the transparency of ARMin IV by decreasing the interaction torques and forces. This is exemplarily shown for the elbow joint and the shoulder internal/external rotation. The P-controller and the PI-controller show distinct decrease of interaction torques. The PI-controller's performance is slightly worse than the one of the P-controller. This may be due to smaller P-gains in the PI-controller compared to the P-controller. Nevertheless, it is assumed that the I-part of the controller could be beneficial for very slow movements. This will have to be tested in future.

#### **Conclusion**

The new force controller detects very small interaction forces/torques between the patient and the robot. The first version of the force controller will be integrated into the current ARMin IV software and the newly developed assessments and allows to include weak patients in the ARMin IV therapy. Furthermore, this improved transparency could be beneficial for impaired children with even smaller and weaker arms and, therefore, the application of the sensors in a planned pediatric ARMin is currently being investigated.

## A.4 Appendix of ChARMin Assessments

### A.4.1 Isometric Torque Validation

A large hysteresis was observed when recording the motor torques which were needed to counteract an externally applied torque by the Mecmesin AFG sensor (Fig. A.15).

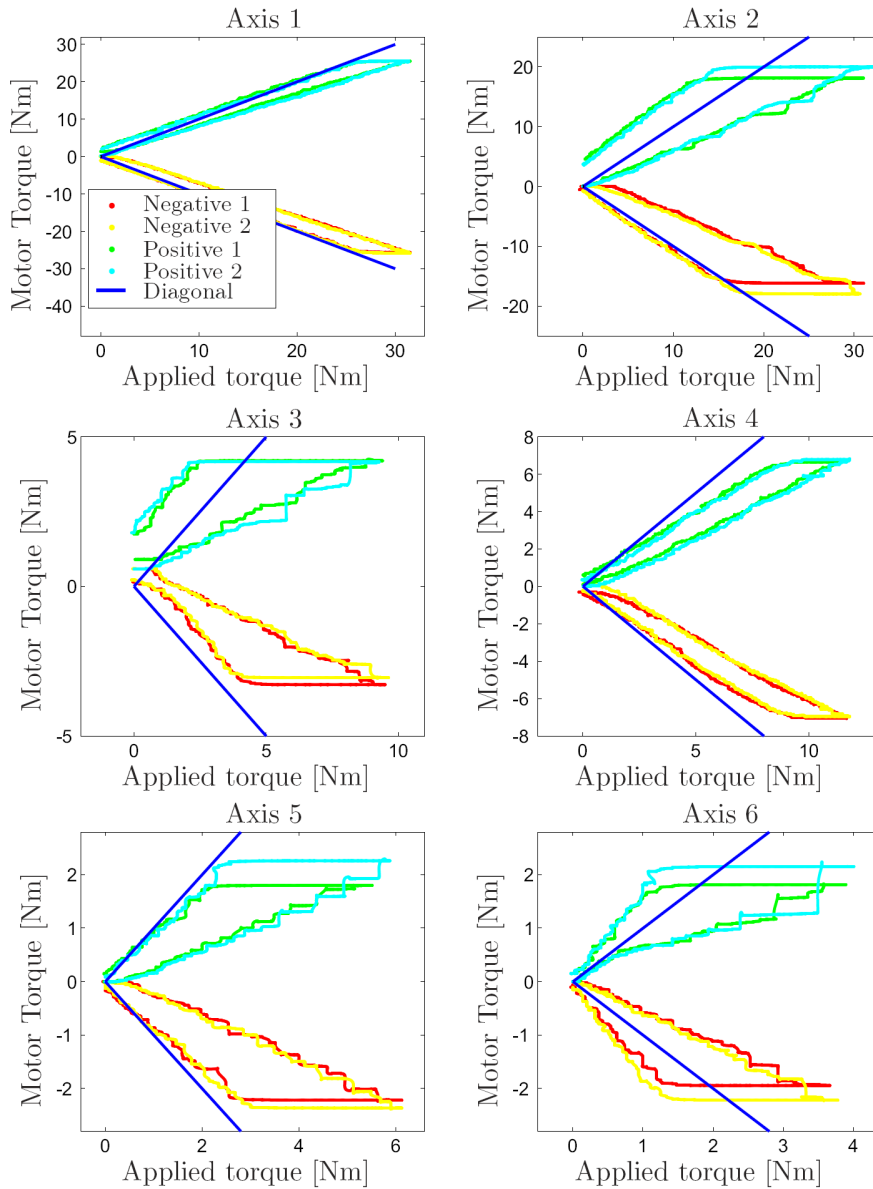


Figure A.15: Isometric torque validation for the six axes of ChARMin equipped with the large distal module (e.g., for isometric torque assessment). On the x-axes are the torques applied by the Mecmesin AFG sensor and on the y-axes are the motor torques applied to the robot joint by the motors to counteract the external forces. The blue line is the diagonal which can be seen as the perfect mapping if the joint was frictionless. The torques were applied twice in both joint directions.

The results of the torque validation for the small distal module were similar to the large distal module. Analogous to the large distal module the joint torque estimation excludes the unloading phase and, therefore, the large hysteresis in the measurement (Fig. A.16).

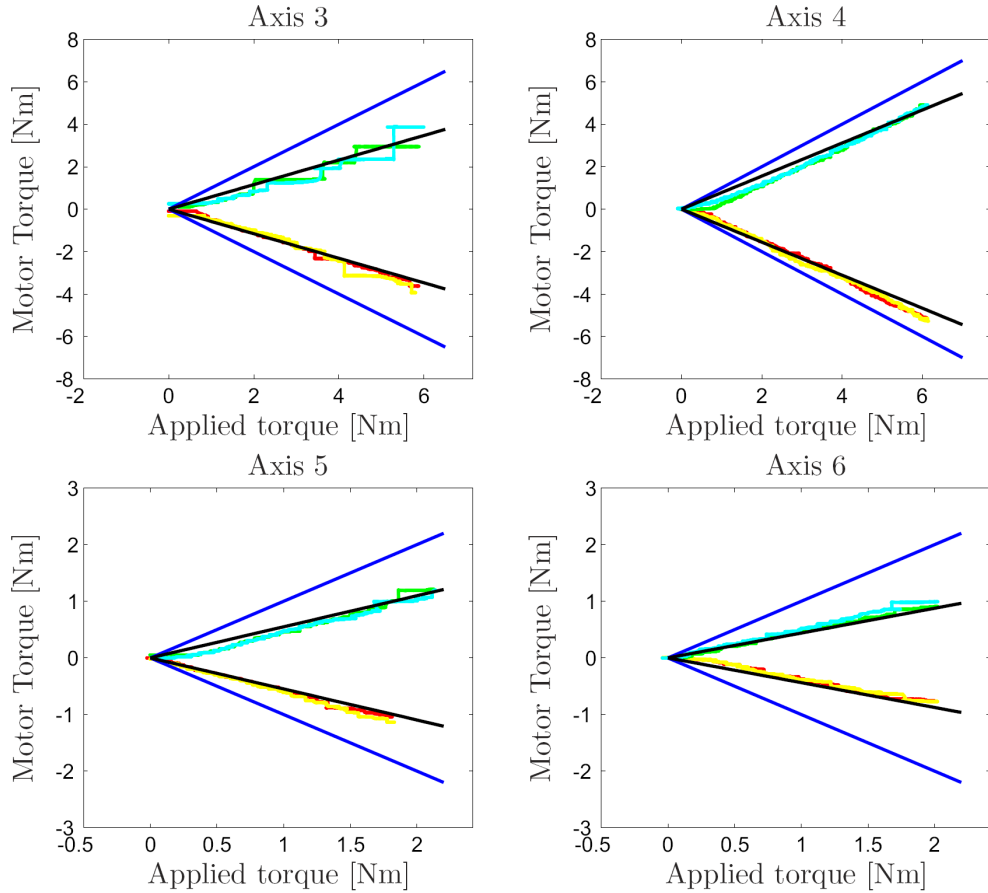


Figure A.16: Isometric torque validation for the four axes of the small distal module. Only the loading of the robot is shown, i.e., without hysteresis. On the y-axes are the motor torques applied to the robot joint by the motors and on the x-axes are the torques applied by the Mecmesin AFG sensor. The blue line is the diagonal which can be seen as the perfect mapping if the joint was frictionless. The torques were applied twice in both joint directions. The black line is the linear fit of the cut data.

### A.4.2 Robot-Assisted Assessments Supplementary Material

	ROM joint measured						
	Lateral shoulder ad-/abduction	Shoulder flexion/extension	Horizontal shoulder ad-/abduction	Shoulder internal-/external rotation	Elbow flexion/extension	Forearm pronation/supination	Wrist flexion/extension
Axis 1: Lateral shoulder ad-/abduction	67 ABD	80 ABD	90 FLEX	90 FLEX	90 FLEX	50 FLEX	50 FLEX
Axis 2: Horizontal shoulder ad-/abduction	90 ABD	20 ABD	90 ABD	20 ABD	20 ABD	90 ABD	90 ABD
Axis 3: Shoulder internal-/external rotation	85 EXR	85 EXR	85 EXR	85 EXR	0	0	0
Axis 4: Elbow flexion/extension	0	0	0	90 FLEX	0	90 FLEX	90 FLEX
Axis 5: Forearm pronation/supination	0	0	0	0	85 SUP	50 SUP	50 SUP
Axis 6: Wrist flexion/extension	0	0	0	0	0	0	0

ABD=Abduction, EXR=External rotation, FLEX=Flexion, SUP=Supination.

Figure A.17: Table S1 - ARMin postures for the different joints measured during the ROM assessment.

	STRENGTH joint measured						
	Lateral Shoulder ad-/abduction	Shoulder flexion/extension	Horizontal shoulder ad-/abduction	Shoulder internal-/external rotation	Elbow flexion/extension	Forearm pronation/supination	Wrist flexion/extension
Axis 1: Lateral shoulder ad-/abduction	60 ABD	80 ABD	90 ABD	90 ABD	90 ABD	50 ABD	50 ABD
Axis 2: Horizontal shoulder ad-/abduction	90 ABD	20 ABD	45 ABD	20 ABD	20 ABD	90 ABD	90 ABD
Axis 3: Shoulder internal-/external rotation	85 EXR	85 EXR	85 EXR	45 EXR	0	0	0
Axis 4: Elbow flexion/extension	0	0	0	90 FLEX	90 FLEX	90 FLEX	90 FLEX
Axis 5: Forearm pronation/supination	0	0	0	0	85 SUP	50 SUP	50 SUP
Axis 6: Wrist flexion/extension	0	0	0	0	0	0	0

ABD=Abduction, EXR=External rotation, FLEX=Flexion, SUP=Supination.

Figure A.18: Table S2 - ARMin postures for the different joints measured during the STRENGTH assessment.



	Assessment parameter	Spearman's correlation coefficient	Bland-Altman t-test significance
WORKSPACE	Mean of cubic volume	0.77* (p=0.014)	0.025
	Workspace levels	0.75* to 1.0** (p<0.02 for all dir.)	p>0.035 (sign. for "down" dir.)
QOM	Mean D-P ratio to target	0.29 (p=0.535)	0.496
	Mean D-P ratio to start	0.48 (p=0.233)	0.298
	Mean Precision	0.68 (p=0.094)	0.112
	Mean Number of peaks to target	0.46 (p=0.294)	0.854
	Mean Number of peaks to start	0.71* (p=0.047)	0.923
	Mean Time to target	0.36 (p=0.432)	0.550
	Mean Time to start	0.21 (p=0.610)	0.069
	Mean Reaction time to target	0.10 (p=0.823)	0.887
	Mean Reaction time to start	0.29(p=0.493)	0.821

\*= p<0.05, \*\*= p<0.01.

Figure A.19: Table S3 - Summary of the inter-rater analysis of WORKSPACE and QOM.

	Mean(Range, i.e. difference between max and min value)								Mean(Standard deviation)	
	m1	m2	m3	m4	m5	m6	m7	m8		
aROM [°]	47.9(4.2) 130.8(1.1)	46.7(3.9) 130.7(1.3)	-34.9(6.3) 123.6(2.0)	-28.6(3.5) 87.9(2.3)	-0.5(0.7) 118.9(2.1)	-88.8(2.9) 44.6(18.3)	-34.1(4.2) 37.4(4.0)	-	QOM Time [ms]	1566(395)
pROM [°]	50.3(7.5) 130.2(0.9)	47.7(3.9) 130.6(0.7)	-29.1(12.1) 121.3(2.5)	-27.5(3.7) 89.7(1.3)	-0.6(0.4) 116.7(4.1)	-89.7(1.1) 85.5(6.9)	-33.8(3.9) 36.6(3.5)	-	QOM Peak [°]	18.6(9.4)
STRENGTH [Nm]	37.7(11.2) 30.6(12.2)	37.5(15.8) 45.5(15.4)	28.6(11.1) 32.5(8.0)	15.9(4.8) 14.8(3.9)	21.8(5.2) 24.3(7.3)	4.9(2.4) 3.1(1.7)	4.2(1.1) 4.6(2.1)	1.4(0.6) 1.5(0.6)	QOM D-P ratio [°]	1.19(0.18)
RPM 30°/s [Nm/rad]	-1.57(3.88) 0.51(5.46)	-	1.03(1.23) 0.58(1.02)	-1.05(0.94) -0.47(0.51)	0.61(0.64) 0.38(0.59)	0.00(0.26) 0.34(1.20)	0.4(0.21) 0.25(0.19)	1.89(1.57) 1.43(1.59)	QOM Reaction [ms]	877(226)
RPM 60°/s [Nm/rad]	-1.53(3.32) 0.73(4.15)	-	0.39(1.96) -0.16(1.90)	-1.42(1.10) -0.38(0.48)	0.64(0.51) 0.39(0.50)	0.09(0.24) 0.31(0.14)	0.47(0.26) 0.27(0.25)	1.67(1.38) 2.27(1.95)	QOM Precision [m]	0.036(0.01)
WORKSPACE [dm <sup>3</sup> ]	139.4(1.3)									

For aROM, pROM, WORKSPACE, STRENGTH and RPM the mean differences are shown between the maximum and minimum values measured during the four recordings of the intra-rater reliability. For the QOM assessment the standard deviation is used as an indicator for the variability of the recorded parameters. m1 = shoulder add-/abduction, m2 = shoulder extension/flexion, m3 = horizontal shoulder add-/abduction, m4 = shoulder internal/external rotation, m5 = elbow extension/flexion, m6 = elbow pro-/supination, m7 = wrist extension/flexion, m8 = hand closing/opening.

Figure A.20: Table S4 - Variability in the assessment parameters measured.

## A.5 Appendix of ChARMin Feasibility

### A.5.1 ChARMin Feasibility Study

The ChARMin feasibility study covers different subprojects which will be conducted over the next five years, involving (out of the ethical application):

1. Feasibility study investigating technical handling and patient comfort. The main objective is to investigate the usability and applicability of the ChARMin. Investigated are technical aspects, patient-related aspects, the different control modes of the device, safety and the software (interface, games, and assessments).
2. Randomized semi-experimental open labeled study investigating the differences between the three control modes of the device. The main objective is to determine whether differences between game scores, kinematic and kinetic metrics provided by ChARMin, additionally applied physiological measures and adverse events differ when participants train with the free non-supported modus, the assist-as-needed modus, and the fully supported modus. In addition, we will investigate what the patient requirements are to train with each modus.
3. The ChARMin has several assessments included, such as Workspace, Quality of Movement, Range of Motion, Strength and Resistance. The main objective is to determine the psychometric properties (validity, reliability and responsiveness) of these assessments.
4. Case series will be performed with the main objective to describe the application of the system and changes in upper extremity motor function that these participants undergo.
5. We plan motor learning experiments to investigate whether children with neurological diagnoses can learn to improve arm and hand task performance during repetitive training with the ChARMin, are able to retain an improved level of task performance and are able to transfer improved task performance to a slightly different task or setting (generalizability).
6. In an observational clinical study, we would like to assess 80-120 children and adolescents who are being referred from our rehabilitation physicians to improve upper extremity function. The idea is that at a certain time point, the ChARMin becomes integrated into our program of technologies that complement conventional occupational therapy. However, as the ChARMin will still not have received a CE certification, we would like to prospectively assess clinical and ChARMin data of each participant that is referred for training in the ChARMin. The main objective is to determine whether at a later stage patient criteria might change (i.e., is a specific patient group being referred for training with the ChARMin), does the number of adverse events change, do changes in upper extremity outcomes are still comparable to those observed in the first series of case studies?

## A.5.2 Feasibility Results - Games

## End-Effector Plots for the Airplane Game

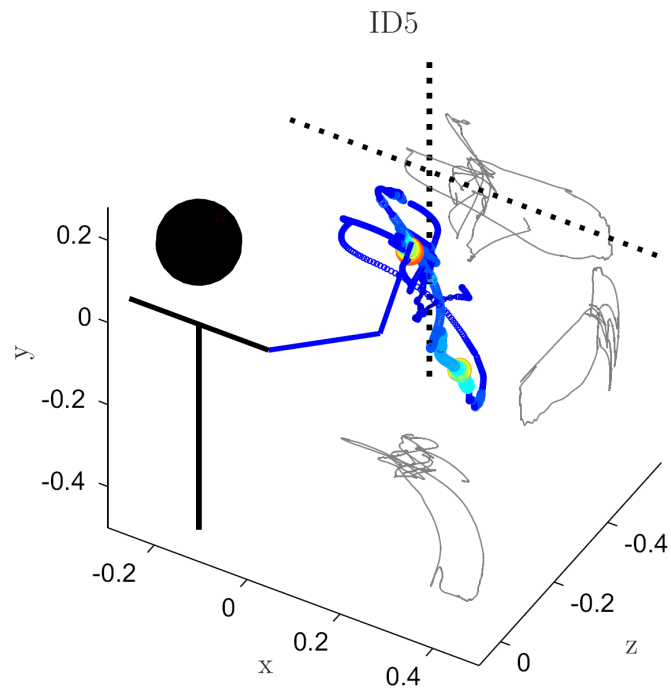


Figure A.21: Example of the end-effector path of patient ID5 during the airplane game. No pressure needs to be applied to play the game, therefore, not a lot of pressure changes are observable.

## End-Effector Plots for the Spaceship Game

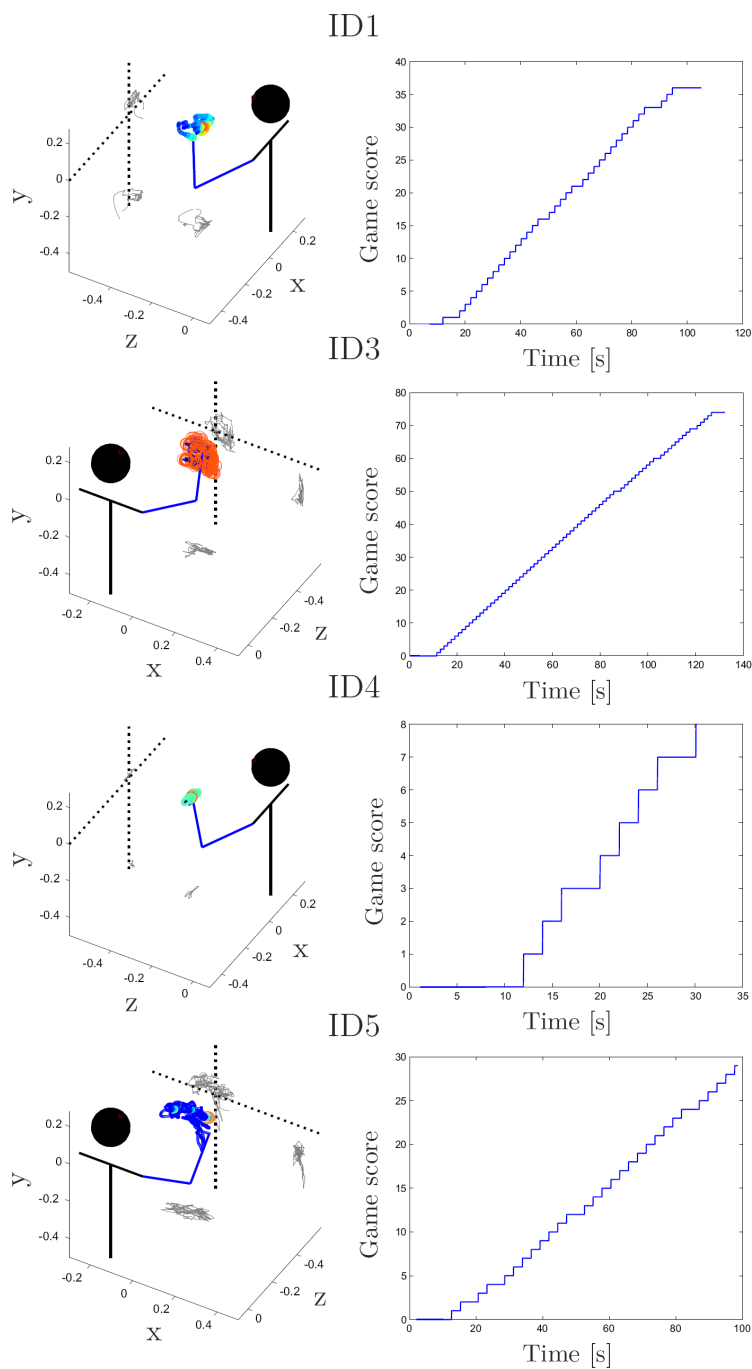


Figure A.22: The spaceship game played by patient ID1, ID3, ID4, and ID5. The first plots show the end-effector path of (a) patient ID1 with 70% support and (b) patient ID3 with 25% support (there was almost no pressure applied to the bulb and, therefore, only very small changes in pressure leading to the discretization in the colored end-effector circles). (c) Patient ID4 played with 60% support for a rather short time and in a small workspace and (d) patient ID5 had 0% support.

### A.5.3 Feasibility Results - Assessments

#### CIRCLE Plots for Patient ID1 (Test 1)

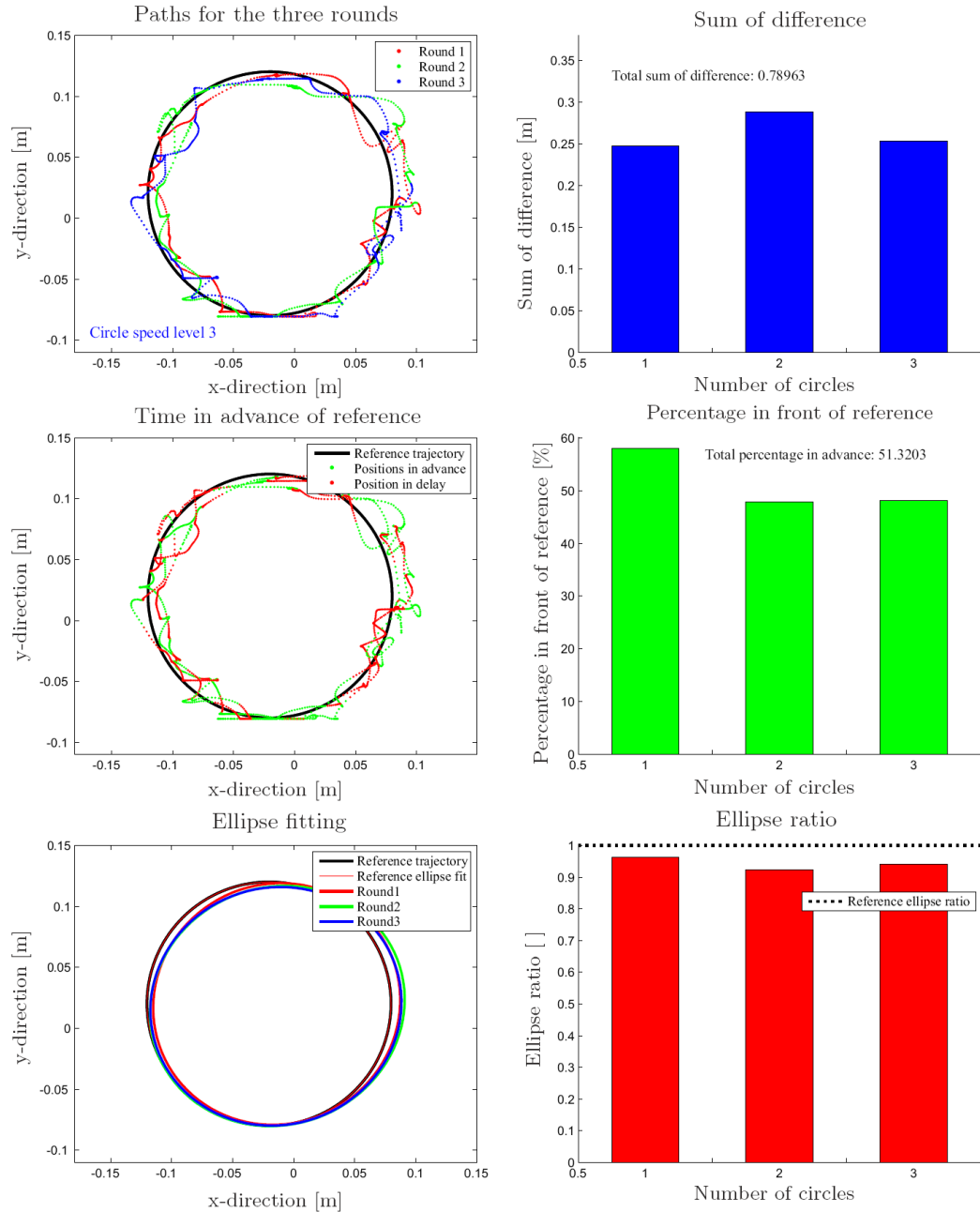


Figure A.23: CIRCLE Assessment results for patient ID1, test1. The first row shows the end-effector paths for the three trials together with the sum of differences between the end-effector position and the reference position. The second row shows the end-effector paths colored in green when the hand is in front of the target and in red, when the hand is delayed. Additionally, the percentage was calculated that the hand was in front of the reference position. The third row shows the ellipses fitted to the end-effector data and the corresponding ellipse ratios.

QOM Plots for Patient ID3 (Test 1)

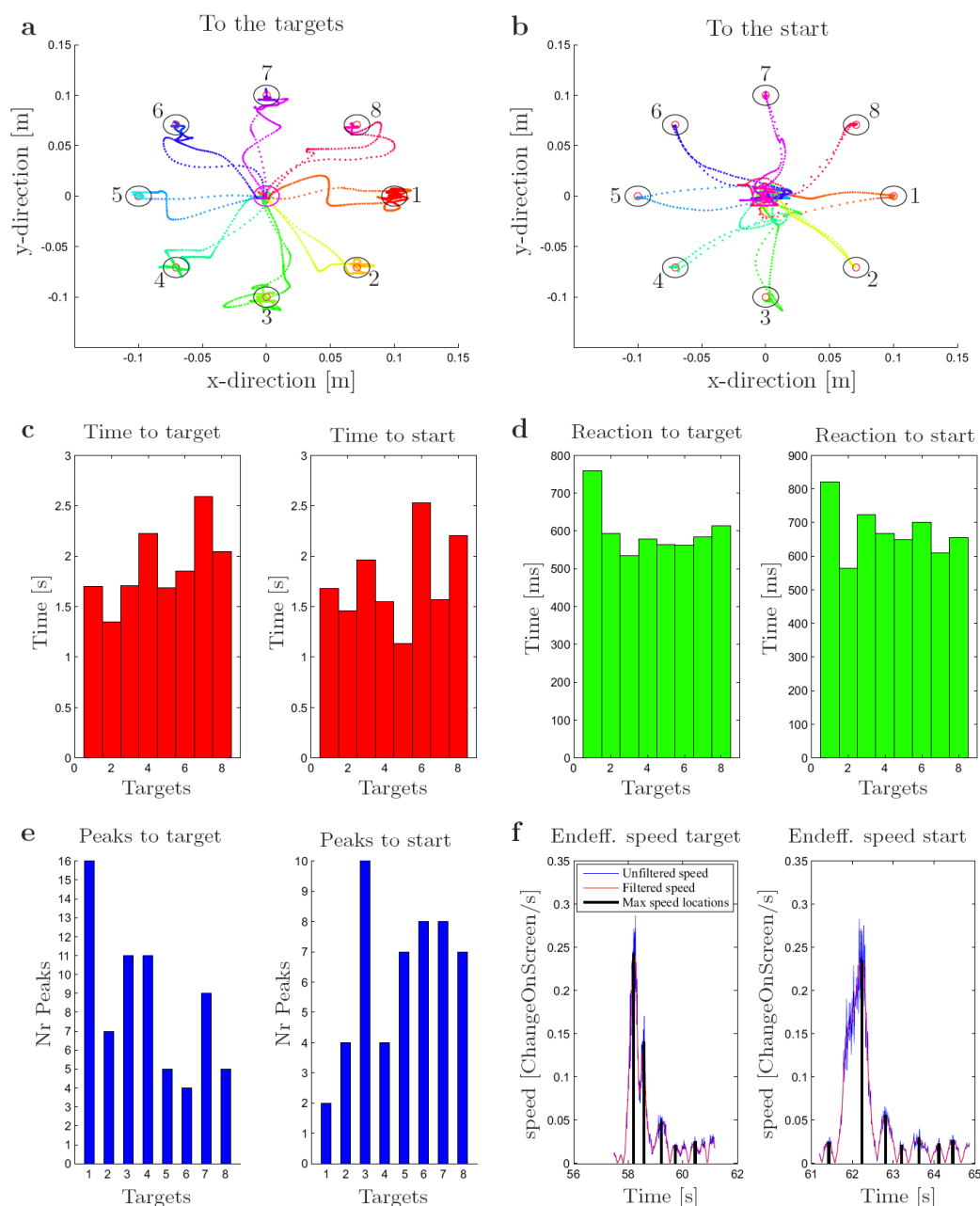




Figure A.24: QOM assessment results for patient ID3. The plots (a) and (b) show the end-effector paths to the eight different targets. (c) The time to target is the time needed to move from the start to the target position. In plot (d) the reaction time is shown which is the time to leave the start position, after the target is displayed. (e) The number of speed peaks were calculated for the eight different targets. Plot (f) shows a detailed view of the end-effector speed to the target number 5 and back to the start. The black lines indicate the peaks detected. The number of peak locations corresponds to the number plotted in (e) for target 5.

## A.5.4 Ethic Approval

	<p>Kanton Zürich <b>Kantonale Ethikkommission</b></p> <p> <b>Prof. Dr. med. Edith R. Schmid</b> Präsidentin Abteilung C</p> <p><b>Niklaus Herzog, lic. iur. et theol.</b> Juristischer Sekretär Stampfenbachstrasse 121 Postfach 8090 Zürich Telefon +41 43 259 79 70 Fax +41 43 259 79 72 gabriela.schlittler@kaz.zh.ch www.kek.zh.ch</p>
<p>Einschreiben Kinderspital Zürich Herr PD Dr. Hubertus van Hedel Mühlebergstrasse 104 8910 Affoltern am Albis</p>	
<p>12. Juni 2015 <b>Beschlussmitteilung der Kantonalen Ethikkommission Zürich</b></p>	
<p><b>Gesuch KEK-ZH-Nr. 2015-0239</b> <b>Feasibility of a new pediatric arm rehabilitation robot ChARMin: A mono-centric interventional study</b></p>	
<b>Gesuchsteller</b>	PD Dr. Hubertus van Hedel, Kinderspital Zürich
<b>Zentren</b>	PD Dr. Hubertus van Hedel, Kinderspital Zürich
<p><b>I. Verfahren</b></p> <p><input type="checkbox"/> ordentliches Verfahren    <input type="checkbox"/> vereinfachtes Verfahren    <input checked="" type="checkbox"/> präsidiales Verfahren</p>	
<p><b>II. Entscheid</b></p> <p><input checked="" type="checkbox"/> <b>Die Bewilligung wird erteilt</b> Bedeutet: Das Vorhaben gemäss bewilligtem Forschungsplan kann gestartet und im Rahmen der anwendbaren rechtlichen Bestimmungen durchgeführt werden.</p>	
<p>Bewilligungen für <b>klinische Versuche der Kategorie B und C</b> stehen unter dem <b>Vorbehalt</b>, dass</p> <ol style="list-style-type: none"><li>1. allfällig durch die zuständige eidgenössische Zulassungsbehörde (Swissmedic/BAG) festgestellte Mängel keine Änderungen der von der Ethikkommission evaluierten Unterlagen erfordern, und dass</li><li>2. die Bewilligung der eidgenössischen Zulassungsbehörde (Swissmedic/BAG) vorliegt.</li></ol>	
<p><small>Beschluss_Abt. C_Version_23.03.2015</small></p>	

## A.5.5 Swissmedic Approval



oem, clinicaltrials.devices@swissmedic.ch  
Kontakt: +41 58 463 22 51  
Seite 1/4

### EINSCHREIBEN

Rehabilitationszentrum für Kinder und Jugendliche  
Herr PD Dr. Huub van Hedel  
Mühlebergstrasse 104  
8910 Affoltern am Albis

Bern, 25. Juni 2015

### Verfügung

#### Bewilligung eines klinischen Versuchs mit Medizinprodukten

- Titel: Feasibility of a new pediatric arm rehabilitation robot ChARMin: A monocentric interventional study
- Sponsor: Rehabilitationszentrum für Kinder und Jugendliche
- Referenznummer Ethikkommission:
- Referenznummer Swissmedic: 2015-MD-0009
- Referenznummer EUDAMED: CIV-15-04-013484

Sehr geehrter Herr Dr. van Hedel

### 1. Erwägungen

Swissmedic trifft den Entscheid zur Bewilligung des Versuchs gemäss Artikel 54 vom Bundesgesetz über Arzneimittel und Medizinprodukte (HMG; SR 812.21) und die bis und mit am 10. Juni 2015 bei Swissmedic eingegangenen Unterlagen und Informationen, insbesondere

- Prüfplan (CIP) Version 31.03.2015
- Datenerhebungsbogen (CRF) Version 31.03.2015
- Prüferinformation (Investigator's Brochure) Version 1.1 vom 3.6.2015
- Aufklärungsbogen (Patient information) Version 31.03.2015
- Bericht zur IEC 62304 vom 3.6.2015

Schweizerisches Heilmittelinstitut  
Institut suisse des produits thérapeutiques  
Istituto svizzero per gli agenti terapeutici  
Swiss Agency for Therapeutic Products

Bewilligung\_an\_Sponsor\_(autom\_d)\_2014-03-31.dotm

Swissmedic | Hallerstrasse 7 | Postfach | CH-3000 Bern 9 | www.swissmedic.ch | Tel. +41 58 462 02 11 | Fax +41 58 462 02 12



## A.5.6 Wheelchair Placement

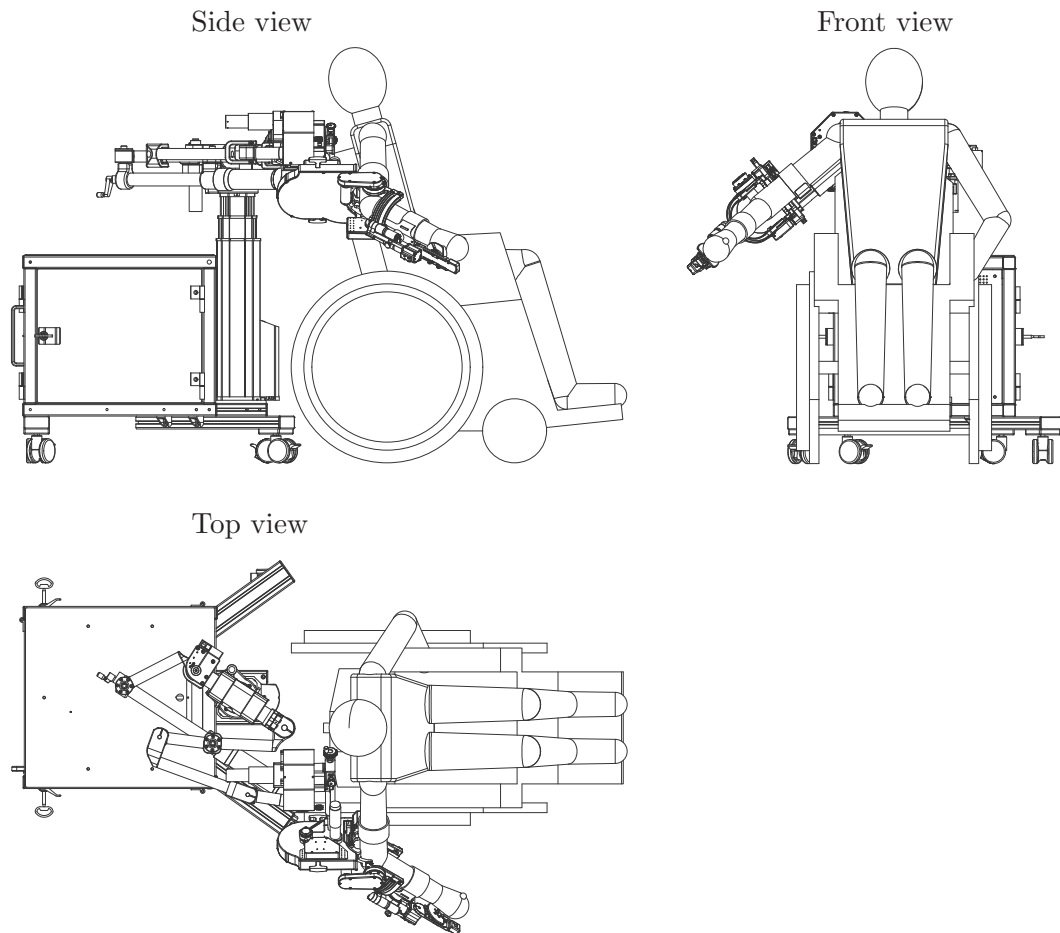


Figure A.25: This figure illustrates how a wheelchair is placed in the ChARMin setup. The different views show that the robot can collide with the backrest or armrest of the wheelchair. Furthermore, handles in the back of the wheelchair can prevent that the wheelchair can be moved enough backwards and, therefore, a proper positioning of the shoulder is not possible. The avatar is a simplified model of an 18-year-old subject. For younger patients with smaller wheelchairs, collisions are even more likely to occur.



# Bibliography

- [1] U. Keller, V. Klamroth, H. J. A. van Hedel, and R. Riener, “ChARMin: A robot for pediatric arm rehabilitation,” in *Robotics and Automation (ICRA), 2013 IEEE International Conference on*. IEEE, 2013, pp. 3908–3913.
- [2] U. Keller and R. Riener, “Design of the Pediatric Arm Rehabilitation Robot ChARMin,” in *Biomedical Robotics and Biomechanics (BioRob), 2014 IEEE International Conference on*. IEEE, 2014, pp. 530–535.
- [3] U. Keller, H. J. A. van Hedel, V. Klamroth-Marganska, and R. Riener, “ChARMin: The first actuated exoskeleton robot for pediatric arm rehabilitation,” *IEEE/ASME Transactions on Mechatronics (TMECH)*, 2016, *in press*.
- [4] U. Keller, G. Rauter, and R. Riener, “Assist-as-needed path control for the PASCAL rehabilitation robot,” in *Rehabilitation Robotics (ICORR), 2013 IEEE International Conference on*. IEEE, 2013, pp. 1–7.
- [5] U. Keller, S. Schölch, U. Albisser, C. Rudhe, A. Curt, R. Riener, and V. Klamroth-Marganska, “Robot-assisted arm assessments in spinal cord injured patients: A consideration of concept study,” *PloS one*, vol. 10, no. 5, 2015.
- [6] U. Keller, M. Guidali, L. Conditt, and R. Riener, “Novel recording and control strategies for robotic therapy,” in *Automed Conference*, vol. 286, 2012, pp. 55–56.
- [7] H.-M. Schmidt and U. Lanz, *Surgical anatomy of the hand*. Thieme, 2011.
- [8] F. E. Cleland and D. L. Gallahue, “Young children’s divergent movement ability,” *Perceptual and Motor skills*, vol. 77, no. 2, pp. 535–544, 1993.
- [9] A. Diamond, “Close interrelation of motor development and cognitive development and of the cerebellum and prefrontal cortex,” *Child development*, vol. 71, no. 1, pp. 44–56, 2000.
- [10] J. G. Bremner, “Motor abilities as causal agents in infant cognitive development,” *Advances in psychology*, vol. 97, pp. 47–77, 1993.
- [11] E. Odding, M. Roebroek, H. Stam *et al.*, “The epidemiology of cerebral palsy: incidence, impairments and risk factors.” *Disability and rehabilitation*, vol. 28, no. 4, p. 183, 2006.
- [12] M. Oskoui, F. Coutinho, J. Dykeman, N. Jetté, and T. Pringsheim, “An update on the prevalence of cerebral palsy: a systematic review and meta-analysis,” *Developmental Medicine & Child Neurology*, vol. 55, no. 6, pp. 509–519, 2013.
- [13] P. Rosenbaum, N. Paneth, A. Leviton, M. Goldstein, M. Bax, D. Damiano, B. Dan, B. Jacobsson *et al.*, “A report: the definition and classification of cerebral palsy april 2006,” *Dev Med Child Neurol Suppl*, vol. 109, no. suppl 109, pp. 8–14, 2007.
- [14] K. Shikako-Thomas, A. Majnemer, M. Law, and L. Lach, “Determinants of participation in leisure activities in children and youth with cerebral palsy: systematic review,” *Physical & occupational therapy in pediatrics*, vol. 28, no. 2, pp. 155–169, 2008.
- [15] H. J. van Hedel and T. Aurich-Schuler, “Clinical application of rehabilitation technologies in children undergoing neurorehabilitation,” *Neurorehabilitation Technology*, 2015, 2nd Edition, chap. 14, *in press*.

- [16] M. Holmefur, L. KRUMLINDE-SUNDHOLM, J. Bergström, and A.-C. ELIASSON, "Longitudinal development of hand function in children with unilateral cerebral palsy," *Developmental medicine & child neurology*, vol. 52, no. 4, pp. 352–357, 2010.
- [17] S. E. Hanna, M. C. Law, P. L. Rosenbaum, G. A. King, S. D. Walter, N. Pollock, and D. J. Russell, "Development of hand function among children with cerebral palsy: growth curve analysis for ages 16 to 70 months," *Developmental Medicine & Child Neurology*, vol. 45, no. 07, pp. 448–455, 2003.
- [18] S. E. Hanna, P. L. Rosenbaum, D. J. Bartlett, R. J. Palisano, S. D. Walter, L. Avery, and D. J. Russell, "Stability and decline in gross motor function among children and youth with cerebral palsy aged 2 to 21 years," *Developmental Medicine & Child Neurology*, vol. 51, no. 4, pp. 295–302, 2009.
- [19] M. K. Gunel, A. Mutlu, T. Tarsuslu, and A. Livanelioglu, "Relationship among the Manual Ability Classification System (MACS), the Gross Motor Function Classification System (GMFCS), and the functional status (WeeFIM) in children with spastic cerebral palsy," *European journal of pediatrics*, vol. 168, no. 4, pp. 477–485, 2009.
- [20] H. Duffau, "Brain plasticity: from pathophysiological mechanisms to therapeutic applications," *Journal of Clinical Neuroscience*, vol. 13, no. 9, pp. 885–897, 2006.
- [21] S. M. Onifer, G. M. Smith, and K. Fouad, "Plasticity after spinal cord injury: relevance to recovery and approaches to facilitate it," *Neurotherapeutics*, vol. 8, no. 2, pp. 283–293, 2011.
- [22] H. Chen, J. Epstein, and E. Stern, "Neural plasticity after acquired brain injury: evidence from functional neuroimaging," *PM&R*, vol. 2, no. 12, pp. S306–S312, 2010.
- [23] J. Liepert, H. Bauder, W. H. Miltner, E. Taub, and C. Weiller, "Treatment-induced cortical reorganization after stroke in humans," *Stroke*, vol. 31, no. 6, pp. 1210–1216, 2000.
- [24] J. Liepert, M. Tegenthoff, and J.-P. Malin, "Changes of cortical motor area size during immobilization," *Electroencephalography and clinical neurophysiology/electromyography and motor control*, vol. 97, no. 6, pp. 382–386, 1995.
- [25] M. Johnston, "Plasticity in the developing brain: implications for rehabilitation," *Developmental disabilities research reviews*, vol. 15, no. 2, pp. 94–101, 2009.
- [26] N. Kuhnke, H. Juenger, M. Walther, S. Berweck, V. Mall, and M. Staudt, "Do patients with congenital hemiparesis and ipsilateral corticospinal projections respond differently to constraint-induced movement therapy?" *Developmental Medicine & Child Neurology*, vol. 50, no. 12, pp. 898–903, 2008.
- [27] M. L. Aisen, D. Kerkovich, J. Mast, S. Mulroy, T. A. Wren, R. M. Kay, and S. A. Rethlefsen, "Cerebral palsy: clinical care and neurological rehabilitation," *The Lancet Neurology*, vol. 10, no. 9, pp. 844–852, 2011.
- [28] W. Kułak, W. Sobaniec, J.-Ś. Kuzia, and L. Boćkowski, "Neurophysiologic and neuroimaging studies of brain plasticity in children with spastic cerebral palsy," *Experimental neurology*, vol. 198, no. 1, pp. 4–11, 2006.
- [29] A. M. Gordon, J. Charles, and S. L. Wolf, "Efficacy of constraint-induced movement therapy on involved upper-extremity use in children with hemiplegic cerebral palsy is not age-dependent," *Pediatrics*, vol. 117, no. 3, pp. e363–e373, 2006.
- [30] J. W. Krakauer, "Motor learning: its relevance to stroke recovery and neurorehabilitation," *Current opinion in neurology*, vol. 19, no. 1, pp. 84–90, 2006.
- [31] R. Boyd, M. Morris, and H. Graham, "Management of upper limb dysfunction in children with cerebral palsy: a systematic review," *European Journal of Neurology*, vol. 8, pp. 150–166, 2001.

- [32] L. Sakzewski, J. Ziviani, and R. N. Boyd, "Efficacy of upper limb therapies for unilateral cerebral palsy: A meta-analysis," *Pediatrics*, vol. 133, no. 1, pp. e175–e204, 2014.
- [33] Y.-p. Chen, S. Pope, D. Tyler, and G. L. Warren, "Effectiveness of constraint-induced movement therapy on upper-extremity function in children with cerebral palsy: a systematic review and meta-analysis of randomized controlled trials," *Clinical rehabilitation*, p. 0269215514544982, 2014.
- [34] Y.-C. Hung and A. M. Gordon, "Motor learning of a bimanual task in children with unilateral cerebral palsy," *Research in developmental disabilities*, vol. 34, no. 6, pp. 1891–1896, 2013.
- [35] G. Kwakkel, R. van Peppen, R. C. Wagenaar, S. W. Dauphinee, C. Richards, A. Ashburn, K. Miller, N. Lincoln, C. Partridge, I. Wellwood *et al.*, "Effects of augmented exercise therapy time after stroke a meta-analysis," *Stroke*, vol. 35, no. 11, pp. 2529–2539, 2004.
- [36] R. P. Van Peppen, G. Kwakkel, S. Wood-Dauphinee, H. J. Hendriks, P. J. Van der Wees, and J. Dekker, "The impact of physical therapy on functional outcomes after stroke: what's the evidence?" *Clinical rehabilitation*, vol. 18, no. 8, pp. 833–862, 2004.
- [37] T. Kitago and J. W. Krakauer, "Motor learning principles for neurorehabilitation," *Handb Clin Neurol*, vol. 110, pp. 93–103, 2013.
- [38] H. Krebs, S. Fasoli, L. Dipietro, M. Fragala-Pinkham, R. Hughes, J. Stein, and N. Hogan, "Motor learning characterizes habilitation of children with hemiplegic cerebral palsy," *Neurorehabilitation and Neural Repair*, 2012.
- [39] N. A. Bernstein, "The co-ordination and regulation of movements," 1967.
- [40] K. Löwing, A. Bexelius, and E. Brogren Carlberg, "Activity focused and goal directed therapy for children with cerebral palsy-do goals make a difference?" *Disability & Rehabilitation*, vol. 31, no. 22, pp. 1808–1816, 2009.
- [41] D. L. Damiano, "Rehabilitative therapies in cerebral palsy: the good, the not as good, and the possible," *Journal of child neurology*, vol. 24, no. 9, pp. 1200–1204, 2009.
- [42] D. Damiano, "Activity, activity, activity: rethinking our physical therapy approach to cerebral palsy," *Physical therapy*, vol. 86, no. 11, pp. 1534–1540, 2006.
- [43] M. Lotze, C. Braun, N. Birbaumer, S. Anders, and L. G. Cohen, "Motor learning elicited by voluntary drive," *Brain*, vol. 126, no. 4, pp. 866–872, 2003.
- [44] N. Hogan, H. Krebs, B. Rohrer, J. Palazzolo, L. Dipietro, S. Fasoli, J. Stein, R. Hughes, W. Frontera, D. Lynch *et al.*, "Motions or muscles? some behavioral factors underlying robotic assistance of motor recovery," *Journal of rehabilitation research and development*, vol. 43, no. 5, p. 605, 2006.
- [45] A. W. Dromerick, P. S. Lum, and J. Hidler, "Activity-based therapies," *NeuroRx*, vol. 3, no. 4, pp. 428–438, 2006.
- [46] R. Teasell, N. Bayona, K. Salter, C. Hellings, and J. Bitensky, "Progress in clinical neurosciences: stroke recovery and rehabilitation," *The Canadian Journal of Neurological Sciences*, vol. 33, no. 4, pp. 357–364, 2006.
- [47] Y. Salem and E. Godwin, "Effects of task-oriented training on mobility function in children with cerebral palsy," *NeuroRehabilitation*, vol. 24, no. 4, pp. 307–313, 2008.
- [48] B. Bobath, "The very early treatment of cerebral palsy," *Developmental Medicine & Child Neurology*, vol. 9, no. 4, pp. 373–390, 1967.
- [49] M. Law, D. Russell, N. Pollock, P. Rosenbaum, S. Walter, and G. King, "A comparison of intensive neurodevelopmental therapy plus casting and a regular occupational therapy program for children with cerebral palsy," *Developmental Medicine & Child Neurology*, vol. 39, no. 10, pp. 664–670, 1997.

- [50] A.-C. Eliasson and M. Holmefur, "The influence of early modified constraint-induced movement therapy training on the longitudinal development of hand function in children with unilateral cerebral palsy," *Developmental Medicine & Child Neurology*, vol. 57, no. 1, pp. 89–94, 2015.
- [51] K. J. Dodd, N. F. Taylor, and D. L. Damiano, "A systematic review of the effectiveness of strength-training programs for people with cerebral palsy," *Archives of physical medicine and rehabilitation*, vol. 83, no. 8, pp. 1157–1164, 2002.
- [52] W. H. Organization, *International Classification of Functioning, Disability, and Health: Children & Youth Version: ICF-CY*. World Health Organization, 2007.
- [53] L. Miller, J. Ziviani, and R. N. Boyd, "A systematic review of clinimetric properties of measurements of motivation for children aged 5-16 years with a physical disability or motor delay," *Physical & occupational therapy in pediatrics*, vol. 34, no. 1, pp. 90–111, 2014.
- [54] A. Majnemer, M. Shevell, M. Law, R. Birnbaum, G. Chilingaryan, P. Rosenbaum, and C. Poulin, "Participation and enjoyment of leisure activities in school-aged children with cerebral palsy," *Developmental Medicine & Child Neurology*, vol. 50, no. 10, pp. 751–758, 2008.
- [55] A. Majnemer, M. Shevell, M. Law, C. Poulin, and P. Rosenbaum, "Level of motivation in mastering challenging tasks in children with cerebral palsy," *Developmental Medicine & Child Neurology*, vol. 52, no. 12, pp. 1120–1126, 2010.
- [56] A.-L. Brunner, E. Rutz, S. Juenemann, and R. Brunner, "Continuous vs. blocks of physiotherapy for motor development in children with cerebral palsy and similar syndromes: A prospective randomized study," *Developmental neurorehabilitation*, vol. 17, no. 6, pp. 426–432, 2014.
- [57] M.-H. Milot, S. J. Spencer, V. Chan, J. P. Allington, J. Klein, C. Chou, J. E. Bobrow, S. C. Cramer, and D. J. Reinkensmeyer, "A crossover pilot study evaluating the functional outcomes of two different types of robotic movement training in chronic stroke survivors using the arm exoskeleton bones," *Journal of neuroengineering and rehabilitation*, vol. 10, no. 1, p. 112, 2013.
- [58] J. Klein, S. J. Spencer, and D. J. Reinkensmeyer, "Breaking it down is better: Haptic decomposition of complex movements aids in robot-assisted motor learning," *Neural Systems and Rehabilitation Engineering, IEEE Transactions on*, vol. 20, no. 3, pp. 268–275, 2012.
- [59] G. Prange, M. Jannink, A. Stienen, H. Van der Kooij, M. Ijzerman, and H. Hermens, "Influence of gravity compensation on muscle activation patterns during different temporal phases of arm movements of stroke patients," *Neurorehabilitation and neural repair*, 2009.
- [60] T. Rahman, W. Sample, S. Jayakumar, M. M. King, J. Y. Wee, R. Seliktar, M. Alexander, M. Scavina, and A. Clark, "Passive exoskeletons for assisting limb movement," *Journal of rehabilitation research and development*, vol. 43, no. 5, p. 583, 2006.
- [61] C. N. Gerber, R. Labruyère, and H. J. van Hedel, "Reliability and responsiveness of upper limb motor assessments for children with central neuromotor disorders a systematic review," *Neurorehabilitation and neural repair*, 2015.
- [62] G. Kwakkel, B. J. Kollen, J. van der Grond, and A. J. Prevo, "Probability of regaining dexterity in the flaccid upper limb impact of severity of paresis and time since onset in acute stroke," *Stroke*, vol. 34, no. 9, pp. 2181–2186, 2003.
- [63] N. Bayona, J. Bitensky, K. Salter, and R. Teasell, "The role of task-specific training in rehabilitation therapies," *Topics in Stroke Rehabilitation*, vol. 12, no. 3, p. 58, 2005.

- [64] M. Guidali, A. Duschau-Wicke, S. Broggi, V. Klamroth-Marganska, T. Nef, and R. Riener, "A robotic system to train activities of daily living in a virtual environment," *Medical and Biological Engineering and Computing*, pp. 1–11, 2011.
- [65] K. Brütsch, A. Koenig, L. Zimmerli, S. Merillat-Koeneke, R. Riener, L. Jäncke, H. van Hedel, and A. Meyer-Heim, "Virtual reality for enhancement of robot-assisted gait training in children with neurological gait disorders," *Journal of Rehabilitation Medicine*, vol. 43, no. 6, pp. 493–499, 2011.
- [66] G. Prange, M. Jannink, C. Groothuis-Oudshoorn, H. Hermens, M. IJzerman *et al.*, "Systematic review of the effect of robot-aided therapy on recovery of the hemiparetic arm after stroke," *Journal of rehabilitation research and development*, vol. 43, no. 2, p. 171, 2006.
- [67] J. Mehrholz, T. Platz, J. Kugler, and M. Pohl, "Electromechanical-assisted training for improving upper limb function and disability after stroke," *The Cochrane Library*, 2008.
- [68] A. Lo, P. Guarino, L. Richards, J. Haselkorn, G. Wittenberg, D. Federman, R. Ringer, T. Wagner, H. Krebs, B. Volpe *et al.*, "Robot-assisted therapy for long-term upper-limb impairment after stroke," *New England Journal of Medicine*, vol. 362, no. 19, pp. 1772–1783, 2010.
- [69] V. Klamroth-Marganska, J. Blanco, K. Campen, A. Curt, V. Dietz, T. Ettl, M. Felder, B. Fellinghauer, M. Guidali, A. Kollmar *et al.*, "Three-dimensional, task-specific robot therapy of the arm after stroke: a multicentre, parallel-group randomised trial," *The Lancet Neurology*, vol. 13, no. 2, pp. 159–166, 2014.
- [70] J. Zariffa, N. Kapadia, J. Kramer, P. Taylor, M. Alizadeh-Meghbrazi, V. Zivanovic, R. Willms, A. Townson, A. Curt, M. Popovic *et al.*, "Feasibility and efficacy of upper limb robotic rehabilitation in a subacute cervical spinal cord injury population," *Spinal cord*, vol. 50, no. 3, pp. 220–226, 2011.
- [71] T. H. Wagner, A. C. Lo, P. Peduzzi, D. M. Bravata, G. D. Huang, H. I. Krebs, R. J. Ringer, D. G. Federman, L. G. Richards, J. K. Haselkorn *et al.*, "An economic analysis of robot-assisted therapy for long-term upper-limb impairment after stroke," *Stroke*, vol. 42, no. 9, pp. 2630–2632, 2011.
- [72] M. Stefano, P. Patrizia, A. Mario, G. Ferlini, R. Rizzello, and G. Rosati, "Robotic upper limb rehabilitation after acute stroke by nerebot: Evaluation of treatment costs," *BioMed research international*, vol. 2014, 2014.
- [73] E. L. Miller, L. Murray, L. Richards, R. D. Zorowitz, T. Bakas, P. Clark, S. A. Billinger *et al.*, "Comprehensive overview of nursing and interdisciplinary rehabilitation care of the stroke patient a scientific statement from the american heart association," *Stroke*, vol. 41, no. 10, pp. 2402–2448, 2010.
- [74] A. C. Lo, "Clinical designs of recent robot rehabilitation trials," *American Journal of Physical Medicine & Rehabilitation*, vol. 91, no. 11, pp. S204–S216, 2012.
- [75] N. Hogan, H. I. Krebs, J. Charnnarong, P. Srikrishna, and A. Sharon, "MIT-MANUS: a workstation for manual therapy and training. I," in *Robot and Human Communication, 1992. Proceedings., IEEE International Workshop on*. IEEE, 1992, pp. 161–165.
- [76] M. Gilliaux, T. Lejeune, C. Detrembleur, J. Sapin, B. Dehez, and G. Stoquart, "A robotic device as a sensitive quantitative tool to assess upper limb impairments in stroke patients: a preliminary prospective cohort study," *Journal of Rehabilitation Medicine*, vol. 44, no. 3, pp. 210–217, 2012.
- [77] M.-S. Ju, C.-C. Lin, D.-H. Lin, I.-S. Hwang, and S.-M. Chen, "A rehabilitation robot with force-position hybrid fuzzy controller: hybrid fuzzy control of rehabilitation robot," *Neural Systems and Rehabilitation Engineering, IEEE Transactions on*, vol. 13, no. 3, pp. 349–358, 2005.

- [78] J. L. Herder, N. Vrijlandt, T. Antonides, M. Cloosterman, and P. L. Mastenbroek, "Principle and design of a mobile arm support for people with muscular weakness," *JRRD: Journal of Rehabilitation Research & Development*, 43 (5), 2006, 2006.
- [79] J. C. Perry, H. Zabaleta, A. Belloso, and T. Keller, "ARMassist: A low-cost device for telerehabilitation of post-stroke arm deficits," in *World Congress on Medical Physics and Biomedical Engineering, September 7-12, 2009, Munich, Germany*. Springer, 2009, pp. 64–67.
- [80] K. Nagai, I. Nakanishi, H. Hanafusa, S. Kawamura, M. Makikawa, and N. Tejima, "Development of an 8 DOF robotic orthosis for assisting human upper limb motion," in *ICRA*, 1998, pp. 3486–3491.
- [81] D. J. Reinkensmeyer, C. D. Takahashi, W. K. Timoszyk, A. N. Reinkensmeyer, and L. E. Kahn, "Design of robot assistance for arm movement therapy following stroke," *Advanced robotics*, vol. 14, no. 7, pp. 625–637, 2001.
- [82] P. S. Lum, C. G. Burgar, P. C. Shor, M. Majmundar, and M. Van der Loos, "Robot-assisted movement training compared with conventional therapy techniques for the rehabilitation of upper-limb motor function after stroke," *Archives of physical medicine and rehabilitation*, vol. 83, no. 7, pp. 952–959, 2002.
- [83] D. Mayhew, B. Bachrach, W. Z. Rymer, and R. F. Beer, "Development of the MACARM - a novel cable robot for upper limb neurorehabilitation," in *Rehabilitation Robotics, 2005. ICORR 2005. 9th International Conference on*. IEEE, 2005, pp. 299–302.
- [84] A. Toth, G. Fazekas, G. Arz, M. Jurak, and M. Horvath, "Passive robotic movement therapy of the spastic hemiparetic arm with reharob: report of the first clinical test and the follow-up system improvement," in *Rehabilitation Robotics, 2005. ICORR 2005. 9th International Conference on*. IEEE, 2005, pp. 127–130.
- [85] G. Rosati, P. Gallina, S. Masiero, and A. Rossi, "Design of a new 5 DOF wire-based robot for rehabilitation," in *Rehabilitation Robotics, 2005. ICORR 2005. 9th International Conference on*. IEEE, 2005, pp. 430–433.
- [86] A. Jackson, R. Holt, P. Culmer, S. Makower, M. Levesley, R. Richardson, J. Cozens, M. M. Williams, and B. Bhakta, "Dual robot system for upper limb rehabilitation after stroke: the design process," *Proceedings of the Institution of Mechanical Engineers, Part C: Journal of Mechanical Engineering Science*, vol. 221, no. 7, pp. 845–857, 2007.
- [87] C. K. Wong, K. Jordan, and M. King, "Robotic arm skate for stroke rehabilitation," in *Rehabilitation Robotics (ICORR), 2011 IEEE International Conference on*. IEEE, 2011, pp. 1–6.
- [88] F. Bovolenta, P. Sale, V. Dall'Armi, P. Clerici, and M. Franceschini, "Robot-aided therapy for upper limbs in patients with stroke-related lesions. brief report of a clinical experience," *J Neuroeng Rehabil*, vol. 8, no. 18, pp. 0003–8, 2011.
- [89] R. C. Loureiro and T. A. Smith, "Design of the ROBIN system: whole-arm multi-model sensorimotor environment for the rehabilitation of brain injuries while sitting or standing," in *Rehabilitation Robotics (ICORR), 2011 IEEE International Conference on*. IEEE, 2011, pp. 1–6.
- [90] V. Bartenbach, C. Sander, M. Pöschl, K. Wilging, T. Nelius, F. Doll, W. Burger, C. Stockinger, A. Focke, and T. Stein, "The BioMotionBot: A robotic device for applications in human motor learning and rehabilitation," *Journal of neuroscience methods*, vol. 213, no. 2, pp. 282–297, 2013.
- [91] [http://www.rehatechnology.com/en/armotion-\\_content—1-1071.html](http://www.rehatechnology.com/en/armotion-_content—1-1071.html).



- [92] M. Johnson, K. Wisneski, J. Anderson, D. Nathan, and R. Smith, "Development of adler: The activities of daily living exercise robot," in *Biomedical Robotics and Biomechanics, 2006. BioRob 2006. The First IEEE/RAS-EMBS International Conference on*. IEEE, 2006, pp. 881–886.
- [93] M. Ellis, T. Sukal, T. DeMott, and J. Dewald, "ACT 3D exercise targets gravity-induced discoordination and improves reaching work area in individuals with stroke," in *Rehabilitation Robotics, 2007. ICORR 2007. IEEE 10th International Conference on*. IEEE, 2007, pp. 890–895.
- [94] R. Loureiro, F. Amirabdollahian, M. Topping, B. Driessen, and W. Harwin, "Upper limb robot mediated stroke therapy - GENTLE/s approach," *Autonomous Robots*, vol. 15, no. 1, pp. 35–51, 2003.
- [95] M. Johnson, X. Feng, L. Johnson, B. Ramachandran, J. Winters, and J. Kosasih, "Robotic systems that rehabilitate as well as motivate: three strategies for motivating impaired arm use," in *Biomedical Robotics and Biomechanics, 2006. BioRob 2006. The First IEEE/RAS-EMBS International Conference on*. IEEE, 2006, pp. 254–259.
- [96] A. H. Stienen, E. E. Hekman, F. C. Van der Helm, G. B. Prange, M. J. Jannink, A. M. Aalsma, and H. Van der Kooij, "Freebal: dedicated gravity compensation for the upper extremities," in *Rehabilitation Robotics, 2007. ICORR 2007. IEEE 10th International Conference on*. IEEE, 2007, pp. 804–808.
- [97] S. J. Ball, I. E. Brown, and S. H. Scott, "A planar 3 DOF robotic exoskeleton for rehabilitation and assessment," in *Engineering in Medicine and Biology Society, 2007. EMBS 2007. 29th Annual International Conference of the IEEE*. IEEE, 2007, pp. 4024–4027.
- [98] N. Tsagarakis, D. Caldwell, and G. Medrano-Cerda, "A 7 DOF pneumatic muscle actuator (pMA) powered exoskeleton," in *Robot and Human Interaction, 1999. RO-MAN'99. 8th IEEE International Workshop on*. IEEE, 1999, pp. 327–333.
- [99] C. Carignan, M. Liszka, and S. Roderick, "Design of an arm exoskeleton with scapula motion for shoulder rehabilitation," in *Advanced Robotics, 2005. ICAR'05. Proceedings., 12th International Conference on*. IEEE, 2005, pp. 524–531.
- [100] J. C. Perry and J. Rosen, "Design of a 7 degree-of-freedom upper-limb powered exoskeleton," in *Biomedical Robotics and Biomechanics, 2006. BioRob 2006. The First IEEE/RAS-EMBS International Conference on*. IEEE, 2006, pp. 805–810.
- [101] T. Nef, M. Mihelj, and R. Riener, "ARMin: a robot for patient-cooperative arm therapy," *Medical and Biological Engineering and Computing*, vol. 45, no. 9, pp. 887–900, 2007.
- [102] A. Frisoli, L. Borelli, A. Montagner, S. Marcheschi, C. Procopio, F. Salsedo, M. Bergamasco, M. C. Carboncini, M. Tolaini, and B. Rossi, "Arm rehabilitation with a robotic exoskeleton in virtual reality," in *Rehabilitation Robotics, 2007. ICORR 2007. IEEE 10th International Conference on*. IEEE, 2007, pp. 631–642.
- [103] G. Fazekas, M. Horvath, T. Troznai, and A. Toth, "Robot-mediated upper limb physiotherapy for patients with spastic hemiparesis: a preliminary study," *Journal of rehabilitation medicine*, vol. 39, no. 7, pp. 580–582, 2007.
- [104] T. G. Sugar, J. He, E. J. Koeneman, J. B. Koeneman, R. Herman, H. Huang, R. S. Schultz, D. Herring, J. Wanberg, S. Balasubramanian *et al.*, "Design and control of RUPERT: a device for robotic upper extremity repetitive therapy," *Neural Systems and Rehabilitation Engineering, IEEE Transactions on*, vol. 15, no. 3, pp. 336–346, 2007.
- [105] P. Garrec, J. Friconeau, Y. Measson, and Y. Perrot, "ABLE, an innovative transparent exoskeleton for the upper-limb," in *Intelligent Robots and Systems, 2008. IROS 2008. IEEE/RSJ International Conference on*. IEEE, 2008, pp. 1483–1488.

- [106] A. Stienen, E. Hekman, F. Van Der Helm, and H. Van Der Kooij, "Self-aligning exoskeleton axes through decoupling of joint rotations and translations," *Robotics, IEEE Transactions on*, vol. 25, no. 3, pp. 628–633, 2009.
- [107] T. Lenzi, S. De Rossi, N. Vitiello, A. Chiri, S. Roccella, F. Giovacchini, F. Vecchi, and M. C. Carrozza, "The neuro-robotics paradigm: NEURARM, NEUROExos, HAN-DEXOS," in *Engineering in Medicine and Biology Society, 2009. EMBC 2009. Annual International Conference of the IEEE*. IEEE, 2009, pp. 2430–2433.
- [108] J. Klein, S. Spencer, J. Allington, J. E. Bobrow, and D. J. Reinkensmeyer, "Optimization of a parallel shoulder mechanism to achieve a high-force, low-mass, robotic-arm exoskeleton," *IEEE Transactions on Robotics*, vol. 26, no. 4, pp. 710–715, 2010.
- [109] A. U. Pehlivan, O. Celik, and M. K. Malley, "Mechanical design of a distal arm exoskeleton for stroke and spinal cord injury rehabilitation," in *Rehabilitation Robotics (ICORR), 2011 IEEE International Conference on*. IEEE, 2011, pp. 1–5.
- [110] Y. Mao and S. K. Agrawal, "Design of a cable-driven arm exoskeleton (CAREX) for neural rehabilitation," *Robotics, IEEE Transactions on*, vol. 28, no. 4, pp. 922–931, 2012.
- [111] <http://www.hocoma.com/products/ameo/ameopower/>.
- [112] A. H. Stienen, E. E. Hekman, F. C. Der Helm, G. B. Prange, M. J. Jannink, A. M. Aalsma, and H. Van der Kooij, "Dampace: dynamic force-coordination trainer for the upper extremities," in *Rehabilitation Robotics, 2007. ICORR 2007. IEEE 10th International Conference on*. IEEE, 2007, pp. 820–826.
- [113] <http://www.hocoma.com/products/ameo/ameospring/>.
- [114] E. Ambrosini, S. Ferrante, M. Rossini, F. Molteni, M. Gföhler, W. Reichenfeller, A. Duschau-Wicke, G. Ferrigno, and A. Pedrocchi, "Functional and usability assessment of a robotic exoskeleton arm to support activities of daily life," *Robotica*, vol. 32, no. 08, pp. 1213–1224, 2014.
- [115] S. Lum, S. L. Lehman, and D. J. Reinkensmeyer, "The bimanual lifting rehabilitator: an adaptive machine for therapy of stroke patients," *Rehabilitation Engineering, IEEE Transactions on*, vol. 3, no. 2, pp. 166–174, 1995.
- [116] J. A. Cozens, "Robotic assistance of an active upper limb exercise in neurologically impaired patients," *Rehabilitation Engineering, IEEE Transactions on*, vol. 7, no. 2, pp. 254–256, 1999.
- [117] S. Hesse, G. Schulte-Tigges, M. Konrad, A. Bardeleben, and C. Werner, "Robot-assisted arm trainer for the passive and active practice of bilateral forearm and wrist movements in hemiparetic subjects," *Archives of physical medicine and rehabilitation*, vol. 84, no. 6, pp. 915–920, 2003.
- [118] C. D. Takahashi, L. Der-Yeghiaian, V. H. Le, and S. C. Cramer, "A robotic device for hand motor therapy after stroke," in *Rehabilitation Robotics, 2005. ICORR 2005. 9th International Conference on*, 2005, pp. 17–20.
- [119] U. Mali and M. Munih, "HIFE-haptic interface for finger exercise," in *Mechatronics, IEEE/ASME Transactions on*, vol. 11, 2006, pp. 93–102.
- [120] O. Lamercy, L. Dovat, R. Gassert, E. Burdet, C. L. Teo, and T. Milner, "A haptic knob for rehabilitation of hand function," *Neural Systems and Rehabilitation Engineering, IEEE Transactions on*, vol. 15, no. 3, pp. 356–366, 2007.
- [121] R. C. V. Loureiro and W. S. Harwin, "Reach & grasp therapy: Design and control of a 9-DOF robotic neuro-rehabilitation system," in *2007 IEEE 10th International Conference on Rehabilitation Robotics, Vols 1 and 2*, 2007, pp. 757–763.

- [122] L. Masia, H. Krebs, P. Cappa, and N. Hogan, "Design, characterization, and impedance limits of a hand robot," in *Rehabilitation Robotics, 2007. ICORR 2007. IEEE 10th International Conference on*. IEEE, 2007, pp. 1085–1089.
- [123] S. Hesse, H. Kuhlmann, J. Wilk, C. Tomelleri, and S. G. Kirker, "A new electromechanical trainer for sensorimotor rehabilitation of paralysed fingers: A case series in chronic and acute stroke patients," *Journal of NeuroEngineering and Rehabilitation*, vol. 5, p. 21, 2008.
- [124] L. Dovat, O. Lambercy, R. Gassert, T. Maeder, T. Milner, T. C. Leong, and E. Burdet, "HandCARE: a cable-actuated rehabilitation system to train hand function after stroke," *Neural Systems and Rehabilitation Engineering, IEEE Transactions on*, vol. 16, no. 6, pp. 582–591, 2008.
- [125] <http://kinetec.fr/en/kinetec-selection/cpm-continuous-passive-motion/attelle-kinetec-maestra-portable-detail.html>.
- [126] J. Podobnik, M. Mihelj, and M. Munih, "Upper limb and grasp rehabilitation and evaluation of stroke patients using HenRiE device ," in *Virtual Rehabilitation International Conference 2009*, 2009, pp. 173–178.
- [127] C. N. Schabowsky, S. B. Godfrey, R. J. Holley, P. S. Lum *et al.*, "Development and pilot testing of HEXORR: hand EXOskeleton rehabilitation robot," *J Neuroeng Rehabil*, vol. 7, no. 1, p. 36, 2010.
- [128] J.-C. Metzger, O. Lambercy, D. Chapuis, and R. Gassert, "Design and characterization of the ReHapticKnob, a robot for assessment and therapy of hand function." in *IROS*. IEEE, 2011, pp. 3074–3080.
- [129] A. Meyer-Heim and H. J. van Hedel, "Robot-assisted and computer-enhanced therapies for children with cerebral palsy: current state and clinical implementation," in *Seminars in pediatric neurology*, vol. 20, no. 2. Elsevier, 2013, pp. 139–145.
- [130] J. F. Farrell, H. B. Hoffman, J. L. Snyder, C. A. Giuliani, and R. W. Bohannon, "Orthotic aided training of the paretic upper limb in chronic stroke: results of a phase 1 trial," *NeuroRehabilitation-An Interdisciplinary Journal*, vol. 22, no. 2, pp. 99–104, 2007.
- [131] F. Amirabdollahian, S. Ates, A. Basteris, A. Cesario, J. Buurke, H. Hermens, D. Hofs, E. Johansson, G. Mountain, N. Nasr *et al.*, "Design, development and deployment of a hand/wrist exoskeleton for home-based rehabilitation after stroke-script project," *Robotica*, vol. 32, no. 08, pp. 1331–1346, 2014.
- [132] <http://www.hocoma.com/en/products/armeo/armeospring/manovospring/>.
- [133] N. Yozbatiran, J. Berliner, M. K. O'Malley, A. U. Pehlivan, Z. Kadivar, C. Boake, and G. E. Francisco, "Robotic training and clinical assessment of upper extremity movements after spinal cord injury: a single case report," *Journal of rehabilitation medicine*, vol. 44, no. 2, pp. 186–188, 2012.
- [134] M. Cortes, J. Elder, A. Rykman, L. Murray, M. Avedissian, A. Stampas, G. W. Thickbroom, A. Pascual-Leone, H. I. Krebs, J. Valls-Sole *et al.*, "Improved motor performance in chronic spinal cord injury following upper-limb robotic training," *NeuroRehabilitation*, vol. 33, no. 1, pp. 57–65, 2013.
- [135] D. Vanmulken, A. Spooren, H. Bongers, and H. Seelen, "Robot-assisted task-oriented upper extremity skill training in cervical spinal cord injury: a feasibility study," *Spinal cord*, 2015.
- [136] I. Carpinella, D. Cattaneo, S. Abuarqub, and M. Ferrarin, "Robot-based rehabilitation of the upper limbs in multiple sclerosis: feasibility and preliminary results," *Journal of rehabilitation medicine*, vol. 41, no. 12, pp. 966–970, 2009.

- [137] D. Gijbels, I. Lamers, L. Kerkhofs, G. Alders, E. Knippenberg, P. Feys *et al.*, “The Armeo Spring as training tool to improve upper limb functionality in multiple sclerosis: a pilot study,” *Journal of neuroengineering and rehabilitation*, vol. 8, no. 5, p. 5, 2011.
- [138] J. M. Veerbeek, E. van Wegen, R. van Peppen, P. J. van der Wees, E. Hendriks, M. Ritberg, and G. Kwakkel, “What is the evidence for physical therapy poststroke? a systematic review and meta-analysis,” *PLoS One*, vol. 9, no. 2, p. e87987, 2014.
- [139] D. L. Turner, W. Winterbotham, and M. Kmetova, “Using assistive robotic technology in motor neurorehabilitation after childhood stroke,” *Journal of Neurology Research*, vol. 2, no. 2, pp. 65–68, 2012.
- [140] D. Wille, K. Eng, L. Holper, E. Chevrier, Y. Hauser, D. Kiper, P. Pyk, S. Schlegel, and A. Meyer-Heim, “Virtual reality-based paediatric interactive therapy system (PITS) for improvement of arm and hand function in children with motor impairment - a pilot study,” *Developmental neurorehabilitation*, vol. 12, no. 1, pp. 44–52, 2009.
- [141] G. Fluet, Q. Qiu, D. Kelly, H. Parikh, D. Ramirez, S. Saleh, and S. Adamovich, “Interfacing a haptic robotic system with complex virtual environments to treat impaired upper extremity motor function in children with cerebral palsy,” *Developmental neurorehabilitation*, vol. 13, no. 5, pp. 335–345, 2010.
- [142] <http://tyromotion.com/en/products/diego/overview>.
- [143] M. Hartwig, “Fun und evidenz - computergestützte Armrehabilitation mit dem Pablo® Plus-System,” *Neurol Rehabil*, vol. 17, no. 1, pp. 42–46, 2011.
- [144] <http://www.hocomma.com/products/armeospring-pediatric/>.
- [145] <http://tyromotion.com/en/products/pablo/overview>.
- [146] S. Fasoli, M. Fragala-Pinkham, R. Hughes, N. Hogan, H. Krebs, and J. Stein, “Upper limb robotic therapy for children with hemiplegia,” *American Journal of Physical Medicine & Rehabilitation*, vol. 87, no. 11, p. 929, 2008.
- [147] M. Gilliaux, A. Renders, D. Dispa, D. Holvoet, J. Sapin, B. Dehez, C. Detrembleur, T. M. Lejeune, and G. Stoquart, “Upper limb robot-assisted therapy in cerebral palsy a single-blind randomized controlled trial,” *Neurorehabilitation and neural repair*, vol. 29, no. 2, pp. 183–192, 2014.
- [148] S. H. Jang, S. H. You, M. Hallett, Y. W. Cho, C.-M. Park, S.-H. Cho, H.-Y. Lee, and T.-H. Kim, “Cortical reorganization and associated functional motor recovery after virtual reality in patients with chronic stroke: an experimenter-blind preliminary study,” *Archives of physical medicine and rehabilitation*, vol. 86, no. 11, pp. 2218–2223, 2005.
- [149] T. Parsons, A. Rizzo, S. Rogers, and P. York, “Virtual reality in paediatric rehabilitation: A review,” *Developmental Neurorehabilitation*, vol. 12, no. 4, pp. 224–238, 2009.
- [150] M. K. Holden, “Virtual environments for motor rehabilitation: review,” *Cyberpsychology & behavior*, vol. 8, no. 3, pp. 187–211, 2005.
- [151] R. Labruyère, C. N. Gerber, K. Birrer-Brütsch, A. Meyer-Heim, and H. J. van Hedel, “Requirements for and impact of a serious game for neuro-pediatric robot-assisted gait training,” *Research in developmental disabilities*, vol. 34, no. 11, pp. 3906–3915, 2013.
- [152] A. Koenig, U. Keller, K. Pfluger, A. Meyer-Heim, and R. Riener, “PASCAL: Pediatric arm support robot for combined arm and leg training,” in *4th International Conference on Biomedical Robotics and Biomechanics (BioRob)*. IEEE, 2012, pp. 1862–1868.
- [153] R. Riener, L. Lünenburger, I. Maier, G. Colombo, and V. Dietz, “Locomotor training in subjects with sensori-motor deficits: an overview of the robotic gait orthosis Lokomat,” *Journal of Healthcare Engineering*, vol. 1, no. 2, pp. 197–216, 2010.

- [154] R. Jensen, "Changes in segment inertia proportions between 4 and 20 years," *Journal of Biomechanics*, vol. 22, no. 6-7, pp. 529–536, 1989.
- [155] B. Falk, C. Usselman, R. Dotan, L. Brunton, P. Klentrou, J. Shaw, and D. Gabriel, "Child-adult differences in muscle strength and activation pattern during isometric elbow flexion and extension," *Applied Physiology, Nutrition, and Metabolism*, vol. 34, no. 4, pp. 609–615, 2009.
- [156] "Centers for disease control and prevention - morbidity and mortality weekly report (MMWR)," vol. 61, no. 20, 2012.
- [157] N. Maclean and P. Pound, "A critical review of the concept of patient motivation in the literature on physical rehabilitation." *Social science & medicine*, 2000.
- [158] M. Csikszentmihalyi, "The concept of flow," in *Flow and the Foundations of Positive Psychology*. Springer, 2014, pp. 239–263.
- [159] B. J. Pollock and T. D. Lee, "Dissociated contextual interference effects in children and adults," *Perceptual and motor skills*, vol. 84, no. 3, pp. 851–858, 1997.
- [160] R. Palisano, P. Rosenbaum, S. Walter, D. Russell, E. Wood, and B. Galuppi, "Development and reliability of a system to classify gross motor function in children with cerebral palsy," *Dev Med Child Neurol*, vol. 39, pp. 214–223, 1997.
- [161] R. Stevenson, M. Conaway, W. Chumlea, P. Rosenbaum, E. Fung, R. Henderson, G. Worley, G. Liptak, M. O'Donnell, L. Samson-Fang *et al.*, "Growth and health in children with moderate-to-severe cerebral palsy," *Pediatrics*, vol. 118, no. 3, pp. 1010–1018, 2006.
- [162] J. Brooks, S. Day, R. Shavelle, and D. Strauss, "Low weight, morbidity, and mortality in children with cerebral palsy: new clinical growth charts," *Pediatrics*, vol. 128, no. 2, pp. e299–e307, 2011.
- [163] R. Snyder *et al.*, "Anthropometry of Infants, Children, and Youths to Age 18 for Product Safety Design. Final Report." 1977.
- [164] K. Petuskey, A. Bagley, E. Abdala, M. James, and G. Rab, "Upper extremity kinematics during functional activities: Three-dimensional studies in a normal pediatric population," *Gait & posture*, vol. 25, no. 4, pp. 573–579, 2007.
- [165] C. Owings, D. Chaffin, R. Snyder, and R. NORCUTT, *Strength characteristics of US children for product safety design*, 1975.
- [166] M. Eek, A. Kroksmark, and E. Beckung, "Isometric muscle torque in children 5 to 15 years of age: normative data," *Archives of physical medicine and rehabilitation*, vol. 87, no. 8, pp. 1091–1099, 2006.
- [167] B. Danneskiold-Samsøe, E. Bartels, P. Bülow, H. Lund, A. Stockmarr, C. Holm, I. Wätjen, M. Appleyard, and H. Bliddal, "Isokinetic and isometric muscle strength in a healthy population with special reference to age and gender," *Acta Physiologica*, vol. 197, pp. 1–68, 2009.
- [168] T. L. Nef, "ARMin-multimodal robot for the movement therapy of the upper extremities," Ph.D. dissertation, Diss., Eidgenössische Technische Hochschule ETH Zürich, Nr. 17476, 2007, 2007.
- [169] P. Culmer, A. Jackson, S. Makower, R. Richardson, J. Cozens, M. Levesley, and B. Bhakta, "A control strategy for upper limb robotic rehabilitation with a dual robot system," *Mechatronics, IEEE/ASME Transactions on*, vol. 15, no. 4, pp. 575–585, 2010.
- [170] M. Guidali, "Robot assisted arm rehabilitation: Cooperative control strategies for activities of daily living," Ph.D. dissertation, Sensory-Motor Systems Lab, ETH Zurich, 2012.

## BIBLIOGRAPHY

---

- [171] T. Nef, M. Guidali, and R. Riener, “ARMin III—arm therapy exoskeleton with an ergonomic shoulder actuation,” *Applied Bionics and Biomechanics*, vol. 6, no. 2, pp. 127–142, 2009.
- [172] H. S. Lo and S. Q. Xie, “Exoskeleton robots for upper-limb rehabilitation: State of the art and future prospects,” *Medical engineering & physics*, vol. 34, no. 3, pp. 261–268, 2012.
- [173] S. H. Scott, I. E. Brown, and S. J. Ball, “Robotic exoskeleton for limb movement,” Patent Application US 2008/0 304 935 A1, 11 06, 2008.
- [174] D. Dörig, “Design of a new hand module for the pediatric ARMin,” *Semester thesis ETH Zurich*, 2012.
- [175] P. Maciejasz, J. Eschweiler, K. Gerlach-Hahn, A. Jansen-Troy, and S. Leonhardt, “A survey on robotic devices for upper limb rehabilitation,” *Journal of neuroengineering and rehabilitation*, vol. 11, no. 1, p. 3, 2014.
- [176] M. Guidali, U. Keller, V. Klamroth-Marganska, T. Nef, and R. Riener, “Estimating the patient’s contribution during robot-assisted therapy.” *Journal of Rehabilitation Research & Development*, vol. 50, no. 3, 2013.
- [177] A. Martin, U. Götz, and R. Bauer, “»IMIC« - Innovative Movement Therapies in Childhood,” *Neurologie & Rehabilitation*, vol. 4, pp. 215–225, 2014.
- [178] N. Dominici, U. Keller, H. Vallery, L. Friedli, R. van den Brand, M. L. Starkey, P. Musienko, R. Riener, and G. Courtine, “Versatile robotic interface to evaluate, enable and train locomotion and balance after neuromotor disorders,” *Nature medicine*, vol. 18, no. 7, pp. 1142–1147, 2012.
- [179] J. von Zitzewitz, H. Vallery, A. Hasse, and G. Courtine, “High-precision force control using selective compliant mechanisms,” in *2013 International Workshop on Soft Robotics and Morphological Computation (SoftRobot2013)*, no. EPFL-TALK-196614, 2013.
- [180] A. H. Stienen, E. E. Hekman, H. T. Braak, A. M. Aalsma, F. C. van der Helm, and H. van der Kooij, “Design of a rotational hydroelastic actuator for a powered exoskeleton for upper limb rehabilitation,” *Biomedical Engineering, IEEE Transactions on*, vol. 57, no. 3, pp. 728–735, 2010.
- [181] J. Patton, M. Stoykov, M. Kovic, and F. Mussa-Ivaldi, “Evaluation of robotic training forces that either enhance or reduce error in chronic hemiparetic stroke survivors,” *Experimental Brain Research*, vol. 168, no. 3, pp. 368–383, 2006.
- [182] R. Schmidt, “Frequent augmented feedback can degrade learning: Evidence and interpretations,” *Tutorials in motor neuroscience*, pp. 59–75, 1991.
- [183] R. Sigrist, G. Rauter, R. Riener, and P. Wolf, “Augmented visual, auditory, haptic, and multimodal feedback in motor learning: A review,” *Psychonomic Bulletin & Review*, pp. 1–33, 2012.
- [184] N. Hogan, “Impedance control: An approach to manipulation,” in *American Control Conference, 1984*. IEEE, 1984, pp. 304–313.
- [185] J. Emken, J. Bobrow, and D. Reinkensmeyer, “Robotic movement training as an optimization problem: designing a controller that assists only as needed,” in *Rehabilitation Robotics, 2005. ICORR 2005. 9th International Conference on*. IEEE, 2005, pp. 307–312.
- [186] R. Riener, L. Lünenburger, S. Jezernik, M. Anderschitz, G. Colombo, and V. Dietz, “Patient-cooperative strategies for robot-aided treadmill training: first experimental results,” *Neural Systems and Rehabilitation Engineering, IEEE Transactions on*, vol. 13, no. 3, pp. 380–394, 2005.

- [187] H. Krebs, J. Palazzolo, L. Dipietro, M. Ferraro, J. Krol, K. Ranneklev, B. Volpe, and N. Hogan, "Rehabilitation robotics: Performance-based progressive robot-assisted therapy," *Autonomous Robots*, vol. 15, no. 1, pp. 7–20, 2003.
- [188] L. Cai, A. Fong, C. Otoshi, Y. Liang, J. Burdick, R. Roy, and V. Edgerton, "Implications of assist-as-needed robotic step training after a complete spinal cord injury on intrinsic strategies of motor learning," *The Journal of neuroscience*, vol. 26, no. 41, pp. 10 564–10 568, 2006.
- [189] S. Banala, S. Agrawal, and J. Scholz, "Active Leg Exoskeleton (ALEX) for gait rehabilitation of motor-impaired patients," in *Rehabilitation Robotics, 2007. ICORR 2007. IEEE 10th International Conference on*. IEEE, 2007, pp. 401–407.
- [190] G. Rauter, R. Sigrist, L. Marchal-Crespo, H. Vallery, R. Riener, and P. Wolf, "Assistance or challenge? Filling a gap in user-cooperative control," in *IEEE/RSJ International Conference on Intelligent Robots and Systems (IROS)*, 2011, pp. 3068–3073.
- [191] A. Duschau-Wicke, J. von Zitzewitz, A. Caprez, L. Lunenburger, and R. Riener, "Path control: A method for patient-cooperative robot-aided gait rehabilitation," *Neural Systems and Rehabilitation Engineering, IEEE Transactions on*, vol. 18, no. 1, pp. 38–48, 2010.
- [192] H. Kim, L. M. Miller, N. Byl, G. Abrams, and J. Rosen, "Redundancy resolution of the human arm and an upper limb exoskeleton," *Biomedical Engineering, IEEE Transactions on*, vol. 59, no. 6, pp. 1770–1779, 2012.
- [193] D. A. Winter, *Biomechanics and motor control of human movement*. John Wiley & Sons, 1990.
- [194] D. Simon, *Optimal state estimation: Kalman, H infinity, and nonlinear approaches*. John Wiley & Sons, 2006.
- [195] B. Ugurlu, M. Nishimura, K. Hyodo, M. Kawanishi, and T. Narikiyo, "Proof of concept for robot-aided upper limb rehabilitation using disturbance observers," *Human-Machine Systems, IEEE Transactions on*, vol. 45, no. 1, pp. 110–118, 2015.
- [196] T. Nef and P. Lum, "Improving backdrivability in geared rehabilitation robots," *Medical & biological engineering & computing*, vol. 47, no. 4, pp. 441–447, 2009.
- [197] B. Armstrong-Hélouvry, P. Dupont, and C. C. De Wit, "A survey of models, analysis tools and compensation methods for the control of machines with friction," *Automatica*, vol. 30, no. 7, pp. 1083–1138, 1994.
- [198] H. Olsson, K. J. Åström, C. Canudas de Wit, M. Gäfvert, and P. Lischinsky, "Friction models and friction compensation," *European journal of control*, vol. 4, no. 3, pp. 176–195, 1998.
- [199] H. F. Olson, "Music, physics and engineering," p. 249, 1967.
- [200] N. I. Badler and D. Tolani, "Real-time inverse kinematics of the human arm," *Center for Human Modeling and Simulation*, p. 73, 1996.
- [201] T. Kang, Y. Shimansky, and J. He, "Angle of elbow elevation depends on the reach target coordinates," in *Engineering in Medicine and Biology, 2002. 24th Annual Conference and the Annual Fall Meeting of the Biomedical Engineering Society EMBS/BMES Conference, 2002. Proceedings of the Second Joint*, vol. 3. IEEE, 2002, pp. 2571–2572.
- [202] T. Kang, J. He, and S. I. H. Tillery, "Determining natural arm configuration along a reaching trajectory," *Experimental Brain Research*, vol. 167, no. 3, pp. 352–361, 2005.
- [203] A. M. Zanchettin, P. Rocco, L. Bascetta, I. Symeonidis, and S. Peldschus, "Kinematic analysis and synthesis of the human arm motion during a manipulation task," in *Robotics and Automation (ICRA), 2011 IEEE International Conference on*. IEEE, 2011, pp. 2692–2697.

- [204] J. J. Marotta, W. Medendorp, and J. Crawford, "Kinematic rules for upper and lower arm contributions to grasp orientation," *Journal of neurophysiology*, vol. 90, no. 6, pp. 3816–3827, 2003.
- [205] H. Vallery, A. Duschau-Wicke, and R. Riener, "Generalized elasticities improve patient-cooperative control of rehabilitation robots," in *International Conference on Rehabilitation Robotics (ICORR)*. IEEE, 2009, pp. 535–541.
- [206] L. Marchal-Crespo and D. Reinkensmeyer, "Review of control strategies for robotic movement training after neurologic injury," *Journal of neuroengineering and rehabilitation*, vol. 6, no. 1, p. 20, 2009.
- [207] L. Marchal-Crespo, G. Rauter, D. Wyss, J. von Zitzewitz, and R. Riener, "Synthesis and control of an assistive robotic tennis trainer," in *4th International Conference on Biomedical Robotics and Biomechatronics (BioRob)*. IEEE, 2012, pp. 355–360.
- [208] A. v. d. Schaft and A. Schaft, *L2-gain and passivity in nonlinear control*. Springer-Verlag New York, Inc., 1999.
- [209] J. E. Colgate, "The control of dynamically interacting systems," Ph.D. dissertation, Massachusetts Institute of Technology, 1988.
- [210] H. Kaufman, I. Barkana, and K. Sobel, *Direct adaptive control algorithms: theory and applications*. Springer Science & Business Media, 1998.
- [211] J. S. Shamma and M. Athans, "Guaranteed properties of gain scheduled control for linear parameter-varying plants," *Automatica*, vol. 27, no. 3, pp. 559–564, 1991.
- [212] J.-H. Ryu, C. Preusche, B. Hannaford, and G. Hirzinger, "Time domain passivity control with reference energy following," *Control Systems Technology, IEEE Transactions on*, vol. 13, no. 5, pp. 737–742, 2005.
- [213] N. Diolaiti, G. Niemeyer, F. Barbagli, and J. K. Salisbury, "Stability of haptic rendering: Discretization, quantization, time delay, and coulomb effects," *Robotics, IEEE Transactions on*, vol. 22, no. 2, pp. 256–268, 2006.
- [214] J. Ghan, R. Steger, and H. Kazerooni, "Control and system identification for the Berkeley lower extremity exoskeleton (BLEEX)," *Advanced Robotics*, vol. 20, no. 9, pp. 989–1014, 2006.
- [215] T. Bukhari, "Developing a patient-specific arm weight compensation for the ARMin control software," 2012, Bachelor Thesis ETH Zurich.
- [216] I. S. Howard, J. N. Ingram, and D. M. Wolpert, "A modular planar robotic manipulum with end-point torque control," *Journal of neuroscience methods*, vol. 181, no. 2, pp. 199–211, 2009.
- [217] J. E. Colgate and J. M. Brown, "Factors affecting the z-width of a haptic display," in *Robotics and Automation, 1994. Proceedings., 1994 IEEE International Conference on*. IEEE, 1994, pp. 3205–3210.
- [218] J.-C. Metzger, O. Lamercy, and R. Gassert, "High-fidelity rendering of virtual objects with the ReHapticKnob - novel avenues in robot-assisted rehabilitation of hand function," in *Haptics Symposium (HAPTICS), 2012 IEEE*. IEEE, 2012, pp. 51–56.
- [219] M. Guidali, P. Schlink, A. Duschau-Wicke, and R. Riener, "Online learning and adaptation of patient support during ADL training," in *Rehabilitation Robotics (ICORR), 2011 IEEE International Conference on*. IEEE, 2011, pp. 1–6.
- [220] J.-C. Metzger, O. Lamercy, A. Califfi, D. Dinacci, C. Petrillo, P. Rossi, F. M. Conti, and R. Gassert, "Assessment-driven selection and adaptation of exercise difficulty in robot-assisted therapy: a pilot study with a hand rehabilitation robot," *Journal of neuroengineering and rehabilitation*, vol. 11, no. 1, p. 154, 2014.



- [221] F. Carrillo, “Online learning controller for the ChARMin arm rehabilitation robot,” 2013, Semester Thesis ETH Zurich.
- [222] B. Siciliano and O. Khatib, *Springer handbook of robotics*. Springer Science & Business Media, 2008.
- [223] A. Gupta and M. K. O’Malley, *Robotic exoskeletons for upper extremity rehabilitation*. INTECH Open Access Publisher, 2007.
- [224] B. Lee, R. Cripps, M. Fitzharris, and P. Wing, “The global map for traumatic spinal cord injury epidemiology: update 2011, global incidence rate,” *Spinal cord*, vol. 52, no. 2, pp. 110–116, 2013.
- [225] N. E. Mayo, S. Wood-Dauphinee, R. Côt, L. Durcan, and J. Carlton, “Activity, participation, and quality of life 6 months poststroke,” *Arch Phys Med Rehabil*, vol. 83, no. 8, pp. 1035–1042, 2002.
- [226] P. Kennedy, P. Lude, and N. Taylor, “Quality of life, social participation, appraisals and coping post spinal cord injury: a review of four community samples,” *Spinal Cord*, vol. 44, no. 2, pp. 95–105, 2005.
- [227] J. D. Schaechter, “Motor rehabilitation and brain plasticity after hemiparetic stroke,” *Progress in neurobiology*, vol. 73, no. 1, pp. 61–72, 2004.
- [228] M. Kloosterman, G. Snoek, and M. Jannink, “Systematic review of the effects of exercise therapy on the upper extremity of patients with spinal-cord injury,” *Spinal Cord*, vol. 47, no. 3, pp. 196–203, 2008.
- [229] World Health Organization and others, *Towards a common language for functioning, disability and health: ICF*. World Health Organisation, 2002.
- [230] O. Lamercy, L. Lünenburger, R. Gassert, and M. Bolliger, “Robots for measurement/clinical assessment,” in *Neurorehabilitation Technology*. Springer, 2012, pp. 443–456.
- [231] J. M. Gregson, M. Leathley, A. P. Moore, A. K. Sharma, T. L. Smith, and C. L. Watkins, “Reliability of the Tone Assessment Scale and the modified Ashworth scale as clinical tools for assessing poststroke spasticity,” *Archives of physical medicine and rehabilitation*, vol. 80, no. 9, pp. 1013–1016, 1999.
- [232] C. Bosecker, L. Dipietro, B. Volpe, and H. I. Krebs, “Kinematic robot-based evaluation scales and clinical counterparts to measure upper limb motor performance in patients with chronic stroke,” *Neurorehabilitation and neural repair*, vol. 24, no. 1, pp. 62–69, 2010.
- [233] L. Dovat, O. Lamercy, B. Salman, V. Johnson, R. Gassert, E. Burdet, C. L. Teo, and T. Milner, “Post-stroke training of a pick and place activity in a virtual environment,” in *Virtual Rehabilitation, 2008*. IEEE, 2008, pp. 28–34.
- [234] M. Gilliaux, T. M. Lejeune, C. Detrembleur, P. Sapin, B. Dehez, C. Selves, and G. Stoquart, “Using the robotic device REAplan as a valid, reliable, and sensitive tool to quantify upper limb impairments in stroke patients,” *Journal of Rehabilitation Medicine*, vol. 46, no. 2, pp. 117–125, 2014.
- [235] O. Lamercy, L. Dovat, H. Yun, S. K. Wee, C. Kuah, K. Chua, R. Gassert, T. Milner, T. C. Leong, and E. Burdet, “Robotic assessment of hand function with the Haptic-Knob,” in *Proceedings of the 4th International Convention on Rehabilitation Engineering & Assistive Technology*. Singapore Therapeutic, Assistive & Rehabilitative Technologies (START) Centre, 2010, p. 33.

- [236] L. Lünenburger, G. Colombo, R. Riener, and V. Dietz, “Clinical assessments performed during robotic rehabilitation by the gait training robot Lokomat,” in *Rehabilitation Robotics, 2005. ICORR 2005. 9th International Conference on*. IEEE, 2005, pp. 345–348.
- [237] M. D. Ellis, T. Sukal-Moulton, and J. P. Dewald, “Progressive shoulder abduction loading is a crucial element of arm rehabilitation in chronic stroke,” *Neurorehabilitation and neural repair*, vol. 23, no. 8, pp. 862–869, 2009.
- [238] G. Kurillo, A. Chen, R. Bajcsy, and J. J. Han, “Evaluation of upper extremity reachable workspace using Kinect camera,” *Technology and Health Care*, vol. 21, no. 6, pp. 641–656, 2013.
- [239] R. Colombo, F. Pisano, S. Micera, A. Mazzone, C. Delconte, M. Carrozza, P. Dario, and G. Minuco, “Assessing mechanisms of recovery during robot-aided neurorehabilitation of the upper limb,” *Neurorehabilitation and neural repair*, vol. 22, no. 1, pp. 50–63, 2008.
- [240] O. Celik, M. K. O’Malley, C. Boake, H. S. Levin, N. Yozbatiran, and T. A. Reistetter, “Normalized movement quality measures for therapeutic robots strongly correlate with clinical motor impairment measures,” *Neural Systems and Rehabilitation Engineering, IEEE Transactions on*, vol. 18, no. 4, pp. 433–444, 2010.
- [241] M. Bolliger, R. Banz, V. Dietz, and L. Lünenburger, “Standardized voluntary force measurement in a lower extremity rehabilitation robot,” *Journal of neuroengineering and rehabilitation*, vol. 5, p. 23, 2008.
- [242] T. J. Tredinnick and P. W. Duncan, “Reliability of measurements of concentric and eccentric isokinetic loading,” *Physical Therapy*, vol. 68, no. 5, pp. 656–659, 1988.
- [243] J. Zariffa, N. Kapadia, J. L. Kramer, P. Taylor, M. Alizadeh-Meghbrazi, V. Zivanovic, U. Albisser, R. Willms, A. Townson, A. Curt *et al.*, “Relationship between clinical assessments of function and measurements from an upper-limb robotic rehabilitation device in cervical spinal cord injury,” *Neural Systems and Rehabilitation Engineering, IEEE Transactions on*, vol. 20, no. 3, pp. 341–350, 2012.
- [244] B. Rohrer, S. Fasoli, H. I. Krebs, R. Hughes, B. Volpe, W. R. Frontera, J. Stein, and N. Hogan, “Movement smoothness changes during stroke recovery,” *The Journal of Neuroscience*, vol. 22, no. 18, pp. 8297–8304, 2002.
- [245] N. Hogan and D. Sternad, “Sensitivity of smoothness measures to movement duration, amplitude, and arrests,” *Journal of motor behavior*, vol. 41, no. 6, pp. 529–534, 2009.
- [246] S. Balasubramanian, A. Melendez-Calderon, and E. Burdet, “A robust and sensitive metric for quantifying movement smoothness,” *Biomedical Engineering, IEEE Transactions on*, vol. 59, no. 8, pp. 2126–2136, 2012.
- [247] T. E. Milner, “A model for the generation of movements requiring endpoint precision,” *Neuroscience*, vol. 49, no. 2, pp. 487–496, 1992.
- [248] J. J. Daly, N. Hogan, E. M. Perepezko, H. I. Krebs, J. M. Rogers, K. S. Goyal, M. E. Dohring, E. Fredrickson, J. Nethery, and R. L. Ruff, “Response to upper-limb robotics and functional neuromuscular stimulation following stroke,” *Journal of rehabilitation research and development*, vol. 42, no. 6, p. 723, 2005.
- [249] L. Zimmerli, C. Krewer, R. Gassert, F. Müller, R. Riener, and L. Lünenburger, “Validation of a mechanism to balance exercise difficulty in robot-assisted upper-extremity rehabilitation after stroke,” *Journal of neuroengineering and rehabilitation*, vol. 9, no. 1, p. 6, 2012.
- [250] L. Dipietro, H. I. Krebs, S. E. Fasoli, B. T. Volpe, J. Stein, C. Bever, and N. Hogan, “Changing motor synergies in chronic stroke,” *Journal of neurophysiology*, vol. 98, no. 2, pp. 757–768, 2007.

- [251] V. C. Cheung, A. Turolla, M. Agostini, S. Silvoni, C. Bennis, P. Kasi, S. Paganoni, P. Bonato, and E. Bizzi, “Muscle synergy patterns as physiological markers of motor cortical damage,” *Proceedings of the National Academy of Sciences*, vol. 109, no. 36, pp. 14 652–14 656, 2012.
- [252] T. Krabben, G. B. Prange, B. I. Molier, A. H. Stienen, M. J. Jannink, J. H. Buurke, and J. S. Rietman, “Influence of gravity compensation training on synergistic movement patterns of the upper extremity after stroke, a pilot study,” *Journal of neuroengineering and rehabilitation*, vol. 9, no. 1, p. 44, 2012.
- [253] M. D. Ellis, B. G. Holubar, A. M. Acosta, R. F. Beer, and J. Dewald, “Modifiability of abnormal isometric elbow and shoulder joint torque coupling after stroke,” *Muscle & nerve*, vol. 32, no. 2, pp. 170–178, 2005.
- [254] K. Perell, A. Scremin, O. Scremin, and C. Kunkel, “Quantifying muscle tone in spinal cord injury patients using isokinetic dynamometric techniques,” *Spinal Cord*, vol. 34, no. 1, pp. 46–53, 1996.
- [255] D. E. Wood, J. Burrige, F. V. Wijck, C. McFadden, R. Hitchcock, A. Pandyan, A. Haugh, J. Salazar-Torres, and I. D. Swain, “Biomechanical approaches applied to the lower and upper limb for the measurement of spasticity: a systematic review of the literature,” *Disability & Rehabilitation*, vol. 27, no. 1-2, pp. 19–33, 2005.
- [256] L. E. Kahn, M. L. Zygmán, W. Z. Rymer, and D. J. Reinkensmeyer, “Robot-assisted reaching exercise promotes arm movement recovery in chronic hemiparetic stroke: a randomized controlled pilot study,” *Journal of NeuroEngineering and Rehabilitation*, vol. 3, p. 12, 2006.
- [257] A. Pandyan, C. Price, H. Rodgers, M. Barnes, and G. Johnson, “Biomechanical examination of a commonly used measure of spasticity,” *Clinical Biomechanics*, vol. 16, no. 10, pp. 859–865, 2001.
- [258] R. T. Kumar, A. D. Pandyan, and A. K. Sharma, “Biomechanical measurement of post-stroke spasticity,” *Age and ageing*, vol. 35, no. 4, pp. 371–375, 2006.
- [259] A. M. Coderre, A. A. Zeid, S. P. Dukelow, M. J. Demmer, K. D. Moore, M. J. Demers, H. Bretzke, T. M. Herter, J. I. Glasgow, K. E. Norman *et al.*, “Assessment of upper-limb sensorimotor function of subacute stroke patients using visually guided reaching,” *Neurorehabilitation and neural repair*, vol. 24, no. 6, pp. 528–541, 2010.
- [260] S. Del Din, S. Patel, C. Cobelli, and P. Bonato, “Estimating Fugl-Meyer clinical scores in stroke survivors using wearable sensors,” in *Engineering in Medicine and Biology Society, EMBC, 2011 Annual International Conference of the IEEE*. IEEE, 2011, pp. 5839–5842.
- [261] H. Krebs, B. Volpe, M. Ferraro, S. Fasoli, J. Palazzolo, B. Rohrer, L. Edelstein, and N. Hogan, “Robot-aided neurorehabilitation: from evidence-based to science-based rehabilitation,” *Topics in stroke rehabilitation*, vol. 8, no. 4, pp. 54–70, 2002.
- [262] B. H. Dobkin, “Progressive staging of pilot studies to improve phase III trials for motor interventions,” *Neurorehabilitation and Neural Repair*, vol. 23, no. 3, pp. 197–206, 2009.
- [263] L. J. Chapman and J. P. Chapman, “The measurement of handedness,” *Brain and cognition*, vol. 6, no. 2, pp. 175–183, 1987.
- [264] W. R. Hepp and H.-A. Locher, *Orthopädisches Diagnostikum*. Georg Thieme Verlag, 2014.
- [265] N. Klopčar, M. Tomšič, and J. Lenarčič, “A kinematic model of the shoulder complex to evaluate the arm-reachable workspace,” *Journal of biomechanics*, vol. 40, no. 1, pp. 86–91, 2007.
- [266] R. W. Bohannon and M. B. Smith, “Interrater reliability of a modified Ashworth scale of muscle spasticity,” *Physical therapy*, vol. 67, no. 2, pp. 206–207, 1987.

- [267] A. Haugh, A. Pandyan, and G. Johnson, "A systematic review of the Tardieu Scale for the measurement of spasticity," *Disability & Rehabilitation*, vol. 28, no. 15, pp. 899–907, 2006.
- [268] S. Kalsi-Ryan, D. Beaton, A. Curt, S. Duff, M. R. Popovic, C. Rudhe, M. G. Fehlings, and M. C. Verrier, "The graded redefined assessment of strength sensibility and prehension: reliability and validity," *Journal of neurotrauma*, vol. 29, no. 5, pp. 905–914, 2012.
- [269] H. M. Clarkson, *Musculoskeletal assessment: joint range of motion and manual muscle strength*. Lippincott Williams & Wilkins, 2000.
- [270] H. J. Hislop and J. Montgomery, *Manuelle Muskeltests: Untersuchungstechniken nach Daniels und Worthingham*. Elsevier, Urban&FischerVerlag, 2007.
- [271] M. Itzkovich, I. Gelernter, F. Biering-Sorensen, C. Weeks, M. Laramee, B. Craven, M. Tonack, S. Hitzig, E. Glaser, G. Zeilig *et al.*, "The Spinal Cord Independence Measure (SCIM) version III: reliability and validity in a multi-center international study," *Disability & Rehabilitation*, vol. 29, no. 24, pp. 1926–1933, 2007.
- [272] M. Post, G. Van Lieshout, H. Seelen, G. Snoek, M. Ijzerman, and C. Pons, "Measurement properties of the short version of the Van Lieshout test for arm/hand function of persons with tetraplegia after spinal cord injury," *Spinal cord*, vol. 44, no. 12, pp. 763–771, 2006.
- [273] J. Soucie, C. Wang, A. Forsyth, S. Funk, M. Denny, K. Roach, and D. Boone, "Range of motion measurements: reference values and a database for comparison studies," *Haemophilia*, vol. 17, no. 3, pp. 500–507, 2011.
- [274] V. Squeri, L. Masia, M. Casadio, P. Morasso, and E. Vergaro, "Force-field compensation in a manual tracking task," *PloS one*, vol. 5, no. 6, p. e11189, 2010.
- [275] S. C. Cuthbert and G. J. Goodheart, "On the reliability and validity of manual muscle testing: a literature review," *Chiropractic & Manual Therapies*, vol. 15, no. 1, p. 4, 2007.
- [276] A. Calota, A. G. Feldman, and M. F. Levin, "Spasticity measurement based on tonic stretch reflex threshold in stroke using a portable device," *Clinical Neurophysiology*, vol. 119, no. 10, pp. 2329–2337, 2008.
- [277] D. Prochnow, S. Bermúdez i Badia, J. Schmidt, A. Duff, S. Brunheim, R. Kleiser, R. Seitz, and P. Verschure, "A functional magnetic resonance imaging study of visuomotor processing in a virtual reality-based paradigm: Rehabilitation gaming system," *European Journal of Neuroscience*, vol. 37, no. 9, pp. 1441–1447, 2013.
- [278] M. K. Holden, "Neurorehabilitation using learning by imitation in virtual environments," *Usability evaluation and interface design: cognitive engineering, intelligent agents and virtual reality*. London: Lawrence Erlbaum, pp. 624–628, 2001.
- [279] R. C. Loureiro and W. S. Harwin, "Reach & grasp therapy: design and control of a 9-DOF robotic neuro-rehabilitation system," in *Rehabilitation Robotics, 2007. ICORR 2007. IEEE 10th International Conference on*. IEEE, 2007, pp. 757–763.
- [280] P. Heo, G. M. Gu, S.-j. Lee, K. Rhee, and J. Kim, "Current hand exoskeleton technologies for rehabilitation and assistive engineering," *International Journal of Precision Engineering and Manufacturing*, vol. 13, no. 5, pp. 807–824, 2012.
- [281] M. C. Hume, H. Gellman, H. McKellop, and R. H. Brumfield Jr, "Functional range of motion of the joints of the hand," *The Journal of hand surgery*, vol. 15, no. 2, pp. 240–243, 1990.
- [282] J. G. Ziegler and N. B. Nichols, "Optimum settings for automatic controllers," *Transactions of the A. S. M. E.*, vol. 5, no. 11, pp. 759–768, 1942.